LA-UR -79-2425

TITLE: PRELIMINARY CALCULATIONS RELATED TO THE ACCIDENT AT THREE MILE ISLAND

Compiled by: W. L. Kirchner and M. G. Stevenson

SUBMITTED TO: Division of Reactor Safety Research, U.S. Nuclear Regulatory Commission and the President's Commission on the Accident at Three Mile Island

los alamos
scientific laboratory
of the University of California
LOS ALAMOS, NEW MEXICO 87544

An Affirmative Action/Equal Opportunity Employer

Form No. 836
St. No. 2629
1/75

UNITED STATES
ENERGY RESEARCH AND
DEVELOPMENT ADMINISTRATION
CONTRACT W-7405-ENG. 36

DISCLAIMER

PRELIMINARY CALCULATIONS RELATED TO THE ACCIDENT AT THREE MILE ISLAND

Draft Report

Prepared by the
Reactor Safety Program
of the
Energy Division

Los Alamos Scientific Laboratory

August 1979

TABLE OF CONTENTS

CONTENTS (cont)

AUTHORSHIP AND ACKNOWLEDGMENTS*

A large number of people from the Reactor Safety Program at LASL have contributed directly and indirectly to the preparation of this report. The main contributors are listed below according to prime responsibility and contribution to each section of this report.

TRAC Base Case Calculation:	J. R. Ireland
TRAC Parametric Calculations:	J. R. Ireland
	P. B. Bleiweis
Core Thermal-Mechanical Response:	P. K. Mast
	T. R. Wehner
Report Compilation:	W. L. Kirchner
	M. G. Stevenson

*Work performed under the auspices of the U.S. Nuclear Regulatory Commission.

1.0 INTRODUCTION AND SUMMARY

The Los Alamos Scientific Laboratory has an extensive program, funded by the U.S. Nuclear Regulatory Commission, in the development, verification, and application of computer methods, specifically the Transient Reactor Analysis Code (TRAC), for the analysis of Light-Water Reactor (LWR) accidents.[1] Additional efforts for NRC involve investigations of phenomena relevant to High-Temperature Gas-Cooled Reactor (HTGR) and Liquid-Metal Cooled Fast Breeder Reactor (LMFBR) accidents. This report discusses preliminary studies of the Three Mile Island Unit 2 (TMI-2) accident based on available methods and data. The work reported includes:

- A TRAC base case calculation out to 3 hours into the accident sequence.
- TRAC parametric calculations. These are the same as the base case except for a single hypothetical change in the system conditions, such as assuming the high pressure injection (HPI) system operated as designed rather than as in the accident.
- Fuel rod cladding failure, cladding oxidation due to zirconium metal-steam reactions, hydrogen release due to cladding oxidation, cladding ballooning, cladding embrittlement, and subsequent cladding breakup estimates based on TRAC calculated cladding temperatures and system pressures. Estimates beyond initial gross fuel rod deformation must be regarded as speculative since the TRAC calculations currently assume intact core geometry.

Some conclusions of this work are:

- The TRAC base case accident calculation agrees very well with known system conditions to nearly 3 hours into the accident.

- The parametric calculations indicate that, loss-of-core cooling was most influenced by the throttling of High-Pressure Injection (HPI) flows, given the accident initiating events and the pressurizer electromagnetic-operated valve (EMOV) failing to close as designed.

- Failure of nearly all the rods and gaseous fission product gas release from the failed rods is predicted to have occurred at about 2 hours and 30 minutes. This is consistent with radiation monitors at TMI-2.

- Cladding oxidation (zirconium-steam reaction) up to 3 hours resulted in the production of approximately 40 kilograms of hydrogen. It is highly probable that hydrogen generation continued beyond that time.

1.1 TRAC Base Case Calculation

A description of the first released version of the TRAC code, TRAC-P1A, and the current status of its verification is contained in Appendix A to this report. TRAC-P1A is a steam-water (two-phase) systems analysis code designed specifically to produce physically accurate (best estimate) predictions of large-break loss-of-coolant accidents (LOCAs). TRAC calculations of a large number of LOCA-related experiments, such as in the Semiscale and LOFT facilities at the Idaho National Engineering Laboratory (INEL), have agreed very well with the experimental data, and considerable confidence can be placed in its modeling of the rapid blowdown, refill, and reflood phases typical of large-break LOCAs. Its calculational capabilities were not developed for and have not been tested against long time duration experiments typical of the TMI-2 accident. In particular, TRAC-P1A does not presently account for non-condensible gases (such as hydrogen generated by zirconium-steam reactions or nitrogen which may be injected from core flooding accumulators), nor does it account for changing core geometry due to cladding ballooning, rupture, oxidation, breakup, or fuel motion. Nevertheless, the TRAC-P1A base case results are in very good agreement with known system conditions during the first 3 hours of the TMI-2 accident. Further, much can be learned concerning the

system hydraulics and the core thermal-mechanical behavior by examining the TRAC results, as summarized below and discussed in detail in Sec. 2.0.

The TRAC model of the TMI-2 system for these calculations used 24 cells in the reactor vessel and 42 cells for the two system loops. The core fuel rods were modeled initially using three axial levels and two azimuthal regions per level, with average, high power, and low power fuel rods per region. This vessel noding was used to calculate the steady-state system conditions and the first 81 minutes of the transient. The pressurizer relief valve (EMOV) was modeled using a pipe module, allowing a direct calculation of the flow out the EMOV. The once-through steam generators (OTSG) were modeled on both primary and secondary sides, but with boundary conditions used to model the balance of the secondary system. Based on the TMI-2 recorded power level, a TRAC steady-state calculation was performed to generate the initial conditions prior to the accident. These conditions are in very good agreement with available TMI-2 data.

Using these self-consistent initial conditions, the TRAC transient calculation was begun. Operator and system actions were simulated in TRAC using plant data, event chronologies, and in certain cases, assumptions necessary to give results which matched known system conditions (these are outlined in detail in Sec. 2). The first 30 minutes of the accident sequence are well simulated by TRAC, particularly system pressure, loop temperatures, and pressurizer level. During the period from 30 minutes to 81 minutes coolant is continuously lost through the EMOV and the letdown system. Calculated core temperatures remain low, however, due to the good cooling provided by boiling in the core, which offsets the coolant losses and maintains the system pressure stable.*

At 81 minutes, a more finely noded vessel model was used to provide more axial levels. This enhances the accuracy of predictions of the core thermal conditions and two-phase natural circulation through the system. Due to continual coolant loss, calculated core void fractions increase and primary coolant pump flow rates slowly decrease due to void formation in the coolant.

---

*Throughout this discussion we will use present tense when describing calculated events and conditions which may or may not be known to have occurred in the accident.

Primary system pressure falls steadily after 91 minutes as increased auxiliary feedwater flow is introduced into the A loop OTSG. After the A loop pumps are tripped at 100 minutes, phase separation occurs throughout the system. This results in partial core uncovering and loss of coolant circulation through the loops. At 120 minutes, upper core temperatures begin to rise rapidly (0.25 K/s). At 138 minutes, the EMOV block valve is closed resulting in a gradual increase in core liquid inventory. At about 160 minutes, the water inventory in the core has boiled down again such that water is in the lower plenum and partially in the lower core, resulting in a steep axial temperature gradient in the core. Since upward-moving steam velocities are very low (less than 0.1 m/s) the steam becomes very superheated in the upper part of the core and, as a result, the cladding and fuel heat up sharply. When the cladding temperatures reach 1300 K, zirconium-steam reactions (exothermic) begin and the upper core temperatures begin rising at about 0.7 K/s. This temperature excursion was probably terminated in the accident when the HPI was returned to nonthrottled flow rates at 3 hours and 20 minutes, enhancing the core cooling rate (TRAC calculations were terminated at 3 hours since the core modeling was no longer realistic).

The results of this TRAC base case calculation show good agreement with measured system parameters out to nearly 3 hours and provide a foundation for: making detailed comparisons against alternative system/operator responses during the accident sequence, investigating longer term TMI-2 accident events, and making estimates of the reactor core thermal-mechanical behavior.

1.2 TRAC Parametric Calculations

This section of the study was performed to investigate hypothetical variations to the TMI-2 accident sequence to determine the significance of system/operator actions on the course of the accident. It is not intended to judge system design or operator response as related to the TMI-2 accident; rather, its purpose is to serve as a basis for future discussion on reactor system design, instrumentation, and operation.

Within the time constraints of this preliminary study, five parametric cases were run with TRAC. These specific cases were requested by the NRC TMI Special Inquiry Group. The INEL is supplying additional parametric cases. The primary variations of interest were: (1) start of auxiliary feedwater supply after initiation of the accident, (2) the effect of degraded high-pressure injection (HPI), (3) the effect of early tripping of the main coolant pumps, and (4) the effect of a cold-leg break of area equivalent to the EMOV throat area. The delay (up to 1 hour) of auxiliary feedwater supply as compared to immediate initiation results, in the TRAC calculations, in very little difference in the long-term behavior of the system from that of the base case. This conclusion is of importance to the TRAC base calculation since it demonstrates that the primary system behavior was a relatively weak function of the details of the secondary system performance.

The parametric case with HPI operating as designed resulted in significant deviations from the base case. After the pressure dropped below the HPI set-point and full flow was initiated, the HPI flow was sufficient to maintain the system pressure at a higher level than the base case. This resulted in a higher break flow than the base case, but, more importantly, maintained the coolant in a subcooled state, preventing a core temperature excursion. This calculation indicates that no core damage would have occurred as long as HPI flow was supplied.

The influence of the main coolant pumps was examined by a parametric case in which the pumps were tripped immediately upon initiation of the accident. This calculation was not run as far out in time as the base case, but the available results indicate that after a flow coastdown transition period of 40 minutes, phase separation begins in the system. Based on comparison with the base case calculation in which phase separation occurred after the A loop pumps were tripped, we expect that this case would result in a similar core temperature transient beginning approximately 45 minutes earlier than the base case.

The final parametric case performed was a cold-leg break simulation. A break area equivalent to the EMOV throat area was assumed and located in the

A loop pump discharge line. The initial transient is characterized by a higher system pressure than in the base case. This occurs because the equivalent area cold-leg small-break flows are lower than out the EMOV in the base case. This case was not run to completion, but, given the same character of letdown and makeup flows as occurred in the base case, this case could depressurize with core flood tank activation and subsequent core flooding.

1.3 Core Thermal-Mechanical Response

The concern in a reactor accident is the potential for release of radioactive materials. The amount of radioactive material available for release is determined by the state of the reactor core before the accident, but the amount actually released is determined by temperatures and other system conditions during the accident. Of particular interest are when significant cladding failures first occur and allow release of fission product gases to the primary coolant system. Continued fuel heatup can result in release of volatile fission products from the surface and matrix of the fuel pellets and, if not terminated, fuel pellet melting. Phenomena which influence the core behavior include cladding ballooning before failure, cladding oxidation, embrittlement, and hydrogen generation from zirconium-steam reactions.

Calculations indicate that considerable local cladding ballooning was likely prior to failure and should have resulted in some degree of local flow blockages. However, the best estimate cladding failure time of about 2-1/2 hours using TRAC-calculated temperatures, while not including local flow starvations, agrees well with indications of substantial radioactive material release. Since there was very little steam flow through the core during the temperature excursion leading to these initial cladding failures, then ballooning should not have influenced failure times substantially. However, local flow reductions due to ballooning could have been a contributor to anamolous fuel bundle outlet temperatures measured later in the accident.

The calculated cladding failure times of about 2-1/2 hours are shown (Sec. 4 of report) to be not very sensitive to initial rod pressures or the accepted criteria used for failure predictions. The major controlling factor is the high cladding temperatures occurring in the upper part of the core after about 2 hours. The calculations indicate that essentially all of the rods should have failed, thus releasing most of the core inventory of gaseous fission products.

Further calculations based on TRAC results indicate about 37 kg of hydrogen were produced by 3 hours into the transient (the TRAC calculations were terminated at that time). This reaction causes swelling and embrittlement of the Zircaloy cladding. Calculations of possible thermal-shock induced failures assuming the hot cladding was quenched shortly after 3 hours show that ductile cladding would not have suffered further failures from thermal shock. However, the swollen and embrittled oxidized cladding probably would have. Thus, the axial length of cladding which was oxidized (roughly the upper third of the core) might have failed extensively during reflood, if reflood occurred quickly. We have not performed detailed calculations beyond 3 hours, and since the TRAC calculations beyond about 2-1/2 hours do not model many of the complicated core phenomena, these estimated cladding conditions are somewhat speculative. However, the TRAC-calculated system pressure does agree quite well with the measured pressure out to almost 3 hours (to the time at which substantial hydrogen generation begins). Thus, the core thermal conditions used for the cladding behavior calculations to this time should not be too unrealistic.

1.4 Hypothetical Sequence Questions

Some specific questions were addressed to us by the President's Commission on the Accident at Three Mile Island. Several of these are covered by the parametric cases summarized in the preceding section. Responses to the complete set are provided below. Those which go beyond the analyses discussed above must be regarded as speculative.

1.4.1 What would have been the effect if the auxiliary feedwater system had been available as designed?

In this case (as discussed above and in Sec. 3.3 of this report), the system would have started depressurizing somewhat earlier than occurred, but after about 30 minutes there would have been little difference in the two cases.

1.4.2 What would have been the effect if the EMOV had closed as designed (assuming auxiliary feedwater was made available at 8 minutes as occurred)?

Although we did not analyze this case, it is likely there would have been no severe problem. In the accident, water was lost through the EMOV and not restored through the HPI system. If the water had not been lost, then a relatively mild pressure transient would have occurred until auxiliary feedwater restored cooling.

1.4.3 What would have been the effect if the HPI had not been throttled?

The TRAC parametric case that examined this situation is reported in Sec. 3.1. There is more water put in by the HPI than lost through the EMOV. The core remains covered and no primary system voids occur. This situation could continue as long as sufficient water was available to the HPI. Eventually, some final heat sink other than this makeup water, such as the low-pressure safety system, would have to be used to continue cooldown.

1.4.4 What would have been the effect if auxiliary feedwater had not been available at any time?

A TRAC parametric case (reported in Sec. 3.2) assumed a 60 minute delay in auxiliary feedwater. The system equilibrates between energy produced in

the core and removed through the EMOV. The system pressure remains about 1.5-2.0 MPa (225-300 psia) higher than in the base case due to the lack of heat transfer in the steam generators. The flow out the EMOV is higher and the system would empty sooner than in the base case. Core uncovering and heatup would probably begin about 1 hour earlier than in the base case.

1.4.5 What would have been the effect if the pressurizer relief block valve had not been closed at 2 hours and 20 minutes?

Although we have not analyzed this case, we expect the system would have depressurized until the core flood tanks were activated, which would probably have reflooded and cooled the core.

1.4.6 What would have been the effect if the HPI had remained throttled indefinitely?

The TRAC base case calculation indicates a core peak temperature rise rate of about 0.7 K/s over the last 1000 s calculated (out to 11000 s). If extrapolated linearly, this indicates initiation of fuel melting at about 3 hours and 45 minutes. However, the TRAC modeling does not include several effects (such as cladding ballooning, cladding swelling, noncondensible gas in the steam flow, radiation heat transfer, natural convection steam cooling inside the vessel) which might have influenced the core heatup rate beyond 2-1/2 hours. This extrapolation to incidence of fuel melting is thus speculati

2.0 TMI-2 BASE CASE CALCULATION

The TRAC-P1A computer code[1] was used to model and simulate the initial part of the accident that occurred at the Three Mile Island, Unit-2, nuclear power plant (TMI-2) on March 28, 1979. The purposes of this calculation were to:

- Provide insight into the system thermal-hydraulic phenomena which occurred during the initial accident stages.

- Provide a basis to evaluate hypothetical alternative system/operator responses during the accident.

- Provide an estimate of core thermal response as a basis for calculations of cladding deformation, oxidization, and failure.

- Evaluate and assess the applicability of TRAC to non-LOCA accident scenarios.

TRAC is a best estimate, nonequilibrium, multidimensional, thermal-hydraulic, steam-water (two-phase) systems analysis computer code written specifically to analyze loss-of-coolant-accidents (LOCAs) in Light-Water Reactors (LWRs). Reference 1 and Appendix A to this report contain a complete description of the code and a demonstration of its successful assessment against a wide range of experiments. One important point concerning TRAC is made here. The maximum time step size for stable computations is limited to a value which when multiplied by the fluid velocity in each computational cell, yields a length smaller than the length of that computational cell. Typically, this results in time step sizes less than a tenth of a second. For application of TRAC to large-break LOCAs, this is not a limiting concern; however, for transients of considerable duration (several thousand seconds) computer running times are quite large (many hours on a CDC-7600 class machine). Finally, even when relatively large time steps (fractions of a

second) are permissible based on the above condition, smaller time steps are necessary to control numerical error. This problem has a direct bearing on the model described in the next section. Typically, TRAC calculations of reactor systems use on the order of 750 cells; for the TMI-2 accident prediction, practical computing limitations constrained the total number to less than 100.

2.1 TRAC TMI-2 Model

A schematic of the TRAC noding used for the TMI-2 model is shown in Fig. 1. The model consists of a vessel and two primary coolant loops. Each loop contains a primary coolant pump and once-through steam generator (OTSG). The high-pressure injection (HPI) to each cold leg is modeled, and the letdown system and pressurizer are attached to the A loop. In the actual system there are two cold legs per loop, each with a primary coolant pump, but these were combined in the TRAC model to reduce the number of cells.

The three-dimensional vessel noding is shown in Fig. 2. The vessel consists of 177 fuel assemblies with 208 fuel rods per assembly (the 15 x 15 array also includes guide tubes). These fuel assemblies are modeled in TRAC using three axial levels, one radial ring, and two azimuthal sectors, for a total of six TRAC core cells. (Levels 2, 3, and 4 in Fig. 2.) With this noding, only two average fuel rods (24.3 kW/m) are used for coupling the fuel rod heat transfer to the fluid dynamics. Two hot rods are also used to model the high power and low power rods in the core (35.8 and 12.0 kW/m, respectively). The lower plenum, upper plenum, and upper head region are each modeled using one axial level. The entire TRAC vessel model consists of 2 radial rings, 6 axial levels, and 2 azimuthal segments for a total of 24 vessel cells. The vessel noding described above was used for the steady-state calculation and during the first 81 minutes of the transient. After 81 minutes, the vessel noding was changed to yield more axial detail for natural convection and core thermal calculations. This revised noding is shown in Fig. 3.

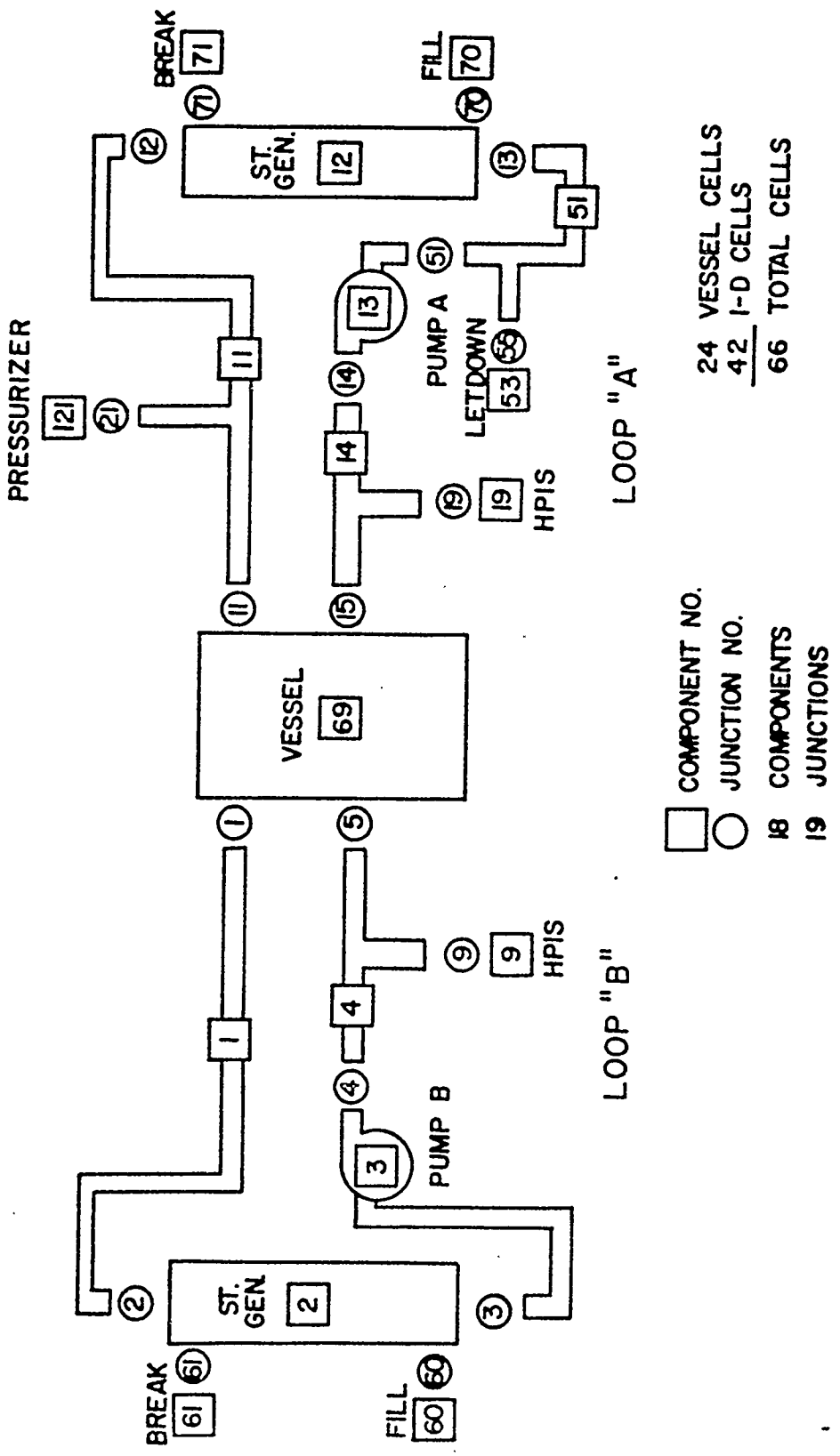

Fig. 1. TRAC nodding schematic for TMI-2.

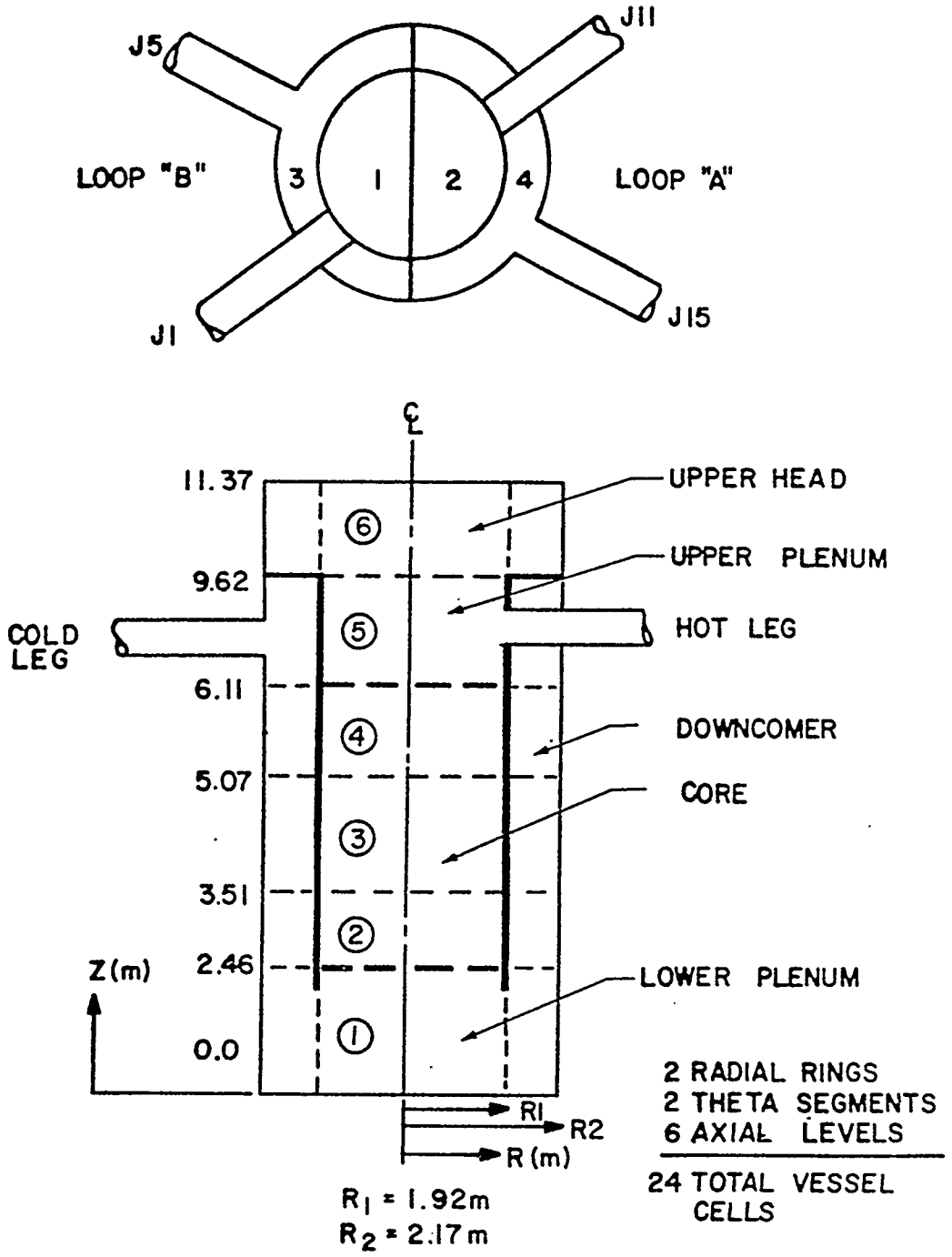

Fig. 2. Vessel noding used for first 81 minutes.

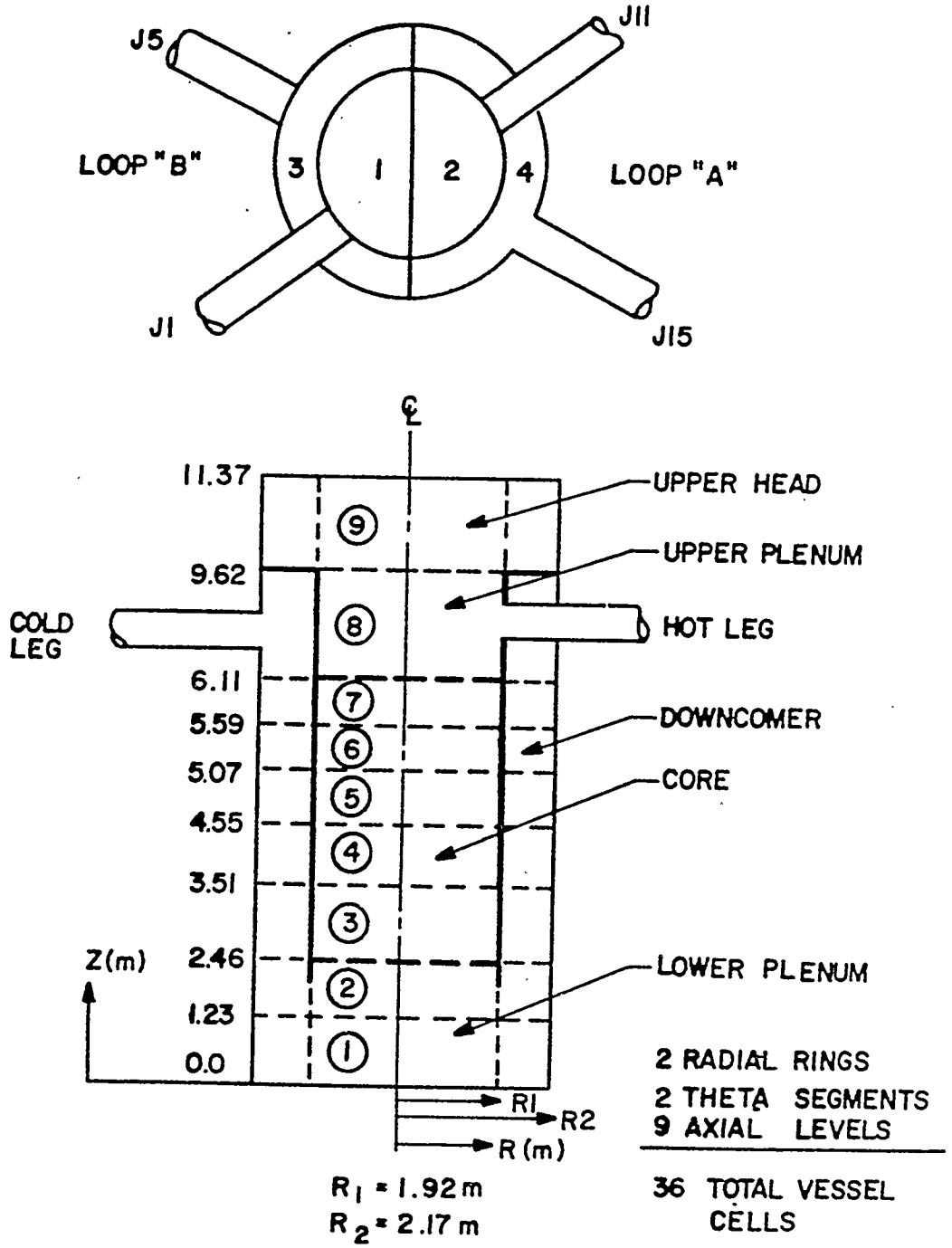

Fig. 3. Vessel noding used after 81 minutes.

The hot-leg noding consists of three cells in each hot leg to model the inlet nozzle, vertical riser, and "candy-cane" regions. (Components 1 and 11, Fig. 1.) The pressurizer is modeled as a constant pressure break for the steady-state calculation (component 121 in Fig. 1). For the transient calculation, however, the pressurizer is modeled using two pipe components as shown in Fig. 4. The lower pipe models part of the pressurizer surge line and the bottom section of the pressurizer and the upper pipe models the top of the pressurizer and the pressurizer relief valve. The choking in the relief valve is modeled by using the fully implicit hydrodynamics option (one-dimensional components) in TRAC. Using very fine noding, the choking is calculated naturally from an implicit solution of the equations of mass, momentum, and energy. The OTSGs are modeled using seven cells on the primary side and five cells on the secondary side (Fig. 5). The complete secondary system is not modeled; the boundary conditions to the OTSGs describing the feedwater flow and steam line back-pressure are given by known system conditions during the accident.

2.2 Steady-State Calculation

Based on the geometry and noding described above, a steady-state calculation was performed to obtain initial conditions prior to the accident. The input parameters for the steady-state calculations are shown in Table I.[2] TRAC calculated initial conditions are shown in Table II along with a comparison with the results from the B&W code CRAFT-2.[3] The agreement appears to be quite good for all parameters. The differences in flow rates and temperatures can be attributed to the fact that CRAFT-2 used 100% power, whereas, for TMI-2 on March 28, 1979, the power was actually 97%, which was the value used in TRAC. The difference between the calculated primary system water masses is due to the fact that TRAC includes the mass of the steam generator secondary side but CRAFT-2 does not.

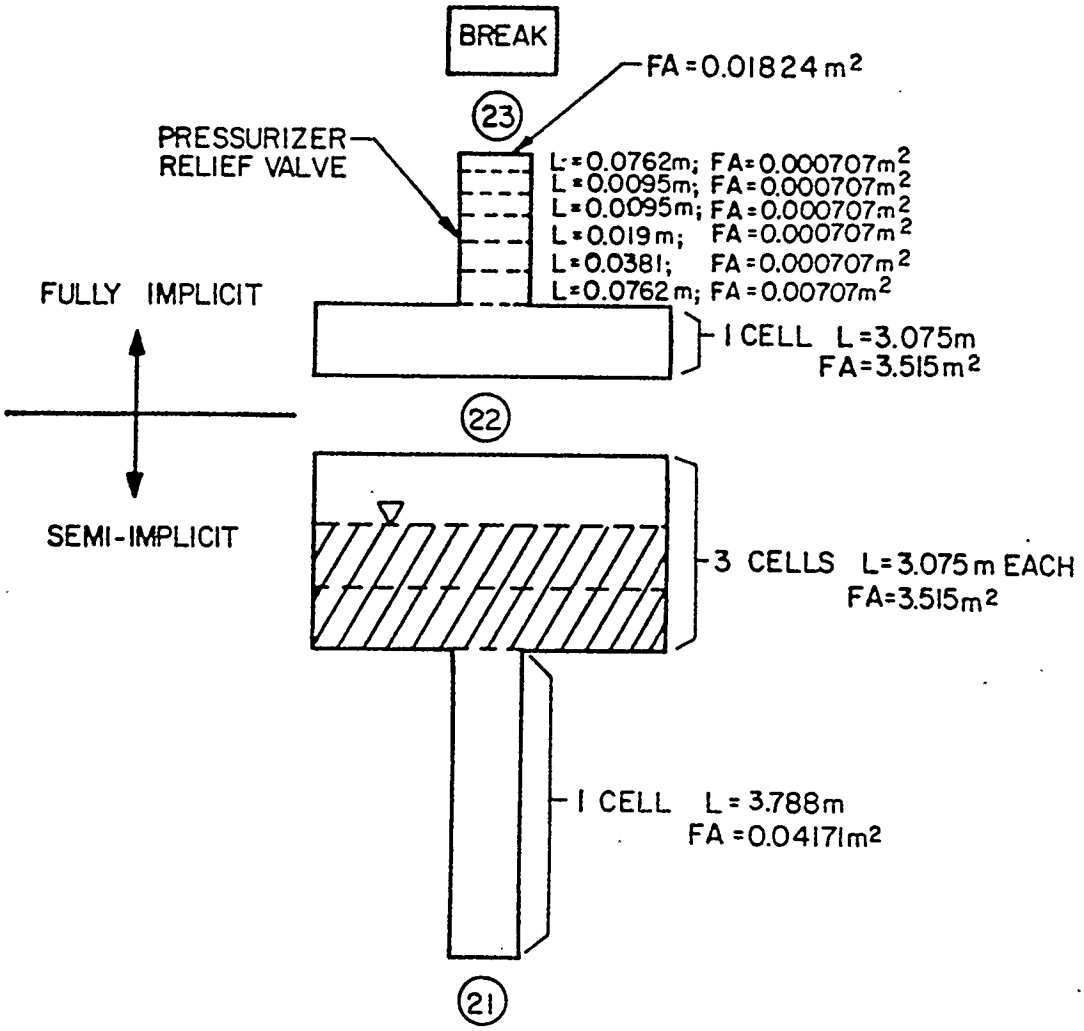

Fig. 4. TRAC pressurizer model.

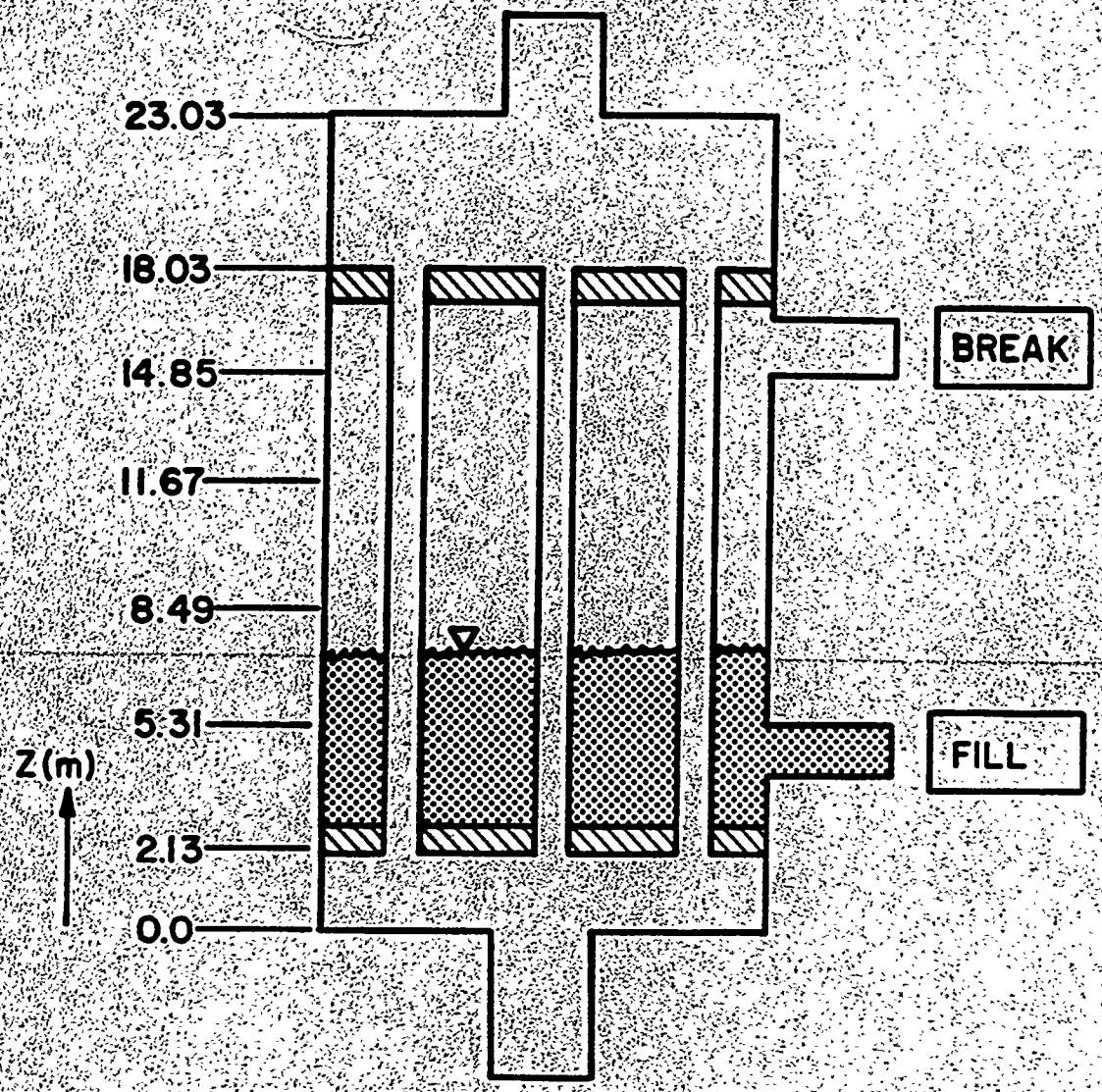

Fig. 5. TRAC steam generator model.

TABLE I

THREE MILE ISLAND - UNIT 2
TRAC Input Parameters

	Parameter	Value
1.	Initial Power (97% of rated)	$2.711\ 78 \times 10^9$ W
2.	Relative Axial Power Shape (3 levels - bottom to top)	0.64, 1.0, 0.76
3.	Relative Radial Power Shape	1.0
4.	Core Average Linear Power	$2.014\ 4 \times 10^4$ W/m
5.	Peak Rod Linear Power	$2.444\ 2 \times 10^4$ W/m
6.	High Power Rod Linear Power	$3.589\ 2 \times 10^4$ W/m
7.	Low Power Rod Linear Power	$1.197\ 5 \times 10^4$ W/m
8.	Pressurizer Pressure	$1.477\ 21 \times 10^7$ Pa

TABLE II

THREE MILE ISLAND - UNIT 2

Calculated Initial Conditions at Steady State

	Parameter	TRAC	CRAFT-2
1.	Average Hot-leg Temperature at Vessel Outlet (K)	592.3	593.0
2.	Average Cold-leg Temperature at Vessel Inlet (K)	564.1	564.5
3.	Total Primary System Flow Rate (2 loops) (kg/s)	17 027.0	17 375.5
4.	Average Hot-leg Pressure at Vessel Outlet (Pa)	1.475×10^7	1.472×10^7
5.	Average Cold-leg Pressure at Vessel Inlet (Pa)	1.504×10^7	1.534×10^7
6.	Pump ΔP (Pa)	7.87×10^5	7.87×10^5
7.	Steam Generator Secondary Side Flow Rate (each) (kg/s)	700.0	
8.	Average Steam Generator Secondary Side Pressure (Pa)	65.5×10^6	
9.	Cladding Surface Temperatures at Core Level 2: (K)		
	a. Average Rod	605.0	
	b. High Power Rod	614.1	
	c. Low Power Rod	595.0	
10.	Total Primary System Water Mass (kg)	2.774×10^5	2.765×10^5

2.3 Transient Calculation

Using the steady-state results, the transient calculation was initiated. For the transient, boundary conditions were required for the steam generator secondary side, pressurizer relief valve back pressure, etc. These boundary conditions are summarized in Table III and shown in Figs. 6-11. A sequence of events was also needed to simulate operator interaction with the system and actual plant signals or trips that occurred. Using available information,[4-7] a sequence of events was developed and is shown in Table IV. The values used for HPI, makeup, and letdown flows were obtained from plant data and event chronology, where available. For certain portions of the transient some of the conditions had to be assumed. These assumptions and others used for the transient are shown in Table V.

The transient calculation was initiated by turning off the feedwater flow to the steam generators. As the system pressurizes above normal operating range the electromagnetically operated valve (EMOV) at the top of the pressurizer opens. The system pressure continues to rise until the reactor is scrammed at about 10 s. A depressurization period then begins and the system pressure drops until the steam generator secondary side dries out at about 2 minutes. The system again begins to pressurize due to loss of heat sink in the steam generators and continues until auxiliary feedwater flow is established at about 8 minutes. Then, the system depressurizes due to enhanced heat transfer in the steam generator until an equilibrium state is achieved between the decay heat produced in the core, energy removal in the steam generator, and energy removal through the break. Figure 12 shows the actual TMI-2 pressure history for the first 30 minutes of the accident and the comparison with the TRAC calculation.[8] Figure 13 shows the loop fluid temperature response for the first 30 minutes and the comparison with TRAC. The pressure and temperature comparisons are in good agreement with the data for this period.

During the first 30 minutes, the pressurizer water level initially drops, then rises as shown in Fig. 12. When the EMOV opens, saturated steam at the top of the pressurizer rapidly escapes and the pressurizer water level rises as the steam volume at the top of the pressurizer is replaced with a two-

TABLE III

THREE MILE ISLAND - UNIT 2

Boundary Conditions

1. Reactor Power vs Time

2. Pump Speed vs Time:

A. Pump Loop B:	$0 \leq t \leq 4\,380.0$	125.7 rad/s
	$t > 4\,380.0$	0.0 rad/s
B. Pump Loop A:	$0 \leq t \leq 6\,000.0$	125.7 rad/s
	$t > 6\,000.0$	0.0 rad/s

3. HPI Flow vs Time

4. Pressurizer Relief Valve Back-pressure vs Time

5. Steam Generator Steam Line Back-pressure vs Time

6. Steam Generator Feedwater Flow vs Time

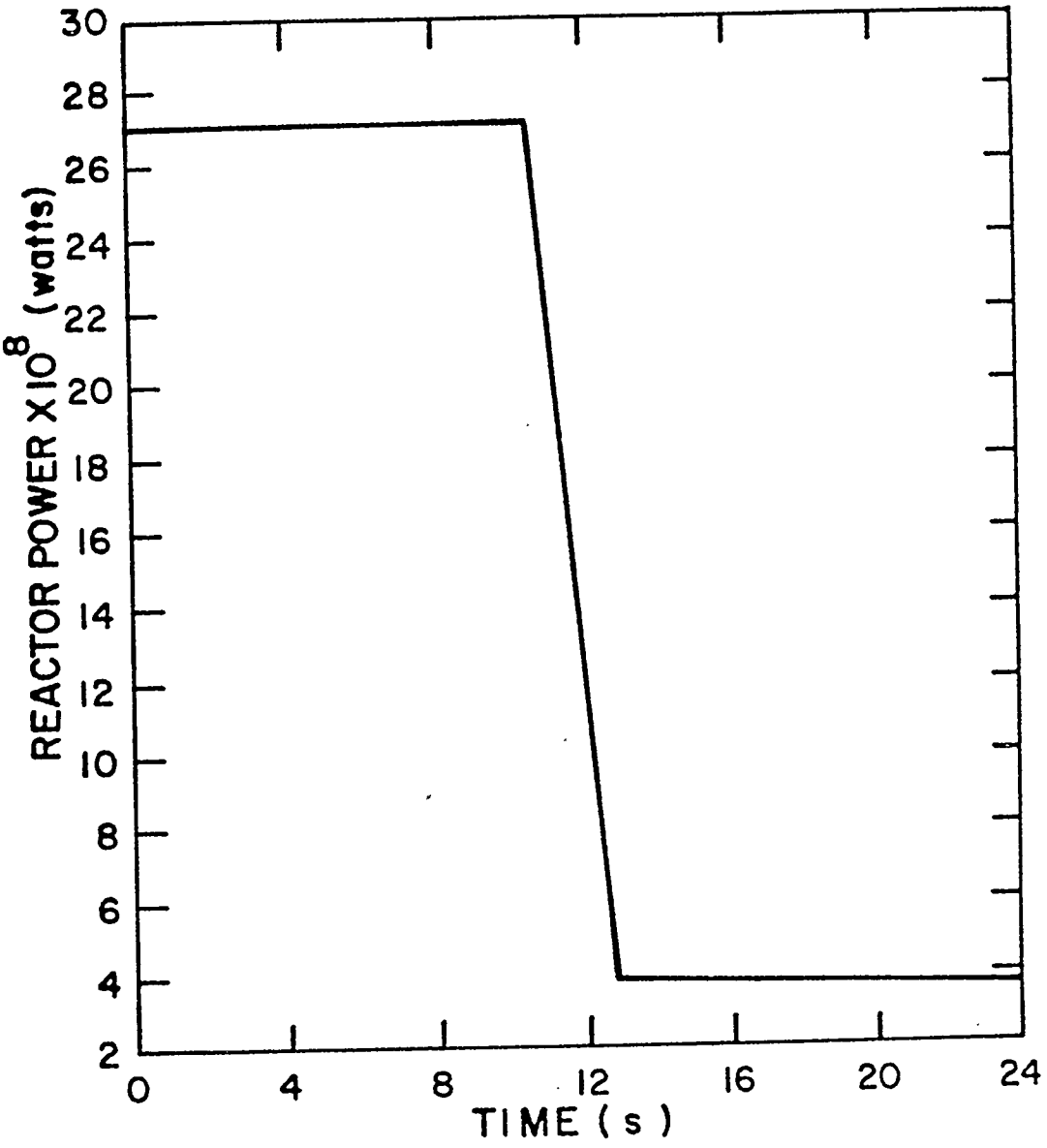

Fig. 6. Reactor power.

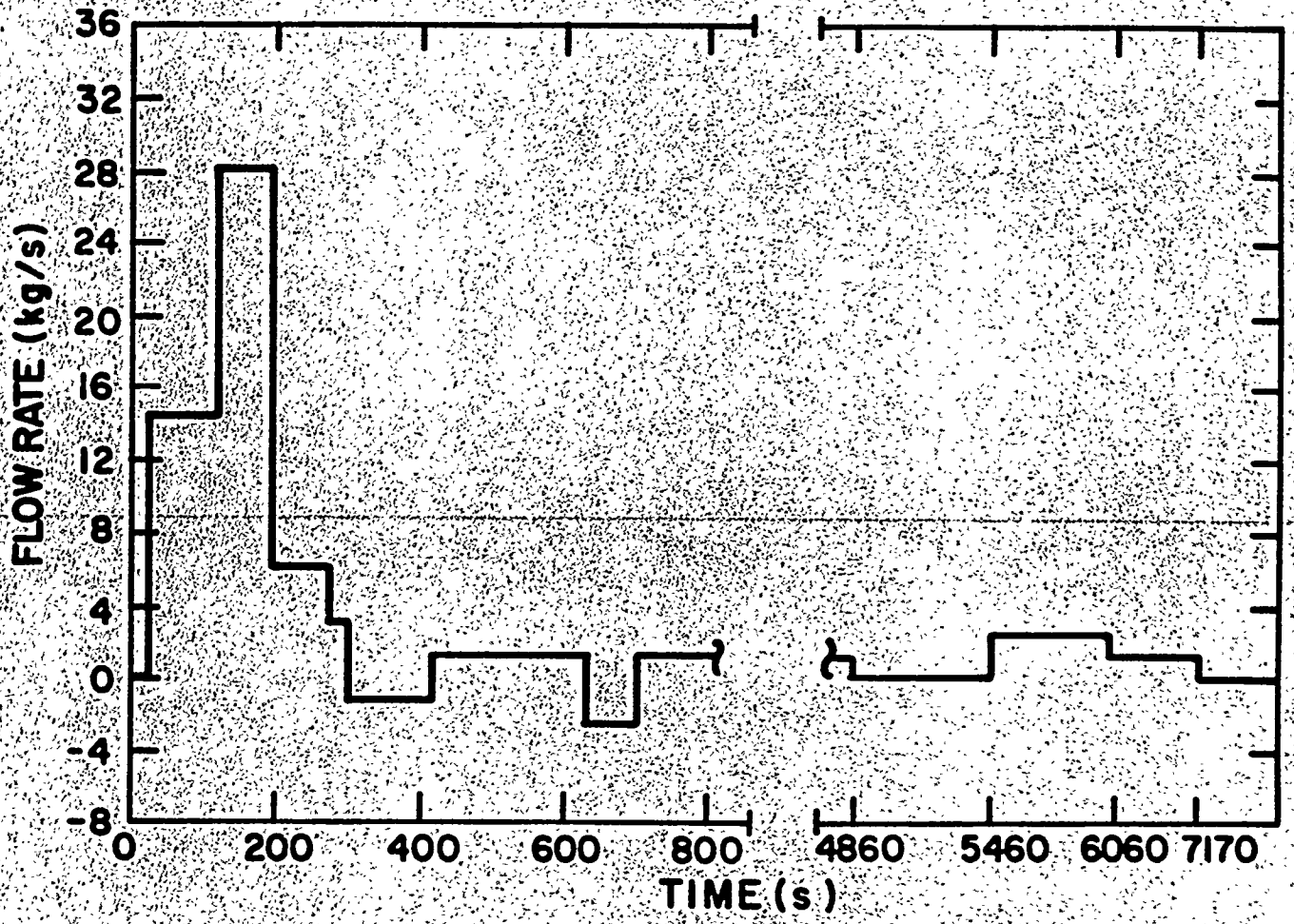

Fig. 7. HPI flow rate for each loop.

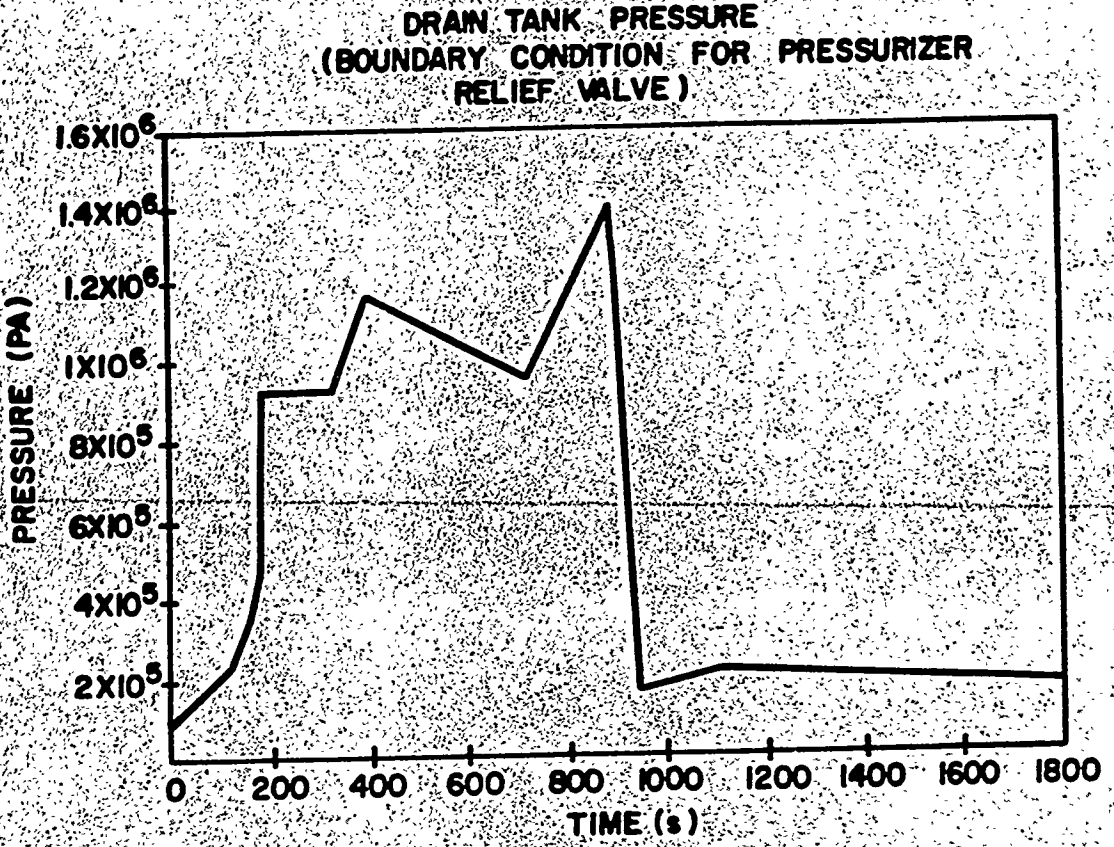

Fig. 8. Relief valve back pressure.

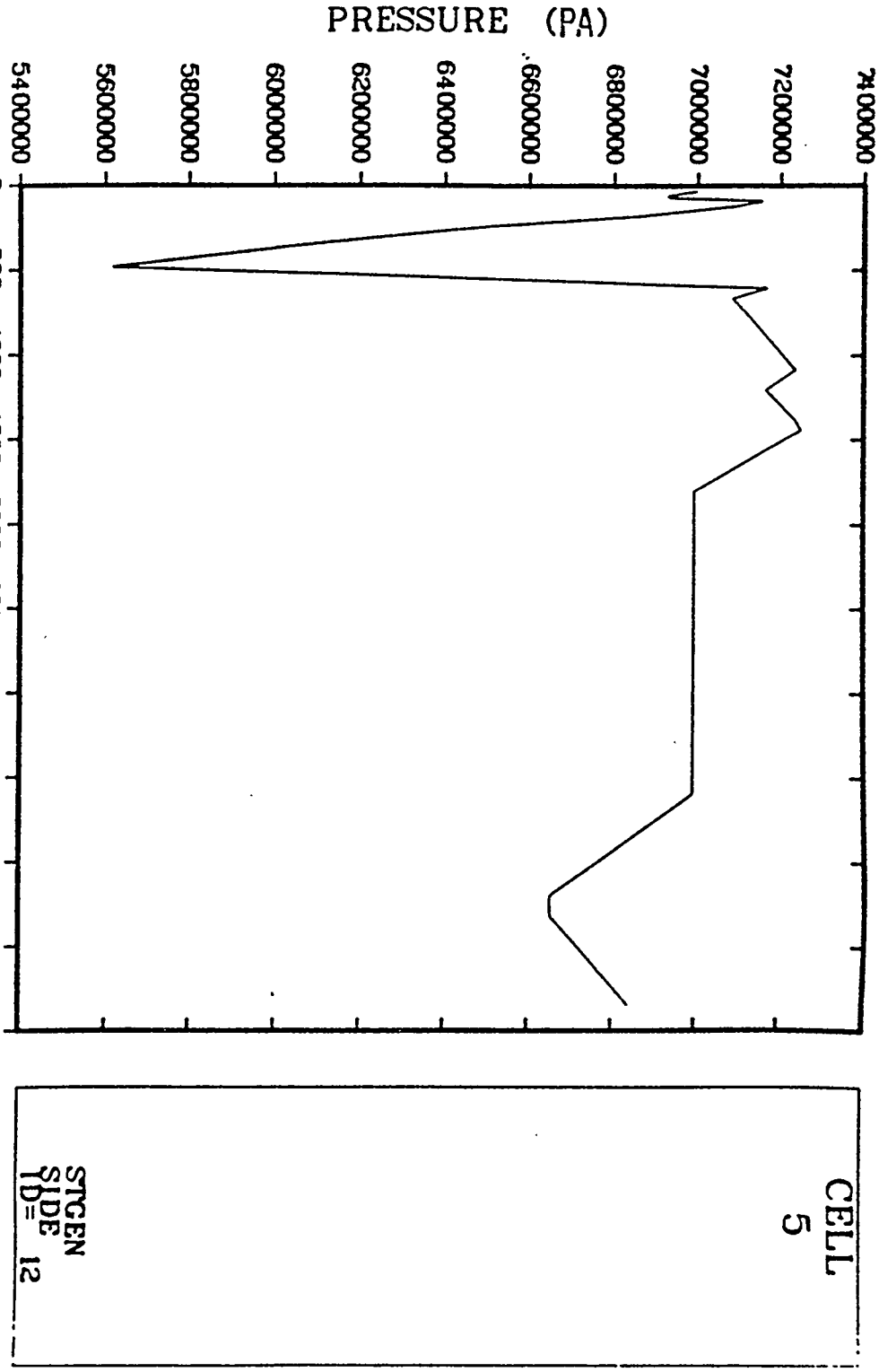

Fig. 9. A Loop steam generator back pressure.

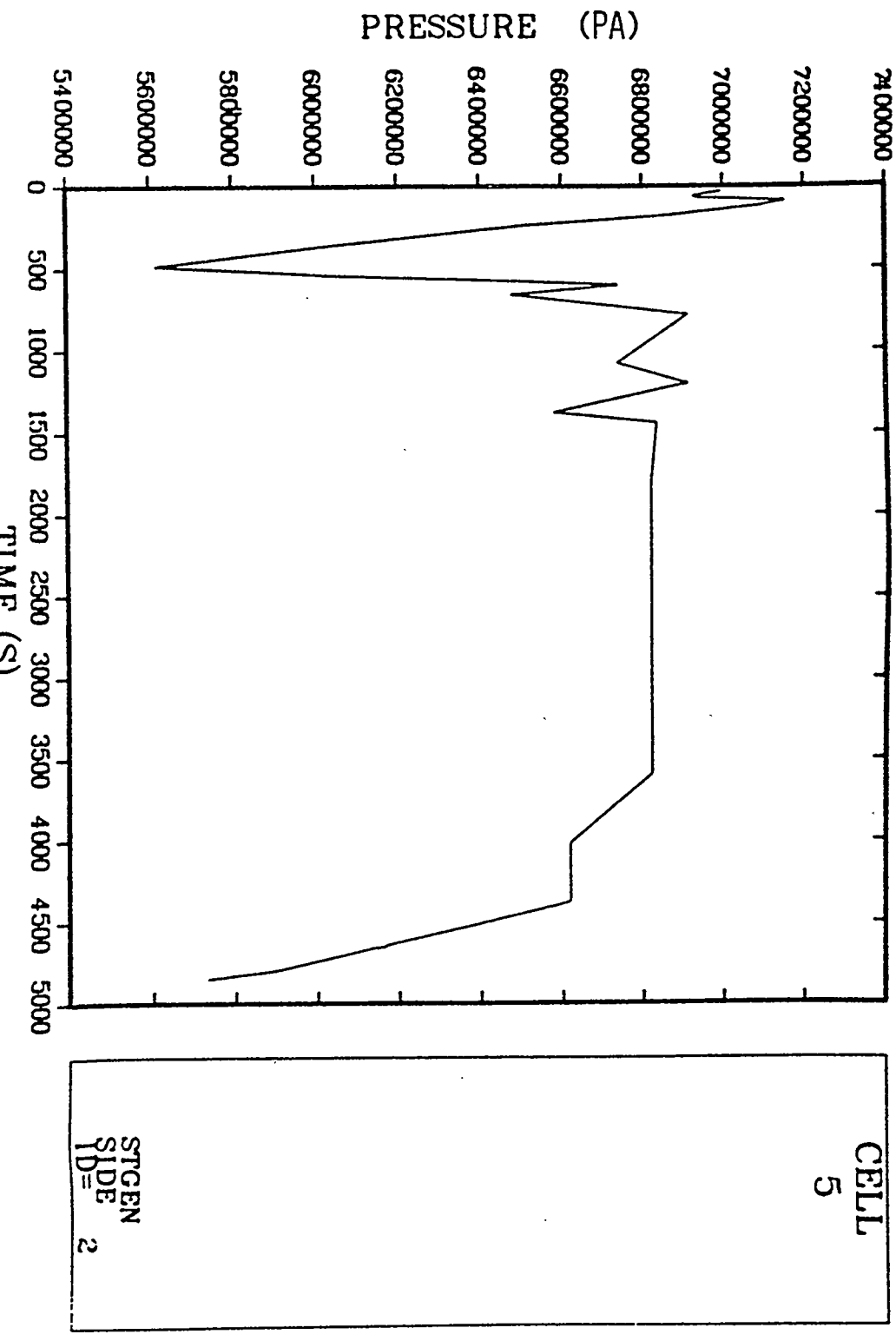

Fig. 10. B Loop steam generator back pressure.

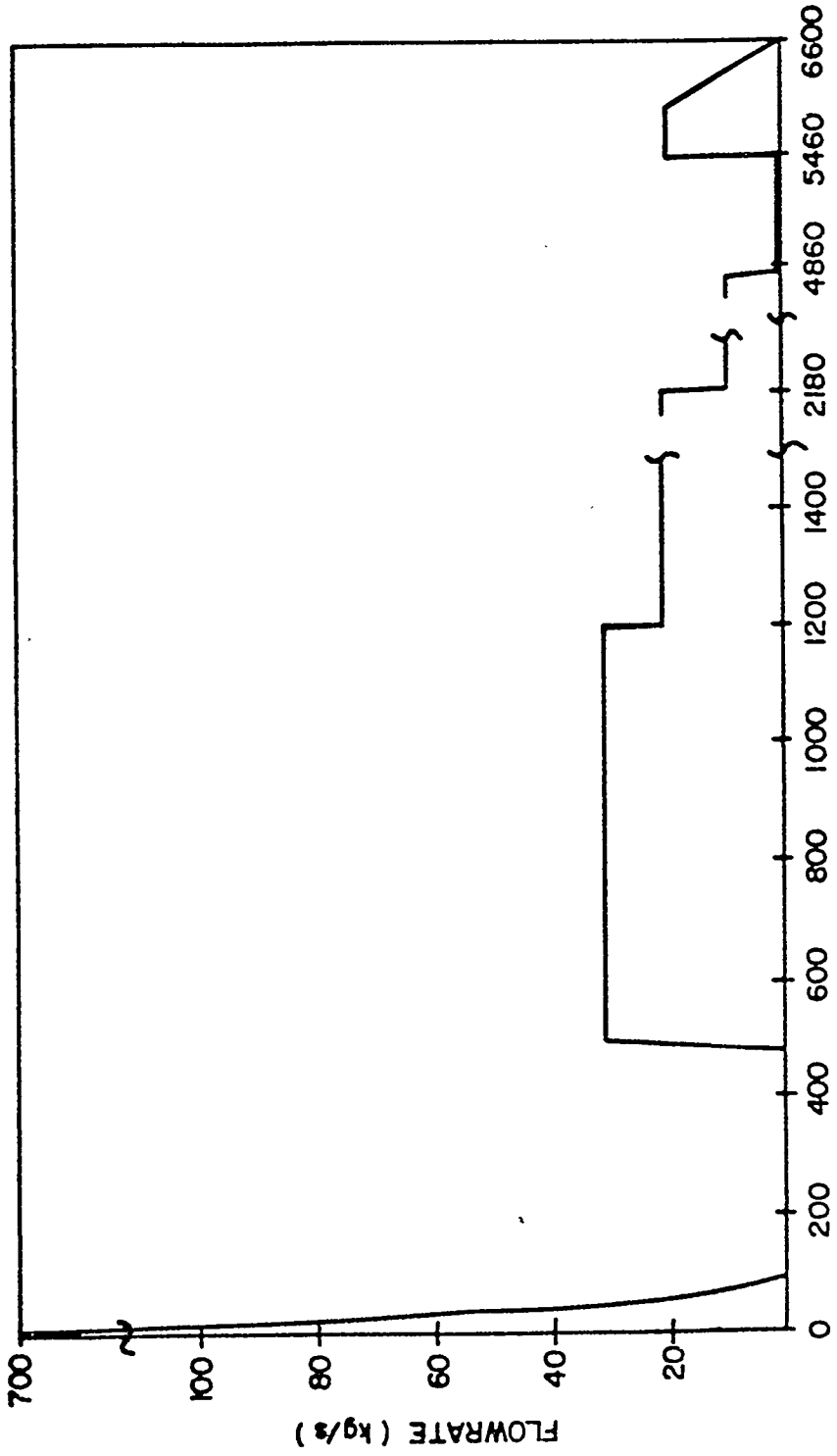

Fig. 11. Auxiliary feedwater flow for each steam generator.

TABLE IV

THREE MILE ISLAND - UNIT 2

Sequence of Events

Used for Base Case Calculations

Time (s)	Event
0.0	Loss of Feedwater Flow
10.5	Trip Reactor Power
13.0	Start Make-up Pump 1A Full Flow 27.5 kg/s
120.0	Start Make-up Pump 1C Full Flow 27.5 kg/s
194.0	Throttle Pumps 1A and 1C to 6.1 kg/s each
278.0	Trip Pump 1C - Continue Pump 1A at 6.1 kg/s
300.0	Initiate Letdown Flow of 8.6 kg/s
418.0	Reduce Letdown Flow to 4.5 kg/s
480.0	Start Auxiliary Feedwater Flow of 30.6 kg/s (each OTSG)
624.0	Trip Pump 1A - Continue Letdown Flow
700.0	Start Pump 1A (Makeup + HPI = 1.85 kg/s)
3824.0	Turn Off Letdown
4380.0	Trip Primary Pumps - Loop B
4860.0	Turn Off HPI and Auxiliary Feedwater Flow
5460.0	Initiate HPI - 4.4 kg/s
	Initiate Letdown - 4.4 kg/s
	Initiate Auxiliary Feedwater Flow to OTSG "A" - 33.4 kg/s
6000.0	Trip Primary Pumps - Loop A
6060.0	Reduce HPI - 2.2 kg/s
	Increase Letdown - 15.0 kg/s
7170.0	Turn Off HPI and Decrease Letdown - 4.5 kg/s
8280.0	Shut Pressurizer Block Valve and Turn Off Letdown

TABLE V

ASSUMPTIONS FOR TMI BASE CASE

1. Decay Power Obtained from "Nuclear Legislative Advisory Service," Issue 17, April 13, 1979.

2. Feedwater Flow vs Time Ramped to Zero Over a 90 s Time Interval at Beginning of Transient. (90 s was used in order to account for the stored water mass in the OTSG downcomer.)

3. Make-up Pump Full Flow Capacity of 27.5 kg/s (each).

4. Throttled Flow Rate for Make-up Pumps of 6.1 kg/s.

5. Letdown Flow is Assumed to be Equal to Make-up Flow for $T < 13$ s and for $T > 8\ 280.0$.

6. Letdown Flow Greater Than Make-up + HPI for $600 \leq t \leq 8\ 280$ s.

7. Auxiliary Feedwater Flow is 31.3 kg/s for Each OTSG (later reduced to match secondary side water level).

8. Pressurizer Relief Valve Noding Determined by Using Rated Saturated Steam Flow Conditions of 15.0 kg/s.

9. From t = 101 Minutes until 120 Minutes, 15 kg/s Letdown Flow was Used to Match Primary System Pressure.

10. Pressurizer heaters were not modeled.

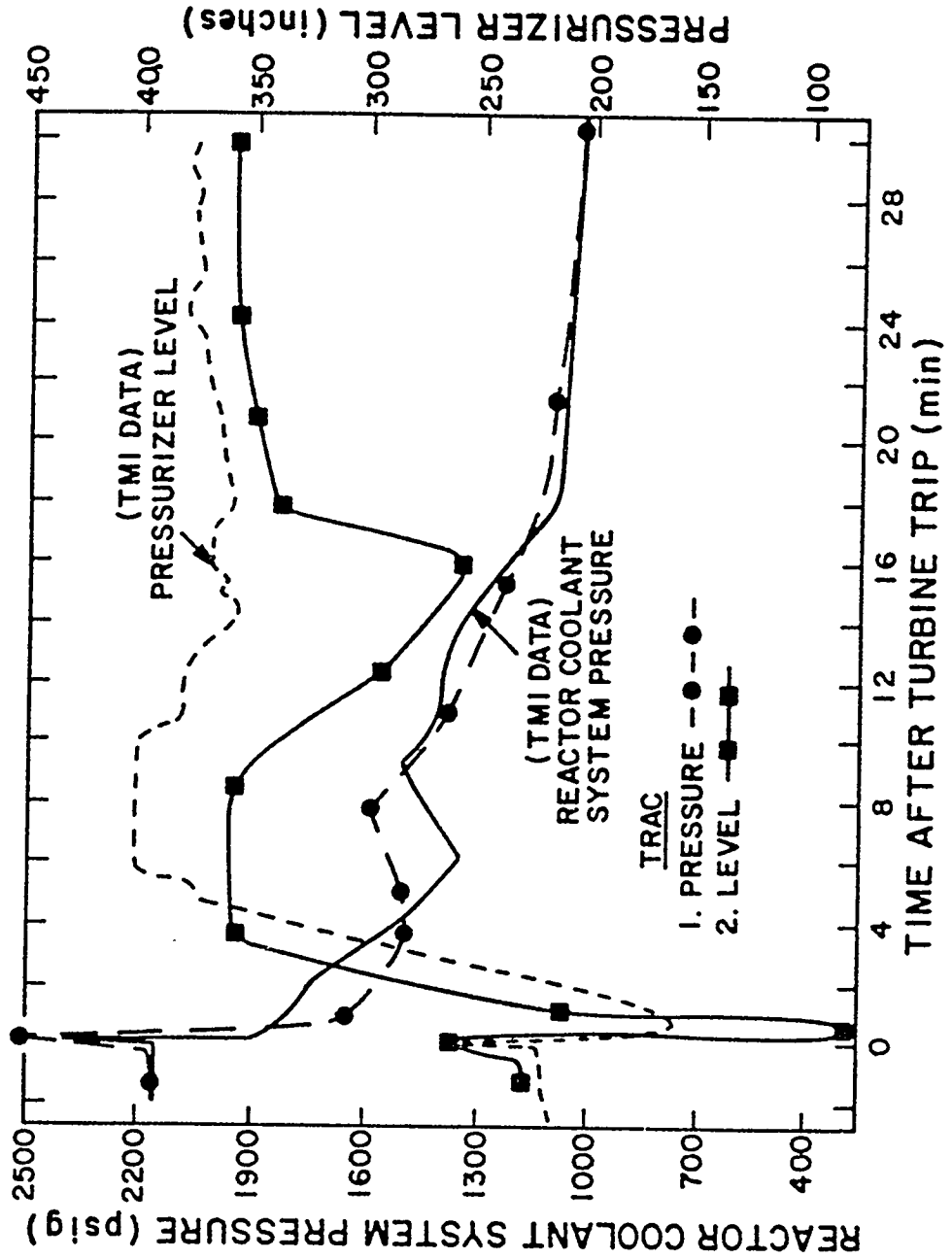

Fig. 12. TRAC comparisons with TMI data for first 30 minutes.

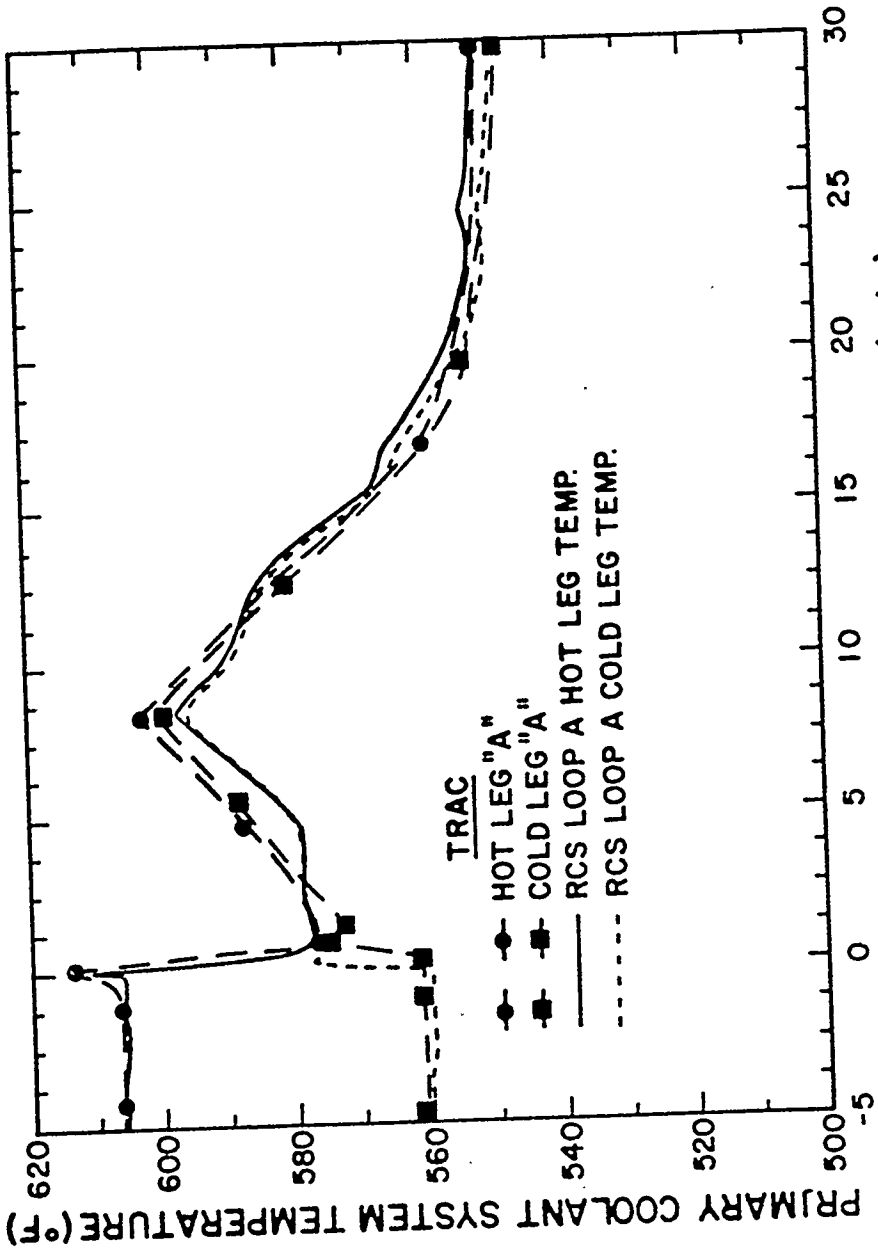

Fig. 13. A Loop fluid temperature comparisons.

phase mixture. When the two-phase mixture begins to leave the EMOV, the mass flow rate increases and the water level begins to drop rapidly as the pressurizer empties. The pressurizer continues to empty until the makeup and HPI systems are started, at which time the water level begins to rise. The makeup, letdown, and HPI flows used during the first 8 minutes were mainly to control the water level in the pressurizer, not to replace the coolant lost out the EMOV. The pressurizer then remains full until the water becomes saturated at about 10 minutes. At this time, flashing of the water begins as the system depressurizes and the water level drops until the system pressure stabilizes. The pressurizer then fills and remains essentially full until approximately 85 minutes.

For the period from 30 minutes until 80 minutes, the system is in a quasi steady-state mode in which the energy produced in the reactor core is removed primarily in the steam generators. Due to good heat transfer in the steam generator, the primary system pressure closely follows the back pressure on the secondary side (Figs. 9, 10, and 14). The fluid temperatures in the system are at saturation during this time and are following the system pressure. Figures 14, 15, and 16 show the actual pressure and temperature histories, along with the TRAC calculation. Since the pressure is relatively constant during this period, the break flow out the EMOV is also constant at about 20 kg/s. (Fig. 17.) Coolant is continually being lost from the system through the EMOV. Also, coolant is being lost through the letdown system since it was assumed that letdown flow was in excess of HPI and makeup flows by about 2.7 kg/s. The system is at saturation during this period and coolant is being continually lost, producing voids throughout the primary side. Figure 18 shows a void fraction profile in the vessel for the first 80 minutes. The curves represent the void fraction in each axial level from the bottom to the top of the vessel (refer to Fig. 2 for the vessel noding diagram). The upper head completely voids at about 27 minutes and remains voided for the entire calculation.

The core regions are producing voids at roughly a constant rate until the B loop pumps are tripped at 73 minutes. At this time, phase separation occurs in the B loop and the resulting elevation head in the loop is high

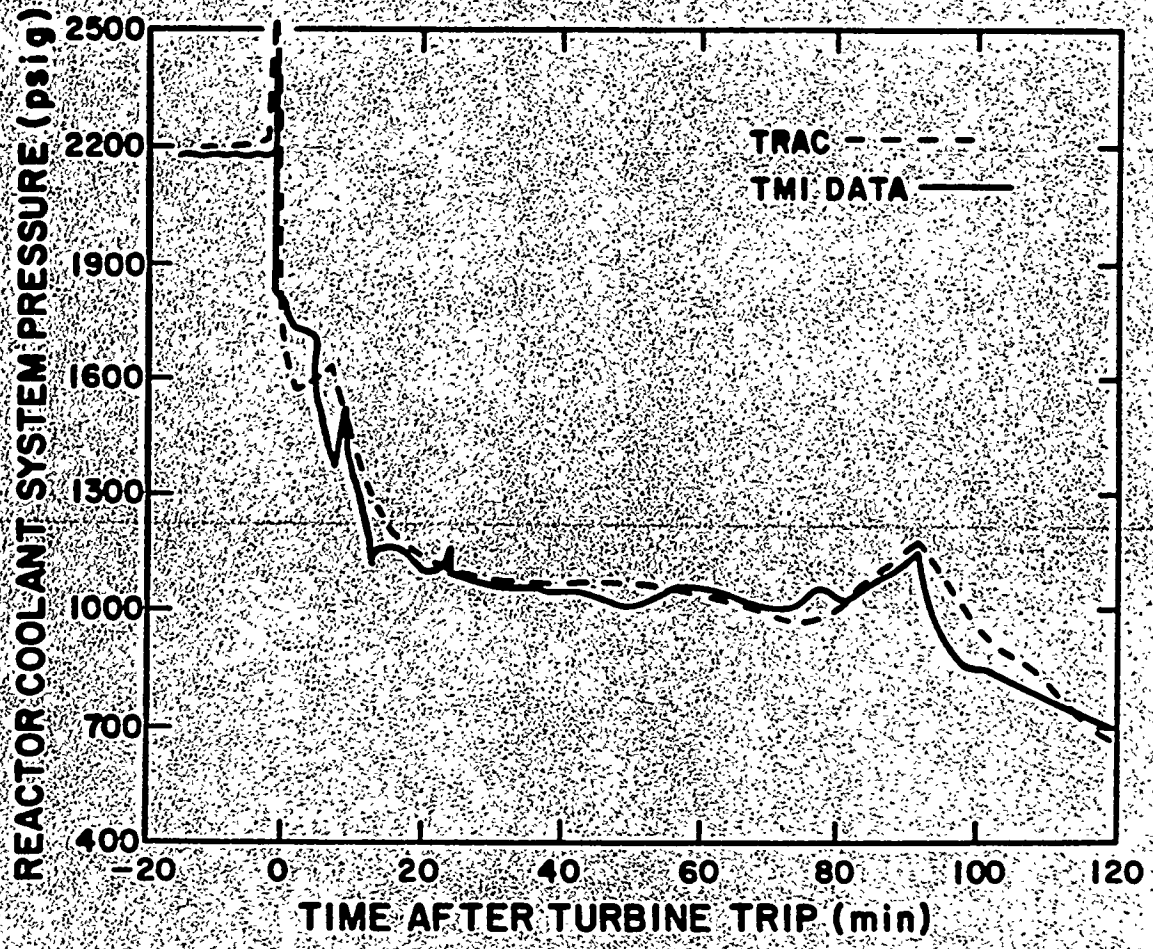

Fig. 14. System pressure comparisons out to 120 minutes.

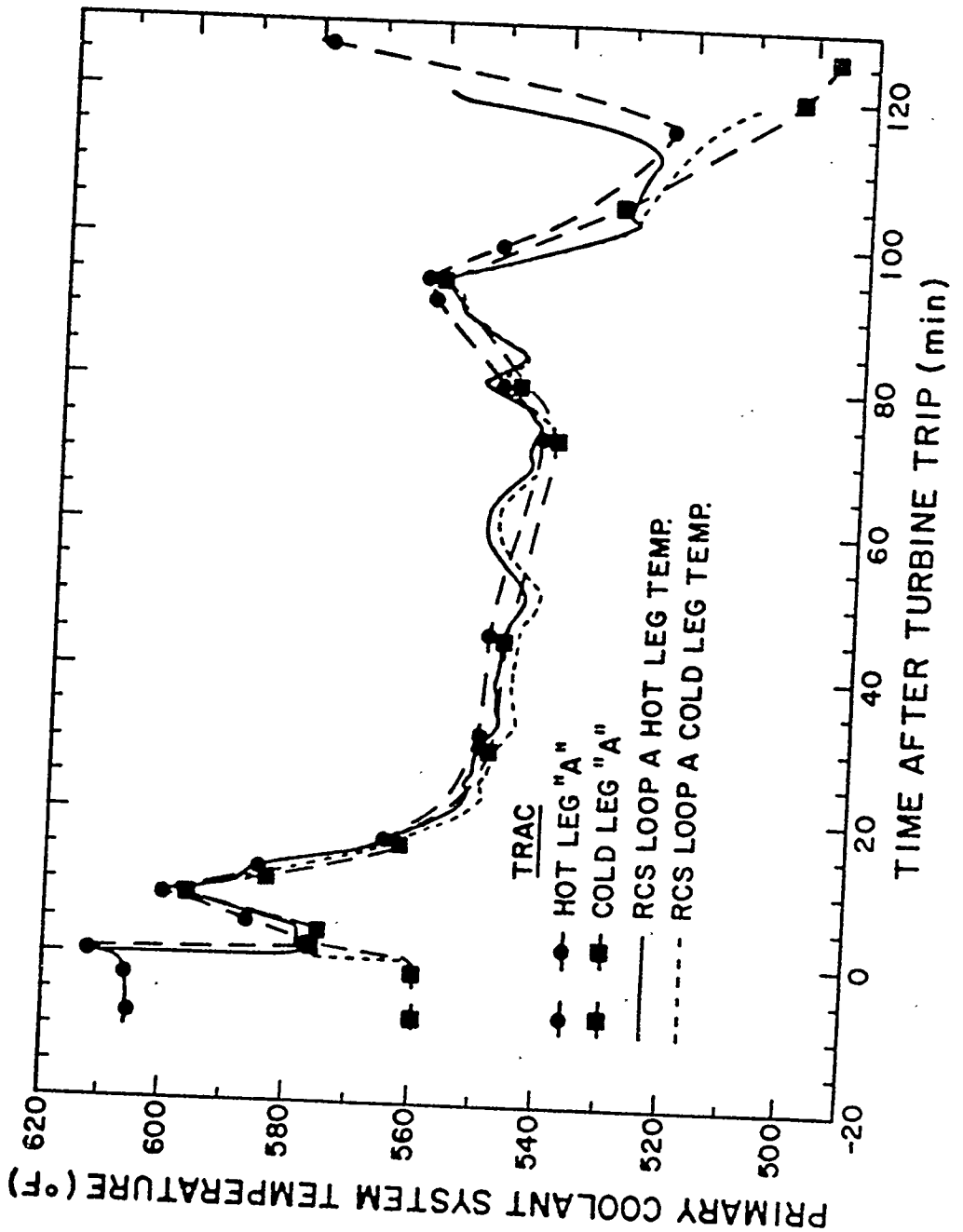

Fig. 15. A Loop fluid temperature comparisons out to 120 minutes.

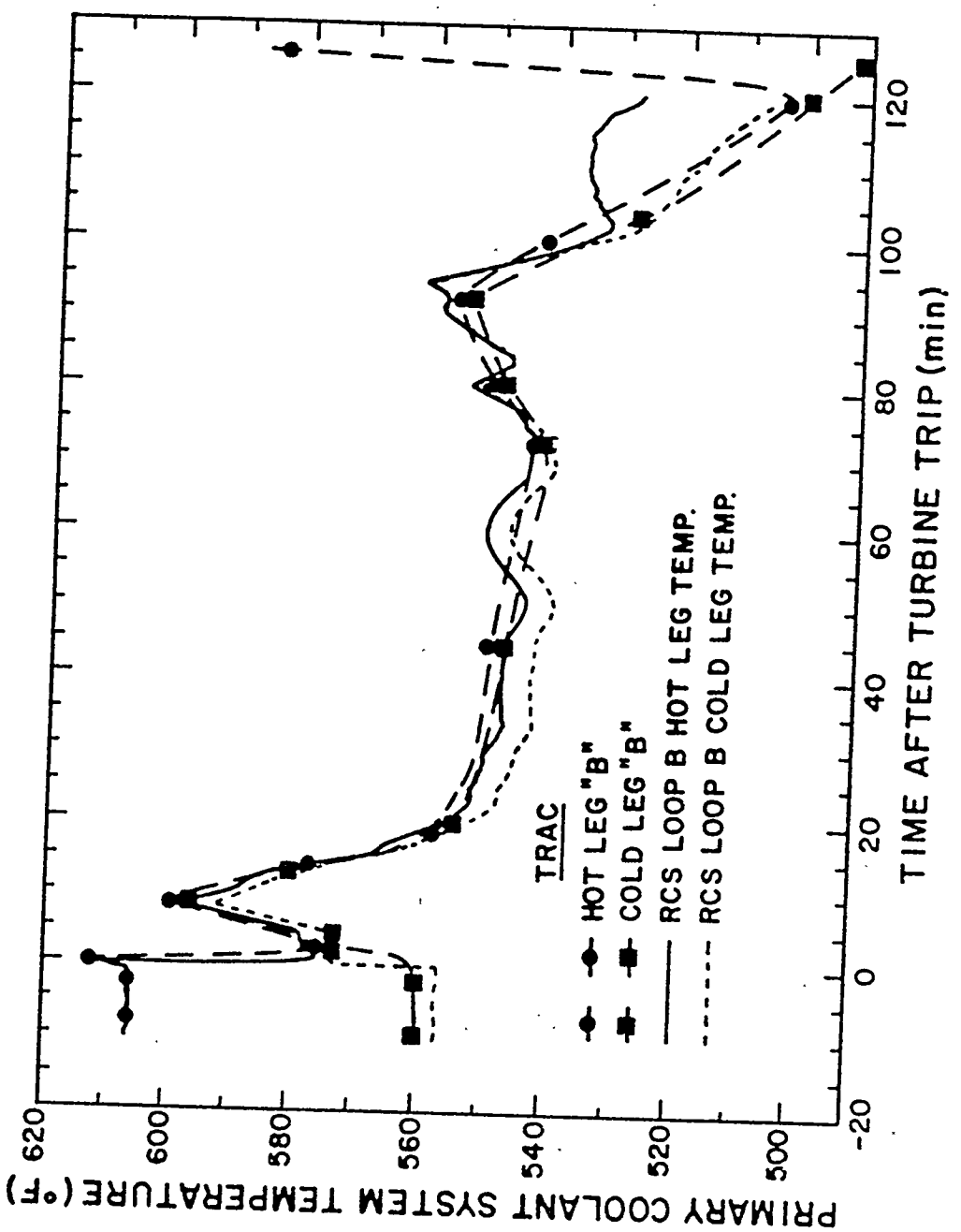

Fig. 16. B Loop fluid temperature comparisons out to 120 minutes.

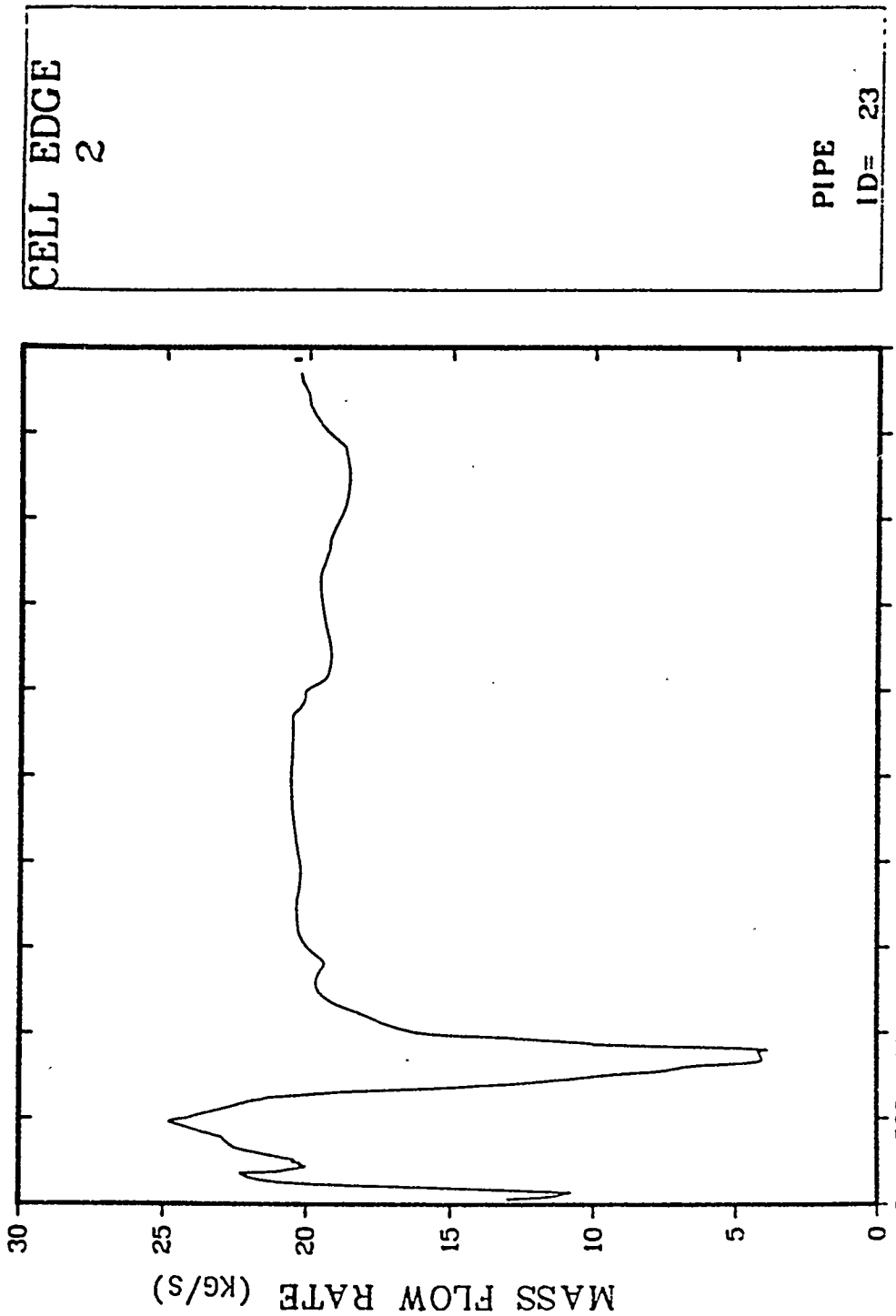

Fig. 17. Pressurizer relief valve flow rate for first 81 minutes.

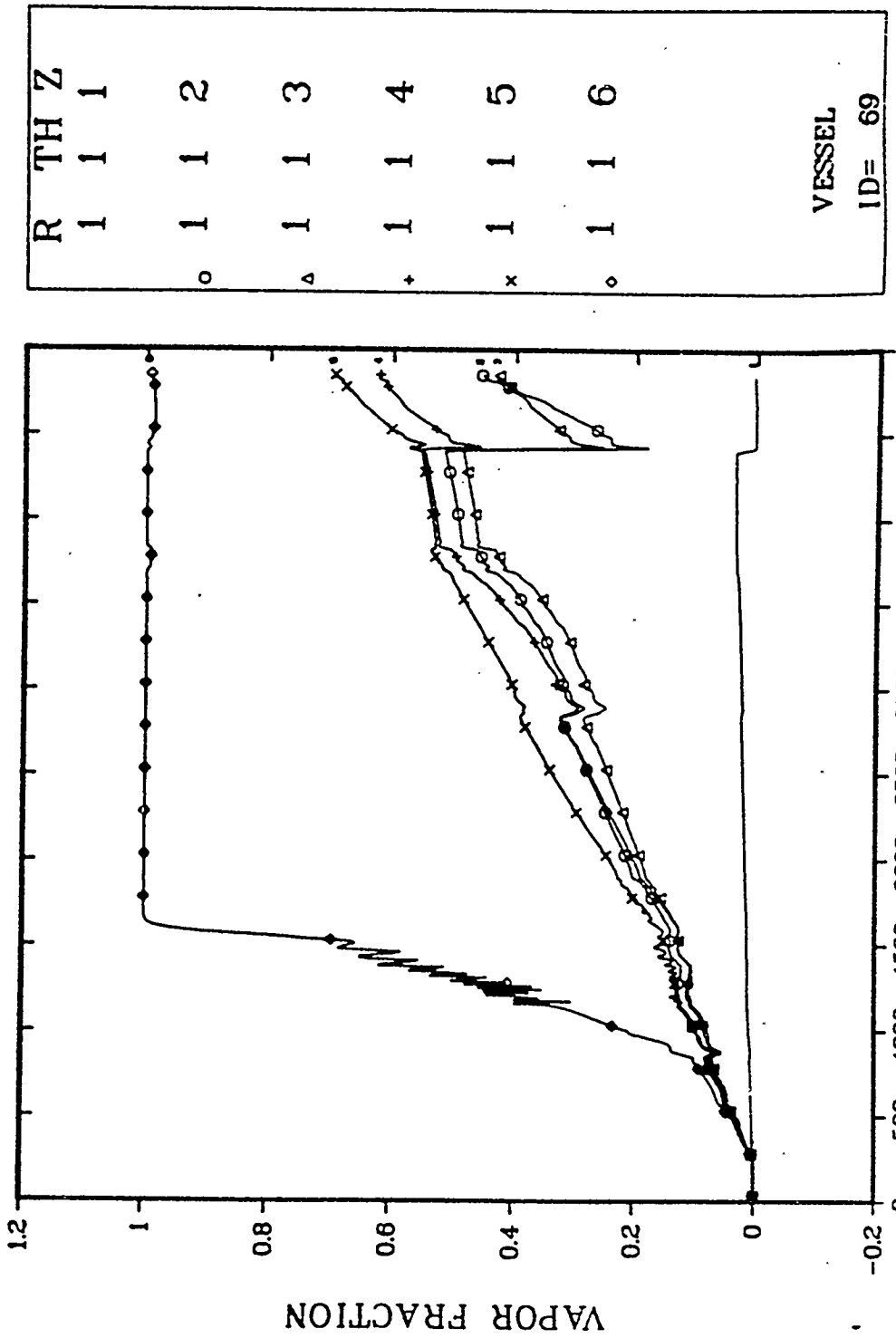

Fig. 18. Vessel void fraction profile out to 81 minutes.

enough to force some water into the vessel. This results in a void fraction drop in the core region, but this additional water is rapidly boiled off. Although the void fraction in the core is increasing during this period, the fuel rods remain cool due to nucleate boiling heat transfer in the core region. The fuel rods remain cool until the core partially uncovers at 101 minutes. Since there are significant voids throughout the system, the pump heads and mass flow rates are degrading due to two-phase flow losses. (See Appendix B for pump mass flow rates and other system variables during this period.) Although the B loop pumps are tripped at 73 minutes, the fuel rods remain cool due to adequate forced convection from the A loop pumps and the EMOV flow.

For the period from 80 minutes to 138 minutes, the system is in more of a transient mode as opposed to the previous quasi steady mode. The transient mode first starts when the B loop pumps are tripped and the secondary side pressure of the B loop OTSG begins to drop (Fig. 10). This drop in back-pressure causes the primary side to also drop slightly in pressure until adequate heat transfer (forced convection) is lost. When this happens, the system pressure begins to rise (Fig. 14) due to loss of heat transfer in the B loop steam generator and the increasing A loop steam generator back-pressure (Fig. 9). Since the A loop pumps are still running, good heat transfer is still available through the A loop steam generator, causing the primary system pressure to follow the secondary side pressure. At 91 minutes, the primary system pressure begins to decrease due to increased auxiliary feedwater flow to the A loop steam generator and increased letdown flow. This also causes the pressurizer water level to decrease (Fig. 19). The system pressure continues to decrease at a constant rate until the A loop pumps are tripped. The slope of the pressure curve then changes due to loss of forced convection through the A loop steam generator. The TRAC calculation does not show this change in slope as dramatically as the data (Fig. 14); however, the agreement is still reasonable. The loop temperatures are shown in Figs. 15 and 16. During this time, the temperatures are essentially following the system pressure.

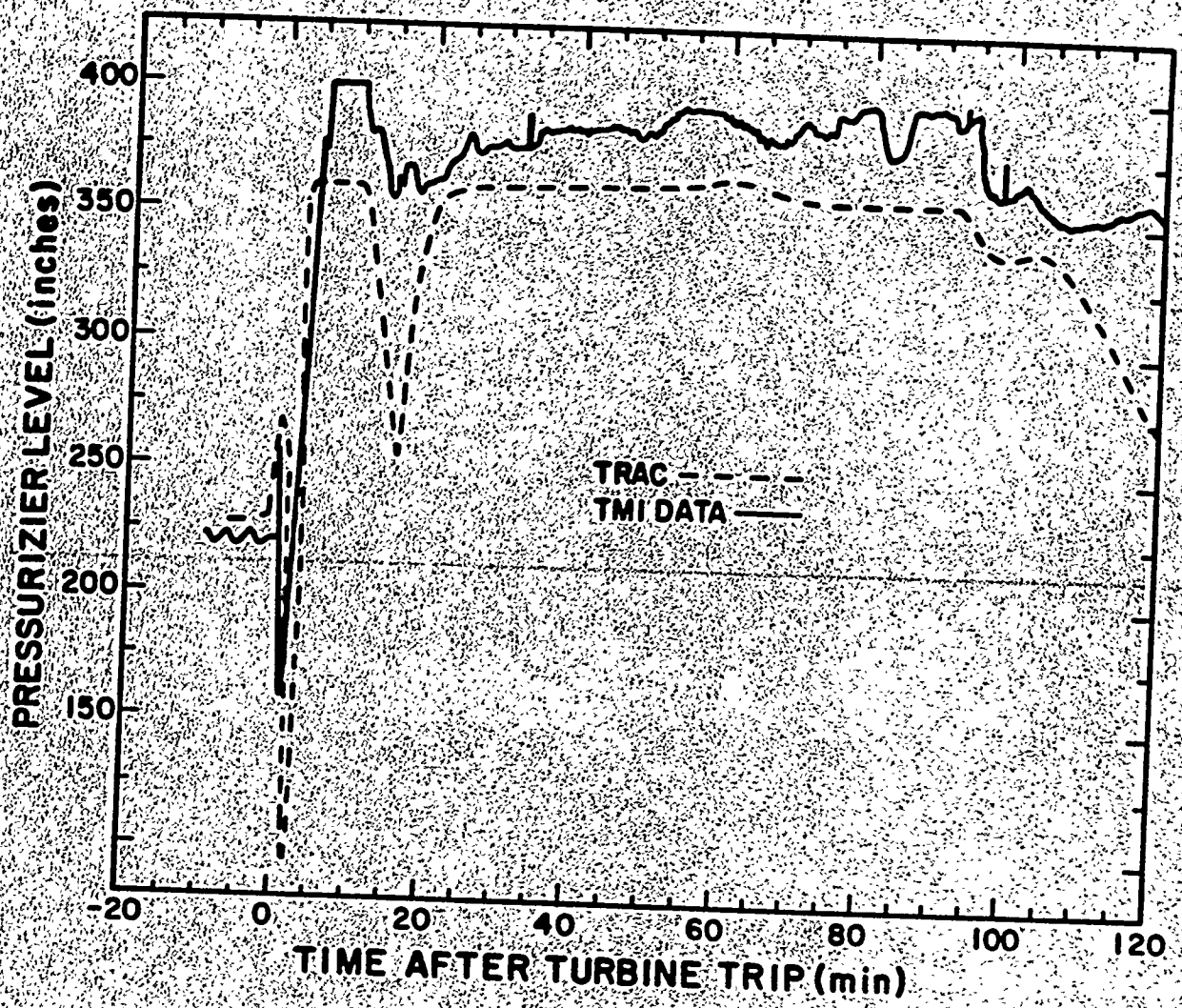

Fig. 19. Pressurizer water level comparisons out to 120 minutes.

When the A loop pumps are tripped at 100 minutes, phase separation occurs throughout the system and the core becomes partially uncovered (top two core levels in the vessel, Fig. 3). This is graphically illustrated in Fig. 20 which shows the void fraction profile in the vessel (note that the vessel noding was refined at 80 minutes to more accurately track the water level in the core, Fig. 3). When the core uncovers, the fuel rod temperatures (hot rod) increase to about 700 K (Fig. 21). This temperature rise was terminated due to core rewetting caused by some of the water in the loops emptying out into the vessel. As in the case when the B loop pumps were tripped, phase separation in the loops results in an elevation head in the steam generators which is large enough to force some water into the vessel. This additional water in the core begins to boil off as the system depressurizes and the core again begins to uncover at about 120 minutes. From this point on, the fuel rods continue to increase in temperature.

The beginning of core uncovering at 100 minutes, as calculated by TRAC, is in agreement with the data analyzed by EPRI.[4] For example, in comparing the mass inventory in the primary system from the TRAC calculation to that reported by EPRI, it is seen that after 100 minutes TRAC calculates the total system mass loss to be 1.275×10^5 kg, while EPRI gives a range of 1.05×10^5 kg (minimum) to 1.235×10^5 kg (maximum). TRAC is calculating about 3% higher mass loss than the EPRI maximum estimate.

It is important to note that in order for TRAC to calculate the depressurization from 100 minutes to 138 minutes, a large letdown flow had to be used (15.0 kg/s). This is because the EMOV flow severely degrades (Fig. 22) after the A loop pumps trip and the water level drops in the pressurizer (Fig. 19). The EMOV flow drops from 20 kg/s to an average of about 6 kg/s over this period. Another variable that is important during this period is the HPI flow rate. Several sequence of events reports state that HPI flow was increased after 100 minutes, but no values are given. If it was increased, condensation would also cause the system to depressurize. However, since no value was given, the best estimate value of 2.2 kg/s was used. The letdown flow used during this period accounts for the flow rate drop in the EMOV and the increased HPI flow.

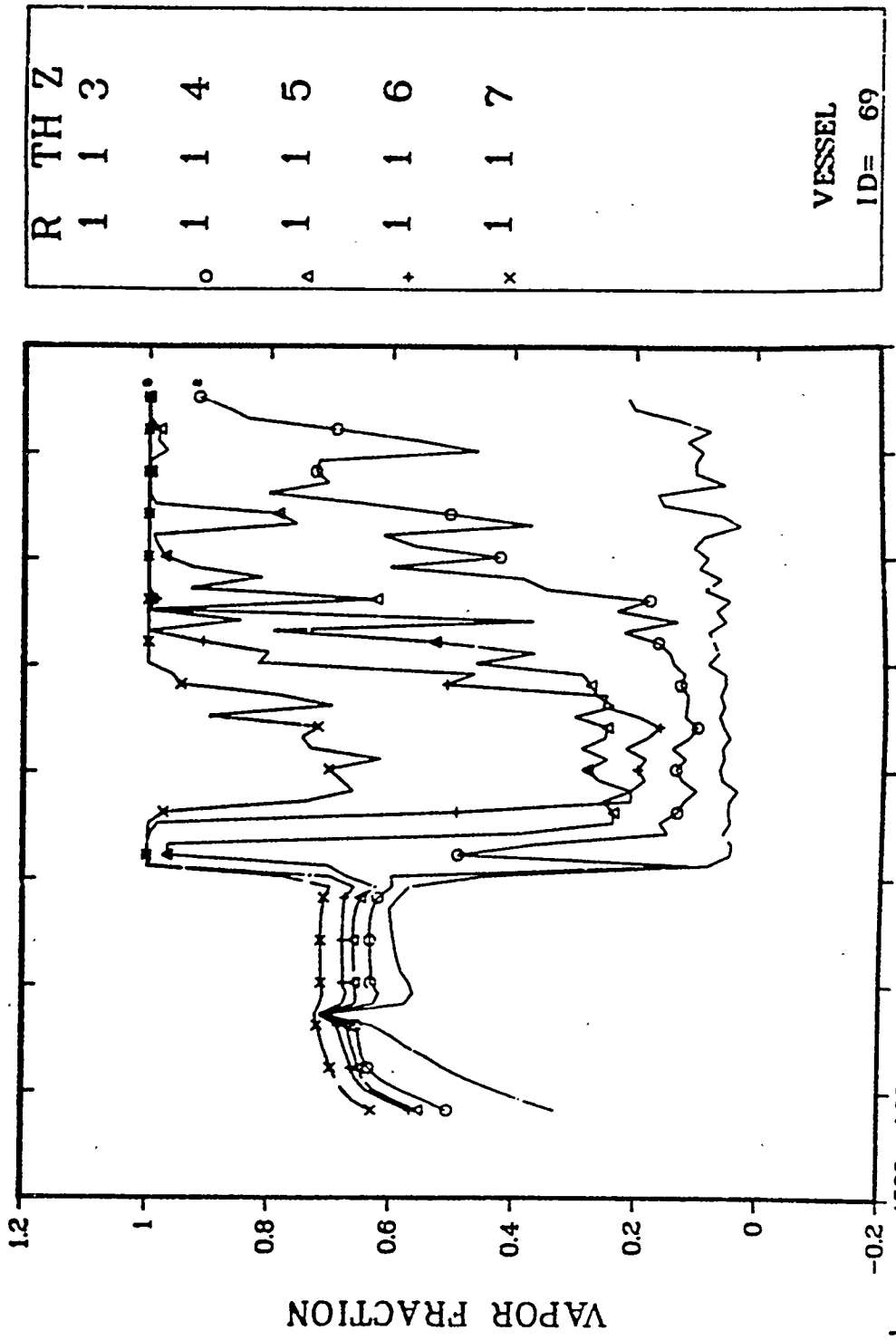

Fig. 20. Core void fraction axial profile after 81 minutes.

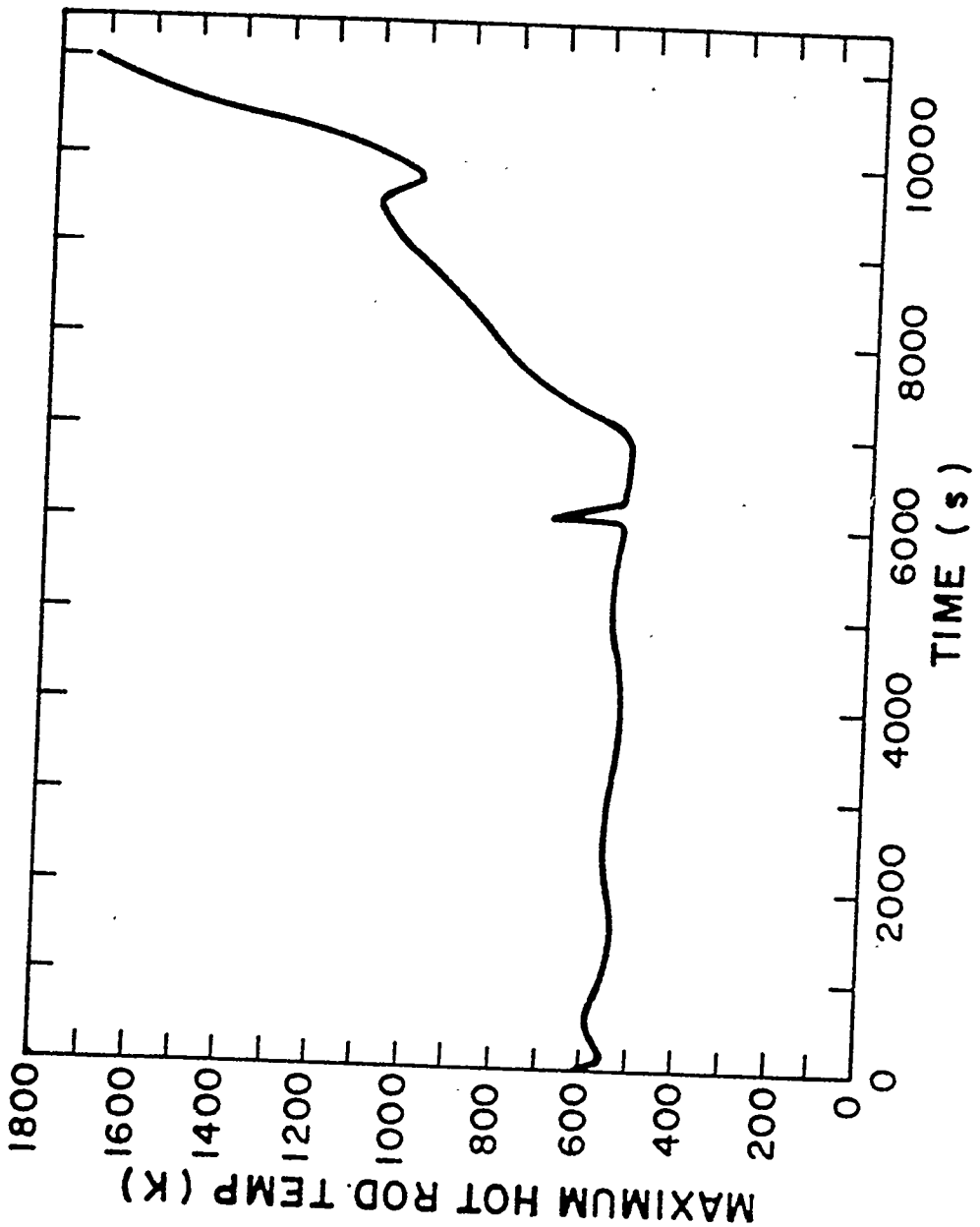

Fig. 21. Maximum hot-rod cladding temperature.

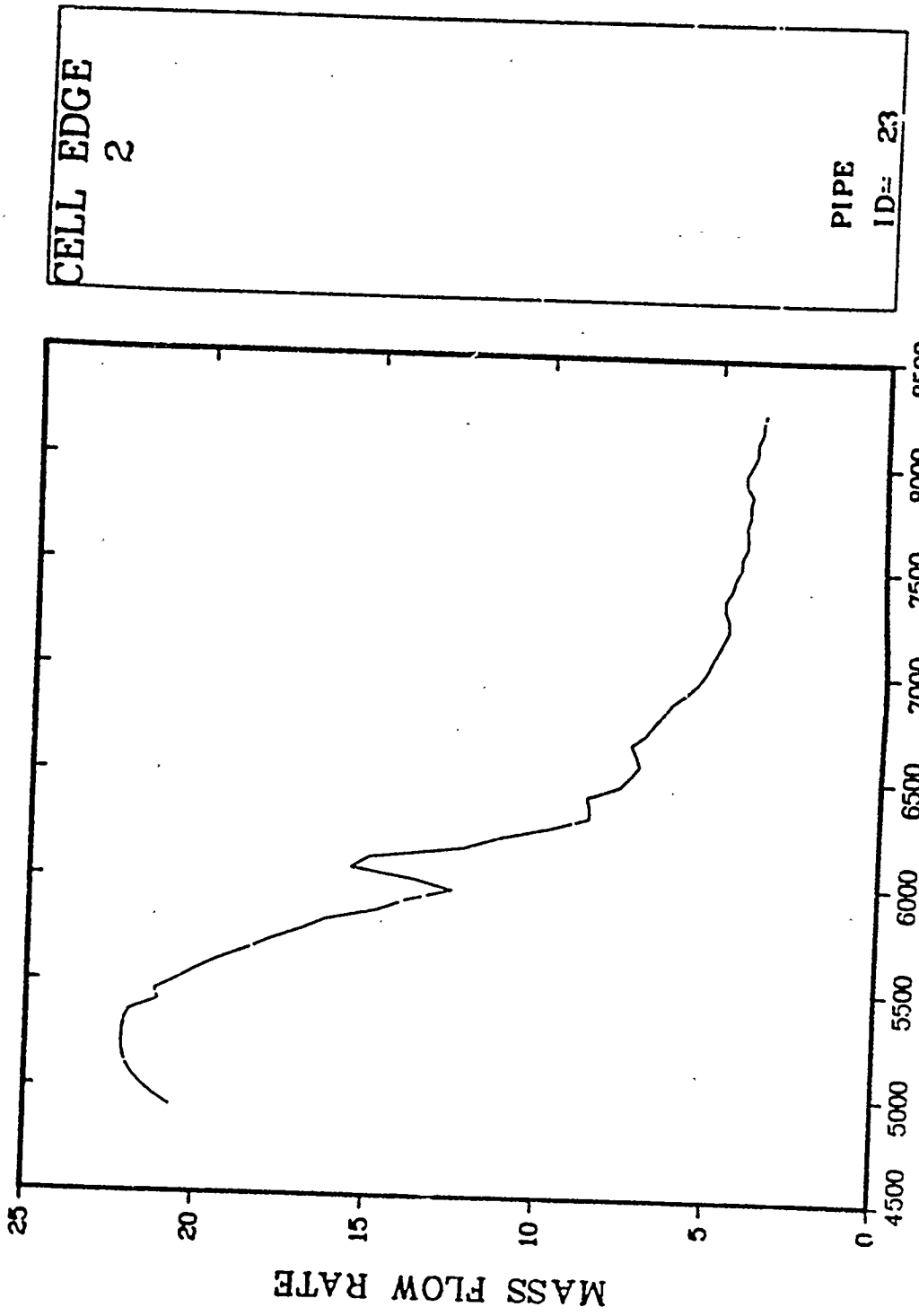

Fig. 22. Pressurizer relief valve flow rate after 81 minutes.

From about 120 minutes to 138 minutes the water level in the core is dropping and the rods are heating up at roughly 1 K every 4 s. The vapor velocities are on the order of 0.5 m/s and the EMOV and letdown flow rates enhance the flow rate through the core. This causes the heat transfer coefficients to be higher than those calculated by natural convection. The loops are essentially void after 138 minutes, water remaining only in the pump suction legs. (Refer to Appendix B for additional plots during this period.) The pressurizer level drops, due mainly to liquid flashing caused by depressurization and increased letdown.

At 138 minutes, the block valve was shut on the pressurizer. In the TRAC calculation, it was also assumed that after 138 minutes the makeup and letdown flows are equal. When the block valve is shut, the steam flow in the core stagnates, since there is no path for the vapor to escape. Also, the water in the pump suction legs (loop seals) prevents any flow through the loops, hence, there is no natural circulation through the system. The system begins to pressurize and continues to pressurize for the remainder of the calculation. Figure 23 shows the TRAC calculated pressure history compared to the TMI data. Also shown is the pressurizer water level history. During this period the vapor velocities through the core are generally less than 0.1 m/s and the heat transfer coefficients are very low (on the order of 50 W/m^2s K, representative of natural convection to superheated steam). The vapor begins to superheat since the flow is stagnant and the rod temperatures continue to increase (Fig. 21). Figure 24 shows the vapor temperature in the core during this period for each axial level in the vessel. The corresponding core void fraction profile is shown in Fig. 25.

As soon as the EMOV is shut, a pressure oscillation moves through the system which causes some of the water in the lower plenum to be forced up into the core. This is the reason core level 4 has a decrease in void fraction for several hundred seconds. Eventually, this core level dries out at about 160 minutes. Before this core region dries out it begins to boil the water rapidly and the boiling causes the vapor velocities through the core to increase for a short period of time. The increased vapor velocities cause the heat transfer coefficients to increase and the vapor temperatures to drop, with a resulting drop in rod temperatures (see Figs.

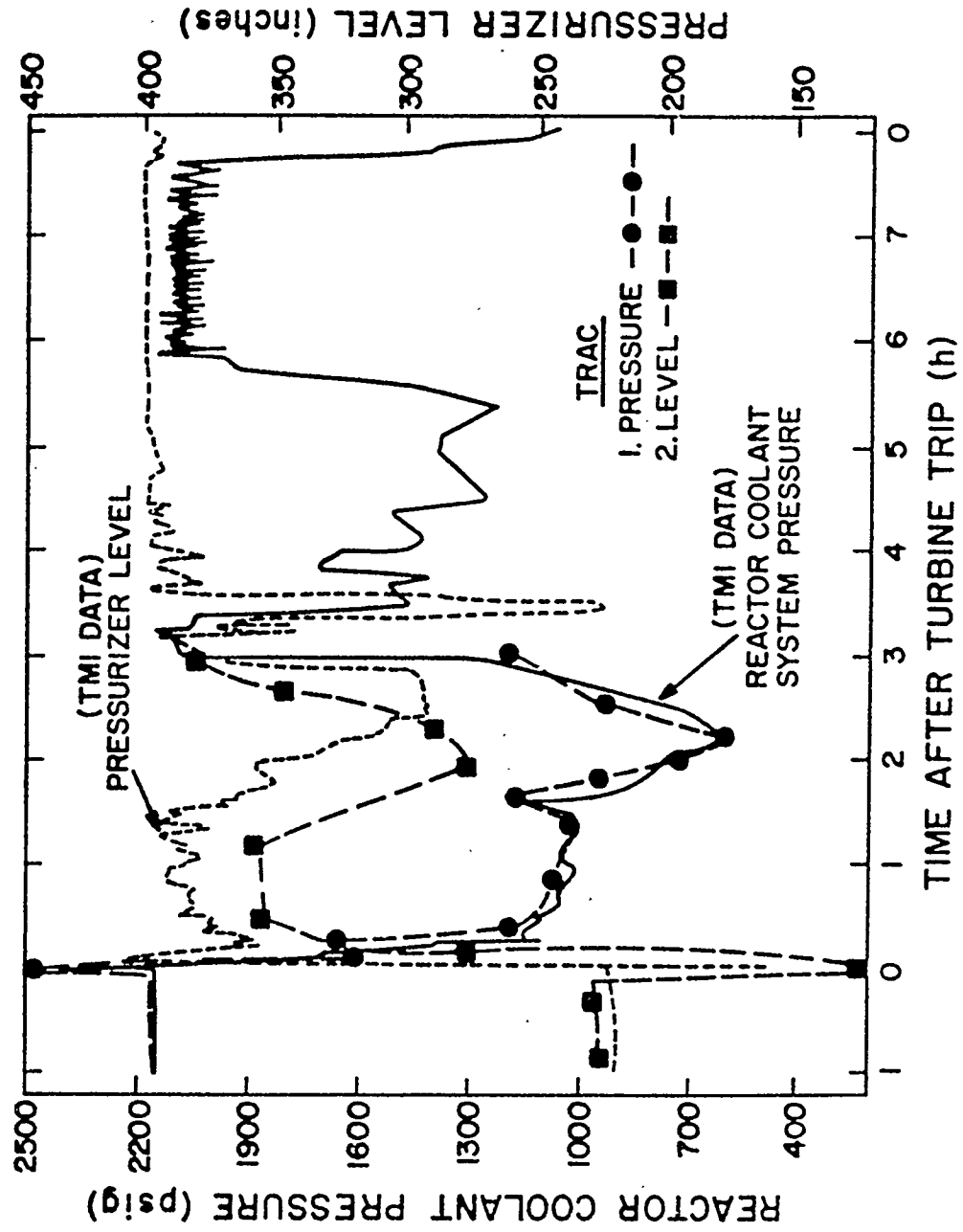

Fig. 23. TRAC comparisons with TMI data out to 3 hours,

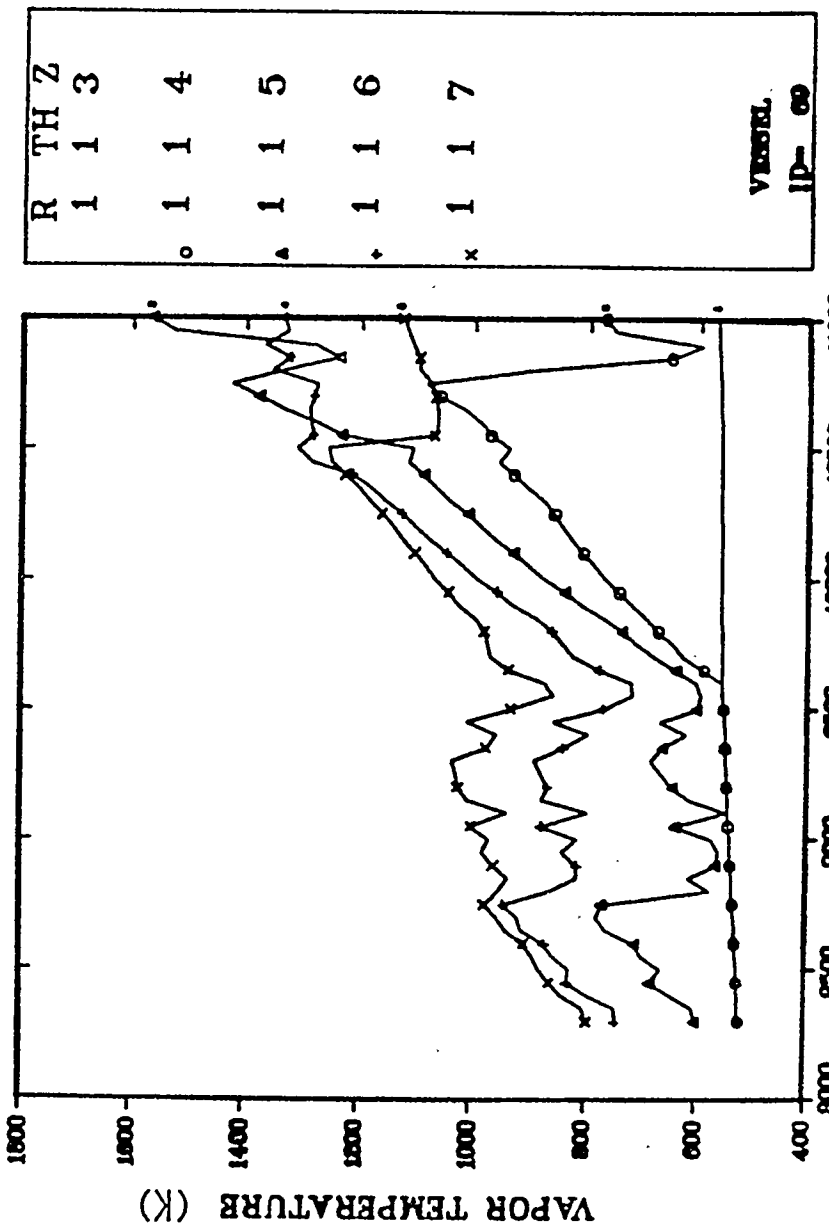

Fig. 24. Core vapor temperature axial profile.

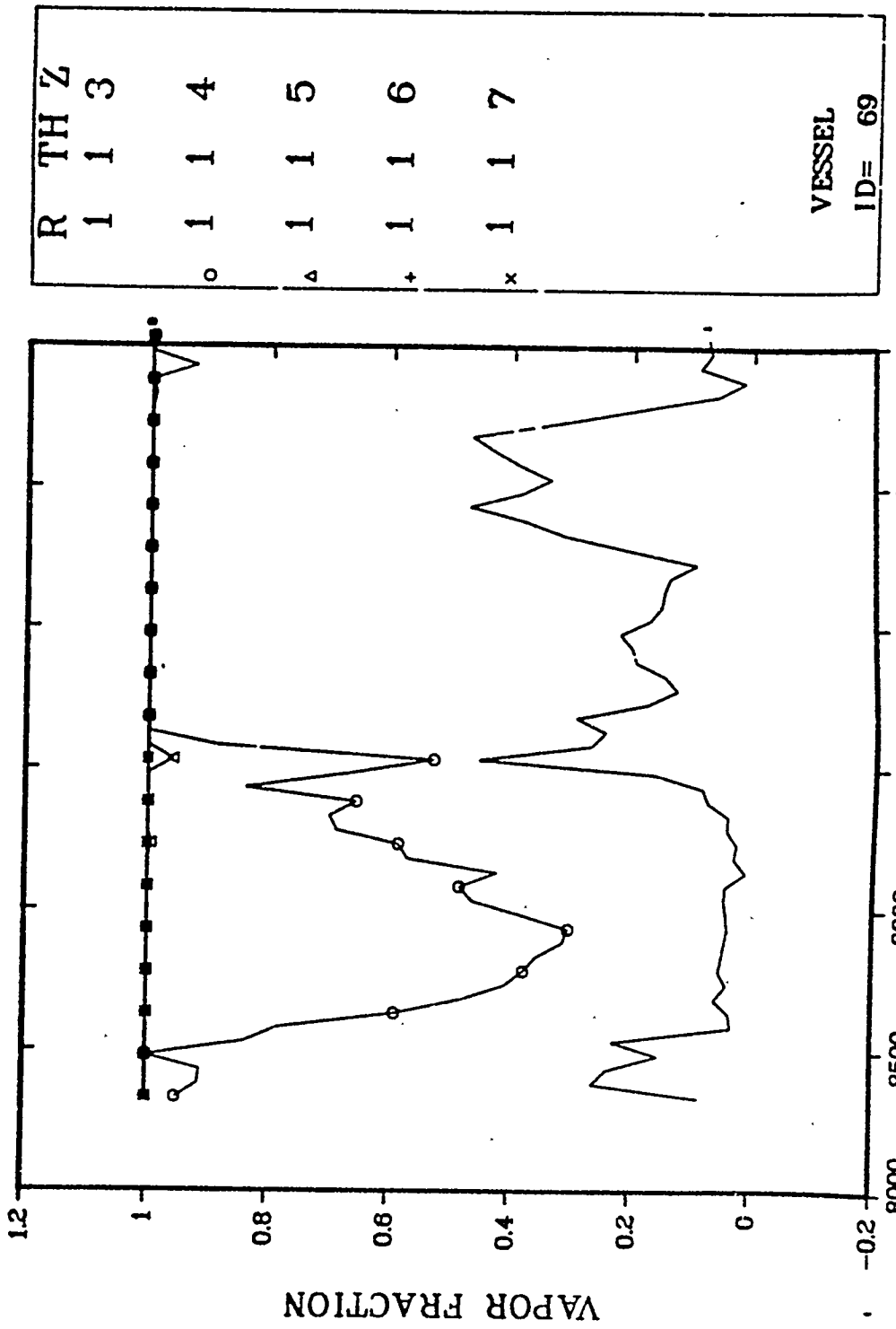

Fig. 25. Core void fraction axial profile after 81 minutes.

21 and 24 at 9600 s). But, as soon as this core level dries out the vapor velocities decrease, the vapor begins to superheat, and the rods again heat up. The rods continue to heat up at roughly the same rate as before (1 K every 4 s) until the zirconium-steam reaction begins to provide a significant additional heat source (at 1273 K). After this time the temperature rise rate increases to about 1 K per s. The calculation was stopped once the temperatures exceeded 1650 K.

During this period, the lower plenum in the vessel remains full of water and the bottom core level has roughly 70% water remaining in it. Only the top 75% of the core is uncovered. The fuel rod temperatures remain relatively cool in the lower core region (see Appendix B for additional plots during this period). Also, referring back to Fig. 23, the pressurizer level is increasing both in the TRAC calculation and the TMI data during this time. The pressurizer never empties because steam produced in the core "holds up" the water in the pressurizer.

Overall, for the sequence of events and assumptions used, the TRAC results are in good agreement with the TMI-2 data and they satisfy the objectives listed at the beginning of this section.

3.0 TRAC PARAMETRIC CALCULATIONS

This section summarizes the results of five TMI-2 parametric calculations performed with TRAC. The first three parametric cases (see Table VI) involve variations in the time of initiation of the auxiliary feedwater and also variations in the HPI flows. The auxiliary feedwater is delayed 60 minutes following accident initiation in cases A-3 and A-6.* Case A-3 uses full HPI when the pressure is less than 110×10^5 Pa (1600 psia) and case A-6 assumes "degraded" HPI flows (degraded means as it happened during the TMI-2 accident). Case A-4 assumes that the auxiliary feedwater is turned on at the time of accident initiation and also assumes degraded HPI flows. The fourth parametric calculation assumes that all main coolant pumps trip simultaneously with the reactor trip at 10 s. The last case investigates the effect of a small break in a primary coolant cold leg. All other boundary and initial conditions for these calculations are the same as in the base case described in the previous section. The pressure on the secondary side of the once-through steam generators (OTSG) used for these cases was assumed to be the same as that used for the base case. Since the steam generator secondary side tends to dry out in the calculations to be described, there is only a weak dependence on OTSG secondary side pressure. The TRAC system noding was also the same as used in the base case (Figs. 1-4).

3.1 Delayed Auxiliary Feedwater/Full HPI (Case A-3)

Figure 26 shows the calculated pressure in a TRAC cell located in the upper plenum for the first 5000 s of the transient in case A-3. Also shown

---

*These specific cases were requested by the NRC/TMI Special Inquiry Group and the case number designations are that groups. (The base case was designated A-5.) Other cases are being provided by the Idaho National Engineering Laboratory.

TABLE VI

TRAC PARAMETRIC CALCULATIONS

Run Conditions	Comments	Case Designation*
1. Auxiliary feedwater delayed until 60 minutes following accident initiation. Full HPI on when P < 1600 psia.		A-3
2. Auxiliary feedwater delayed until 60 minutes following accident initiation. Degraded HPI.	"Degraded" HPI means as occurred during TMI-2 accident.	A-6
3. Auxiliary feedwater turned on at accident initiation. Degraded HPI.		A-4
4. All main coolant pumps tripped at accident initiation. Degraded HPI.		D-2
5. Cold-leg break with area equivalant to EMOV. Degraded HPI.		---

*Case nomenclature adopted by NRC/TMI Special Inquiry Group.[5] Base case was designated A-5.

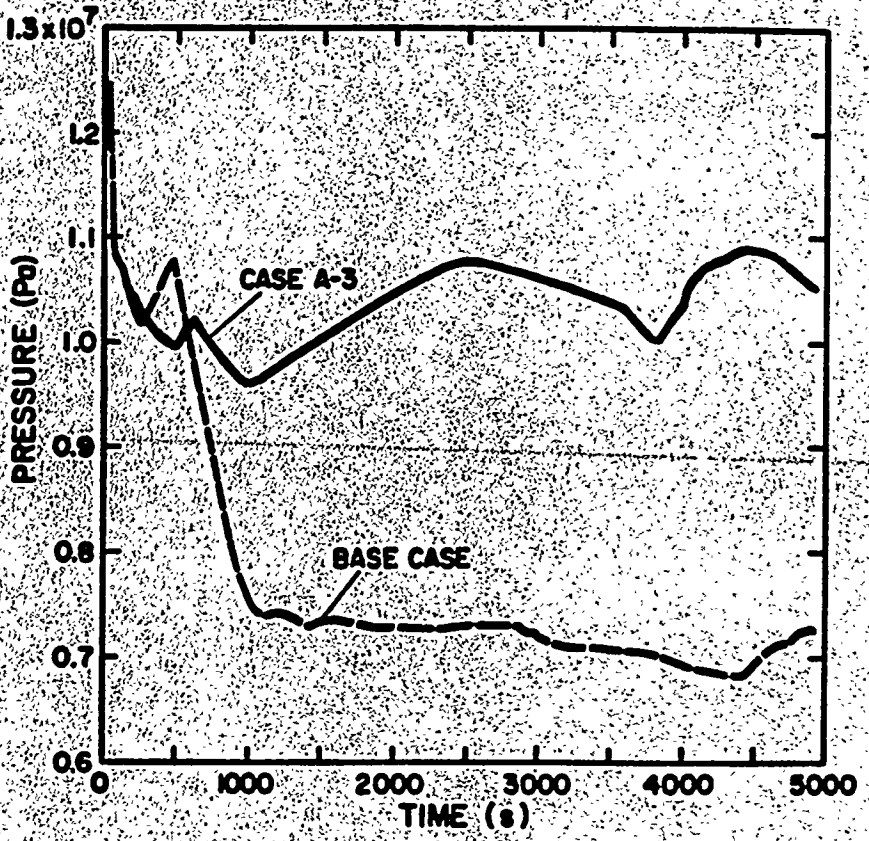

Fig. 26. Parametric case A-3 pressure comparison with base case.

is the base case pressure for the same cell (other pressures in the vessel are similar). As mentioned previously, case A-3 assumes full HPI flows at a setpoint of approximately 110×10^5 Pa (1600 psia) and a delay in auxiliary feedwater of 60 minutes. As can be seen from Fig. 26, the initial pressure for case A-3 matches that of the base case until the HPI setpoint is reached. Beyond this point, the HPI is sufficient to keep the pressure in case A-3 at a quasi steady-state level much higher than the pressure of the base case. Figures 27 and 28 show an HPI mass flow rate (there are two HPI systems with equal flow rates) and the mass flow rate out of the break for case A-3, respectively. Due to a lack of detailed information, the HPI flows are modeled as constant velocity fills after the setpoint is reached. Thus, both HPI flows remain constant at approximately 32 kg/s. The total HPI flows exceed the flow out of the break for the first 3000-4000 s of the transient. From this point on the total HPI flow rate is approximately equal to the break mass flow rate. Thus, the system is essentially running in a steady-state forced convection mode throughout the transient (assuming the main coolant pumps remain on) and there are no voids formed in the vessel at all for case A-3. Figure 29 shows midplane hot-rod temperatures for case A-3 and the base case. Since no voids form in the core for case A-3 the rod temperatures are well below those of the base case. This calculation was run further out in time than shown in the graphs and the rod temperatures for case A-3 remained low. The delay in auxiliary feedwater injection of 60 minutes had no effect on the long-term results of this transient. Thus, for this particular case the importance of full HPI flows far outshadows any delay in the auxiliary feedwater and makes the consequences of this transient mild compared to the base case.

3.2 Delayed Auxiliary Feedwater/Degraded HPI (Case A-6)

Case A-6 is similar to case A-3 except that degraded HPI flows are used rather than full HPI flows. Figure 30 shows the time history of the pressure for case A-6 and the base case for the first 5000 s of the transient. Since the auxiliary feedwater is delayed 60 minutes in case A-6, the pressure in

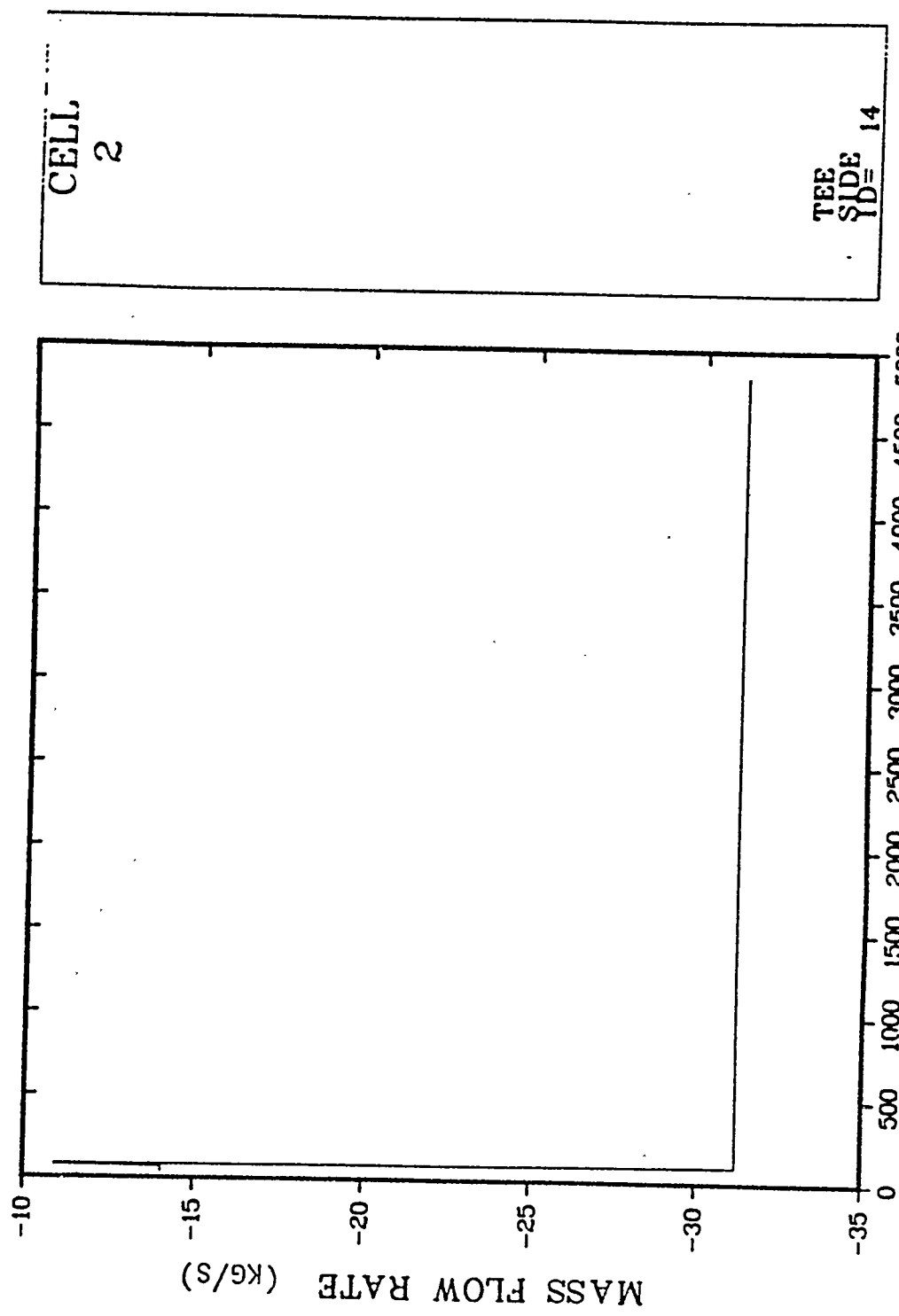

Fig. 27. Case A-3 HPI flow rate (minus indicates flow into system).

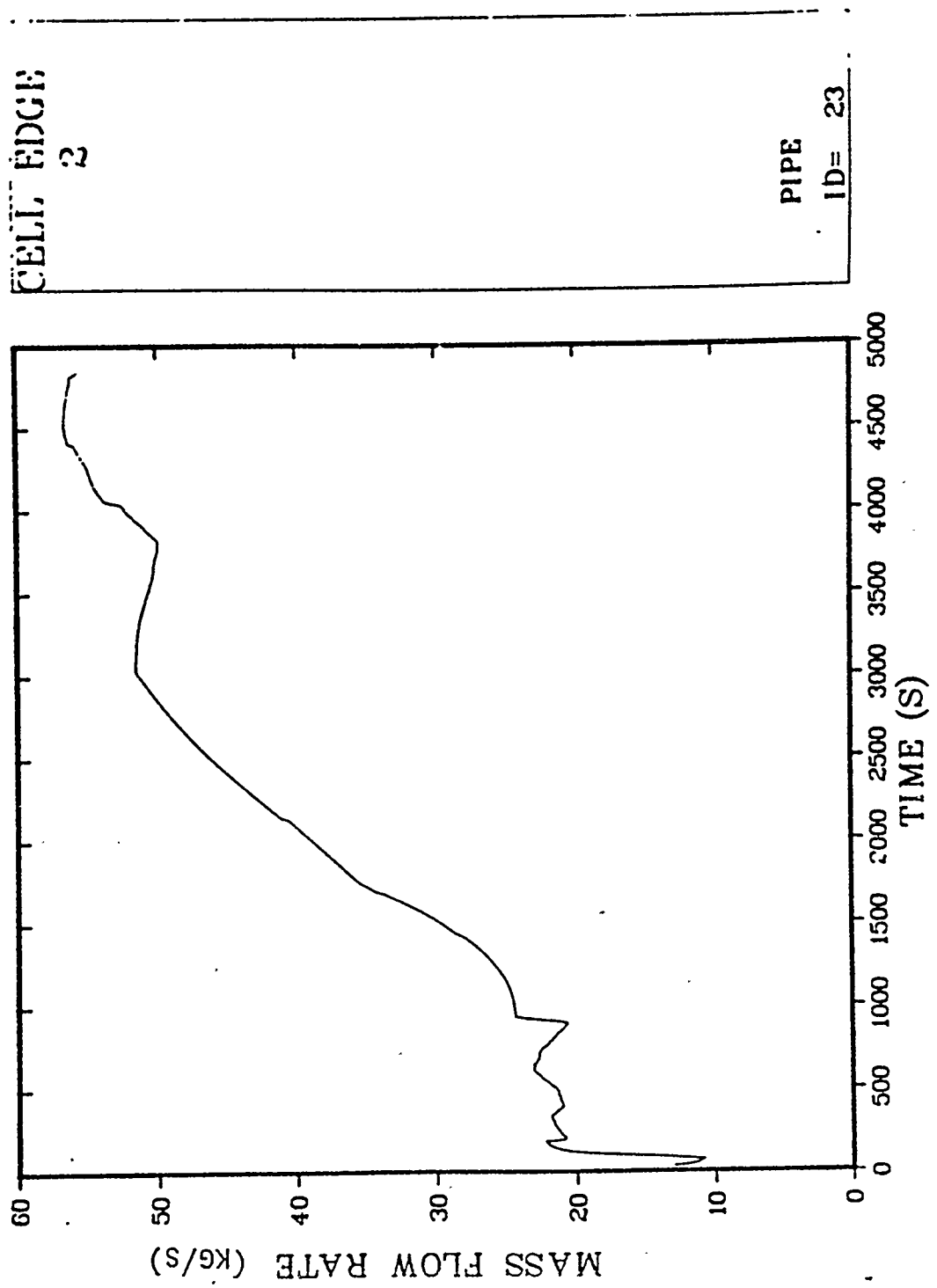

Fig. 28. Case A-3 mass flow out EMOV.

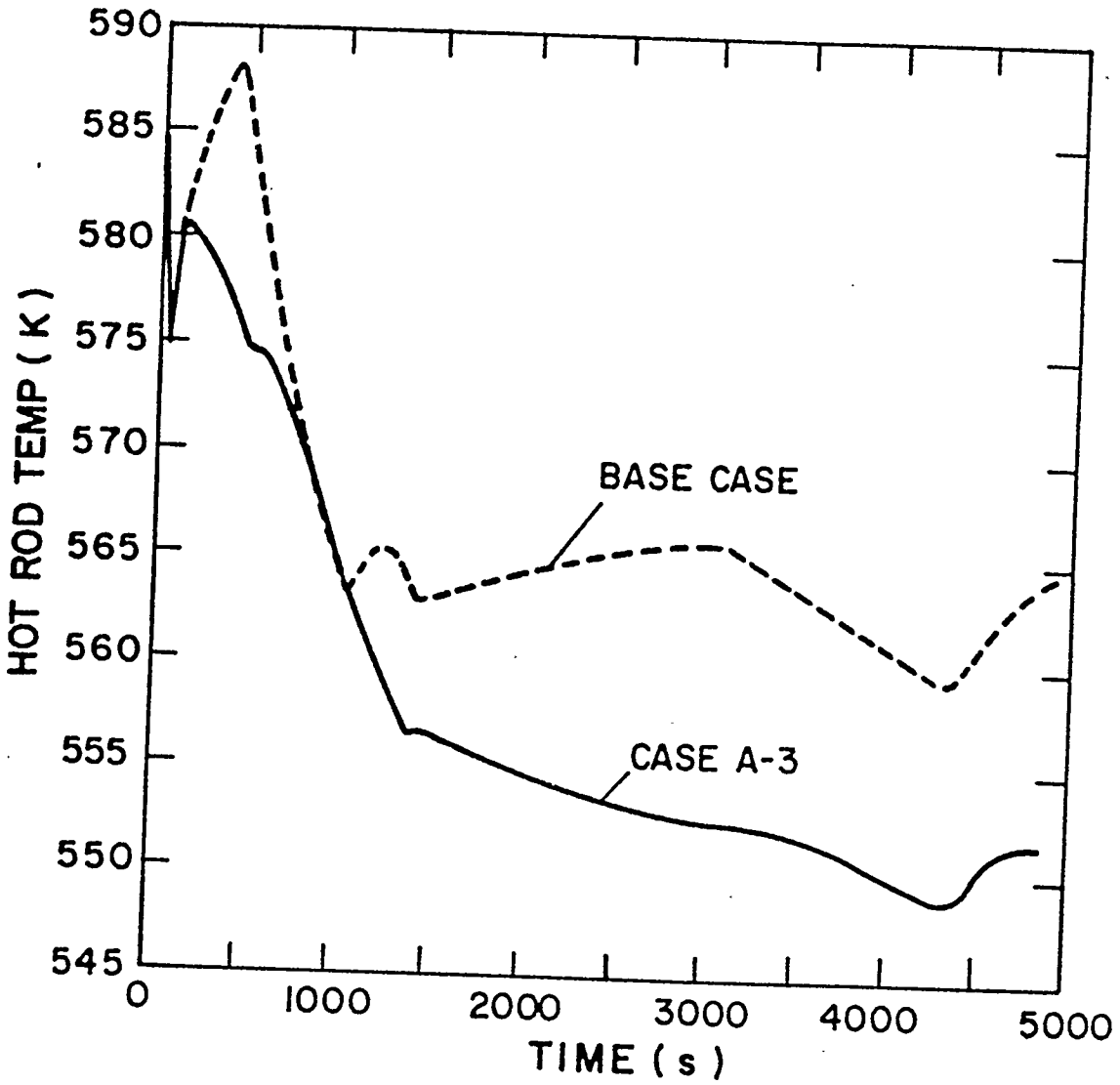

Fig. 29. Case A-3 hot-rod temperature vs base case.

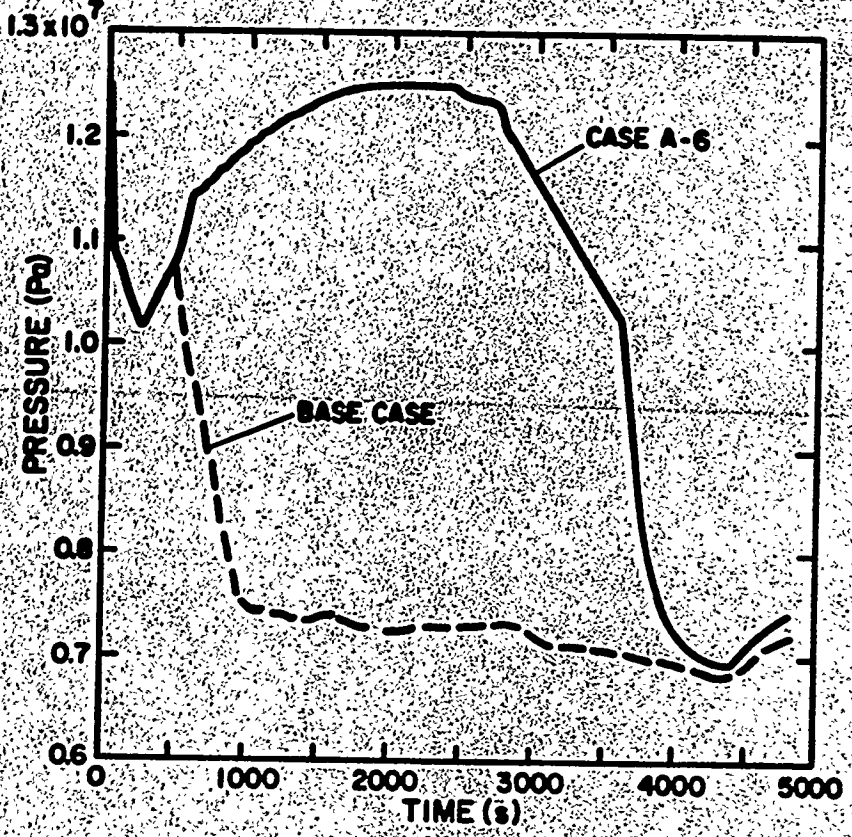

Fig. 30. Case A-6 pressure history vs base case.

this case remains high compared to the base case until the heat sink is restored at 3600 s (the base case auxiliary feedwater comes on at about 500 s). Unlike case A-3, the pressure remains high due to vapor production and a lack of adequate energy removal, since there is very little HPI flow entering the vessel. The upper head in the base case voids more rapidly than case A-6 while the core and upper plenum in case A-6 void more rapidly than the base case, which explains the higher pressures in case A-6. Hot-rod temperature comparisons are shown in Fig. 31 for case A-6 and the base case. The behavior is very similar to that of the pressure. Case A-6 temperatures are 30-40 K higher than the base case until the auxiliary feedwater is initiated at 3600 s, then these temperatures drop because of more efficient energy removal and follow the base case. It appears that a delay in auxiliary feedwater, at least during the initial 5000 s of the accident, does not make an appreciable difference in the long-term response of the system since the behavior of case A-6 matches, very closely, that of the base case after initiation of auxiliary feedwater flows.

3.3 Full Auxiliary Feedwater/Degraded HPI (Case A-4)

Case A-4 differs from the base case and case A-6 since there is no time delay assumed for the initiation of auxiliary feedwater. Case A-4 assumes degraded HPI flows. Figure 32 shows a pressure comparison of case A-4 and the base case for the first 3500 s of the transient. Since the base case assumes a delay of about 500 s for auxiliary feedwater, the pressure decay for the base case is not as rapid as that of case A-4. However, after about 1000 s, the pressures for the two cases are almost identical. The hot-rod temperatures follow this same trend as shown in Fig. 33, where the base case temperatures remain higher than those for case A-4 until 500 s, at which time the base case temperatures drop to about the same level as those for case A-4. It is obvious from the results of case A-4 that, again, auxiliary feedwater delay makes little difference on the long-term behavior of the transient.

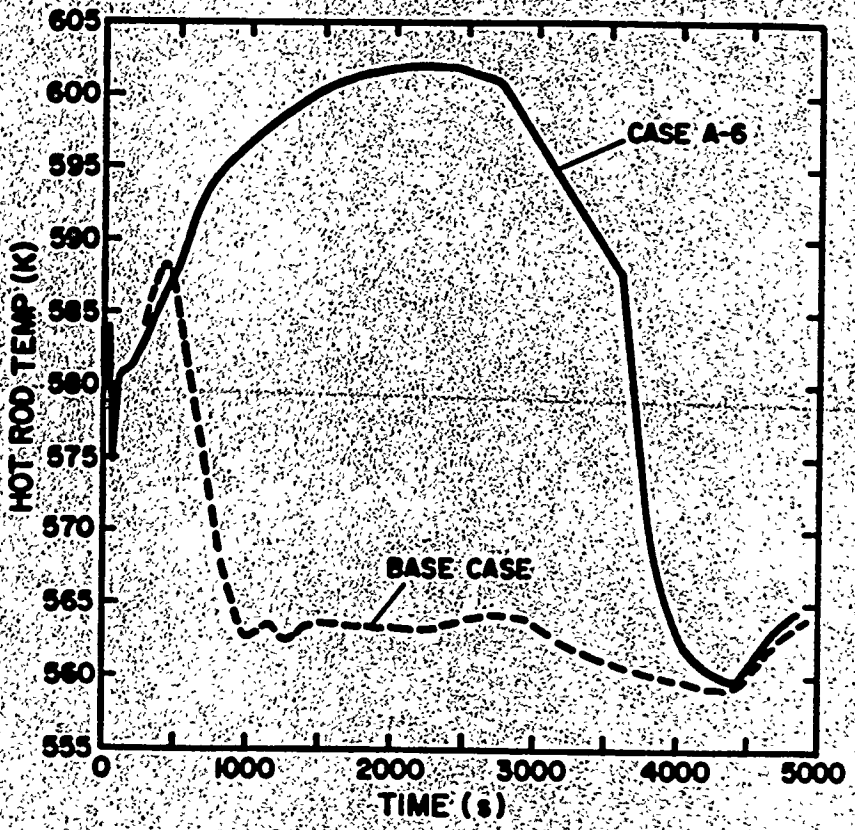

Fig. 31. Case A-6 hot-rod temperature vs base case.

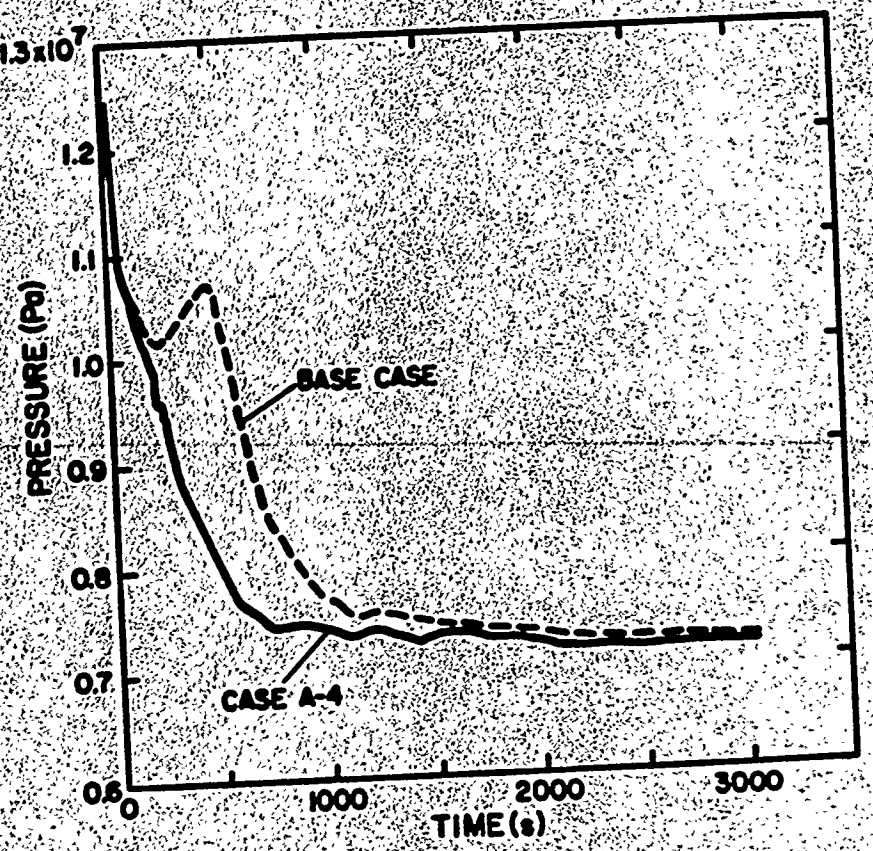

Fig. 32. Case A-4 pressure history vs base case.

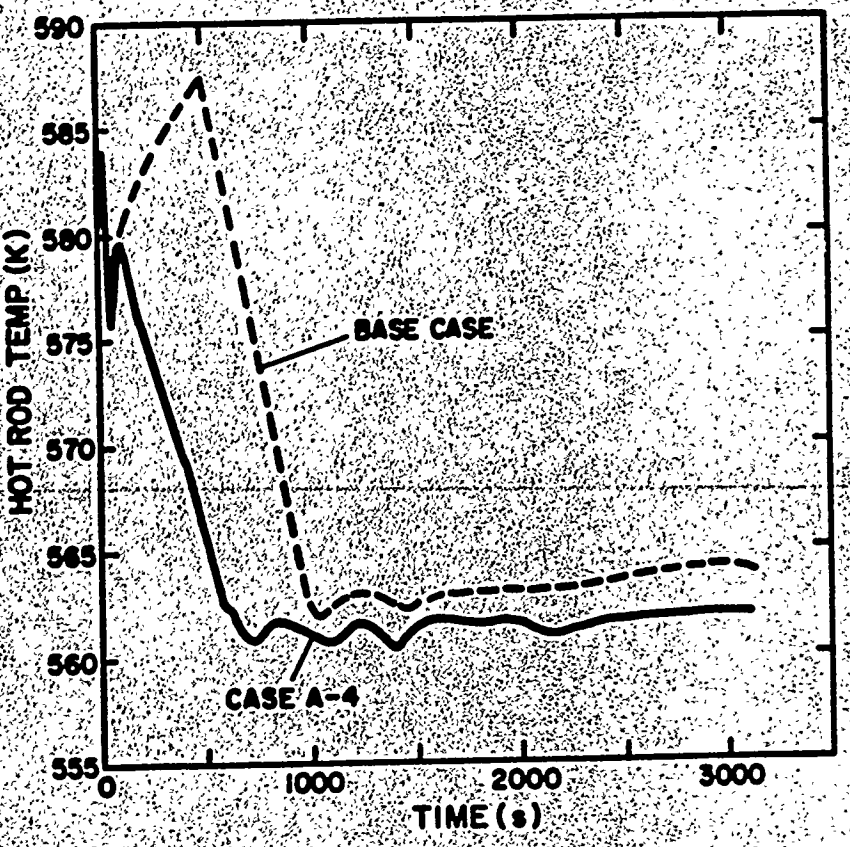

Fig. 33. Case A-4 hot-rod temperature vs base case.

3.4 Main Coolant Pumps Tripped (Case D-2)

This parametric calculation is designated case D-2 and assumes that all main coolant pumps trip at the time of reactor trip ($t \cong 10$ s). The calculation was not run far enough to be compared in detail with the base case. The discussion to follow will be based on comparisons of calculations of the first 4000 s of the transient and somewhat speculative extrapolations beyond that time. Figure 34 shows a plot of the upper plenum pressures for the base case and case D-2 for the first 4000 s of the transient. Initially, the pressure decays monotonically for the first 600 s to a level slightly higher than the base case. At about 2500 s the pressure rises back up to a level much higher than the base case. This is mainly due to increased vapor production in the core and upper plenum resulting from phase separation in the vessel. Figure 35 shows void fraction plots for each level in the vessel at the same radial and axial position. It can be seen from this figure that phase separation occurs in case D-2 around 2500 s (the lower levels fill with water and the upper levels void). A similar plot for the base case can be found in Fig. 18. Partial phase separation in the base case occurs at about 4400 s (when the B loop pump is tripped). A more complete phase separation occurs in the base case at about 6000 s when the other pump trips. Therefore, it might be expected that the cladding temperatures in case D-2 would increase rapidly on the order of 1 hour before they do in the base case. One might also expect cladding failure to occur at 1-1/2 to 2 hours into the transient for this case.

3.5 Cold-Leg Break Parametric Case

As a comparison to the base case, a cold-leg break was calculated using TRAC with the same break flow area as the EMOV in the base case. The break was located on the A loop in the pump discharge line (Fig. 1). All other conditions were the same as in the base case with the exception of the HPI on the A loop, which was not modeled.

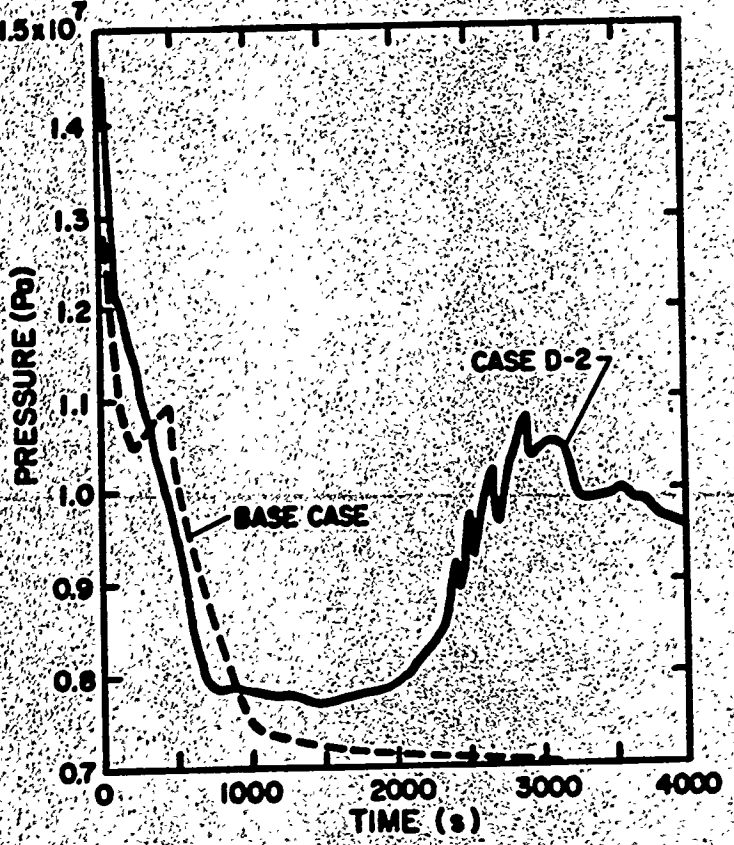

Fig. 34. Case D-2 pressure history vs base case.

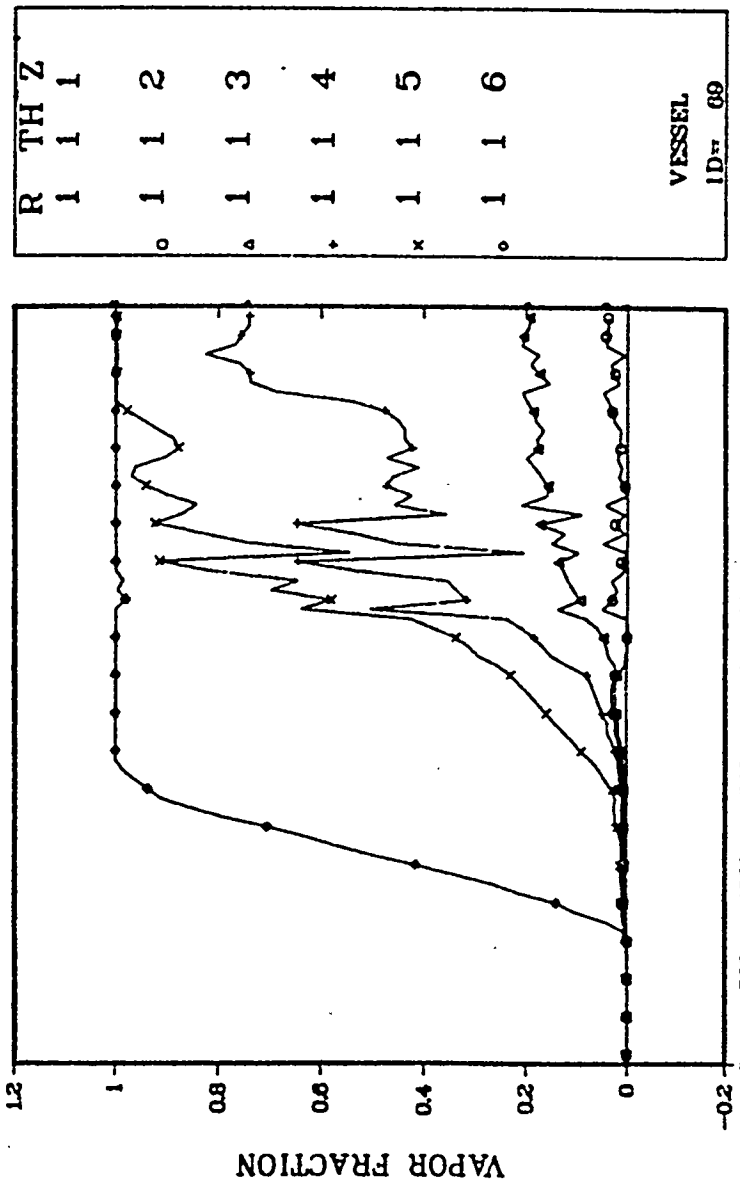

Fig. 35. Case D-2 core void fractions indicating onset of flow separation.

The calculation was carried out to about 20 minutes when the system pressure had stabilized. The pressure after 20 minutes was about 15 bars higher than the base case. Since the break is located on the cold leg, a lower quality two-phase mixture escapes from the system than in the base case; thus the volumetric flow rate is lower and the pressure remains higher. During this time the pressurizer remains almost full of water as in the base case.

Thus, it appears from the calculation that if the break occurred in the cold leg with the same flow area as the EMOV, the system would have depressurized at a slower rate as compared to the base case. Based on these results, after the pumps trip on A loop and phase separation occurs as in the base case, the water in A loop would probably drain out the break rather than empty into the vessel as in the base case. This would result in the core uncovering and remaining uncovered. Some flow would still come into the vessel from B loop as in the base case, but this probably would not be sufficient enough to completely quench the core. The fuel rods would then heat up similar to the base case after 100 minutes. If is possible, however, that in this case the system would depressurize sufficiently (block valve closure prevents this in the base case) such that the core flood tanks would be activated and terminate the heat up.

4.0 CORE THERMAL-MECHANICAL RESPONSE

The severe off-normal conditions that the Zircaloy-clad fuel rods were subjected to during the TMI accident were likely to have caused several potentially important phenomena, including cladding ballooning prior to failure, cladding failure (rupture), cladding swelling and hydrogen evolution caused by zirconium oxidation, and, finally, possible thermal stress-induced cladding fracture and fragmentation during reflood. Each of these five phenomena will be considered in detail based on the TRAC calculations out to 3 hours in the accident. Included below is a section detailing the calculations related to each particular phenomenon. Where possible, the predicted behavior will be compared to the actual behavior as inferred from the data accumulated during the accident. Thus, for example, the predicted fuel rod failure (rupture) time can be compared to the time at which high radiation levels were first observed.

The calculations reported below used the results of the base case TRAC calculation. The information used from TRAC included the system pressure and cladding temperatures as a function of time. For the system pressure, we used the upper plenum pressure shown in Fig. 36. This single pressure can be used to represent the pressure everywhere in the core since the pressure drop across the core is small compared to the average system pressure. The TRAC representation of the core includes 1 radial node, 2 azimuthal sectors, and 5 axial nodes in the core. Thus, we have cladding temperature data for two average rods (the two azimuthal nodes) at 5 axial levels (Figs. 37 and 38). In addition to the average rods, TRAC also calculates temperatures for a hot rod. The hot-rod cladding temperatures (for the two azimuthal nodes) are shown in Figs. 39 and 40. In addition, the vapor fractions at each of the 5 axial levels (representing the water inventory in the core as a function of time) are shown in Fig. 41. This plot is useful in understanding some of the axial variations in the cladding temperature.

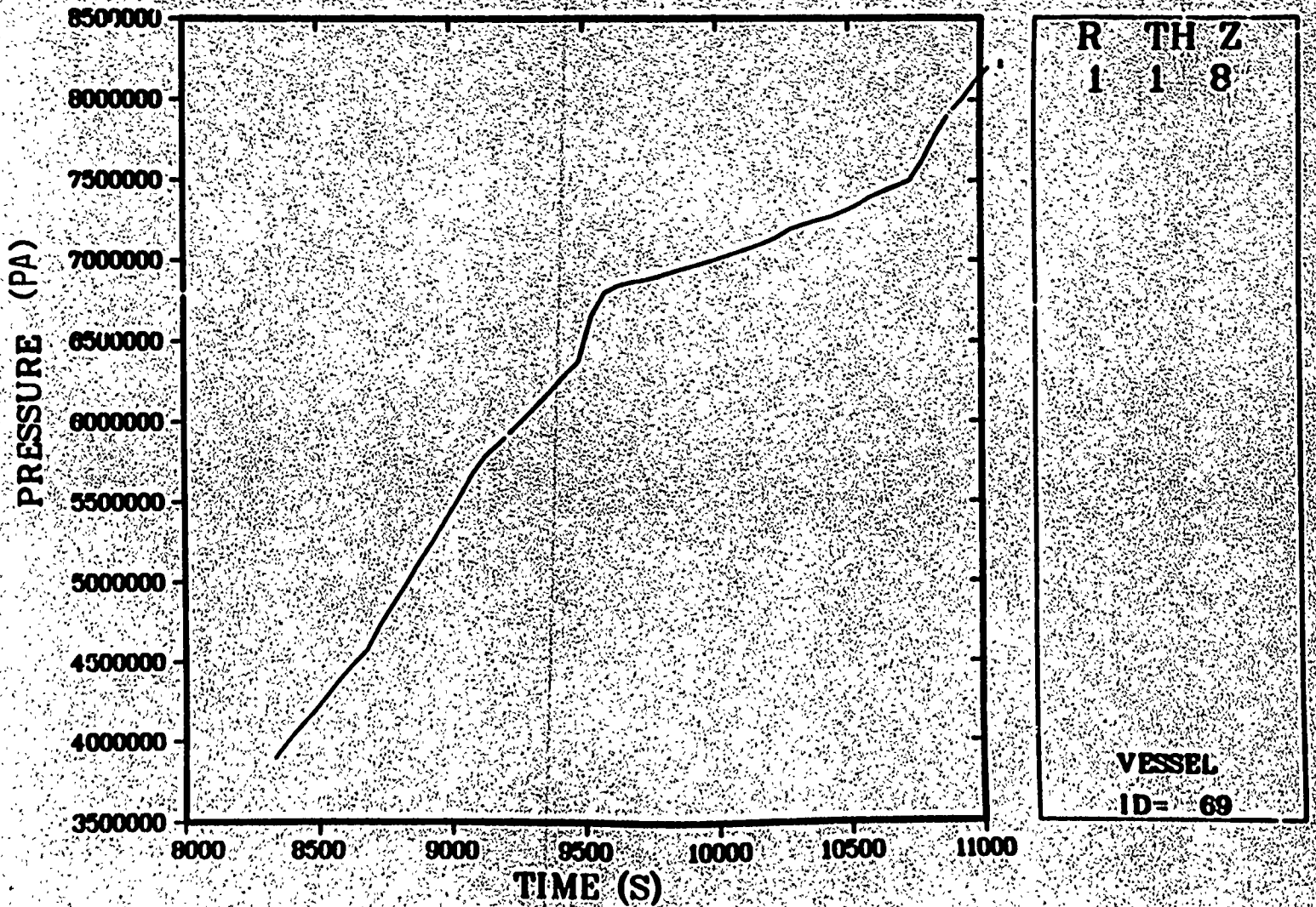

Fig. 36. Upper plenum pressure history.

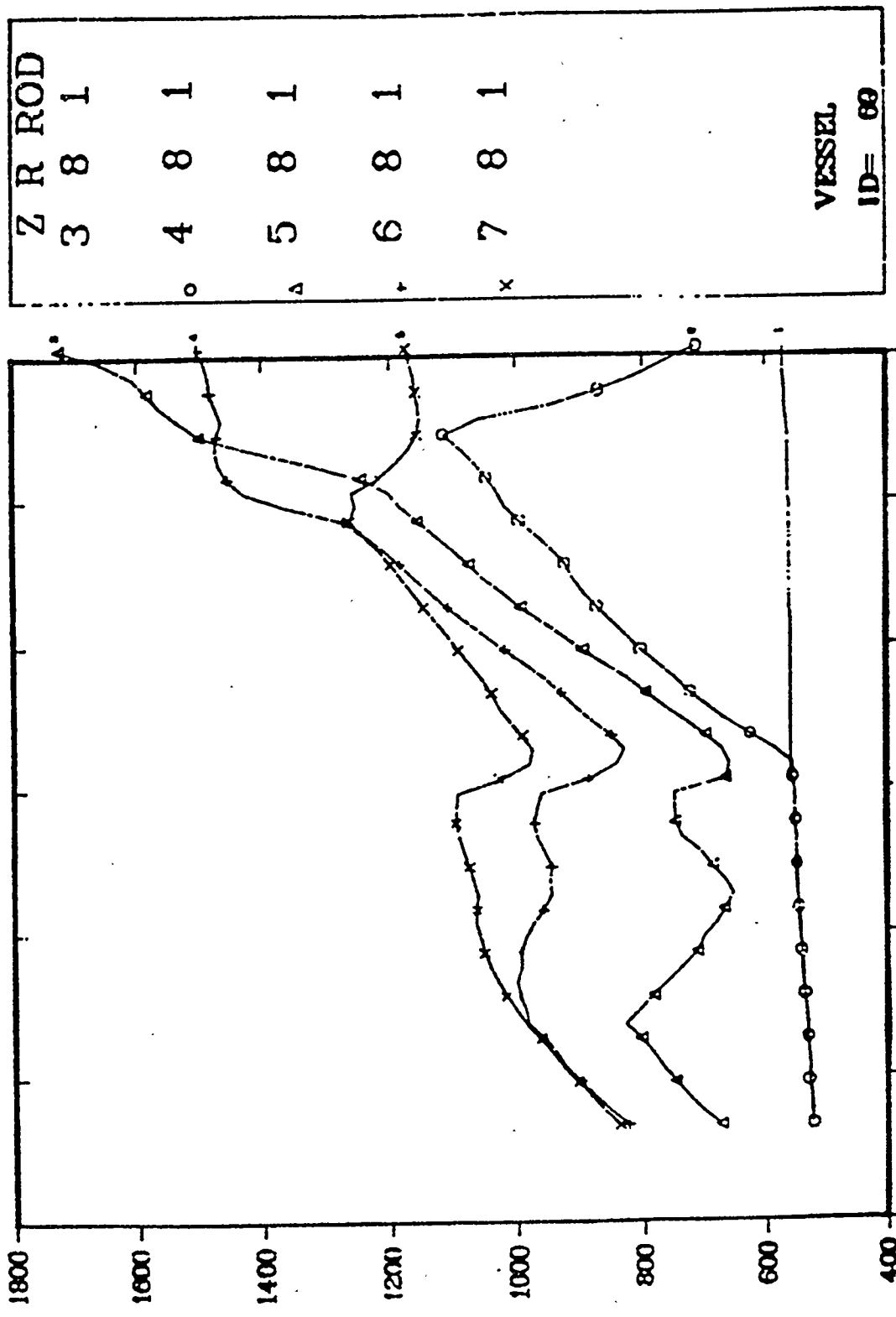

Fig. 37. Axial distribution of average cladding temperatures (azimuthal zone one).

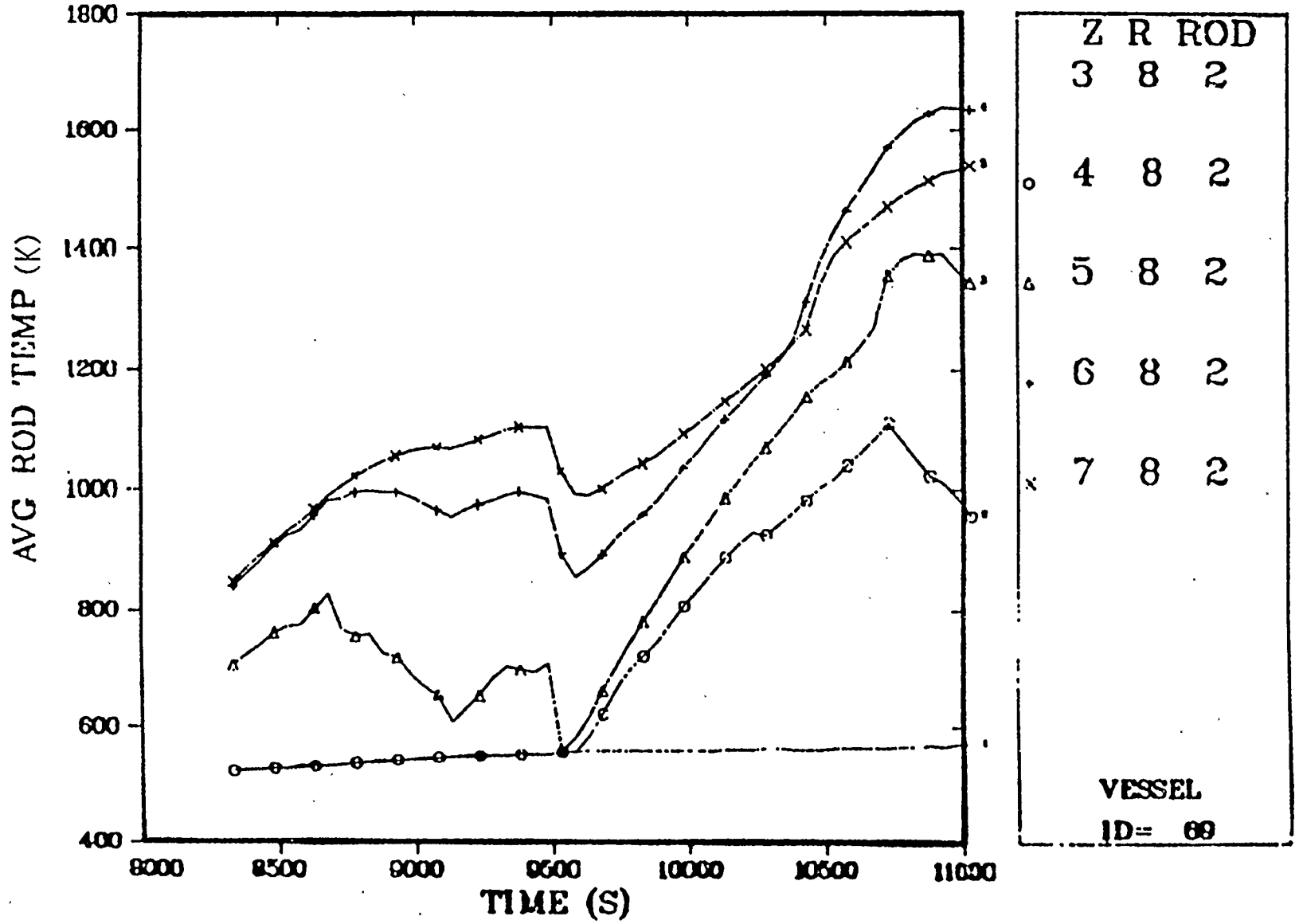

Fig. 38. Axial distribution of average cladding temperatures (azimuthal zone two).

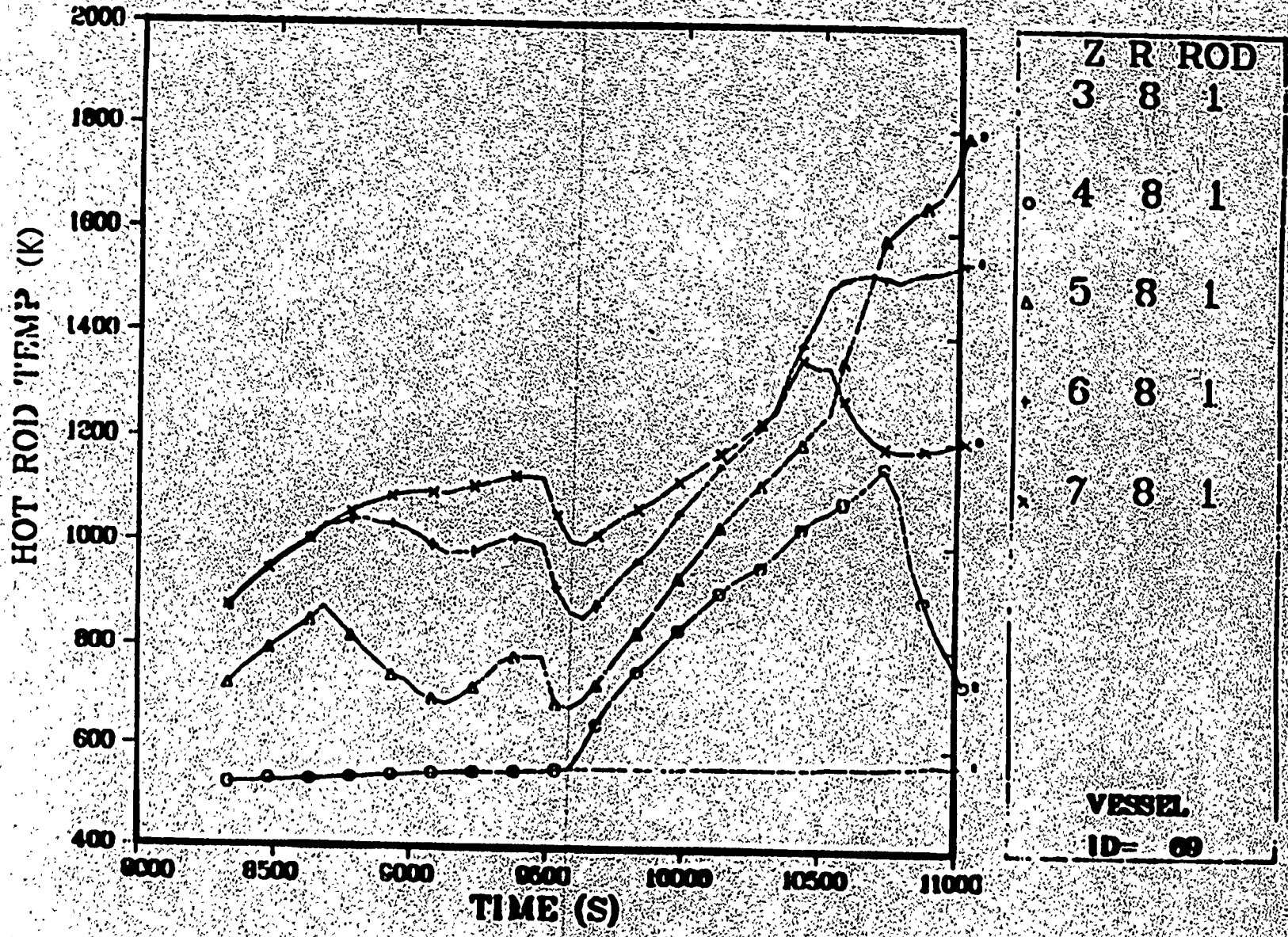

Fig. 39. Axial distribution of hot-rod cladding temperatures (azimuthal zone one).

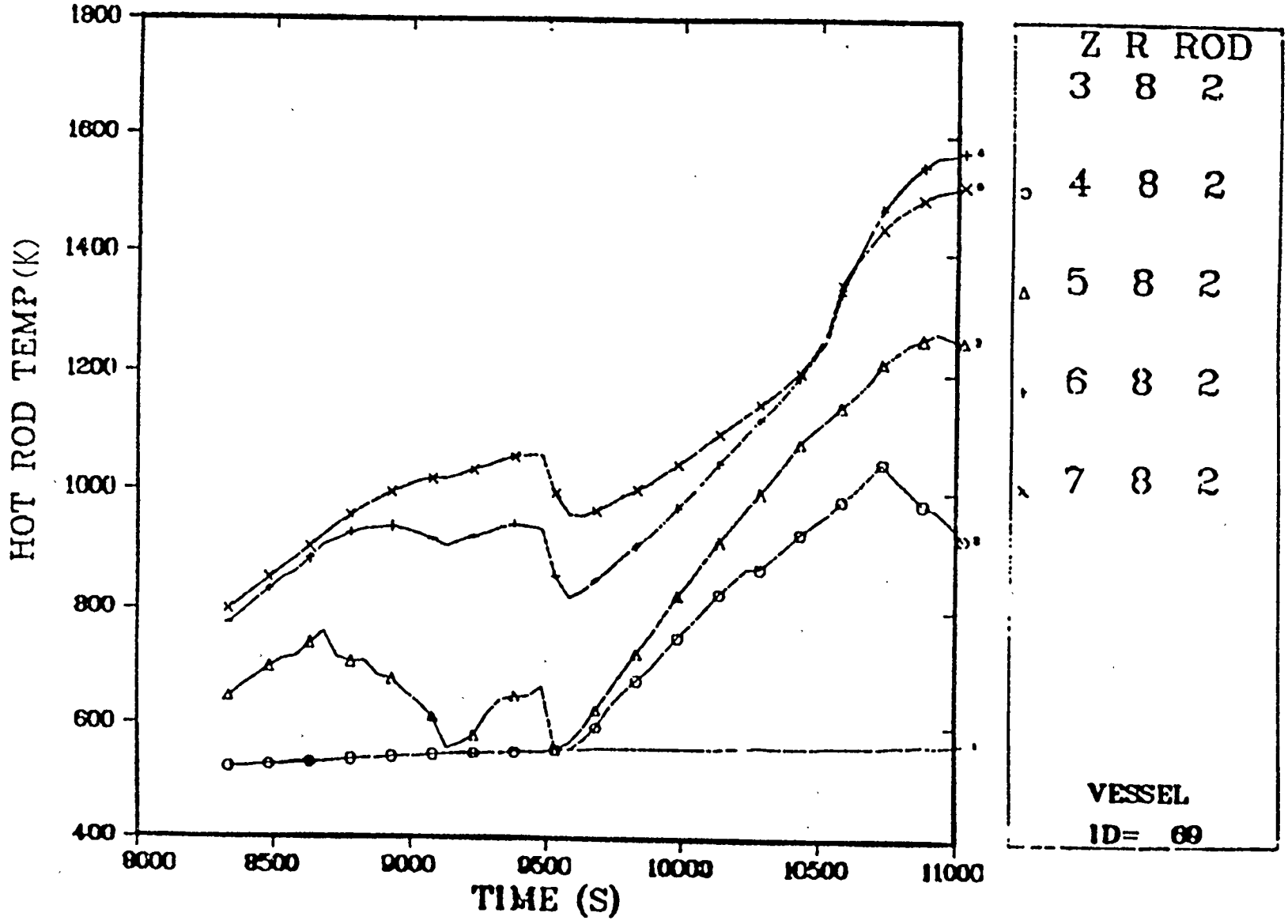

Fig. 40. Axial distribution of hot-rod cladding temperatures (azimuthal zone two).

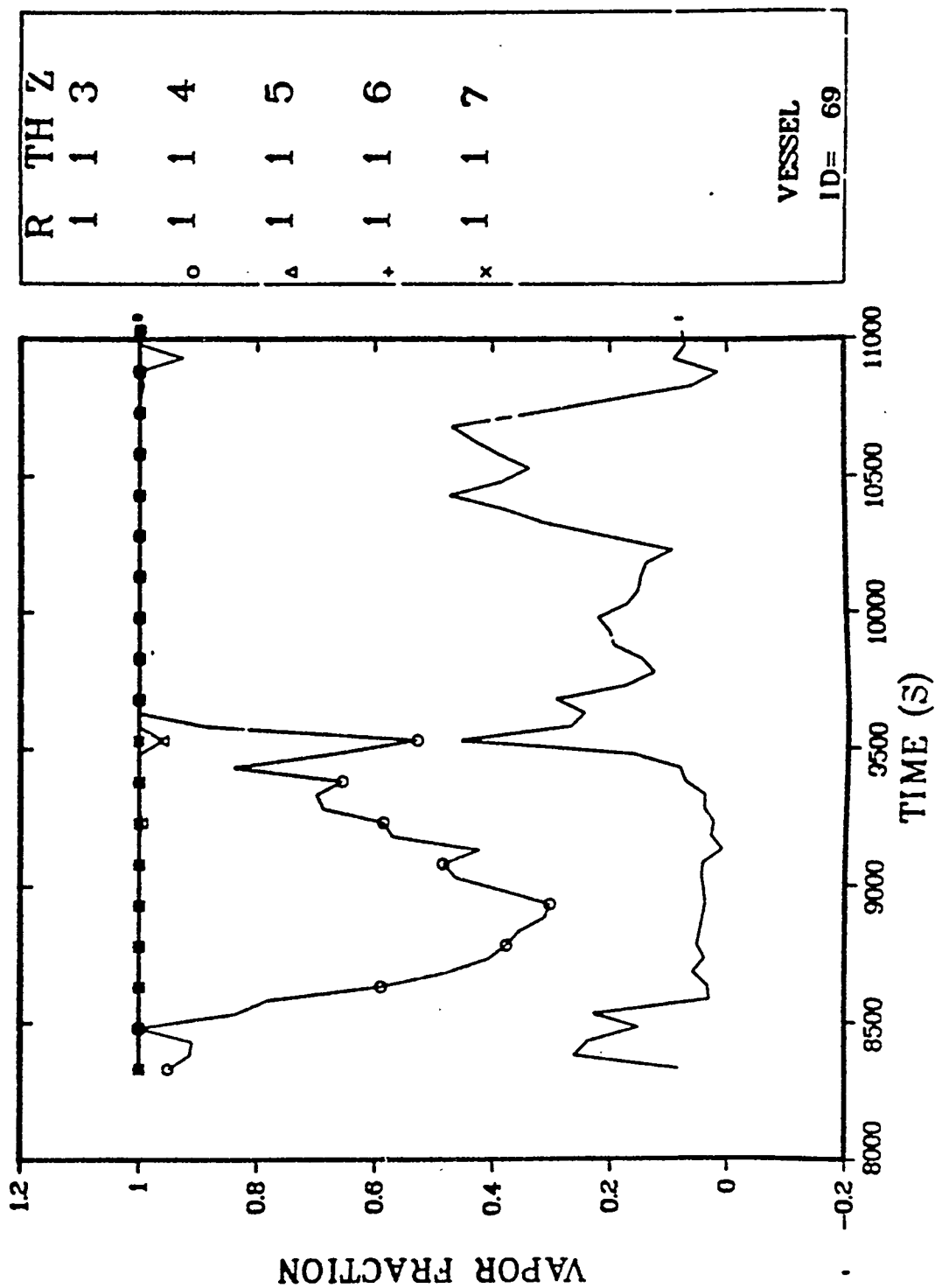

Fig. 41. Axial distribution of void fraction in reactor vessel.

4.1 Cladding Ballooning

Cladding ballooning is the relatively large permanent increase in diameter (also called azimuthal or diametral strain) that the Zircaloy cladding experiences during a transient prior to eventual failure. There are four features of the fuel rods and/or the transient that tend to promote ballooning. These are:

1. Zircaloy cladding is very ductile (that is it experiences large deformations prior to failure)

2. The rods are initially prepressurized to about 30 atmospheres (at room temperature) to prevent cladding creepdown during normal steady-state operation

3. The system pressure during the transient is considerably below the normal operating pressure of about 2200 psia.

4. The cladding temperature is considerably above the normal steady-state operating temperature.

Ballooning is directly related (to first order) to the pressure drop across the cladding (rod internal pressure minus system pressure) and the local cladding temperature. The large pressure drop across the cladding and the high cladding temperature are expected to lead to large cladding ballooning and likely cladding failure. As will be shown in the next section, cladding failure is indeed calculated to occur.

A large diametral cladding strain is potentially important because of the effect on the coolability of the fuel rods. The increased size of the fuel rods leads to a decrease in the volume available for the coolant (steam and/or water). Hence, to maintain the same level of cooling, it would be necessary to increase the coolant velocity by an amount that is (neglecting changes in the heat transfer coefficient) inversely proportional to the change (decrease)

in the coolant channel area. This change in coolant channel area with increase in cladding diameter is illustrated in Fig. 42.

For the TMI plant design, the pitch-to-diameter ratio (S/D) is about 1.3 and the flow area A can be expressed as

$$A = S^2[1 - (\pi/4)\, D^2/S^2] \tag{1}$$

$$\sim 0.536\, S^2.$$

In other words, the volume occupied by the coolant is 53.6% of the core volume.

The maximum increase in cladding diameter that can occur prior to contact between adjacent fuel rods, occurs when the deformed cladding diameter D; just equals the rod pitch, S. The diametral strain for this case is given by

$$\frac{\Delta D}{D} \equiv \frac{D' - D}{D} \tag{2}$$

$$= \frac{S - D}{D}$$

$$\sim 0.3\ .$$

Thus, a diametral strain of 30% just barely results in rod-to-rod contact. The restricted coolant channel area, A', for this case is given by

$$A' = S^2 - \pi \frac{D'^2}{4} \tag{3}$$

$$= 0.215\, S^2\ .$$

In other words, the coolant volume fraction has been reduced from about 53.6% down to 21.5%.

In the next section of this report, it will be shown that the fuel rods are calculated to fail (rupture) during the first 3 hours of the accident. Using this fact, it is relatively simple to calculate a maximum cladding

S = rod-to-rod spacing (rod pitch)

D = undeformed cladding diameter

A = initial coolant channel area per rod

$$A = S^2 - \pi \frac{D^2}{4}$$

D' = deformed cladding diameter

A' = restricted coolant channel area per rod

$$A' = S^2 - \pi \frac{(D')^2}{4}$$

Fig. 42. Reduction in channel area with cladding ballooning.

fission gas plenum

cladding

fuel-cladding gap volume

fuel pellets

Fig. 43. Fuel rod model.

diametral strain that occurs just at the time of failure. The accepted handbook of materials properties for use in the analysis of LWR fuel rod behavior, MATPRO-Version 11,[9] provides a correlation that relates the circumferential cladding elongation (or diametral strain) to the local tempeature.[10] (Note that this correlation is quite approximate because the effects of cladding stress, strain, and strain rate are ignored.) This correlation is given by

for $T < 1090$

$$\frac{\Delta D}{D} = (0.198 + 4.16 \times 10^{-4}\, T + 2.06 \times 10^{-7}\, T^2) R\, F \qquad (4)$$

for $1090 < T < 1170$

$$\frac{\Delta D}{D} = (9.0623 - 7.492 \times 10^{-3}\, T) F \qquad (5)$$

for $1170 < T < 1600$

$$\frac{\Delta D}{D} = (-1.436 + 2.045 \times 10^{-3}\, T - 4.82 \times 10^{-7}\, T^2) F \qquad (6)$$

for $T > 1600$

$$\frac{\Delta D}{D} = 0.6021\, F \qquad (7)$$

where

T = cladding temperature (K),
R = factor to account for the effect of cold work and irradiation, and
F = factor to account for the effect of cladding temperature gradient.

The calculated failure temperatures from Sec. 4.2 are high (about 1000 K). It can be seen from Eq. (5) that this temperature is very close to the temperature of 1090 above which the effects of cold work and irradiation no longer

need to be considered (they are completely annealed out). Furthermore, the cladding is shown to be hot for an extended period of time prior to failure (Figs. 37-40). Thus, it is reasonable to assume that the effects of cold work and irradiation are very nearly annealed out and R is about 1.0. In addition, the temperature gradient across the cladding is very small (a few degrees) because the transient is much longer than the thermal time constant of the fuel rod. The expression for the factor F^{11} is given as

$$F = \exp(-\ 0.0111\ \Delta T) \tag{8}$$

where ΔT = temperature variation across the cladding (K). For a ΔT of only a few degrees, F is also very close to 1.0.

Making these approximations and using a typical calculated failure temperature of about 1000 K, Eq. (4) predicts a diametral failure strain of 0.82. This is clearly larger than the strain of 0.3 that is required to cause rod-to-rod contact. Thus, it appears that even if we are overpredicting the cladding strain using Eq. (4), it is most likely that enough strain does occur to cause rod-to-rod contact and the associated restriction in flow area. Any possible feedback on the subsequent coolability of the core (see for example Ref. 12) is not included in the TRAC calculations.

The large strains calculated above do not occur over the entire axial extent of the fuel pins. From Figs. 37-40 it can be seen that only axial nodes 6 and 7 (the upper third of the core) reach a high temperature prior to cladding failure at about 1000 K. The axial level just below these two nodes is almost 200 K cooler at the time of rod failure. Thus, the cladding ballooning in all but the upper third of the core is expected to be much smaller. Also, the largest deformations are likely to be localized so that the flow area reductions may not be as large as noted above.

4.2 Initial Cladding Rupture

Fuel rod cladding rupture is an important phenomenon because of the associated release into the system of the free (not in the fuel matrix)

gaseous fission product inventory contained in the rod. This section of the report details the assumptions used and the calculations done in determining the time of initial fuel rod rupture during the TMI accident. The points discussed will be the time of initial fuel rod failures (predictions for the hot rods), the temporal coherence of these failures (failure of the hot rod vs the average rod, for example), and the sensitivity of the calculated rod failure time to the assumed pressure in the rod.

The conditions that lead to fuel rod failure are the same conditions listed as causing cladding ballooning (high internal rod pressure, low system pressure, and high cladding temperature). The consequences of fuel rod failure are release of the free gaseous fission product inventory in the rod. For this particular calculation, it is possible to check on the accuracy of the prediction since the time at which high radioactivity levels were first measured should correspond to the time of multiple fuel rod failures.

Two separate predictions of rod failure were made; both of which require a knowledge of the Zircaloy cladding hoop stress and temperature. To calculate the cladding hoop stress, we model the fuel rod as a closed cylinder as shown in Fig. 43. The void volume inside this fuel rod (fission gas plenum, fuel-cladding gap volume, fuel crack volume, pellet dish volume, etc.) is pressurized by the initial fill gas (the rods are prepressurized to about 30 atmospheres to prevent creepdown of the cladding during steady-state irradiation) as well as any fission gas released from the fuel matrix during power operation. Because of the long time scale of the TMI-2 accident, it is reasonable to assume that this internal rod pressure is axially uniform within the rod.

Given the internal rod pressure as well as the pressure outside the fuel rod in the coolant channel, we can approximate the three principal stresses (radial, circumferential, and axial) in the cladding as

$$\sigma_r = (P_i + P_o)/2 \tag{9}$$

$$\sigma_\theta = (P_i - P_o)\frac{d}{2t} \tag{10}$$

$$\sigma_z = (P_i - P_o)\frac{d}{4t} \tag{11}$$

where

P_i = internal rod pressure,

P_o = coolant channel pressure,

d = average diameter of Zircaloy cladding, and

t = thickness of the cladding.

The circumferential stress [Eq. (10)], together with the local cladding temperature can be used to make a prediction of cladding failure. In our analysis, we have used two separate, independent failure criteria. The first of these is a failure hoop stress criterion as given in MATPRO-11.[13] This criterion predicts cladding failure to occur when the circumferential stress [as calculated in Eq. (10)] exceeds a rupture stress given by

$$\sigma_{rupture} = 10^{(8.42 + 2.78 \times 10^{-3} T - 4.87 \times 10^{-6} T^2 + 1.49 T^3)} \quad (12)$$

where T = the cladding temperature (K).

To check the validity of this criterion, we also used a failure criterion based on the results of some Zircaloy creep-rupture tests performed at the Chalk River Facility in Canada.[14] In these tests, sections of unirradiated cladding were pressurized to some known internal pressure and heated to temperatures typical of those that might be experienced during an accident. The measured cladding failure times from these tests are shown in Fig. 44 as a function of cladding temperature and internal pressure.

To use this cladding rupture data, it is necessary to extrapolate from the temperature/pressure data points in the experiments to the conditions encountered during the TMI-2 accident. The Larson-Miller parameter[15] is a useful tool to aid in this extrapolation. It has been found that, to a good approximation, one can define a temperature independent constant that relates the stress-rupture lifetime of a material to the material temperature. For any given stress state, this constant (the Larson-Miller parameter) is given by

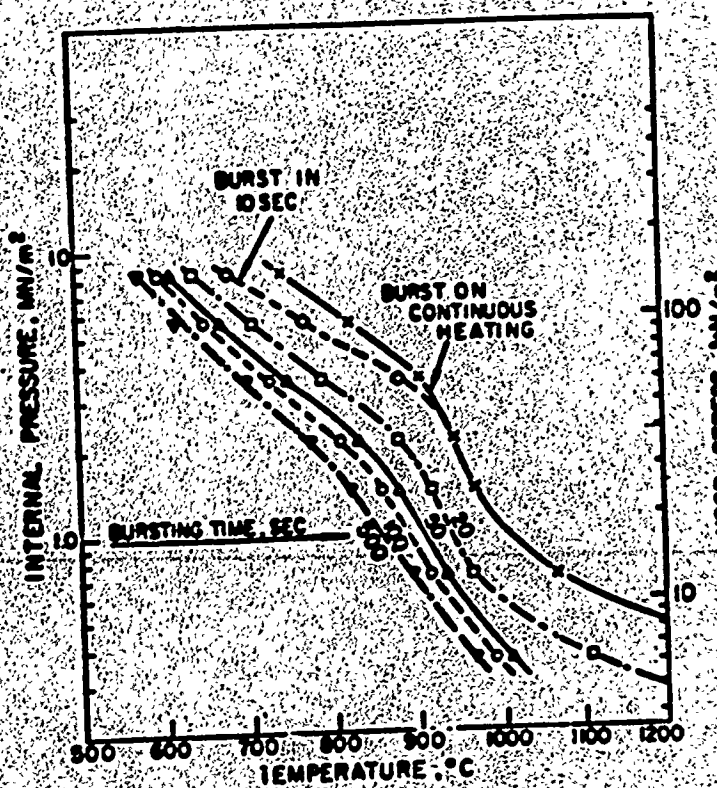

Fig. 44. Cladding burst failure conditions.

$$LMP = T \cdot [\log t_r + c] \tag{13}$$

where

T = material temperature,

t_r = stress-rupture lifetime, and

c = constant dependent only on what the material is (usually taken as about 20).

A least squares fit of the stress-rupture data (from Fig. 44) to Eq. (13) was made in order to determine the Larson-Miller parameter as a function of cladding circumferential stress. (Actually, the Larson-Miller parameter was calculated at seven stress levels and a linear interpolation was used elsewhere). Thus, knowing the cladding hoop stress, one can calculate an appropriate Larson-Miller parameter. This value, along with the cladding temperature, can then be used [Eq. (13)] to calculate the cladding stress-rupture lifetime.

Knowing the stress-rupture lifetime as a function of time, one can use a linear life fraction rule failure criterion[16] to calculate cladding failure. Such a criterion states that over an increment of time Δt during which the cladding stress-rupture lifetime is $t_r(\sigma_\theta, T)$ (thus σ_θ and T are constant during the time increment), a fraction of the cladding "life" is consumed equal to

$$LF = \frac{\Delta t}{t_r(\sigma_\theta, T)} \cdot \tag{14}$$

This can easily be extended to the case where σ_θ and T vary with time (as during the accident) by defining a life fraction as a function of time given by

$$LF(t) = \int_o^t \frac{dt'}{t_r(\sigma_\theta(t'), T(t'))} \cdot \tag{15}$$

Failure is assumed to occur when $LF = 1.0$.

For each prediction of cladding failure, the state of the fuel rod was obtained from the results of the base case TRAC calculation. The TRAC calculation provided the hot and average rod temperatures (Figs. 37-40) and the system pressure (Fig. 36). To calculate the cladding hoop stress, it was also necessary to estimate the rod internal pressure. As was mentioned previously, the rods were prepressurized to about 30 atm (room temperature) to prevent cladding creepdown. In addition, the fission gas produced during steady-state operation (that gas not trapped within the fuel grains) also contributes to the rod pressurization. B&W estimates[17] of this contribution raise the effective initial rod pressure (at room temperature) to about 42 atmospheres.

Knowing the initial internal pressure, the pressure during the transient can be estimated from

$$P_i = P_{io} \cdot \frac{\langle T_{gas} \rangle}{298} \qquad (16)$$

where

P_{io} = room temperature pressure of gas in rod and

$\langle T_{gas} \rangle$ = average temperature of gas in rod (K).

For simplicity, the axially averaged cladding temperature $\langle T_{clad} \rangle$ is used as the average gas temperature (since this is readily available from the TRAC results).

It should be noted that Eq. (16) does not account for potential changes in the amount of volume available to accommodate fission gas (due to the locally large cladding strains discussed in the previous section, for example). Because of the possible error associated with ignoring this effect, as well as the uncertainty in the initial (room temperature) pressure in the rod, we analyzed rod failure for a range of initial rod pressures (25-42 atmospheres).

A first item of concern is the relative agreement between the two methods of predicting failure. In most cases, the calculated agreement is excellent

(within 2 minutes). Only for low initial rod pressure is it possible to see a discrepancy of as much as 10 minutes. This occurred when failure was calculated to occur near the dip in the cladding temperature (at about 9700 s). In this case, the life fraction failure prediction gave the earlier prediction in all cases. This is reasonable because a life fraction criterion is capable of calculating incremental "damage" during the period of time from about 9600 s to about 10000 s, whereas the ultimate hoop stress criterion would not predict failure to occur within that range. Based on these results, we will use the life fraction rule failure prediction as the best estimate.

Cladding failure was calculated for average rod No. 1 for initial rod pressures ranging from 25-42 atmospheres. These results are shown in Table VII. For a wide range of initial pressures (30-42 atmospheres), cladding failure is calculated to have occurred over a narrow 8-minute period of time lasting from 2 hours and 25 minutes to 2 hours and 33 minutes. Only at the lowest initial pressure of 25 atmospheres does the cladding survive through the entire dip in cladding temperature (at about 9700 s) and fail at the later time of 2 hours and 50 minutes. In all cases, failure is calculated to occur in the top axial fuel rod node (in the top 0.5 m of the core).

The general insensitivity in cladding failure time with changes in initial rod pressure is an indication of how rapidly the cladding temperature is increasing at that time (about 0.5 K/s or more). Thus, since the failure temperature at 25 atmospheres (initial pressure) vs 42 atmospheres (initial pressure) varies by a few hundred degrees, it is only a matter of minutes before the cladding temperature increases from the lower failure temperature (high pressure) to the higher failure temperature (low pressure).

A similar analysis was performed for the hot rod. A comparison of Figs. 37 and 39 shows the general similarity between the temperature traces for the hot and average rods. Thus, we expect similar behavior to that calculated for the average rod with somewhat earlier failure times. The results of the analysis for the hot rod are shown in Table VIII. As can be seen from this table, the failure times for the hot rod are about 2-6 minutes earlier than the failure times for the average rod. Thus, there is little variation

TABLE VII

VARIATION IN AVERAGE ROD FAILURE TIME WITH INITIAL ROD PRESSURE

Initial Rod Pressure (atm)	Failure Time (s)
25	10 230 (2 hours and 50 minutes)
30	9 195 (2 hours and 33 minutes)
32.5	8 985 (2 hours and 30 minutes)
35	8 872 (2 hours and 28 minutes)
40	8 743 (2 hours and 26 minutes)
42	8 711 (2 hours and 25 minutes)

TABLE VIII

VARIATION IN HOT ROD FAILURE TIME WITH INITIAL ROD PRESSURE

Initial Rod Pressure (atm)	Failure Time (s)
25	9 237 (2 hours and 34 minutes)
30	8 840 (2 hours and 27 minutes)
35	8 679 (2 hours and 25 minutes)
40	8 614 (2 hours and 24 minutes)
42	8 582 (2 hours and 23 minutes)

in failure time across the core. However, these results have not accounted for the possibility of random early and late failure.

Using the TRAC base case for temperature histories, it is concluded that multiple fuel rod failures occurred at between 2 hours and 25 minutes and 2 hours and 35 minutes into the accident somewhere in the upper 0.5 m of the core. For very low internal rod pressures, the failures could have been delayed as late as until 2 hours and 55 minutes. In addition, it is concluded that most of the rods in the core failed (based on the comparison between the average and hot rod). The calculated failure time of 2 hours and 30 minutes is consistent with the observed response of the containment dome radiation detector. A large increase in the radiation level was observed at about 2 hours and 35 minutes into the accident,[18] very close to the time of our failure prediction.

4.3 Oxidation of Cladding

This section summarizes results of calculations to determine the cladding zirconium dioxide layer thickness, the flow area reduction due to the volumetric expansion associated with oxidation, cladding weight gain due to oxidation, and hydrogen generation during the early stages of the TMI accident. Cladding temperatures, from the axial segment of the fuel rod with the highest temperatures, and plenum pressures used in the calculations come from TRAC code results. Cladding properties used are taken from MATPRO-11.[9]

Temperature data can be used to determine the extent of oxidation of the other cladding surface exposed to water or steam. Cladding temperatures vs time are obtained from TRAC code results as shown in Figs. 37-40.

Cladding oxidation during the approximately three months steady-state reactor operation prior to the start of the transient is negligible. Because oxidation is so much faster at higher temperatures[19] only high-temperature oxidation is considered. For temperatures above 1083 K the oxide thickness[20] in meters can be calculated from

$$X_2 = \left[(X_1)^2 + 2.252 \times 10^{-6} \int_{t_1}^{t_2} \exp(-1.806 \times 10^4 T(t))dt\right]^{1/2}, \quad (17)$$

where

t = time (s),

t_1 = time at beginning of time interval (s),

t_2 = time at end of time interval (s),

T = temperature (K),

X_1 = oxide thickness at beginning of time interval (m), and

X_2 = oxide thickness at end of time interval (m).

The integral in Eq. (17) is evaluated with the trapezoidal rule. Temperatures vs time, extracted from Fig. 37 for evaluating the integral, are shown in Table IX. Linear interpolation is used between tabulated values. The oxide thickness, plotted vs time in Fig. 45, reaches a maximum of about 113 μm at about 11050 s (3:04:10).

Although cladding oxidation results in a 50% volume expansion, the reduction of the effective cross-sectional coolant flow area is negligible because of the insignificant increase in cladding diameter. Of the original 675 μm thickness of Zircaloy cladding, 600 μm of Zircaloy remains at 11050 s (3:04:10). The oxidation is significant also since it embrittles the cladding, making it more susceptible to brittle fracture.

In the same manner, the cladding weight gain from oxidation is calculated. For temperatures above 1083 K, the total weight gain[20] in kg/m^2 can be calculated from

$$W_2 = \left[(W_1)^2 + 3.360 \times 10^1 \int_{t_1}^{t_2} \exp(-2.007 \times 10^4/T)dt\right]^{1/2}, \quad (18)$$

where

W_1 = total weight gain at beginning of time interval (kg/m^2),

TABLE IX

TEMPERATURES VS TIME USED IN CALCULATION OF OXIDE THICKNESS AND WEIGHT GAIN

Time (s)	Temperature (K)
9 379	1 033
9 930	1 103
10 020	1 133
10 170	1 173
10 260	1 216
10 330	1 305
10 470	1 433
10 570	1 503
10 660	1 523
10 760	1 620
10 330	1 643
11 000	1 710
11 050	1 732

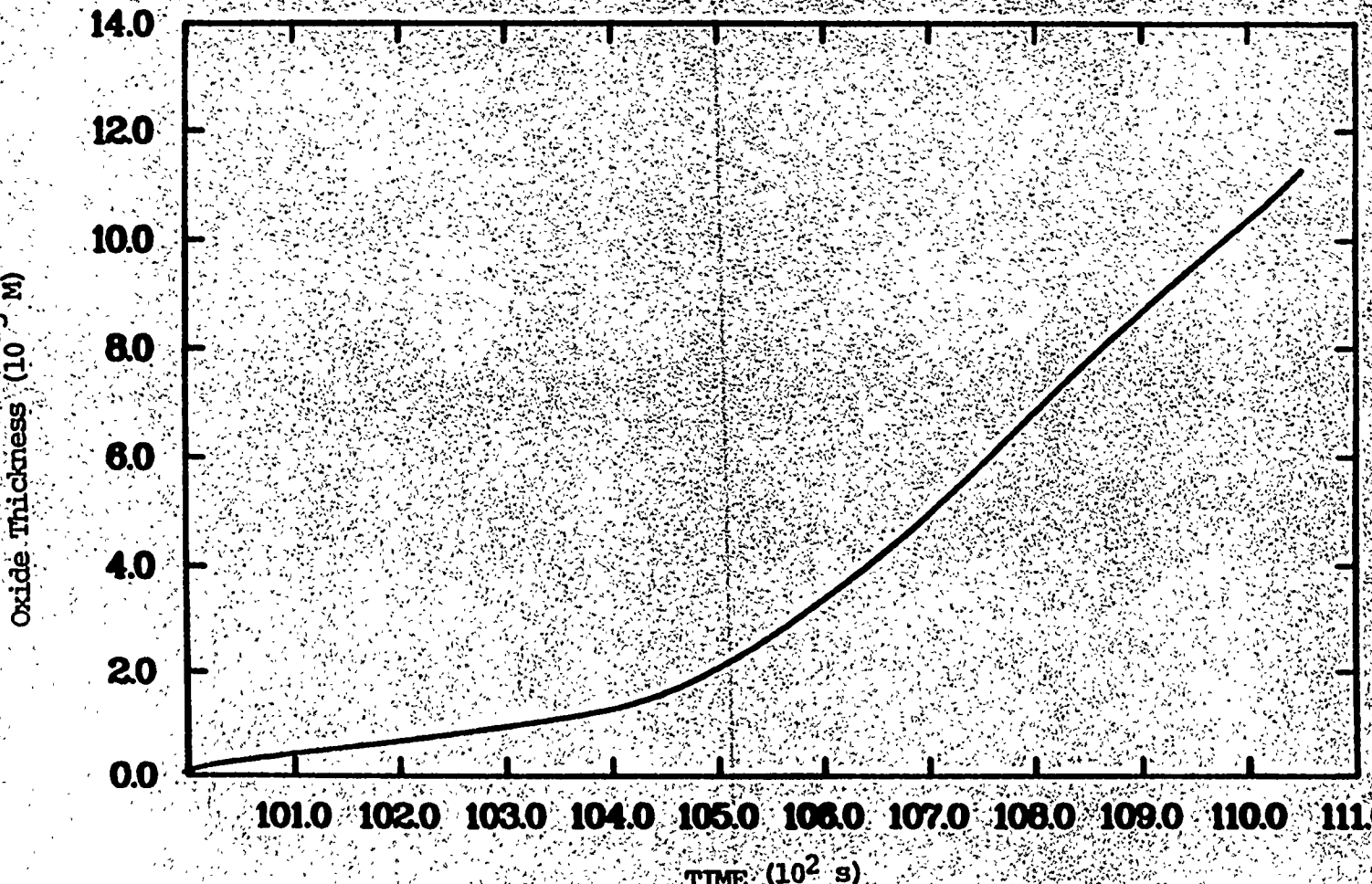

Fig. 45. Plot of zirconium oxide thickness vs time.

W_2 = total weight gain at end of time interval (kg/m^2),

and other quantities are as previously defined. The total weight gain, plotted vs time in Fig. 46, reaches a maximum of about 0.23 kg/m^2 at about 11050 s (3:04:10).

Since the outside diameter of the cladding is 10.92 mm, the weight gain per unit length of fuel rod is calculated to be 7.9 g/m. This is the mass of oxygen per unit length of fuel rod that has reacted with the cladding. Assuming that all of this oxygen was produced by dissociation of water and based on the molecular weights of hydrogen and oxygen, the mass of hydrogen released is one-eighth the mass of oxygen reacted, about 1.0 g/m.

The perfect gas law is used to determine the volume of hydrogen released per unit length of fuel rod

$$V = \frac{mRT}{MP} \quad , \tag{19}$$

where

V = volume of hydrogen per unit length of fuel rod (m^3/m),
m = mass of hydrogen per unit length of fuel rod (kg/m),
R = universal gas constant, 8.31 (J/mole·K),
T = plenum temperature (K),
M = molecular weight of hydrogen (kg/mole), and
P = plenum pressure (Pa).

Values for plenum temperature and pressure of 1500 K and 8.5 MPa, respectively, are estimated from TRAC code results.

$$V = \frac{(1.0 \times 10^{-3})(8.31)(1500)}{(2 \times 10^{-3})(8.5 \times 10^{6})}$$

$$= 7.3 \times 10^{-4} \ m^3/m$$

$$= 0.73 \ \ell/m.$$

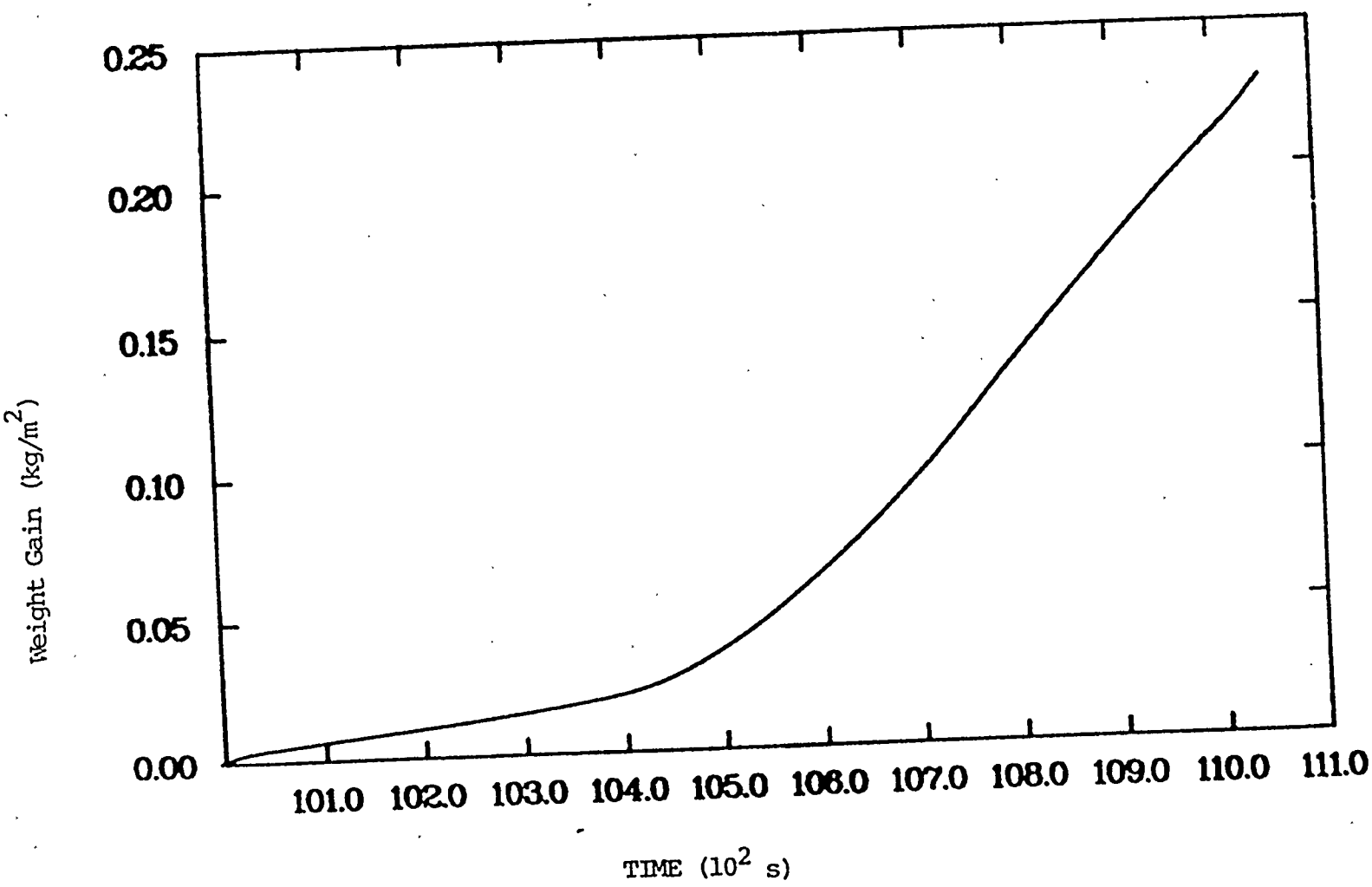

Fig. 46. Zirconium-oxide weight gain per unit cladding area.

Thus, approximately 0.73 liters of hydrogen are generated per meter of oxidized fuel rod. From TRAC results, the total amount of hydrogen generated can be determined by assuming a 1 m length of cladding surface has oxidized on each of the 36, 816 fuel rods. The resultant volume of hydrogen produced is 27 m^3 (37 kg), a substantial quantity of hydrogen.

This calculation may be incorrect compared to the actual condition of the reactor. Not all of the full rods were at the temperatures indicated from TRAC code calculations. In fact, in-core thermocouple readings 4-5 hours after the start of the accident[21] indicate some large variations in temperature from subassembly to subassembly. In addition, the length and thickness of cladding oxidized on each fuel rod can be expected to vary considerably across the core. In light of these considerations, the calculated oxidation and hydrogen generation are thought to be an overestimate of the actual oxidation and hydrogen generation in the early states (before 3 hours) of the TMI accident. However, hydrogen generation probably continued after 3 hours.

For cladding temperatures above 1273 K, the TRAC code calculates the oxide penetration depth and the heat generation from the exothermic metal-water reaction. Oxidation penetration depth is calculated from an empirical rate law developed from isothermal experiments.[22] The TRAC code does not include the effect of the change in cladding properties due to oxidation, nor does it include the effect of the reduced cross-sectional coolant flow area due to the 50% volume expansion of Zircaloy upon oxidation.

The TRAC calculations include five axial levels in the core. This greater detail shows that almost all cladding oxidation occurs near, or above, the core midplane. The lower portion of the core is cooled by water which remains in the lower portion of the core during much of the first 3 hours. Figure 41 shows void fraction for various core levels. The lower level has a consistently low void fraction indicating the presence of water in the lower region of the core. The upper portion of the core is probably not as oxidized as the midplane region because temperatures are lower due to a smaller heat rate near the top of the core.

By determining the volume of oxygen reacted from the oxygen penetration depths calculated by the TRAC code, it is possible to quantify the amount of hydrogen produced by the metal-water reaction. The resultant mass of hydrogen calculated with this method is 39 kg. The two methods of determining hydrogen generation are close enough to give confidence in the results. Agreement is very good because the axially varying amount of oxidation calculated by the TRAC code can be approximated by considering oxidation of a 1 m section of the core's cladding.

4.4 Cladding Mechanical Response During Subsequent Cooldown

During the first 3 hours of the TMI accident, the cladding of the fuel rods experienced increasingly higher temperatures. Shortly after 3 hours, relatively cold water was added to the reactor core due to resumed high-pressure injection (HPI). The mechanical reaction of the cladding can be severe in these circumstances. In particular, it is important to determine whether the cladding could have failed and perhaps fragmented due to thermal shock.

The life fraction calculations discussed above showed that the cladding failed at approximately 9000 s (2:30:00). This failure was due to pressure difference between the inner and outer walls of the cladding at the elevated temperatures. This ductile type of failure, not caused by the temperature gradient in the cladding, can be expected to produce a perforation in the cladding. This perforation permits venting of fission gas to the coolant channel, thus eliminating any pressure difference between the inside and outside of the cladding. Therefore, pressure effects cannot enhance further failure due to thermal shock.

To determine the possibility of cladding failure due to thermal shock, some estimation of the spatial temperature variation in the cladding with time during reflood is essential. Without a thermal gradient in the cladding, thermal stresses would not be induced. To simplify the analysis of temperature in the cladding, any zirconium dioxide layer is ignored and the initial temperature of the cladding is assumed uniform.

At the time of reflood, the outer surface is assumed to be suddenly cooled by the cold water being pumped into the core. Because the cladding thickness-to-diameter ratio is small, less than 7%, the curvature effects can be neglected and the cladding can be modeled as a slab. We assume that immediately before reflood, the cladding and coolant temperatures are approximately equal, and given by T_o. At the time of reflood we assume that the coolant temperature instantaneously changes to some lower temperature, T_∞.

An approximate technique using Kantorovich profiles[23] can be used to determine the temperature distribution with time. Initially, the outer surface temperature will decrease while the inner surface temperature remains constant. The temperature change at the outer surface of the cladding when the inner surface just begins to change, approximates the largest expected differential temperature change, ΔT, to be used in the determination of thermal stress. With the approximate technique outlined above, ΔT can be shown to be given by the expression

$$\Delta T = \frac{(T_o - T_\infty)}{(1 + 2/Bi)} \quad , \tag{20}$$

where Bi, the Biot number, is given by

$$Bi = \frac{ht}{k} \quad . \tag{21}$$

h is the heat transfer coefficient, t is the cladding thickness, and k is the thermal conductivity of the cladding. The dimensionless Biot number is a ratio of convective heat transfer to conductive heat transfer. The larger Biot number becomes, the larger ΔT becomes.

To estimate the largest reasonable ΔT, the larger values of $(T_o - T_\infty)$ and Bi should be used. From TRAC code results an acceptable large value of h is 10^4 $w/m^2 \cdot K$. The thickness of TMI cladding is 0.675 mm. The thermal conductivity of Zircaloy[24] is about 25 $w/m \cdot K$. From Eq. (21), Bi = 0.27.

At approximately 3 hours into the accident, the cladding temperature is about 1650 K. The largest possible change in coolant temperature, $(T_o - T_\infty)$,

at reflood is approximately 1000 K. With these values the largest ΔT to expect, from Eq. (20), is about 120 K. The value of $\Delta T = 120$ K is used in the subsequent stress calculations. This value represents the largest possible differential temperature change in the cladding.

The maximum stress in the cladding will be the tensile hoop stress at the outer surface given by the expression[25]

$$\sigma = f \frac{E\alpha\Delta T}{(1-\nu)} \tag{22}$$

where σ is stress, E is Young's modulus, α is the linear coefficient of thermal expansion, ν is Poisson's ratio, and f is a factor to take into account inelastic, or plastic, deformation. Young's modulus is approximately 3×10^{10} Pa,[26] the linear coefficient of thermal expansion is about 4×10^{-3} K^{-1},[27] and Poisson's ratio is approximately 0.5, the correct value for a material which behaves plastically.

The factor f can be shown to be given by the expression[28]

$$f = \left[1 + \frac{3}{2} \frac{E}{(1-\nu^2)} \left(\frac{\partial\sigma}{\partial\varepsilon}\right)^{-1}\right]^{-1} , \tag{23}$$

where ε is strain. From the MATPRO expression for the yield surface,[29] for strains between 1 and 50% with a strain rate of 10^{-4} s^{-1}, $\partial\sigma/\partial\varepsilon$ is between 1 and 50 MPa. An average value of 10 MPa is used to evaluate f. Results of the calculation yield $f = 3 \times 10^{-4}$.

The maximum stress is calculated to be 7.2 MPa. This value of stress is far below the stress at which failure due to thermal shock can occur according to MATPRO-11 data for unoxidized Zircaloy. However, oxidation embrittled cladding may fail due to thermal shock. Experiments by Kassner, et al.,[30] showed that for isothermal oxidation at 1300 K, 1400 K, 1500 K, and 1600 K for 10000 s, 2000 s, 700 s, and 300 s, respectively, followed by a quench from 840 K to 410 K, cladding failed. Temperature results from the TRAC code calculation indicated that this oxidation criterion is met. If reflooding of the oxidized upper section of the core occurred rapidly, then thermal shock failure may have occurred. If thermal shock failure did occur,

then the oxidized upper portion of the cladding is expected to have fragmented. This assumes that the Zircaloy had not melted before reflood.

4.5 Summary of Core Thermal-Mechanical Response

We have presented calculations detailing the likely fuel rod damage that occurred during the first 3 hours of the accident. The first form of damage that was calculated to occur was ballooning of the very ductile Zircaloy cladding prior to rupture. The amount of ballooning that was calculated is substantial, up to 80% including the large strains at the localized rupture site. The TMI fuel bundle design allows 30% ballooning before rod-to-rod contact occurs. Thus, at least some substantial reductions in flow area in about the upper 1 m of the core seems likely.

This reduction in flow area should have resulted in some degree of local flow starvation. However, the agreement between the best estimate massive cladding failure times and the time of the first substantial radioactive material release indicate that the TRAC calculated cladding temperatures (at that time in the accident) are reasonably accurate. Since there was very little steam flow through the core during the temperature excursion leading to these initial rod failures, ballooning should not have influenced failure times substantially. However, local flow reductions due to ballooning (and oxidation-induced swelling) could have been a contributor to some of the anomalous fuel bundle outlet temperatures measured later in the accident.

The large pressure drops across the cladding and the high cladding temperatures led to cladding failures (rupture). The best estimate prediction indicates that failure in most rods occurred at between 2 hours and 25 minutes and 2 hours and 35 minutes into the accident in the upper 1 m of the core. The local cladding temperature at this time was about 1000 K. As previously mentioned, these times correspond well with the time at which high radiation levels were first measured.

The range of failure times indicated represents both the estimated variation in failure time with radial location in the core as well as the uncertainty in failure time due to uncertainty in internal rod pressure. Calculations indicated that failure times were relatively insensitive to the rod pressure. Rather the dominant controlling factor was the high cladding temperature. In addition, the difference in calculated failure times between the TRAC average and hot rods is small, on the order of 10 minutes. Thus, it appears likely that most of the rods in the core failed around 2 hours and 30 minutes into the accident.

Subsequent to the initial cladding failures and radioactivity release, the major phenomenon the fuel rod undergoes is cladding oxidation. This oxidation of the Zircaloy leads to three important consequences: swelling of the oxidized cladding layer release of hydrogen gas during the oxidation process, and embrittlement of the cladding due to oxidation.

The calculations done to predict oxide layer formation indicate that up to about 3 hours into the accident, the maximum oxide layer thickness for the average rod is about 113 μm cladding thickness. Thus, the effective increase in cladding diameter due to oxidation to this point is only about 76 μm. This represents a negligible increase (initial cladding diameter is about 11 mm) and should not affect the coolability of the fuel pin.

Oxidation of about 75 μm of the cladding thickness does, however, lead to significant hydrogen generation. Because of the small difference between the cool, average, and hot-rod temperatures, cladding oxidation is predicted to occur radially throughout the core. Axially, about the upper one-third to one-half of the core is affected. Using these assumptions, the calculated amount of hydrogen generated at 3 hours is about 40 kg. At the temperature/pressure conditions calculated (by TRAC) to exist in the core at between 2 to 3 hours into the accident, this amount of gas would occupy a volume of about 27 m^3. Further hydrogen release should have occurred after 3 hours.

One other consequence of cladding oxidation is cladding embrittlement. This phenomenon is important relative to the possible fracture and fragmentation of the cladding during the first reflood. While the TRAC calculation

terminates well short of the (at least partial) reflood that occurs at about 3 hours and 20 minutes, estimates have been made of the thermal stress induced in the cladding during reflood and the likelihood of fracture at that time. These calculations indicate that the ductile unoxidized Zircaloy as well as the lightly oxidized cladding will survive the quenching process. Only the cladding that has seen prolonged periods of high temperatures (greater than about 1600 K) is likely to fail under these conditions. Thus, if reflood occurred rapidly, it is possible that up to about one-third of the axial extent of the core may have undergone cladding fragmentation. It should be remembered, however, that since detailed TRAC calculations were not done for this stage of the accident, these estimates of cladding fragmentation are speculative.

REFERENCES

1. "TRAC-P1A, An Advanced Best-Estimate Computer Program for PWR LOCA Analysis," Los Alamos Scientific Laboratory report LA-7777-MS (May 1979).

2. "Three Mile Island Nuclear Station, Unit 2," License Application, FSAR, Vol. 1-10 (Metropolitan Edison Co., 1974).

3. B&W communication.

4. EPRI communication.

5. L. S. Tong, U.S. Nuclear Regulatory Commission, private communication (July 26, 1979).

6. "Investigation Into the March 28, 1979 Three Mile Island Accident By Office of Inspection and Enforcement'" U.S. Nuclear Regulatory Commission Investigative Report No. 50-320/79-10, NUREG-0600 (August 1979).

7. "Nuclear Legislative Advisory Service," Issue 17 (April 13, 1979).

8. General Public Utilities communication to U.S. Nuclear Regulatory Commission (May 15, 1979).

9. "MATPRO-Version 11: A Handbook of Materials Properties for Use in the Analysis of Light-Water Reactor Fuel Rod Behavior," compiled and edited by D. L. Hagrman and Gregory A. Reymann, EG&G Idaho, Inc., report NUREG/CR-0497, TREE-1280, Idaho Falls, Idaho (February 1979).

10. Ibid, p. 404.

11. Ibid, p. 412.

12. P. C. Holland and R. B. Duffey, "A Method of Calculating the Effect of Clad Ballooning on Loss-of-Coolant-Accident Temperature Transients," Nuclear Science and Engineering 58 (1975) pp. 1-20.

13. MATPRO, op. cit., p. 405.

14. D. G. Hardy, "High-Temperature Expansion and Rupture Behavior of Zircaloy Tubing," Topical Meeting on Water-Reactor Safety, Salt Lake City, Utah (March 1973).

15. J. B. Conway, "Stress-Rupture Parameters: Origin, Calculation, and Use," Gordon and Breach, Science Publishers, New York (1969).

16. J. L. Straalsund, et al., "Correlation of Transient-Test Data with Conventional Mechanical Properties Data," Nuclear Technology 25 (March 1975).

17. M. L. Picklesimer, "Bounding Estimates of Damage to Zircaloy Fuel Cladding in the TMI Core at Three Hours After the Start of the Accident, March 28, 1979," Memorandum for File NRC (June 20, 1979).

18. NUREG-0600, op. cit., p. II-3-75.

19. MATPRO, op, cit., p. 439.

20. MATPRO, op. cit., pp. 451-454.

21. NUREG-0600, op. cit., p. I-4-63.

22. J. V. Cathcart, et al., "Zirconium Metal-Water Oxidation Kinetics IV: Reaction Rate Studies," Oak Ridge National Laboratory report ORNL/NUREG-17.

23. V. S. Arpaci, Conduction Heat Transfer (Addison-Wesley Publishing Co., Reading, Massachusetts, 1966) pp. 76-83.

24. MATPRO, op. cit., p. 217.

25. J. H. Faupel, Engineering Design (John Wiley and Sons, Inc., New York, 1964) p. 867.

26. MATPRO, op. cit., p. 251.

27. Ibid, pp. 244-245.

28. P. K. Mast, "The Los Alamos Failure Model (LAFM): A Code for the Prediction of LMFBR Fuel Pin Failure," Los Alamos Scientific Laboratory informal report LA-7161-MS, NRC-7, (March 1978) pp. 27-37.

29. MATPRO, op. cit., pp. 318-324.

30. T. F. Kassner, et al., "LWR Safety Research Program Quarterly Progress Reports, Part III," Argonne National Laboratory report ANL-78-25, NUREG/CR-0089 (October-December 1977) pp. 31-44.

APPENDIX A
TRAC DEVELOPMENT AND ASSESSMENT

J. C. Vigil
R. J. Pryor

Submitted for publication in Nuclear Safety

TRANSIENT REACTOR ANALYSIS CODE (TRAC) DEVELOPMENT AND ASSESSMENT*

J. C. Vigil and R. J. Pryor

Energy Division
University of California
Los Alamos Scientific Laboratory
Los Alamos, New Mexico 87545

ABSTRACT

TRAC is an advanced best-estimate computer program for the safety analysis of light-water reactors. TRAC-P1A provides this analysis capability for pressurized water reactors. Its advanced features include nonhomogeneous, nonequilibrium, and multidimensional hydrodynamics with flow-regime-dependent constitutive relations; quench front tracking capability for both bottom flood and falling films; consistent treatment of entire accident sequences including generation of initial steady-state conditions; and modular design which allows representation of a wide variety of experimental configurations ranging from single components to multiloop systems. TRAC-P1A has been tested against an initial set of separate- and integral-effects experiments. Further assessment of the code through pretest and posttest predictions of other experiments is in progress. Overall results of these testing and assessment activities are encouraging.

*Work performed under the auspices of the U.S. Nuclear Regulatory Commission.

I. INTRODUCTION

The Los Alamos Scientific Laboratory (LASL) is developing, testing, and applying theoretical and numerical methods for analysis of Loss-of-Coolant Accidents (LOCAs) and other transients in Light Water Reactors (LWRs) through funding provided by the Division of Reactor Safety Research, United States Nuclear Regulatory Commission. Improved methods are being developed for the numerical calculation of two-phase flow processes in one, two, and three dimensions and results of calculations are being compared with experimental data. Basic research is also being conducted to assess questions of accuracy, sensitivity, and alternative solution procedures. The entire effort is focused on achieving a better understanding of two-phase flows and on the production of an advanced multidimensional computer program for the analysis of postulated and anticipated transients in LWRs. This computer program is called the Transient Reactor Analysis Code (TRAC).

Primary goals of the TRAC project are to provide a tested analysis capability for LWR system transients, evaluate margins of conservatism in licensing codes, provide detailed analyses of key problem areas such as multi-dimensional and system effects, and provide design and analysis assistance for new large-scale reactor safety experiments. Therefore the TRAC project includes not only methods, models, and code development, but also code assessment and application activities. Close cooperation and liaison are maintained with other LASL projects involving basic thermal-hydraulic research, component code development, and LWR safety experiments in support of model development activities. The purpose of this article is to:

1. review the current capabilities and features of TRAC,
2. present an overview of the current code assessment status, and
3. summarize TRAC development and assessment work now in progress or planned for the near future.

The first documented[1] version of TRAC, called TRAC-P1, was completed in December 1977 and was made available to various organizations following a TRAC Workshop held at LASL in March 1978. Models in TRAC-P1 are directed toward Pressurized Water Reactors (PWRs) and the analysis of LOCAs but other types of problems can be analyzed. An improved version, called TRAC-P1A, was released through the National Energy Software Center in March 1979. Included with the

release was a user's manual[2] which provides detailed descriptions of the thermal-hydraulic models, numerical solution methods, programming features, and user information. A report[3] containing detailed results of initial assessment calculations performed with TRAC-P1A will be released shortly. TRAC-P1A is twice as fast as the first version and includes improvements in the solution methods, constitutive relations, graphics capability, and code structure. All code features described in Section II are based on TRAC-P1A.

TRAC has been tested against an initial set of experiments involving separate and integral effects. Further assessment of TRAC is in progress through pretest and posttest predictions of other experiments. Overall results of these code testing and assessment activities are summarized in Sec. III. Work is in progress on improving the PWR version of TRAC, development of a fast running version, and extension of the code to other accident types. This work is described in Sec. IV.

II. TRAC CHARACTERISTICS

A. General

TRAC can be characterized as an advanced, best-estimate LWR systems computer program. Within limitations imposed by computer running time, it incorporates state-of-the-art methods and models. The models in TRAC are designed to yield realistic solutions as opposed to conservative evaluation models used in licensing codes. TRAC mainly differs from other existing LWR systems codes (e.g. RELAP4 code[4]) in its more detailed geometrical models of system components and its more basic treatment of two-phase thermal hydraulics. These features are reviewed in subsequent sections and described in detail in Refs. 2 and 5-9.

User-selected options are minimized in the basic fluid dynamics and heat transfer modeling. This approach, as opposed to that which allows modeling options, places great demands on the basic thermal-hydraulic modeling because the code must determine local flow topology and supply appropriate constitutive relations. Thus, the development of accurate flow-regime-dependent constitutive relations is vital to the TRAC effort. The ultimate

goal of the TRAC program is to produce computer programs that have a demonstrated capability to adequately predict the results of a broad range of experiments with no tuning of basic physical models from one test to another.

Because of the advanced features in TRAC, most of the physical phenomena that are important in LOCA analysis can be treated. Included among these phenomena are:

- o emergency core coolant (ECC) downcomer penetration and bypass including the effects of countercurrent steam flow and hot walls,
- o lower plenum refill, sweepout, and phase separation effects,
- o bottom flood and falling film reflood quench fronts,
- o multidimensional flow patterns in the downcomer, core, and plenum regions,
- o pool formation and countercurrent flow-limited fallback at the upper core support plate (UCSP),
- o steam binding effects during reflood, and
- o direct injection of subcooled ECC water at any location in the system without the requirement for artificial mixing zones.

The code can be used to obtain steady-state solutions to provide self-consistent initial conditions for subsequent transient calculations. Both a steady-state and transient calculation can be performed in the same run if desired. Efficient solution strategies ranging from semi-implicit to fully implicit are used.

An important characteristic of TRAC is the ability to address the entire LOCA (blowdown, bypass, refill, and reflood) in one continuous and consistent calculation. This eliminates the necessity of interfacing and combining calculations performed with different codes for each major accident phase. Trips can be specified to simulate protective system actions or operational procedures (e.g. opening or closing of a valve).

A sophisticated graphics package, including movie generation capability, is available to help analyze and digest the large amount of output information generated during a TRAC run. A dump/restart feature allows the user to restart a calculation from any point in a transient. This feature is very useful in performing parametric studies and in minimizing loss of computer time due to hardware failure or input errors.

TRAC is designed to run on a CDC 7600 computer but standard programming techniques are being used to ease its conversion to other computers. All storage arrays are dynamically allocated so that the only limit on problem size is the available core memory. A capacity of 60K words of small core memory and 220K words of large core memory is sufficient to handle most problems of interest.

B. Component and Functional Modularity

TRAC is completely modular by component and by function. Component modules, which consist of subroutines or sets of subroutines, are available to model vessels (with associated internals), steam generators, pressurizers, etc. Component modules currently available in TRAC are described in Table I. The user can construct a wide variety of configurations by joining together an arbitrary number of these components in a meaningful way. Thus, the user can solve problems ranging from a simple pipe blowdown to a multiloop PWR LOCA. Component modularity allows component models to be improved, modified, or added without disturbing the rest of the code.

Functional modules, which also consist of subroutines or sets of subroutines, are available for the multidimensional two-fluid hydrodynamics, one-dimensional drift-flux hydrodynamics, thermodynamic and transport properties, wall heat transfer, etc. These functional modules are described in Table II. Functional modularity allows the code to be easily upgraded as improved correlations and experimental information become available. A multinational research effort is underway to develop improved correlations and a better understanding of two-phase flows. This information will be incorporated into TRAC as appropriate.

C. Multidimensional Fluid Mechanics

A three-dimensional cylindrical (r-θ-z) or two-dimensional Cartesian (x-y) hydrodynamic calculation can be performed within the reactor vessel. Components outside the vessel are treated in one-dimensional geometry. A

typical arrangement of components and mesh cells for one loop of a PWR is shown in Fig. 1.

The vessel module is used to model all regions inside the pressure vessel including the downcomer (darkened region in Fig. 1), lower plenum, core, upper plenum, and upper head. It is in these regions of the reactor system that significant multidimensional effects are likely to occur during a LOCA and other postulated accidents. Examples are two-dimensional and countercurrent steam/water flow patterns in the downcomer during the blowdown and refill periods and preferential rewetting of the cooler fuel rods in the core during reflood.

A simplified but typical three-dimensional grid that might be used to model a PWR vessel is shown in Fig. 2. The user has the capability in TRAC of restricting flow across the mesh cell boundaries. A total flow restriction is used to form the downcomer boundaries and a partial flow restriction can be used to account for structural material that does not completely obstruct the fluid flow. In addition to area restrictions, the user can specify reduced mesh cell volumes to account for structural material within the cell.

One-dimensional components are coupled to any mesh cell in the vessel (including interior cells as shown in Fig. 2) through source terms in the hydrodynamic equations. This feature is required to model the outlet nozzles that penetrate the downcomer and it also permits TRAC to handle upper head injection.

D. Nonhomogeneous, Nonequilibrium Hydrodynamics

Two-phase flow in the various TRAC components is treated using non-homogeneous, nonequilibrium models. That is, liquid and vapor velocities are not assumed to be equal and furthermore liquid and vapor temperatures are in general unequal with neither phase assumed to be at saturation conditions.

A two-fluid six-equation model is used to describe the liquid-vapor flow field within the reactor vessel. These equations are based on conservation of mass, momentum, and energy for the separate liquid and vapor fields. Supplementing these field equations are so-called constitutive

relations or closure equations that specify (1) the transfer of mass, energy, and momentum between the liquid and vapor phases and (2) the interaction of these phases with the system structure. The nature of these interfacial transfers and interactions is dependent on flow topology and therefore a flow-regime-dependent constitutive equation package is included in TRAC. This package is continually being tested and upgraded as new information becomes available and as our understanding of two-phase flow improves.

The flow in the one-dimensional loop components is described by a five-equation drift-flux model. These equations are based on conservation of mass, energy, and momentum for the mixture and conservation of mass and energy for the vapor. Liquid and vapor velocities are not assumed to be equal but are expressed in terms of a relative velocity which is dependent on flow topology.

E. Comprehensive Heat Transfer

Heat transfer models in TRAC include (1) conduction models to calculate temperature fields in structural materials and fuel rods and (2) convection models to provide heat transfer between structure and coolant. Heat transfer to the two-phase fluid is calculated using a generalized boiling curve constructed from a library of heat transfer correlations based on local surface and fluid conditions.

Conduction models are available for obtaining temperature fields in one-dimensional (cylindrical) pipe walls, lumped-parameter slabs, and one-dimensional (cylindrical) fuel rod geometries. Pipe wall conduction is used in the components outside the vessel whereas the slab and fuel rod conduction models are used in the vessel module. The fuel rod conduction analysis accounts for gap conductivity changes, metal-water reaction, and quenching phenomena. A fine-mesh axial renoding capability is available for fuel rods to allow more detailed modeling of reflood heat transfer and tracking of quench fronts due to bottom flooding and falling films. Precooling effects and consistency between quench front propagation and stored energy considerations are included in the reflood heat transfer methodology.

Each fluid mesh cell in the core region can contain an arbitrary number of fuel rods. However, heat transfer calculations are only performed on one average rod and one hot rod in each core mesh cell as shown in Fig. 2. The average rod represents the average of the ensemble of rods in the mesh cell and its thermal calculation couples directly to the fluid dynamics. A spatial power peaking factor and local fluid conditions in the mesh cell are used in the hot rod calculation but this calculation does not feed back to the hydrodynamics. The total core power level is determined from either a table lookup or from the solution of the point-reactor kinetics equations including decay heat (6 delayed neutron groups and 11 decay heat groups). The spatial power distribution is specified by separate radial and axial power shapes in the core plus a radial distribution in the fuel rod.

The TRAC library of heat transfer correlations includes data for the following heat transfer regimes: laminar and turbulent forced convection to a single-phase liquid or vapor and to a two-phase mixture; nucleate boiling and forced convection vaporization; pool boiling and high flow critical heat flux (CHF); transition boiling; minimum stable film boiling; film boiling including subcooling and radiation effects; and horizontal, vertical, and turbulent film condensation.

F. Solution Strategies

The system of field and constitutive equations in TRAC is solved by standard spatial finite-difference techniques. A semi-implicit time differencing technique is normally used in most components. This technique is subject to the Courant stability limitation which restricts the time step size in regions of high-speed flow. A fully implicit time differencing option is available for the fluid dynamics in most of the one-dimensional components. This option allows fine spatial resolution in regions of high velocity (e.g. in a nozzle) without restricting the time step size.

Iterative methods are used to solve the time-dependent, nonlinear, finite-difference equations in TRAC. Each time step in the transient calculation consists of several passes through all the components in the system.

These passes, whose purpose is to converge to the solution of the nonlinear finite-difference equations, are called outer iterations. If the outer iteration process fails to converge, the integration time step size is reduced and the time step is repeated.

The solution procedure during an outer iteration begins with a linearization of the finite-difference equations for each one-dimensional component. This results in a block tridiagonal system in which linear variations in pressure and other independent variables (vapor fraction, liquid temperature, and vapor temperature) are solved in terms of variations in the junction velocities for that component. If there are no vessels in the calculation, these linearized equations are combined with the linearized junction momentum equations to obtain a closed linear system for the junction velocity variations. This system is solved by direct methods and a back-substitution is made to update the remaining independent variables. Therefore there is no inner iteration process involved for one-dimensional components.

When one or more vessels are present, the variations in the one-dimensional component junction velocities are solved in terms of the pressure variations at the vessel junctions. These equations are combined with the remaining linearized equations in the vessel to provide a closed set of linear equations. Because the matrix is usually too large for direct inversion, this set of linear equations is solved by Gauss-Seidel iteration. When this vessel inner iteration process has converged, back substitution through the one-dimensional components again completes the solution of the full linear system.

A single pass through the above procedure provides the solution for the linearized finite-difference equations. Subsequent passes through the procedure for the same time step result in a Newton-Raphson iteration scheme with quadratic convergence on the nonlinear difference equations.

Computer running time is highly problem dependent. It is a function of the total mesh cells in the problem and the maximum allowable time step size. The total run time for a given transient can be estimated from a unit run time of 2 to 3 ms per mesh cell per time step and an average time step size of 5 ms.

The TRAC steady-state capability is designed to provide time-independent solutions which may be of interest in their own right or as initial conditions for transient calculations. Two distinct calculations are available within the steady-state capability: (1) a Generalized Steady-State calculation and (2) a PWR Initialization calculation. The first is used to find steady-state conditions for a system of arbitrary configuration. The second is applicable only for configurations typical of current PWR systems and is used to adjust certain loop parameters to match a set of user-specified flow conditions.

Both calculations utilize the transient fluid dynamics and heat transfer routines to search for steady-state conditions. The search is terminated when the normalized rates of change of fluid and thermal variables are reduced below a user-specified criterion throughout the system. For a given problem, computer running times for steady-state calculations are generally much smaller than those for transient calculations.

Although the same subroutines are used in the transient and steady-state calculations, there are important differences between the two calculations. Time step sizes used by the heat transfer and fluid flow calculations are not required to be equal during a steady-state calculation. The ratio of these time step sizes is user-specified and permits compensation for the difference in natural time scales of the two processes. Occurrence of CHF is inhibited during the steady-state calculation and results in a heat transfer coefficient which cannot undergo a rapid reduction due to burnout. Pressurizers are automatically modeled as pressure boundary conditions during steady-state calculations so that each pressurizer's energy and mass inventory, as well as pressure, remain constant regardless of the flow rate between it and the remainder of the system. Trips are inhibited during steady-state calculations. Finally, reactor power is set to zero for a period at the beginning of the steady-state calculation and is increased to its nominal value once the fluid velocity has approached its equilibrium value.

III. TRAC ASSESSMENT AND TESTING

The general procedure for TRAC assessment and testing is outlined in Fig. 3. Note that two stages of code checkout are involved. Developmental code assessment is the first stage and involves primarily posttest analyses of a wide variety of thermal-hydraulic experiments. The primary objective of this activity, which is closely coupled to the code development activity, is to define the limits of validity of the methods, models, and correlations in the developmental version of TRAC by comparing calculated results with experimental measurements. Other objectives include determination of code sensitivity to input data, model assumptions, and solution techniques; recommendation of standard calculational procedures for various classes of problems; and identification of code and model improvements or additional experiments needed for assessment of the advanced models in TRAC.

When a particular code version substantially meets its performance objectives, the code is released for external use and the second checkout stage begins. This is the independent assessment stage that involves pretest and posttest predictions of tests in designated facilities using the publicly released and documented version of TRAC. The primary objective of this activity is to determine the predictive capability of TRAC when applied to new tests involving different scales and experimental configurations. Discrepancies between calculation and experiment are resolved by performing additional posttest analyses as required. Guidance for future code development and recommendations for future experiments are also provided by this activity. If the results of the independent assessment process are satisfactory, the code can then be applied with confidence to full-scale LWR transients.

Pretest predictions are performed before the test and are referred to as "double blind" predictions because the analyst does not have access to either the actual initial conditions or the transient test results. Anticipated initial conditions are used in the pretest prediction. Posttest predictions are performed after the test and are "single blind" in that the actual initial conditions are specified but the transient results have been impounded and are not available to the analyst. After the transient results are released, calculations are referred to as posttest analyses.

A. Developmental Testing

Experimental tests selected for developmental assessment of TRAC-P1A, and the more important thermal-hydraulic effects occurring during these tests are given in Table III. Note that the first five analyses use only the one-dimensional capability in TRAC whereas the remainder involve the multidimensional capability as well. Tests selected for developmental assessment include separate effects (tests involving basically only one component), synergistic effects (several coupled components but only one LOCA phase), and integral effects (several components and more than one LOCA phase). Detailed comparisons between code results and experimental measurements for the tests in Table III are reported in Ref. 3. Therefore, only brief summaries and typical comparisons are given below for each test.

The Edwards experiment,[10] referred to as Standard Problem 1, was the depressurization of a straight horizontal pipe (0.073 m i.d. x 4.1 m long) initially filled with subcooled water at approximately isothermal conditions. A glass rupture disk at one end of the pipe was broken to initiate the blowdown. TRAC best-estimate calculations are in reasonable agreement with available experimental measurements of fluid pressures and temperatures and with the single density measurement. Examples of the typical agreement obtained are given in Figs. 4 and 5 which show the pressure and void fraction, respectively, at gage station 5 (about 1.5 m from the closed end of the pipe). Mass flow rate and pipe wall temperature measurements were not made. In addition there are experimental uncertainties as to the initial temperature distribution, rupture disk dynamics, and the effect of residual disk fragments (about 13% of the pipe area) on the flow field. The calculated results are sensitive to these uncertainties and also to the wall friction factor correlation used. The TRAC model for this problem contains 46 fluid cells and the transient calculation requires 24 s of Central Processor Unit (CPU) time on the CDC 7600.

In the CISE (Centro Informazoni Studi Esperienze) experiments,[11] subcooled water was circulated through a tubular test section consisting of a coiled feeder (0.017 m i.d. x 9.9 m long), a straight vertical pipe (0.021 m i.d. x 4.15 m long) whose walls could be electrically heated, and a coiled

riser (0.026 m i.d. x 10.0 m long). The blowdown was initiated by simultaneously closing two test section isolation valves and opening a discharge valve at the bottom of the feeder section. In the reference test (Test R) a power of 110 kW was input to the heater section whereas in Test 4 there was no power input.

TRAC best-estimate calculations of the CISE tests are in good overall agreement with the measured data including fluid pressure and temperature at several locations in the test section, pipe wall temperature in the heater section, and mass holdup measurements. Figures 6 and 7 are typical of the results obtained for these tests and show, respectively, the fluid pressure near the break (P4) and the pipe wall temperature near the top of the heater section (THW4) for the heated test. In the heated CISE test, the heater wall experiences dryout during the blowdown and the calculation slightly overpredicts the time to CHF. Because of the large length-to-diameter ratio, the calculated results are very sensitive to the wall friction factor correlation. Transfer to the fluid of stored energy in the pipe wall also has a significant effect on the computed results. The models for the CISE problems contained 38 fluid cells and the transients required 1 min and 3 min CPU time for the unheated and heated cases, respectively.

The Marviken critical flow tests[12] are designed to determine how well code models developed using small-scale experiments actually apply to full-scale systems. These tests involve the blowdown of a large (5.2 m i.d. x 21.5 m high) pressure vessel through a discharge pipe (0.75 m i.d. x 6.3 m long) which protrudes 0.74 m into the bottom of the vessel. In Test 4 a nozzle with a minimum diameter of 0.51 m was attached to the bottom of the discharge pipe. The blowdown is initiated by overpressurizing the gap between two rupture disks at the downstream end of the nozzle.

TRAC best-estimate results for Marviken Test 4 are in very good overall agreement with fluid pressure and temperature measurements at various locations and with mass fluxes derived from differential pressure and Pitot tube measurements. Results for the break mass flux and the pressure near the vessel top are shown in Figs. 8 and 9, respectively. The use of deionized

water in the experiment apparently caused delayed nucleation resulting in an initial pressure dip and recovery. Delayed nucleation is not yet modeled in TRAC but can easily be incorporated. Calculated results for this problem are sensitive to the initial nonuniform temperature distribution and to the noding in the pressure vessel. The CPU time required for the transient was 1.6 min using a model containing 60 fluid cells.

Tests in the Semiscale 1-1/2 Loop Isothermal Test Facility[13] provided the first system-effects hydraulic data from a multiloop system. The configuration for Test 1011 consisted of a pressure vessel with internals; an intact loop with a steam generator, pump, and pressurizer; a blowdown loop with a simulated steam generator, simulated pump, and two rupture assemblies each containing nozzles with 80% of the normal break area; and a pressure suppression tank. The standard lower plenum (L/D = 2.8) and an oversize (0.043 m) downcomer gap were used in Test 1011. The volume scale between this apparatus and a large PWR is approximately 1/3000. Prior to the blowdown test the system was brought to an approximately uniform temperature of 575 K at a system pressure of about 15.7 MPa using energy addition from the nine electrically heated core rods, pressurizer heaters, and intact loop pump. Power to the heater rods was turned off after these conditions were attained and the system was then subjected to a double-ended offset cold-leg break.

TRAC analysis of Test 1011 included a steady-state calculation to provide self-consistent initial conditions for the blowdown transient and a transient calculation utilizing the restart dump from the steady-state calculation. Calculated steady-state initial conditions for Test 1011 agree well with measurements of the vessel outlet temperature, intact loop volumetric flow rate, pump differential pressure, system pressures, etc. Agreement between calculated and experimental results for the blowdown transient was generally very good for all system variables that were compared. These included mass flow rates, system pressures, fluid densities and temperatures, and differential pressures. The comparisons for the lower plenum pressure and pump discharge mass flow rate are given in Figs. 9 and 10, respectively. Test 1011 represents the first developmental assessment problem involving a large variety of components arranged in a multiloop configuration. It is encouraging that the one-dimensional TRAC model is adequate since the

experiment was designed to minimize multidimensional effects. With a TRAC model containing 122 fluid cells, the steady-state and transient calculations required 0.5 and 19 min of CPU time, respectively.

The Semiscale Mod-1 system[14] was very similar to the 1-1/2 loop configuration described previously. However, the Mod-1 vessel contained 39 electrically heated rods (which could be programmed to simulate the surface heat flux of a nuclear rod) and a 0.011 m downcomer gap. Test S-02-8 consisted of a 200% double-ended cold-leg break with a programmed power decay curve to simulate decay heat in a nuclear core. The transient was initiated from a steady state core and loop temperature distribution at a power level of 1.6 MW.

The best-estimate TRAC model of Test S-02-8 contains a total of 263 fluid cells including 152 cells in the three-dimensional vessel model. Although multidimensional effects are not too significant in this facility, the three-dimensional vessel module was used because fuel rod heat transfer is not available in the one-dimensional pipe module. As was the case for Test 1011, calculated steady-state initial conditions and transient results for Test S-02-8 agree well with measurements of system variables. Typical transient results are shown in Figs. 12-14. Figure 12 shows the lower plenum pressure and Fig. 13 shows the mass flow rate from the pump side of the break. The calculated cladding temperature in the high power zone is compared in Fig. 14 with the band of temperatures measured in the same zone. Although the overall agreement in cladding temperature response is good, some detailed features were not predicted by TRAC. These include what appear to be random variations in the time to CHF and rewetting of some rods after the initial dryout. Running times for the steady-state and blowdown calculations were 50 min and 2 hrs, respectively.

The primary purpose of the 1/15-scale Creare downcomer experiments[15] was to study the effect of countercurrent steam flow rate, ECC water subcooling, and downcomer wall superheat on the delivery of ECC water from the downcomer to the lower plenum. The apparatus consisted of a vessel with downcomer, lower plenum, four cold leg ports, four simulated hot leg penetrations, and a steam injection port at the top. In the quasistatic experiments, a steady steam flow rate is established up the downcomer and water is then injected at a constant flow rate into three of the cold leg

ports; the other cold leg port simulates the broken cold leg. After an initial transient period, the steam and water flows reach a quasistatic state in which some or all of the injected water is bypassed and the remainder penetrates into the lower plenum. Data from these experiments are used to generate flooding curves which specify the amount of water delivered to the lower plenum as a function of the reverse steam flow rate. Flooding curves are generated for several values of ECC subcooling and liquid flow rate.

The TRAC best-estimate model for the Creare experiments consists of a three-dimensional vessel containing 112 fluid cells and one-dimensional piping connections for the injection and break ports. The calculational procedure closely parallels the experimental procedure. Results of the Creare calculations are in excellent overall agreement with experimental flooding curves for a wide range of ECC injection rates and subcoolings. This is shown in Figs. 15 and 16 which contain flooding curves for two different ECC injection rates and temperatures. The complete bypass and complete delivery points on the curves are well predicted by TRAC for both low and high subcooling cases. Computed results for the Battelle Columbus Laboratory (BCL) 2/15-scale facility[16] are in similar good agreement with the data indicating that scale effects in this range are properly treated. The CPU time for the steady-state (initial condition) runs was 5-30 min depending on steam flow rate. For the transient (ECC injection) calculations, the CPU time was 20-60 min depending on steam flow rate and ECC liquid temperature.

Assessment of the reflood heat transfer and quench front propagation models in TRAC has to date focused on the forced bottom flooding experiments in the PWR-FLECHT facility.[17] These experiments were run using a full-length fuel bundle containing electrically heated rods mounted in a square flow housing with upper and lower plenum regions. A chopped-cosine axial power profile representative of a PWR was used. Power to the fuel bundle was programmed to simulate reactor decay heat during the reflood phase of a LOCA. Prior to the reflood test the core test section and housing were preheated by supplying power to the rods and auxiliary housing heaters. With the lower plenum full of water and the test section containing only saturated steam, ECC

injection into the lower plenum was initiated when the desired maximum rod temperature was reached during the preheating period. The test program investigated the effects of initial clad temperature, flooding rate, power, inlet coolant temperature, and system pressure on reflood heat transfer.

The single-channel geometry of these experiments lends itself very well to the use of the slab vessel option in TRAC. As a matter of fact, a one-dimensional representation was obtained by using only one cell per axial level. The base case model contained 9 axial levels in the core with each of these levels containing 5 fine-mesh axial intervals for the reflood heat transfer calculation. Conduction in the electrically heated rod was represented with 8 radial nodes. Test conditions for the three cases calculated are given in Table IV and a summary of the calculated and measured results is given in Table V. TRAC-P1A predicts the maximum temperature (and hence the temperature rise) quite well for all three tests. For the high flooding rate case (Test 03541), the calculated turnaround time and quench time also agree very well with the data. This is not the case, however, for the low flooding rate tests where the code predicts early turnaround and quenching. Underprediction of the carryover rates results in a rapid refill of the core region and partially accounts for early quenching. TRAC-P1A does not contain an explicit entrainment model but this capability will be available when the droplet field is added in a future version (see Sec. IV). This capability, along with a better definition of a rewetting criterion, should significantly improve the code results for low flodding rates. The ratio of CPU time to transient time is about 25 for the FLECHT calculations.

The Loss of Fluid Test Facility (LOFT)[18] is a scale model of a large PWR with volume scaling of about 1:60. Test L1-4 was the fourth in a series of five isothermal blowdown tests in the non-nuclear LOFT program. The system consisted of a pressure vessel containing upper and lower plena, a downcomer, and a hydraulic core simulator; an intact loop containing a U-tube steam generator, two centrifugal pumps, and a pressurizer; a blowdown loop containing a simulated steam generator, simulated pump, and two quick-opening

valves; and a pressure suppression system. Test L1-4 was a 200% double-ended cold leg break starting from initial isothermal conditions of 552 K and 15.75 MPa. The ECCS consisted of accumulator, high pressure injection, and low pressure injection systems.

Test L1-4 was modeled with 26 TRAC components containing a total of 215 fluid cells 72 of which were used in the three-dimensional vessel model. Calculated initial steady state conditions were within 2% of the experimental values. The blowdown calculation was started from these initial conditions using the dump/restart feature of TRAC. Calculated transient results are in good overall agreement with the experimental measurements including mass flow rates, fluid temperatures, densities, and pressures throughout the system. Some typical examples are shown in Figs. 17-19. Figure 17 indicates the agreement obtained for pressures in the intact loop at the hot leg, cold leg, and pressurizer. The mass flow rate from the vessel side of the break is shown in Fig. 18 and the reactor vessel liquid mass is shown in Fig. 19. Effects resulting from the delayed ECC injection appear to be properly represented by the models in TRAC. Results for Test L1-4 indicate that TRAC provides a good representation of integral effects in LOFT during the blowdown and refill phases of a LOCA. The computer CPU times on the CDC 7600 were 40 s for the steady-state calculation and 40 min for the transient calculation.

In addition to LOFT Test L1-4, TRAC has been used to analyze Test L1-5. This test was also an isothermal blowdown experiment but with the nuclear core in place and in a shutdown state. The agreement between the code results and experimental measurements is similar to that for Test L1-4.

Posttest analyses have been performed for other experiments using earlier versions of TRAC. The most noteworthy of these were Semiscale Mod-1 integral tests S-06-3 (Standard Problem 8) and S-02-6 (Standard Problem 6). Test S-06-3 was a full 200% break LOCA from blowdown through reflood while S-02-6 was a single-ended small break experiment. Coarse-mesh models were used in these analyses to evaluate the accuracy of fast-running TRAC computations. Overall results of these computations were quite good, particularly for the large break test, and are reported in Refs. 19 and 20. The large-break integral test required 169 min of CPU time for the 250 s transient. For the small-break test, 85 min of CPU time were required for the 500 s transient.

A TRAC-P1A posttest analysis of Semiscale Mod-3 Test S-07-6 is currently in progress. The Mod-3 facility differs from Mod-1 in that it has a longer core (3.66 m vs 1.66 m), an active rather than a passive broken loop, and an external downcomer pipe instead of the normal internal annular downcomer. Test S-07-6 was the first integral LOCA test in the Mod-3 baseline series and was a 200% cold leg break with cold leg ECC injection. Some of the future developmental assessment activities for TRAC-P1A will include posttest analyses of FLECHT gravity reflood experiments, upper and lower plenum injection tests and condensation-induced transients in Semiscale, Creare and BCL ECC bypass transients, and blowdown heat transfer tests in the Thermal Hydraulic Test Facility (THTF) at ORNL.

B. Independent Assessment

Independent assessment of TRAC is being performed using tests from a wide variety of thermal-hydraulic facilities both in the United States and abroad. The principal facilities for this activity are given in Table VI. Note that these facilities span a wide range of scales and types.

Pretest and posttest predictions have been performed[21] for the first LOFT nuclear test L2-2 (Test L2-1 was cancelled) and posttest analyses are in progress[22]. Tests in the L2 series[23] are loss-of-coolant experiments conducted at gradually increasing power levels to determine the nuclear core and systems response during all phases of a LOCA. Experiments in this series simulate a 200% double-ended offset shear in the cold leg. Test L2-2 was conducted at a 50% power level of 25 MWt and an intact hot leg temperature of 580 K. The actual initial conditions for Test L2-2 were quite different from those estimated before the test. These differences significantly affected the overall dynamics of the calculation. TRAC posttest predictions of Test L2-2 were in good agreement with most of the data except that early rewetting and subsequent sequence of dryouts and rewets of the rods in the highest power region were not predicted. At other locations the calculated cladding response was in good agreement with experiment. An example is shown in Fig. 20 where the calculated cladding temperature near the core midheight of the lower power rods is compared with thermocouple readings

in the same zone. The calculated peak clad temperature was 840 K compared to the measured value of 790 K. Posttest analyses of this test indicate that an improved rewet correlation is required to more accurately model this phenomenon. These analyses also indicate that the rewetting behavior is not sensitive to reasonable variations in the fuel rod gap conductance during the transient. In addition there is a possibility that the fin effect due to the external thermocouples could initiate early rewetting of the cladding to which they are attached.

A pretest calculation for Test L2-3 is currently in progress. This test is similar to L2-2 but will be conducted at 37 MW. Pretest and posttest predictions and posttest analyses will be performed for all future tests in the LOFT facility. A posttest prediction for a small break test (S-07-10B) in the Semiscale Mod-3 facility is also in progress. This test is being treated as a standard problem by the NRC.

The LOBI facility at Ispra, Italy will offer the first opportunity for a TRAC prediction of a "new" test facility. LOBI is a full-height and approximately 1/700 volume scale model of a 4-loop PWR. It consists of a 5.3 MW electrically heated rod bundle within a pressure vessel and two active coolant loops. The facility will be used to study the blowdown and bypass/refill phases of a LOCA. Design information for the LOBI facility has been received and a TRAC prediction of the first experiment is in progress.

The FLECHT-SEASET (Full-Length Emergency Cooling Heat Transfer-Separate Effects And System Effects Tests) experiments at Westinghouse (W) are a continuation of the original PWR FLECHT and FLECHT-SET programs. They are designed to study fuel rod heat transfer and two-phase flow effects during the reflood phase of a LOCA. As implied by the title, both separate effects and system effects tests will be conducted in this facility. The separate effects tests will be performed first and will focus on rod bundle heat transfer and thermal-hydraulic behavior. The system effects tests will be performed in a closed loop which includes simulation of the downcomer, core, upper plenum, and steam generator. Two forced flooding separate effects tests are the first TRAC predictions that will be performed for the SEASET facility. It is anticipated that these tests, which have been designated as standard problems, will be performed by June 1979. TRAC predictions of subsequent separate effects and system effects tests will be performed as appropriate.

The PKL (primarkreislaufe) facility in West Germany is a full-height integral refill/reflood facility containing a 340-rod electrically heated core, external downcomer, and three coolant loops with steam generators. As compared to a full-scale PWR, the volume scaling of PKL is approximately 1:130. A posttest analysis is currently in progress for Core I of this facility. Another Core I test has been designated a standard problem and a TRAC posttest prediction for this test is also in progress. Future testing in PKL will use a better instrumented core (Core II) and TRAC predictions (pretest and posttest) will be performed as appropriate.

The Japanese Cylindrical and Slab Core Test Facilities (CCTF and SCTF) and the German Upper Plenum Test Facility (UPTF) are part of a multinational (U.S., Germany, Japan) program to investigate refill/reflood phenomena during a LOCA. The LASL role in this program is to provide design assistance and test predictions/analyses using TRAC, provide advanced instrumentation (stereo lens), and perform small-scale entrainment/de-entrainment experiments. CCTF is very similar to PKL but contains 2000 heater rods rather than 340. System shakedown tests have been performed and a base-case test is planned in May 1979. TRAC analysis of the last shakedown test and a pretest prediction for the base test are in progress at this writing.

SCTF and UPTF are full-scale separate-effects facilities which address multidimensional phenomena in the reactor vessel during the reflood process. These facilities are in the design stage and complement each other in that they model different regions of the reactor vessel internals in great detail. The main feature of SCTF is a full-scale two-dimensional (slab) core containing 2000 electrically heated rods; the UPTF features a full-scale three-dimensional upper plenum with the associated upper plenum internals. At present TRAC is being used to provide design assistance by performing calculations for these two facilities and for full-scale PWRs. The PWR calculations provide prototypical initial and boundary conditions for the separate-effects tests. Testing in these facilities is expected to begin in 1980 (SCTF) and 1982 (UPTF).

IV. FUTURE DEVELOPMENTS

Based on the TRAC results for LOFT Test L2-2, a sensitivity study was initiated to determine if one of the rewet correlations available in the literature is more suitable than the one currently in TRAC. This study is still in progress but initial results indicate that a correlation that takes into account quality and mass flux, in addition to liquid and wall properties as in the current one, will greatly improve agreement with experiment. The entire reflood heat transfer methodology is being re-examined to improve the reliability of the computations. Development of a dynamic fuel-rod gap model is in progress. Improvements to other constitutive relations will continue to be made based on further code testing and new experimental data.

Development of more efficient and faster numerical integration schemes is a continuing activity. We are currently investigating the use of higher order spatial integration methods to allow better treatment of sharp liquid/vapor interfaces and the use of larger hydrodynamic mesh cells. A fast-running TRAC version, suitable for sensitivity studies and parametric analyses, is scheduled for future development. This code will be either a one-dimensional version or a coarse-node multidimensional version with appropriately modified constitutive relations.

A two-fluid one-dimensional hydrodynamics capability has been developed and is being tested. This capability can be used in both the development of the one-dimensional code and the development of a vessel module for Boiling Water Reactors (BWRs). Another major capability under development is addition of a droplet field to allow entrainment, transport, and de-entrainment of drops as well as countercurrent flow of drops and films. This capability will allow better treatment of carryover phenomena and entrainment/deentrainment/film formation on the upper plenum internals and pool formation above the upper core support plate. An initial code version containing this capability is currently being tested.

Injection of nitrogen into the primary system when the accumulators empty during a LOCA can have a significant effect on fluid properties, phase-change rates, wall heat transfer, etc. Therefore work is in progress on adding a noncondensable-gas field to TRAC.

TRAC versions to handle anticipated transients without scram, reactivity insertion accidents, and operational transients are scheduled for future development. The major requirements here are a one- or two-dimensional treatment of core neutronics with feedback and development of code modules for the required secondary loop components and plant protection system.

V. ACKNOWLEDGEMENTS

A large number of people have contributed to the work described in this article and it is impossible to acknowledge all of them here. Key LASL personnel and their primary area of contribution are D. R. Liles, hydrodynamic methods; J. H. Mahaffy, numerical methods; W. L. Kirchner, heat transfer methods; J. M. Sicilian, code architecture and programming; K. A. Williams, code assessment; and J. F. Jackson, project management.

REFERENCES

1. "TRAC-P1: An Advanced Best-Estimate Computer Program for PWR LOCA Analysis. Volume I: Methods, Models, User Information, and Programming Details," Los Alamos Scientific Laboratory report LA-7279-MS, Vol. I (NUREG/CR-0063) (June 1978).

2. "TRAC-P1A: An Advanced Best-Estimate Computer Program for PWR LOCA Analysis," Los Alamos Scientific Laboratory report LA-7777-MS (NUREG/CR-0665) (May 1979).

3. J. C. Vigil and K. A. Williams (Compilers), "TRAC-P1A Developmental Assessment Calculations," Los Alamos Scientific Laboratory report (to be published).

4. K. V. Moore and W. H. Rettig, "RELAP4: A Computer Program for Transient Thermal-Hydraulic Analysis," Aerojet Nuclear Company report ANCR-1127 (December 1973).

5. D. R. Liles and K. A. Taggart, "A Three-Dimensional Two-Fluid Hydrodynamics Code for a PWR Reactor Vessel," Proc. ANS Topical Meeting on Thermal Reactor Safety, Sun Valley, Idaho, CONF-770708, 2, 81 (1977).

6. Wm. H. Reed and W. L. Kirchner, "Fluid Dynamics and Heat Transfer Methods for the TRAC Code," Proc. Thermodynamics and Fluid Mechanics Group Conference, University of Manchester, C205/77, p. 97 (1977).

7. D. R. Liles and Wm. H. Reed, "A Semi-Implicit Method for Two-Phase Fluid Dynamics," Journal of Computational Physics, 26, 390 (March 1979).

8. J. H. Mahaffy and D. R. Liles, "Application of Implicit Numerical Methods for Problems in Two-Phase Flow," Los Alamos Scientific Laboratory report LA-7770-MS, NUREG/CR-0763 (April 1979).

9. R. J. Pryor, D. R. Liles, and J. H. Mahaffy, "Treatment of Water Packing Effects," Trans. ANS 1978 Winter Meeting, Washington, D.C., 30, 208 (1978).

10. A. R. Edwards and T. P. O'Brien, "Studies of Phenomena Connected with the Depressurization of Water Reactors," J. British Nucl. E. Soc., 9, 125 (April 1970).

11. A. Premoli and W. T. Hancox, "An Experimental Investigation of Subcooled Blowdown with Heat Addition," Submission to Committee on Safety of Nuclear Installations, Specialists Meeting on Transient Two-Phase Flow, Toronto, Ontario (August 1976).

12. L. Ericson, L. Gros d'Aillon, D. Hall, J. Ravnsborg, O. Sandervag, and H. Akesson, "The Marviken Full-Scale Critical Flow Tests Interim Report; Results from Test 4," Marviken draft interim report MXC-204 (May 1978).

13. S. A. Noff and P. A. Pinson, "1-1/2 Loop Semiscale Isothermal Test Program and System Description in Support of Experiment Data Reports," Aerojet Nuclear Company report ANCR-1143 (February 1974).

14. L. J. Ball, D. J. Hanson, K. A. Dietz, and D. J. Olson, "Semiscale Program Description," Idaho National Engineering Laboratory report TREE-NUREG-1210 (May 1978).

15. C. J. Crowley, J. A. Block, and C. N. Cary, "Downcomer Effects in a 1/15-Scale PWR Geometry: Experimental Data Report," Creare, Inc. report NUREG-0281 (May 1977).

16. R. A. Cudnik, L. J. Flanigan, R. C. Dykhuizen, W. A. Carbiener, and J. S. Liu, "Topical Report on Baseline Plenum Filling Behavior in a 2/15-Scale Model of a Four Loop Pressurized Water Reactor," Battelle Columbus Laboratories report BMI-1997 (NUREG/CR-0069) (April 1978).

17. J. O. Cermak, "PWR Full-Length Emergency Cooling Heat Transfer (FLECHT) Group I Test Report," Westinghouse Electric Company report WCAP-7435 (January 1970).

18. H. C. Robinson, "LOFT Systems and Test Description (Loss-of-Coolant Experiments Using a Core Simulator)," Idaho National Engineering Laboratory report, TREE-NUREG-1019 (November 1976).

19. J. R. Ireland and P. B. Bleiweis, "TRAC Calculations of U.S. Standard Problem 8," reported in "Nuclear Reactor Safety Quarterly Progress Report, July 1 - September 30, 1978," Los Alamos Scientific Laboratory report LA-7567-PR (NUREG/CR-0522), p. 12 (December 1978).

20. K. A. Williams, "TRAC Calculation of Standard Problem 6," reported in "Nuclear Reactor Safety Quarterly Progress Report, July 1 - September 30, 1978," Los Alamos Scientific Laboratory report LA-7567-PR (NUREG/CR-0522), p. 21 (December 1978).

21. K. A. Williams, "Pretest and Posttest Predictions of LOFT Nuclear Test L2-2," reported in "Nuclear Reactor Safety Quarterly Progress Report, October 1 - December 31, 1978," Los Alamos Scientific Laboratory report LA-7769-PR (NUREG/CR-0762), p. 49 (May 1979).

22. D. A. Mandell and K. A. Williams, "L2-2 Parametric Study," reported in "Nuclear Reactor Safety Quarterly Progress Report, January 1 - March 31, 1979," Los Alamos Scientific Laboratory report LA-7867-PR (NUREG-CR/0868), p. 18 (July 1979).

23. D. L. Reeder, "LOFT System and Test Description (5.5-ft Nuclear Core 1 LOCES)," EG&G Idaho, Inc. report TREE-1208 (NUREG/CR-0247) (July 1978).

TABLE I. TRAC COMPONENT MODULES

Module	Description
VESSEL	Models a PWR vessel and associated internals using either a three-dimensional (r-θ-z) or two-dimensional (x-y) geometrical representation and a six-equation two-fluid model to evaluate fluid flows within the vessel. VESSEL includes rod heat transfer with reflood dynamics in one-dimensional and cylindrical geometry, slab heat transfer from structure, and point reactor kinetics with decay heat.
PIPE	Models thermal-hydraulic flow in a one-dimensional duct or pipe using the five-equation drift-flux model. PIPE can treat area changes, wall heat sources, wall friction, and heat transfer across the inner and outer wall surfaces. Both semi-implict and fully implicit solution algorithms are available in this module.
PRIZER	Simulates a pressurizer using the one-dimensional drift-flux model with drift velocities specified to produce a sharp liquid/vapor interface during discharge. The pressurizer walls are adiabatic but energy transfer from a heater/sprayer system is simulated.
PUMP	Describes the interaction of the two-phase fluid with a centrifugal pump using the PIPE capabilities and pump correlations for the mixture momentum source.
ACCUM	Simulates an accumulator filled with ECC water and pressurized with nitrogen gas using the one-dimensional drift-flux model. The vapor-phase properties are those for nitrogen gas and drift velocities are specified to produce a sharp liquid/vapor interface during discharge. Nitrogen is not allowed to discharge from the accumulator because a noncondensible field is not yet available in the basic hydrodynamics model.
STGEN	Models either a "U-tube" or "once-through" type steam generator using the one-dimensional drift-flux model. Primary and secondary side hydrodynamics are treated separately with coupling through wall heat transfer.

TABLE I (cont'd)

Module	Description
TEE	Models the thermal-hydraulics of three piping branches (two of which lie along a common line with the third entering at an arbitrary angle) using essentially two pipes.
VALVE	Models the thermal-hydraulic flow in a valve using the basic PIPE capabilities. Valve action is modeled by controlling the flow area and hydraulic diameter between the two fluid cells.
BREAK	Imposes a fixed or time-dependent pressure boundary condition one cell away from its adjacent component. BREAK is not actually a system component but is treated as such with respect to input, initialization, and identification procedures.
FILL	Imposes fixed or time-dependent velocity boundary conditions at the junction with its adjacent component. The observation made for BREAK applies here also.

TABLE II. TRAC FUNCTIONAL MODULES

Module	Description
DF1D	Solves the finite-difference equations for the one-dimensional drift-flux model using either a semi-implicit or fully implicit algorithm.
TF3D	Solves the finite-difference equations for the multidimensional two-fluid model using a semi-implicit algorithm. TF3D includes a constitutive package to provide wall and interfacial shears and interfacial mass and heat transfer.
THERMO	Provides thermodynamic properties of water and steam.
FWALL	Computes two-phase wall friction factors and loss coefficients associated with abrupt area changes.
SLIP	Calculates relative velocities between vapor and liquid phases for the one-dimensional drift-flux model. The procedure is based on a flow regime map similar to that used in the three-dimensional vessel hydrodynamics.
RODHT	Solves the one-dimensional (cylindrical) finite-difference thermal-conduction equations in the fuel rod including pellet, gap, and clad regions.
SLABHT	Solves for the lumped parameter temperature of a slab of arbitrary configuration.
CYLHT	Solves the one-dimensional (cylindrical) finite-difference thermal-conduction equations in pipe walls.
HTCOR	Provides heat transfer coefficients from wall to fluid based on local conditions.

TABLE III

TRAC-P1A DEVELOPMENTAL ASSESSMENT ANALYSES

Experiment	Thermal-Hydraulic Effects
1. Edwards Horizontal Pipe Blowdown (Standard Problem 1)	Separate effects, one-dimensional critical flow, phase change, slip, wall friction
2. CISE Unheated Pipe Blowdown (Test 4)	Same as 1 plus pipe wall heat transfer, flow area changes, and gravitational effects
3. CISE Heated Pipe Blowdown (Test R)	Same as 2 plus critical heat flux (CHF)
4. Marviken Full-Scale Vessel Blowdown (Test 4)	Same as 1 plus full-scale effects
5. Semiscale 1-1/2 Loop Isothermal Blowdown (Test 1011, Standard Problem 2)	Synergistic and system effects, one-dimensional flow, phase change, slip, wall friction, critical nozzle flow
6. Semiscale Mod-1 Heated Loop Blowdown (Test S-02-8, Standard Problem 5)	Same as 5 plus 3-D vessel model with rod heat transfer including nucleate boiling, DNB, and post-DNB
7. Creare Quasistatic Downcomer/ECC Bypass Experiments	Separate effects, countercurrent flow, interfacial drag and heat transfer, condensation
8. FLECHT Forced Flooding Tests	Separate effects, reflood heat transfer, quench front propagation, liquid entrainment and carryover
9. Nonnuclear LOFT Blowdown with Cold Leg Injection (Test L1-4, Standard Problem 7)	Integral effects during blowdown and refill, scale midway between Semiscale and full-scale PWR

TABLE IV

FLECHT EXPERIMENTAL TEST CONDITIONS FOR TRAC CALCULATIONS

Test Number	Pressure (MPa)	Inlet Fluid Temperature (K)	Flooding Rate (m/s)	Peak Power (kW/m)
03541	0.39	337.6	0.25	4.07
04831	0.28	324.8	0.04	3.12
02414	0.28	327.1	0.02	2.76

TABLE V

SUMMARY OF CALCULATED AND MEASURED RESULTS AT THE FLECHT BUNDLE MIDHEIGHT

	Test 03541		Test 04831		Test 02414	
	Exp.	TRAC	Exp.	TRAC	Exp.	TRAC
Initial Temperature (K)	1143	1144	1144	1144	1144	1144
Max. Temperature (K)	1193	1190	1333	1333	1453	1449
Temperature Rise (K)	50	46	189	189	308	305
Turnaround Time (s)	8	6	74	40	96	80
Quench Time (s)	71	72	219	170	345	210

TABLE VI. TRAC INDEPENDENT ASSESSMENT FACILITIES

Facility	Location	Scale	Description
Semiscale Mod-3	INEL	Small	Integral LOCA facility with full-height core, two active coolant loops, external downcomer, and UHI capability.
LOBI	Ispra	Small	Blowdown/refill facility with two active coolant loops and full-height simulation of a PWR.
FLECHT-SEASET	W	Small	Separate and systems effects reflood facility with a single-bundle full-height core and one external loop.
Nuclear LOFT	INEL	Intermediate	Integral LOCA test facility with nuclear core and two active coolant loops.
PKL	FRG	Intermediate	Full-height refill/reflood facility with three coolant loops (no pumps), external downcomer, and 340-rod core.
CCTF	Japan	Intermediate	Reflood facility with two coolant loops (no pumps) and a 2000-rod cylindrical core.
SCTF	Japan	Large	Separate-effects reflood facility with full-scale slab core, upper and lower plena, and simulated downcomer.
UPTF	FRG	Large	Separate-effects full-scale upper plenum (including internals) test facility with downcomer and lower plenum.
Marviken III	Sweden	Large	Separate-effects facility for full-scale critical pipe flow.

FIGURES

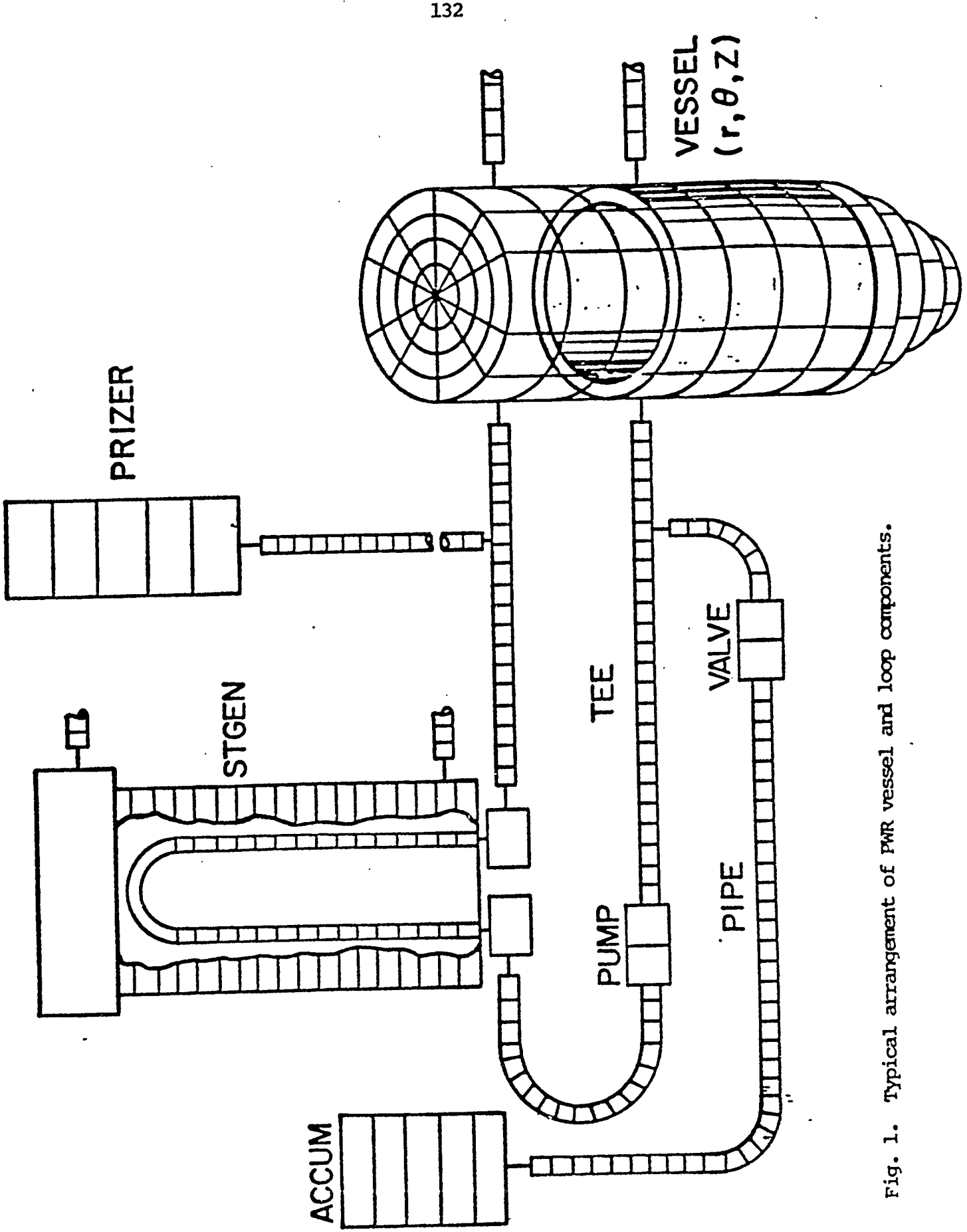

Fig. 1. Typical arrangement of PWR vessel and loop components.

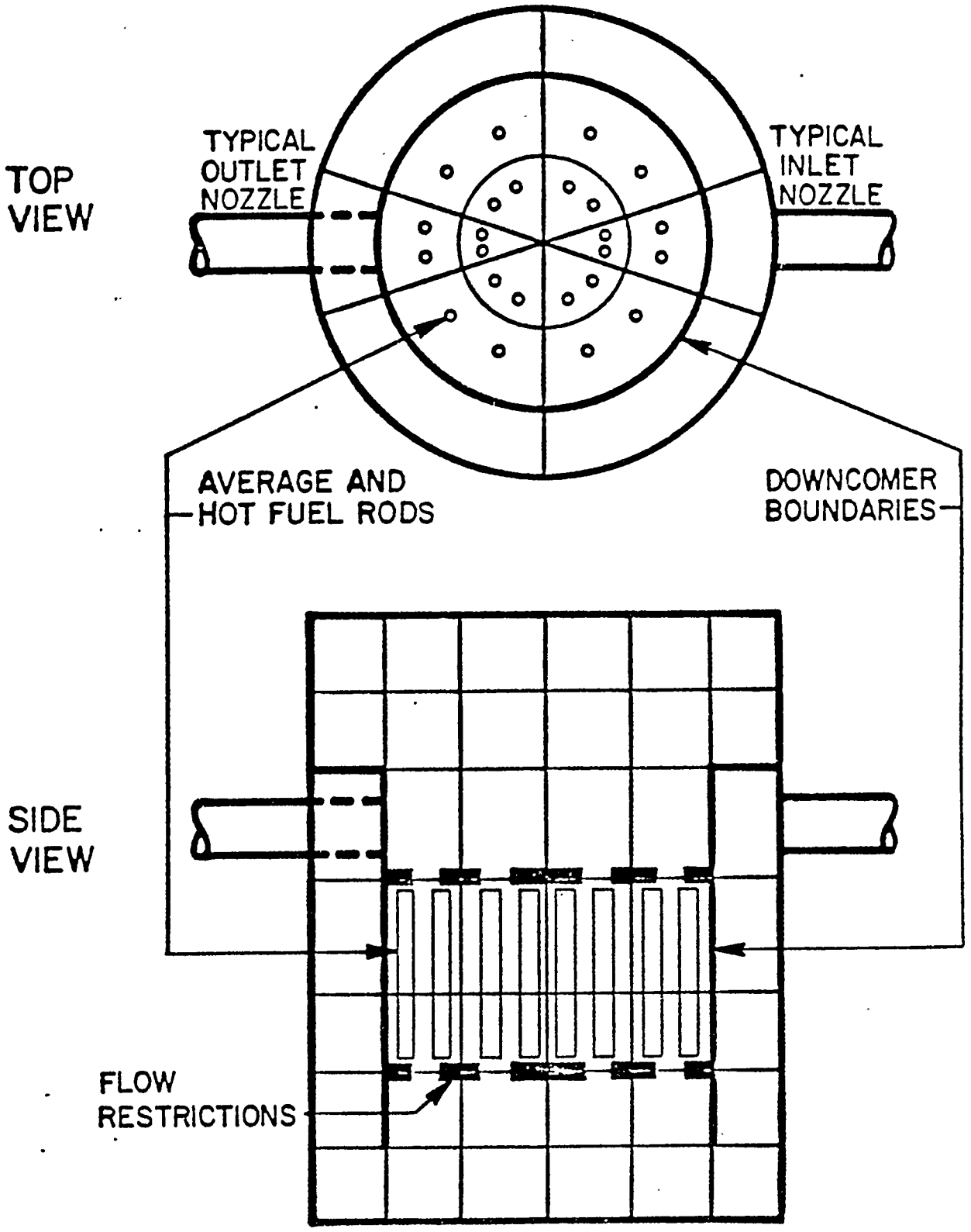

Fig. 2. Typical noding schematic for a three-dimensional reactor vessel.

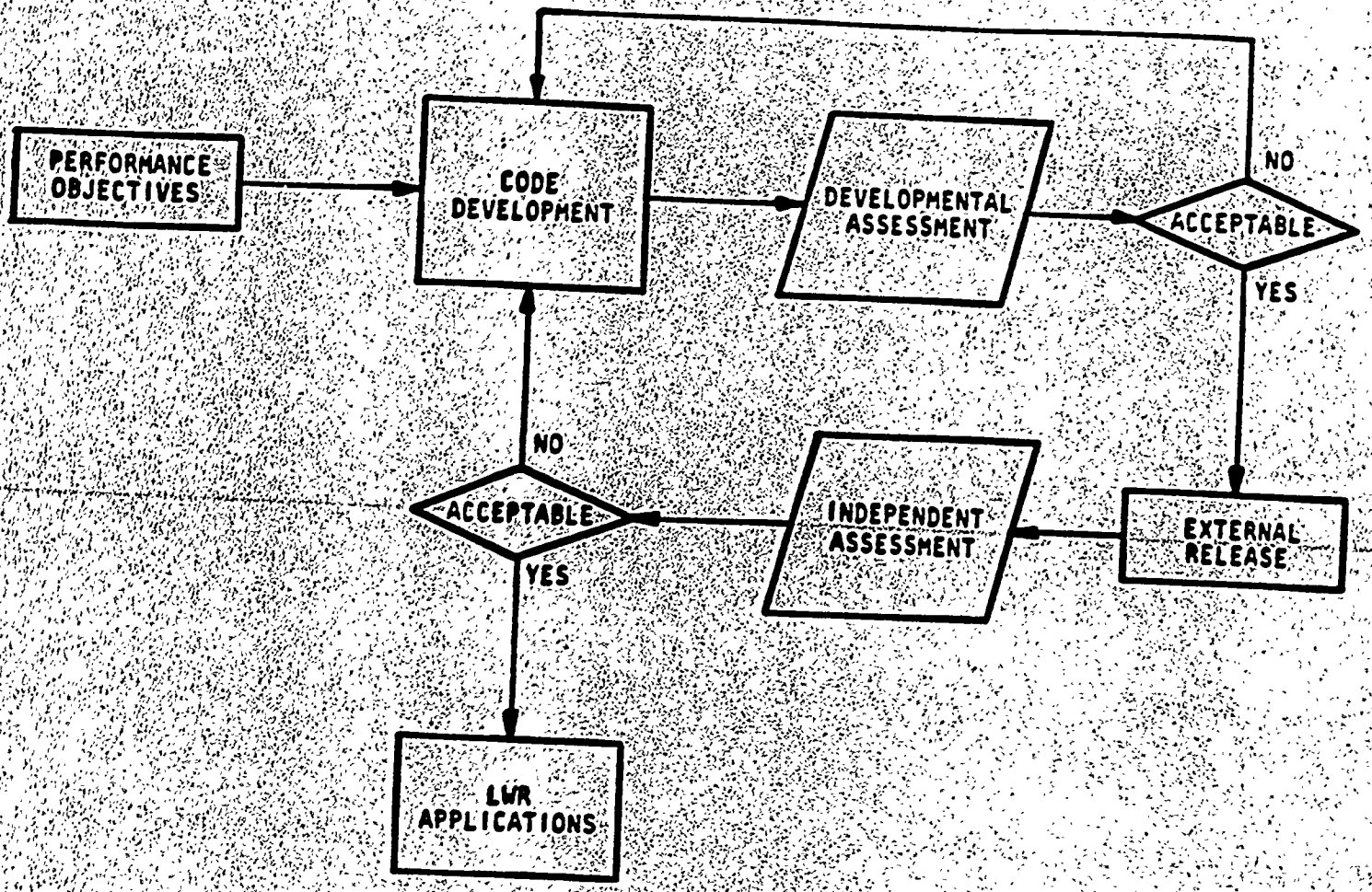

Fig. 3. Procedure for TRAC assessment.

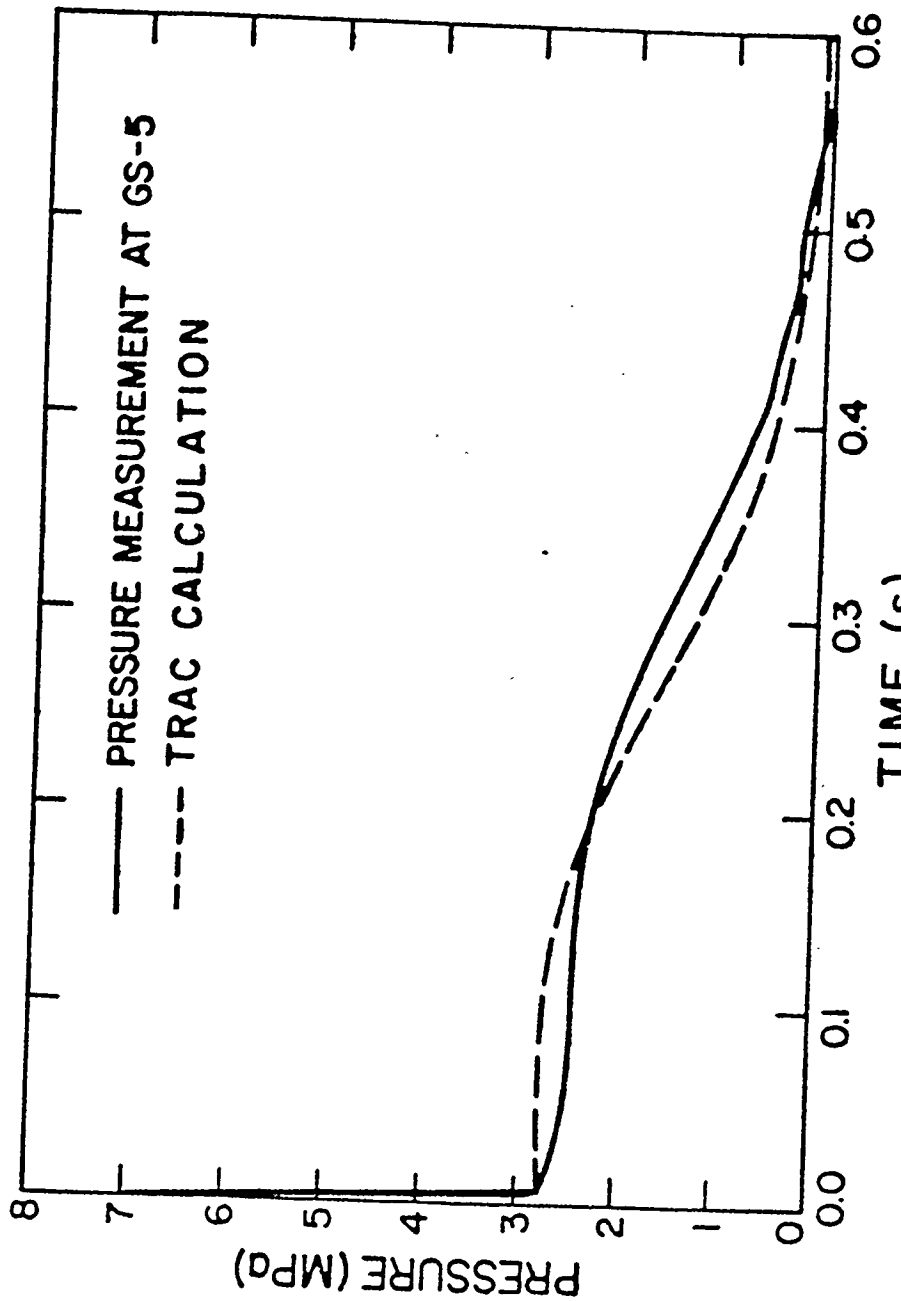

Fig. 4. Fluid pressure for Edwards blowdown experiment at location GS-5.

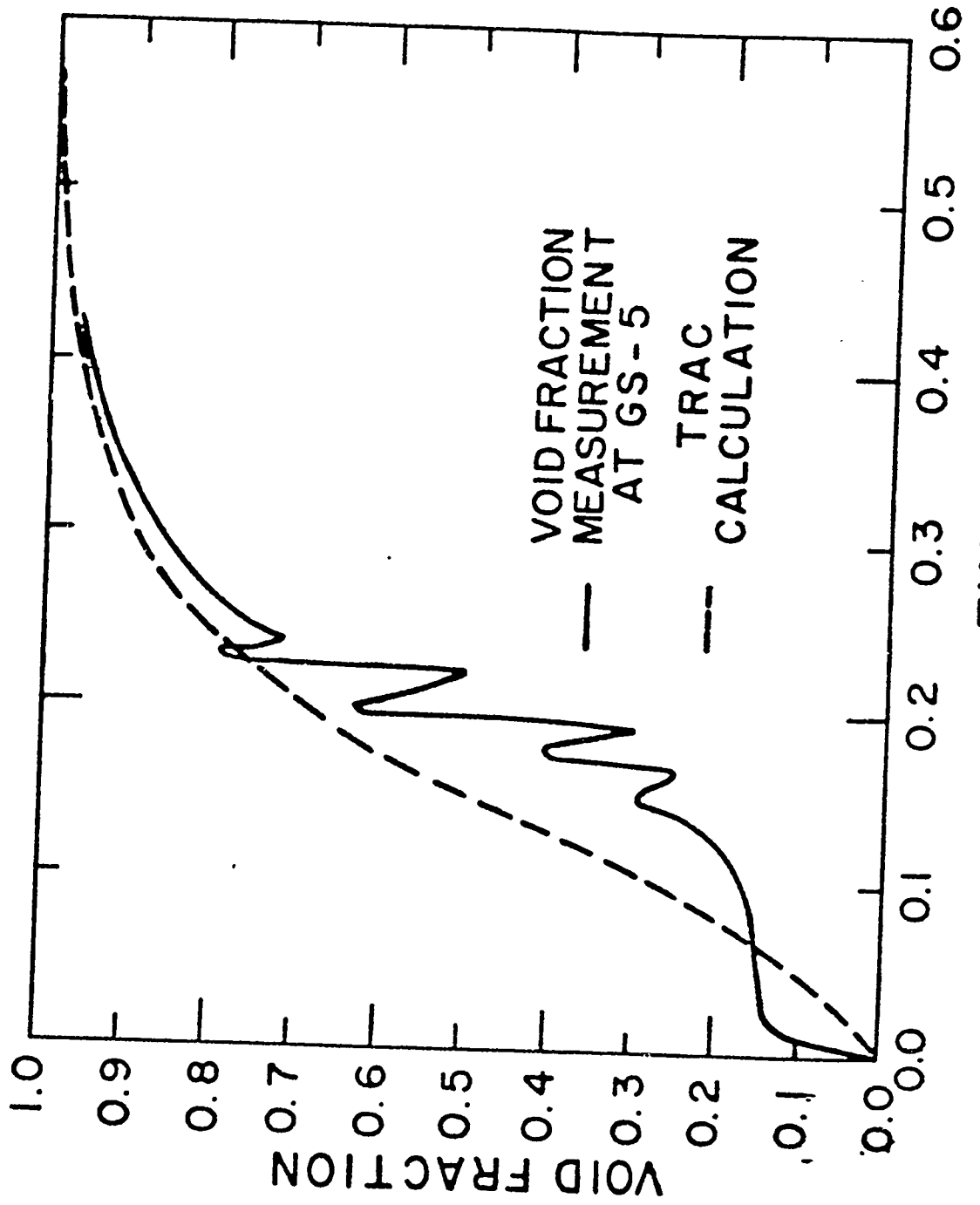

Fig. 5. Void fraction for Edwards blowdown experiment at location GS-5.

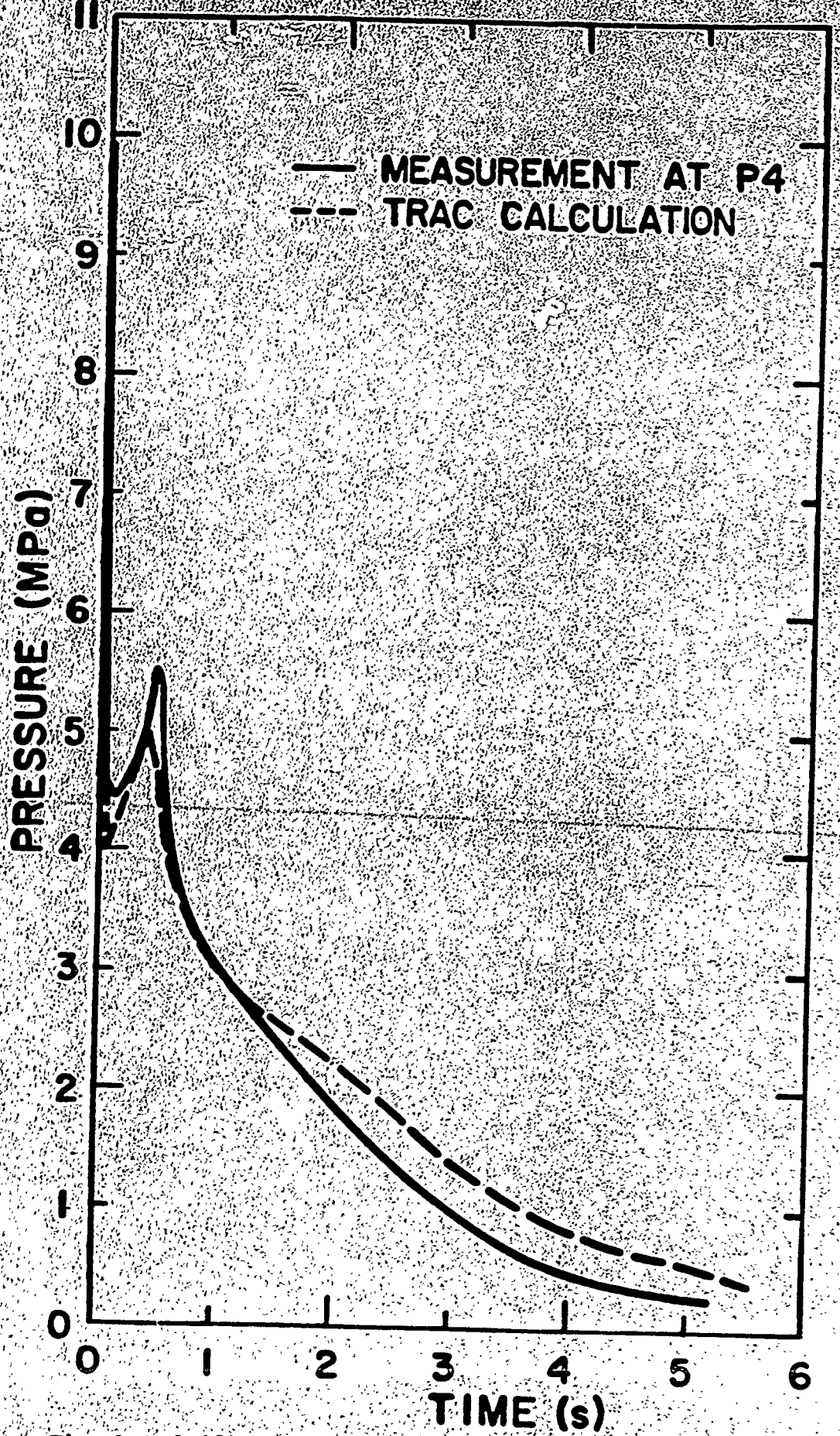

Fig. 6. Fluid pressure near the break for CISE heated blowdown test.

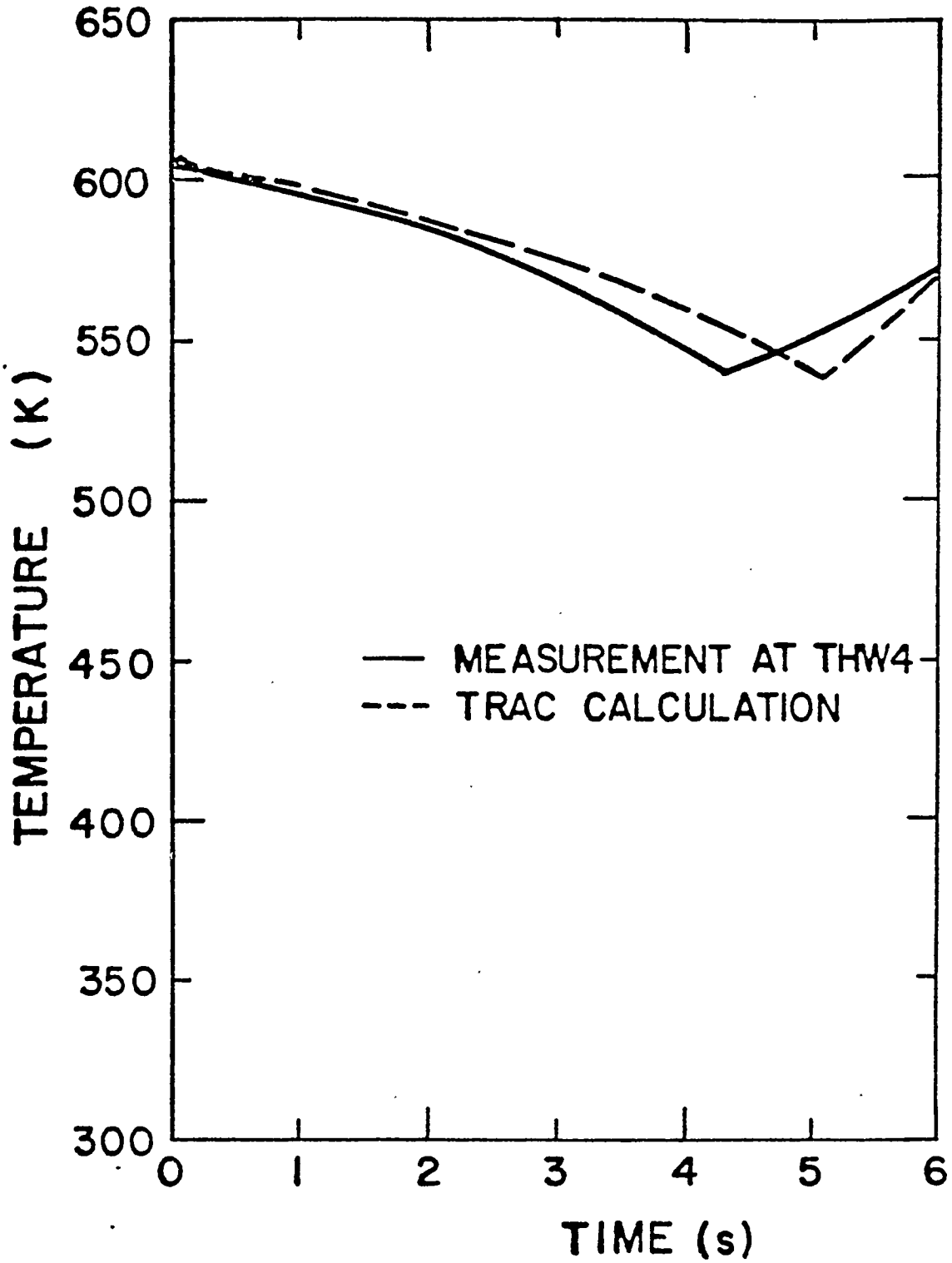

Fig. 7. Heater wall temperature for CISE heated blowdown test.

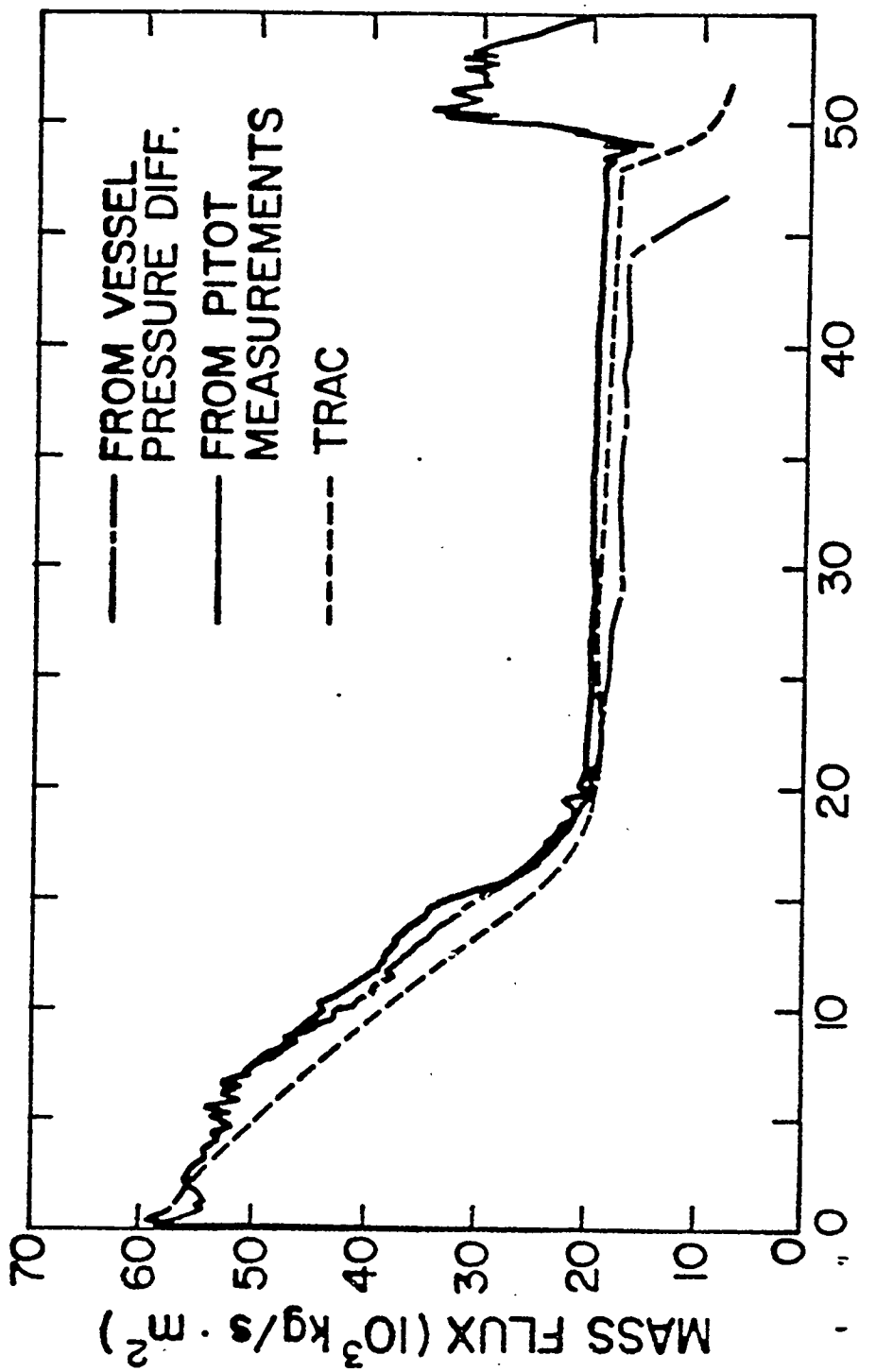

Fig. 8. Mass flux for Marviken blowdown experiment (Test 4).

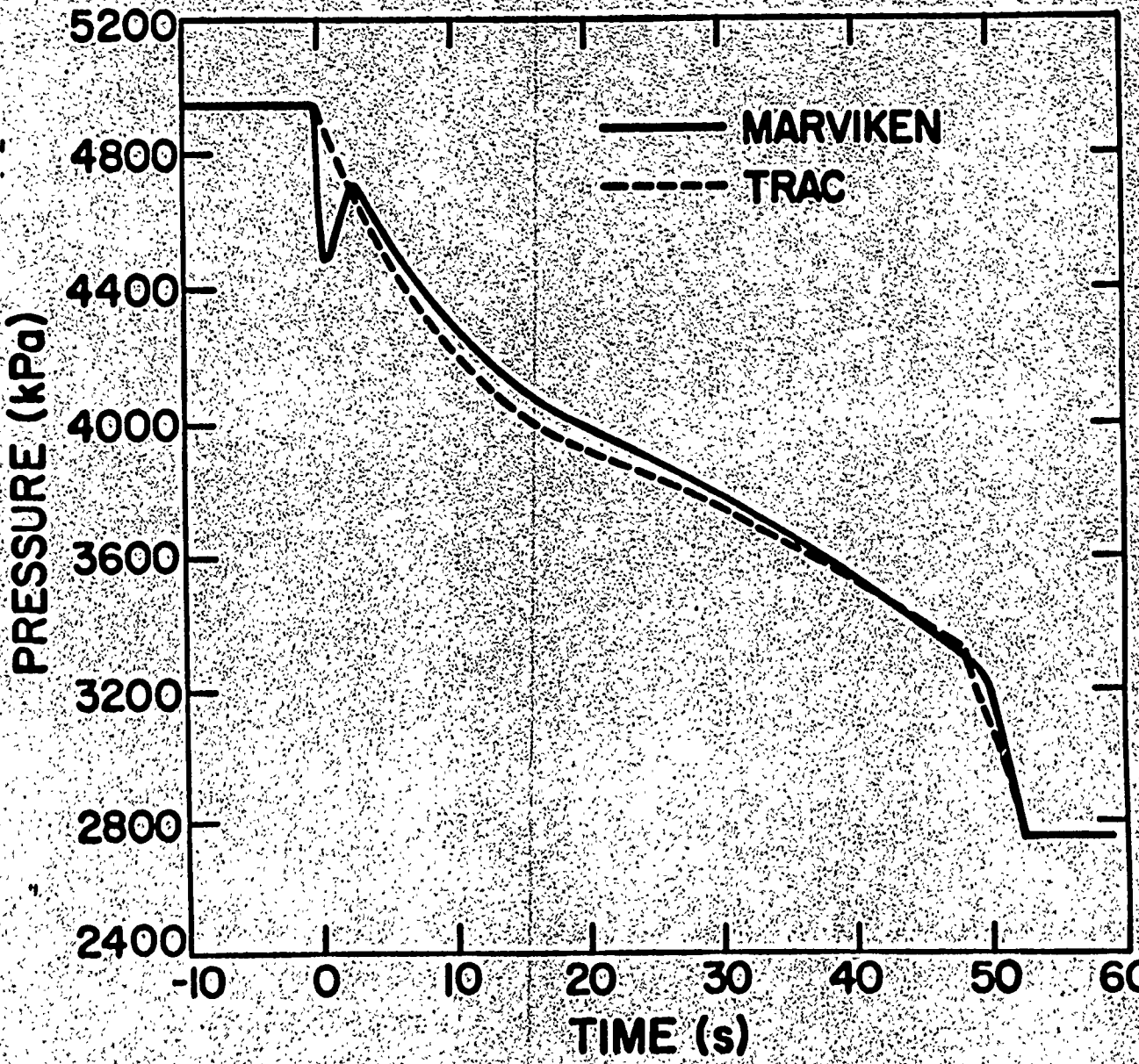

Fig. 9. Pressure near top of vessel for Marviken Test 4.

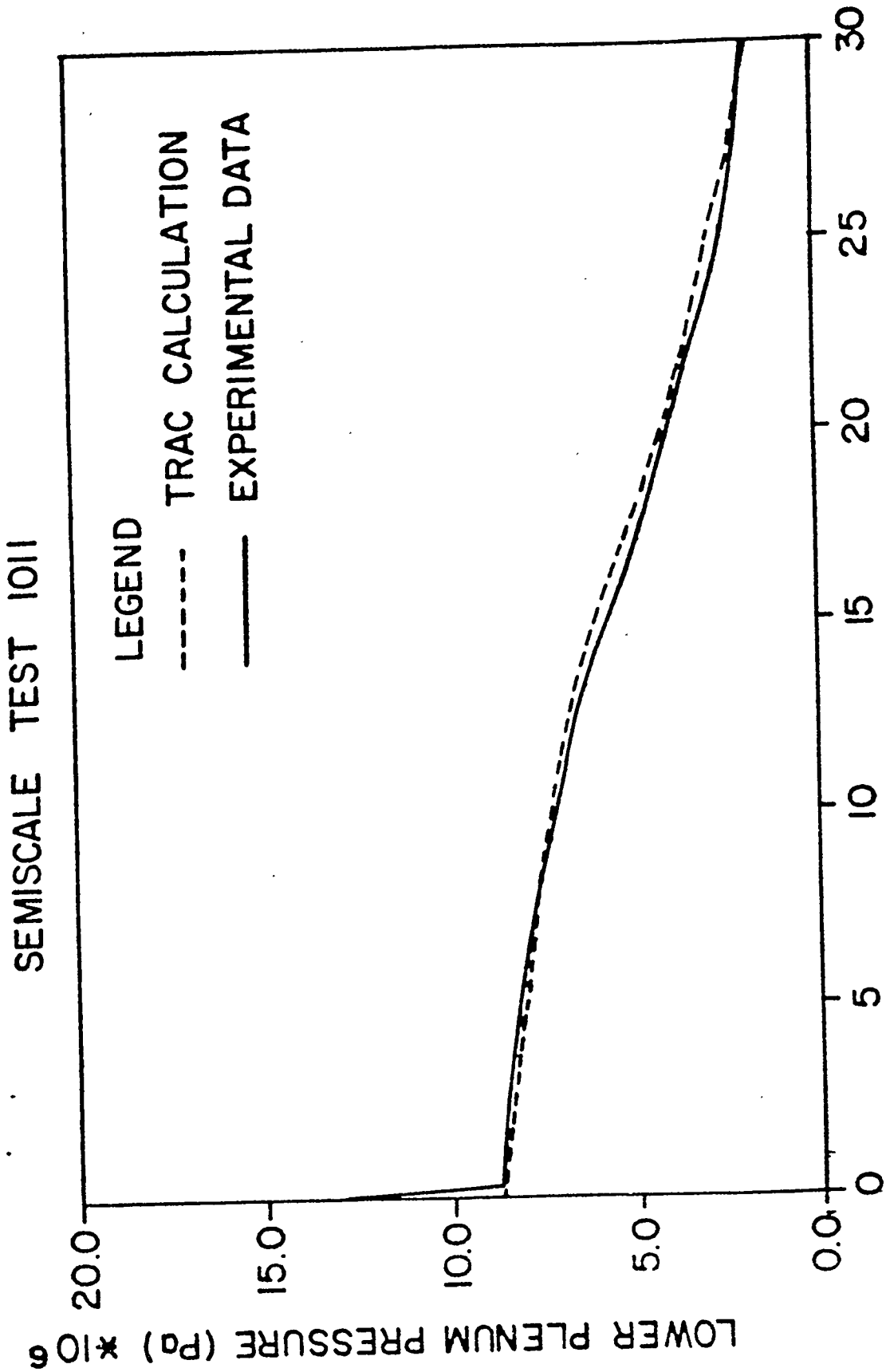

Fig. 10. Lower plenum pressure for Semiscale isothermal blowdown (Test 1011).

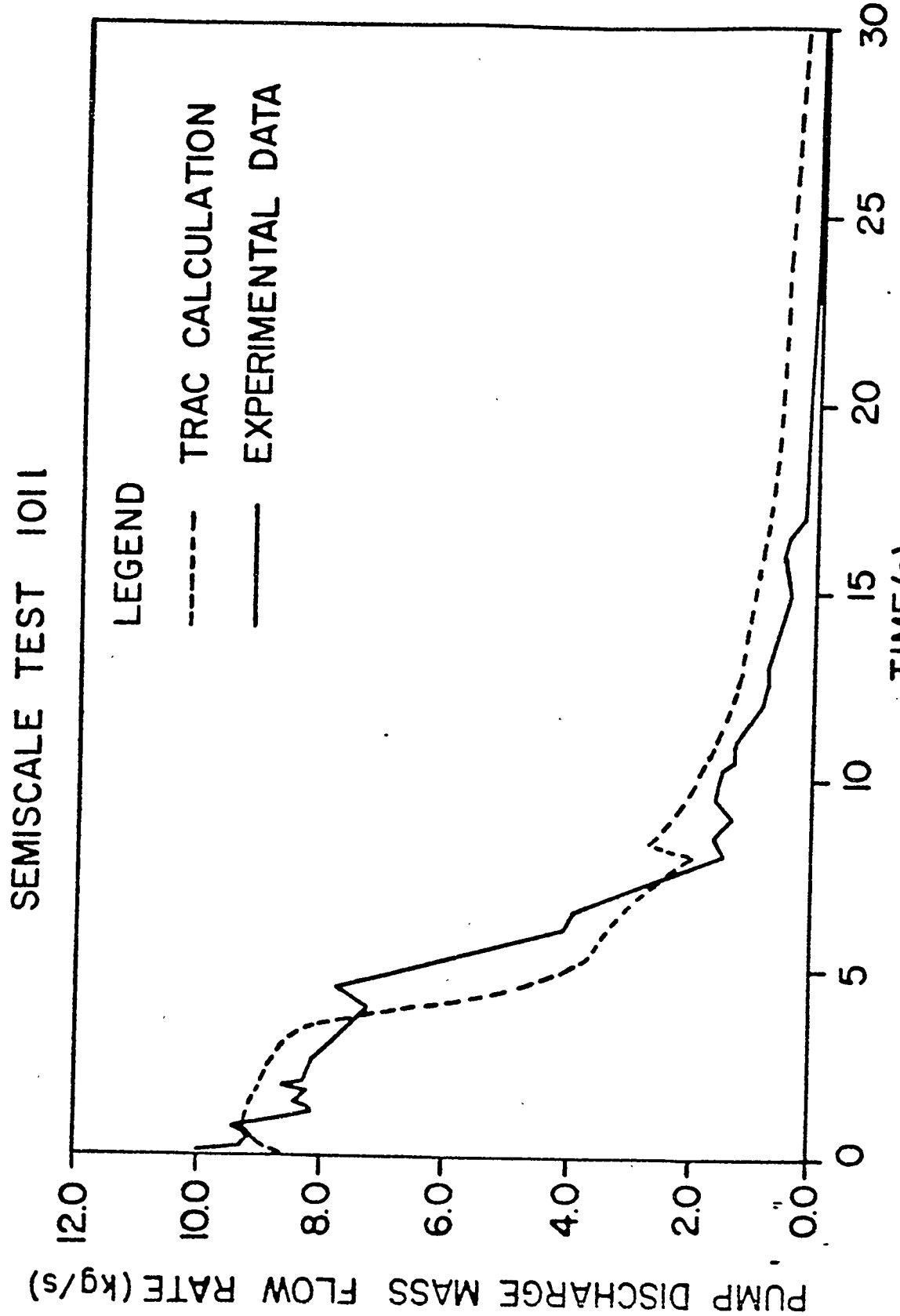

Fig. 11. Pump discharge mass flow rate for Semiscale isothermal blowdown (Test 1011).

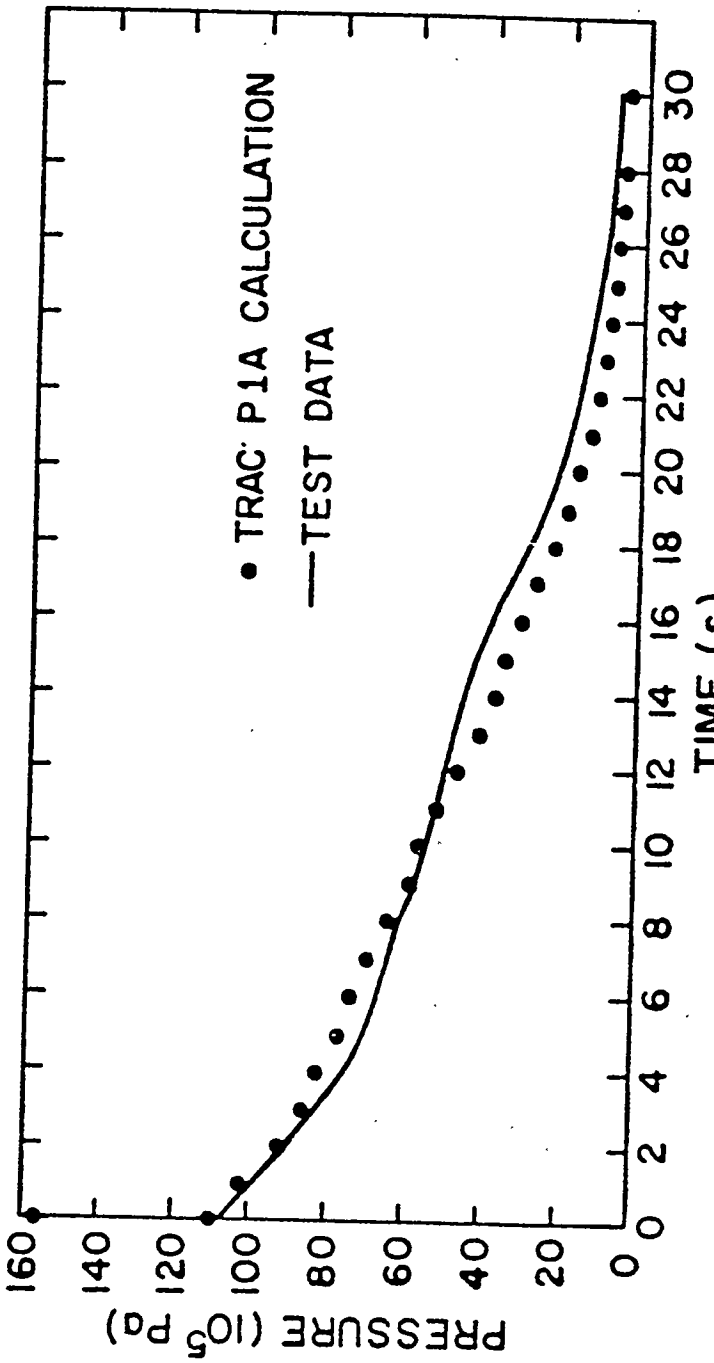

Fig. 12. Lower plenum pressure for Semiscale heated blowdown (Test S-02-8).

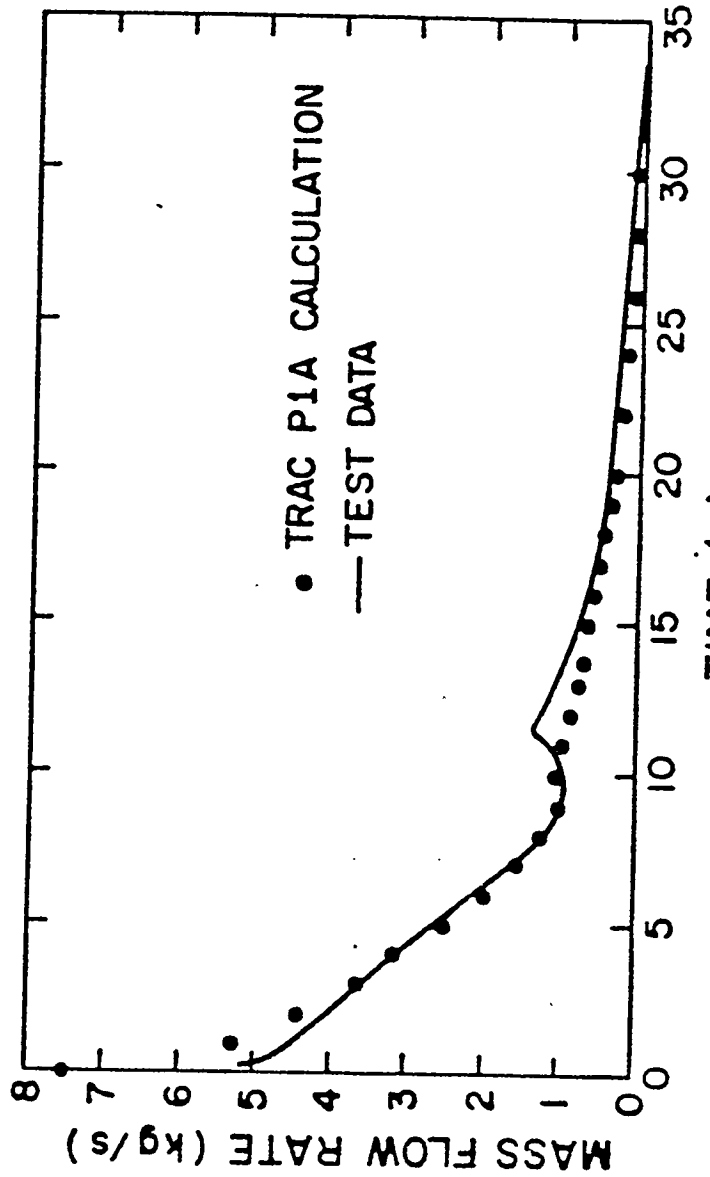

Fig. 13. Hot-leg break mass flow rate for Semiscale Test S-02-8.

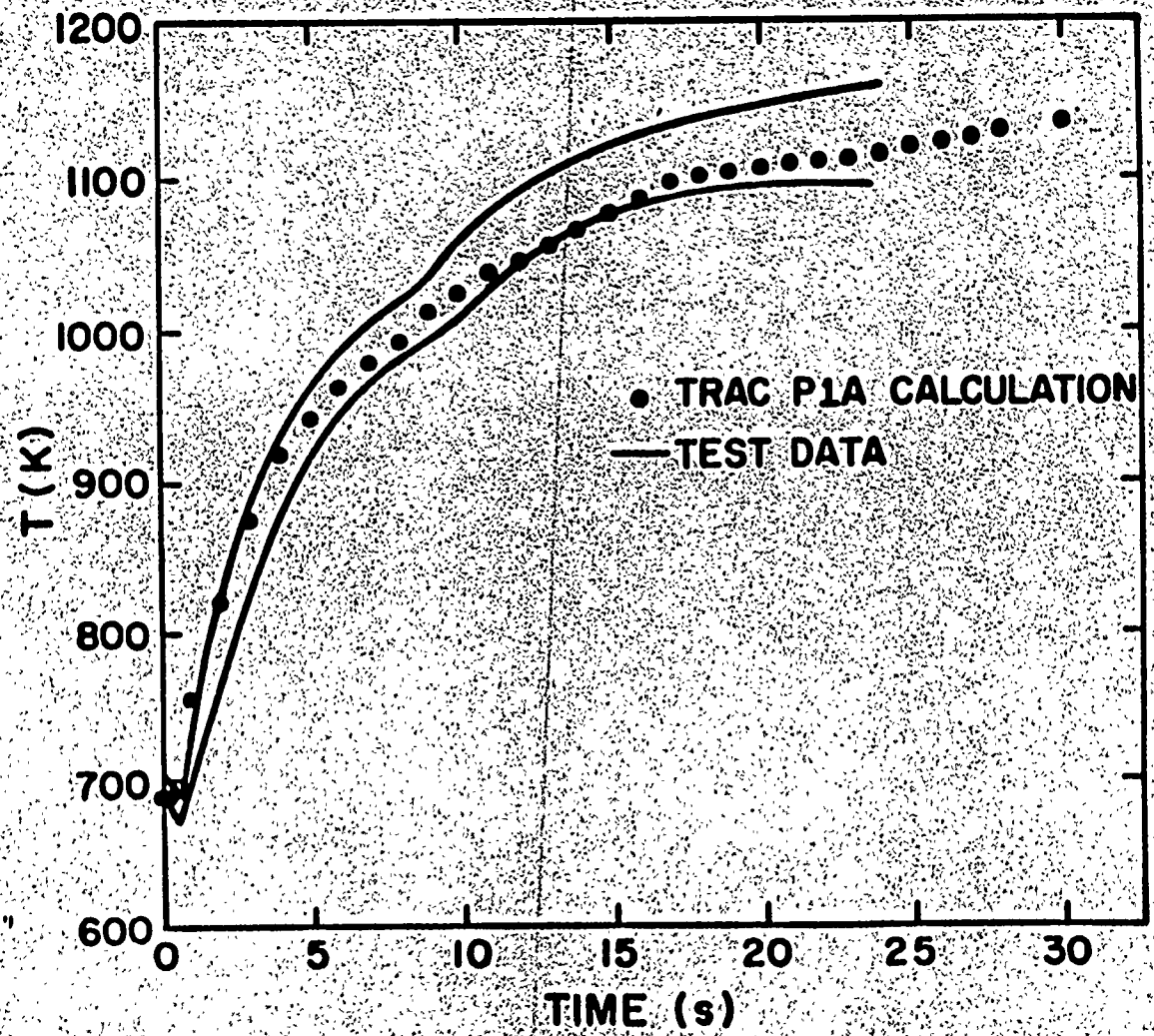

Fig. 14. Cladding temperature in high power zone for Semiscale Test S-02-8.

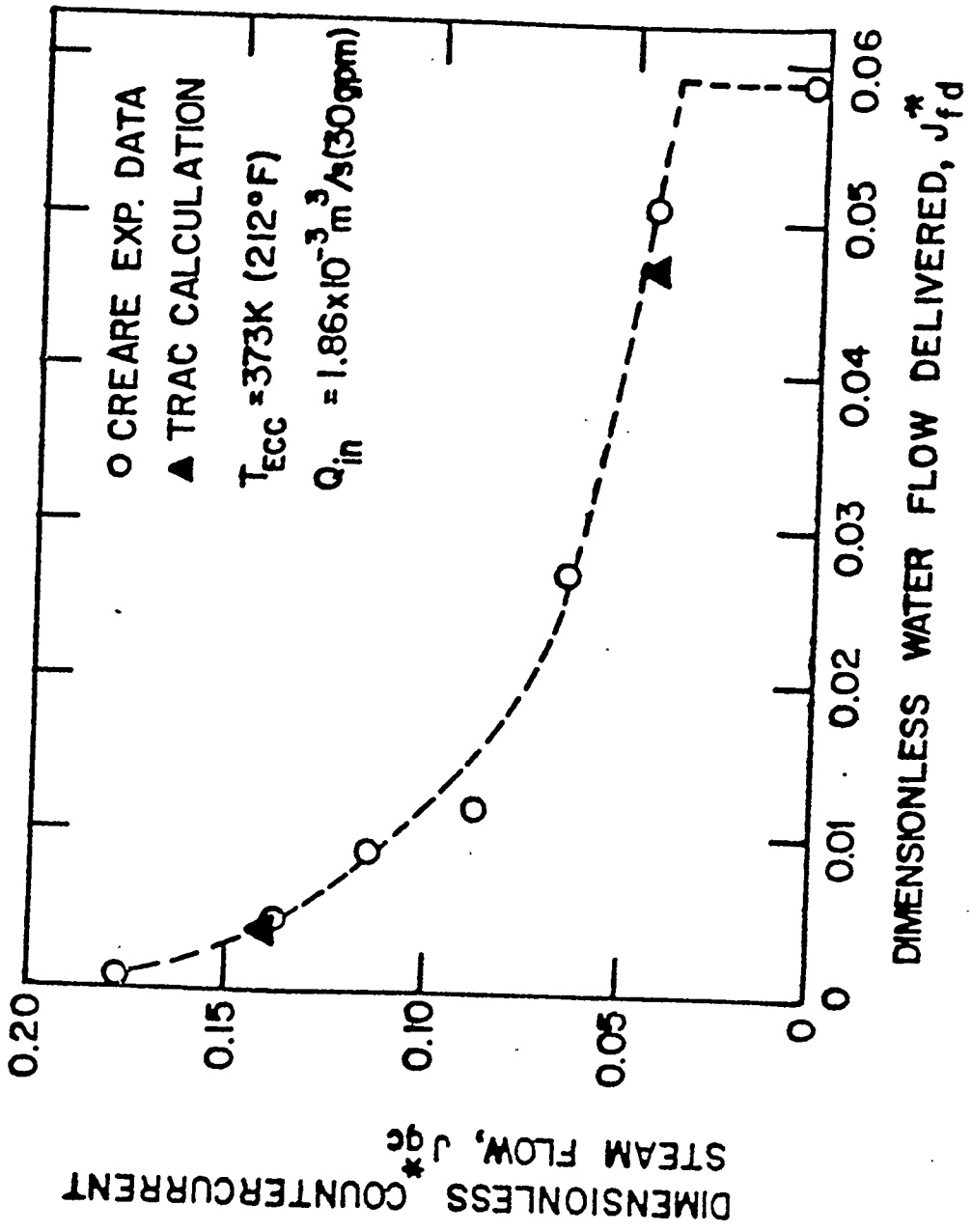

Fig. 15. Flooding curve for Creare low subcooling tests.

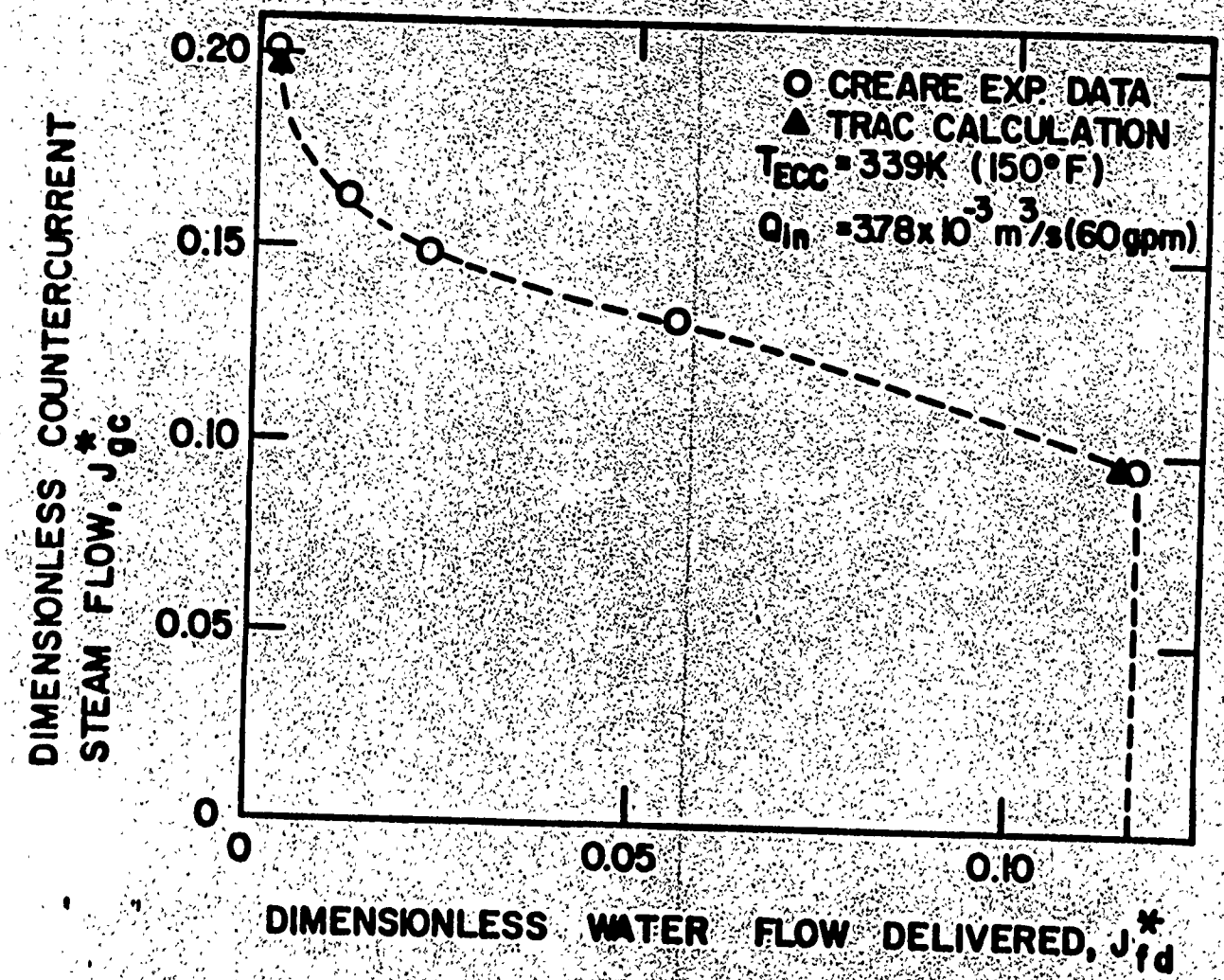

Fig. 16. Flooding curve for Creare high subcooling tests.

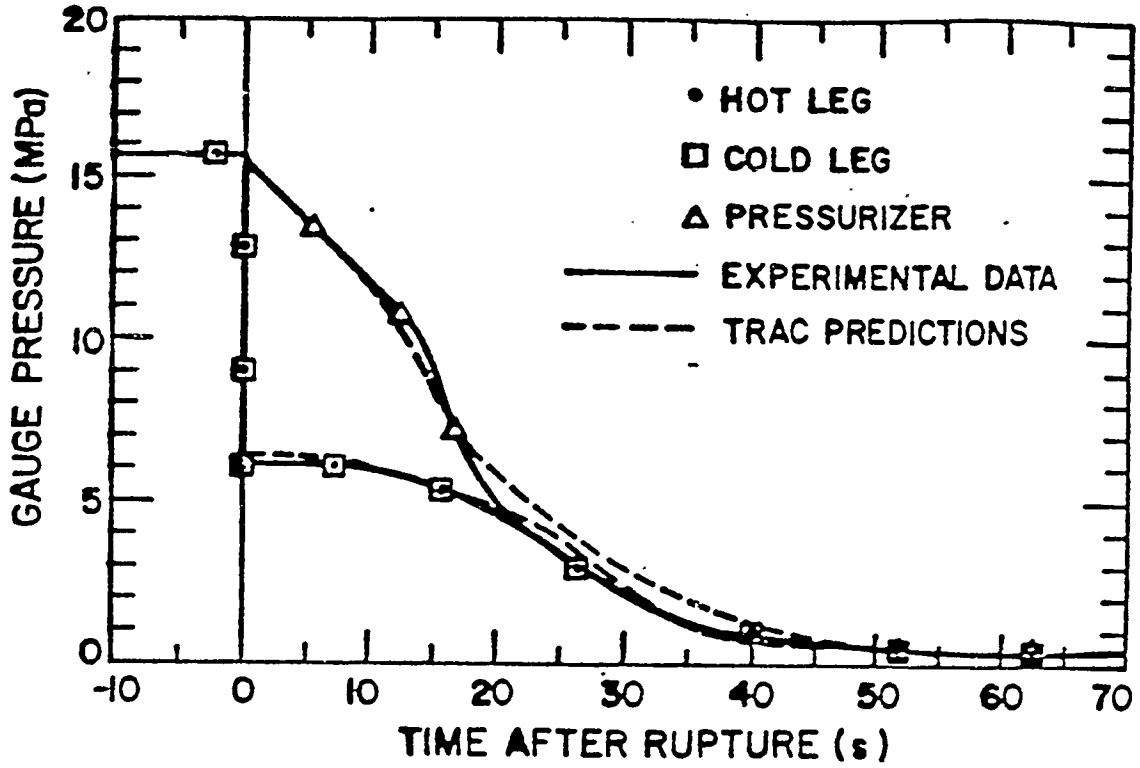

Fig. 17. Intact loop pressures for LOFT Test L1-4.

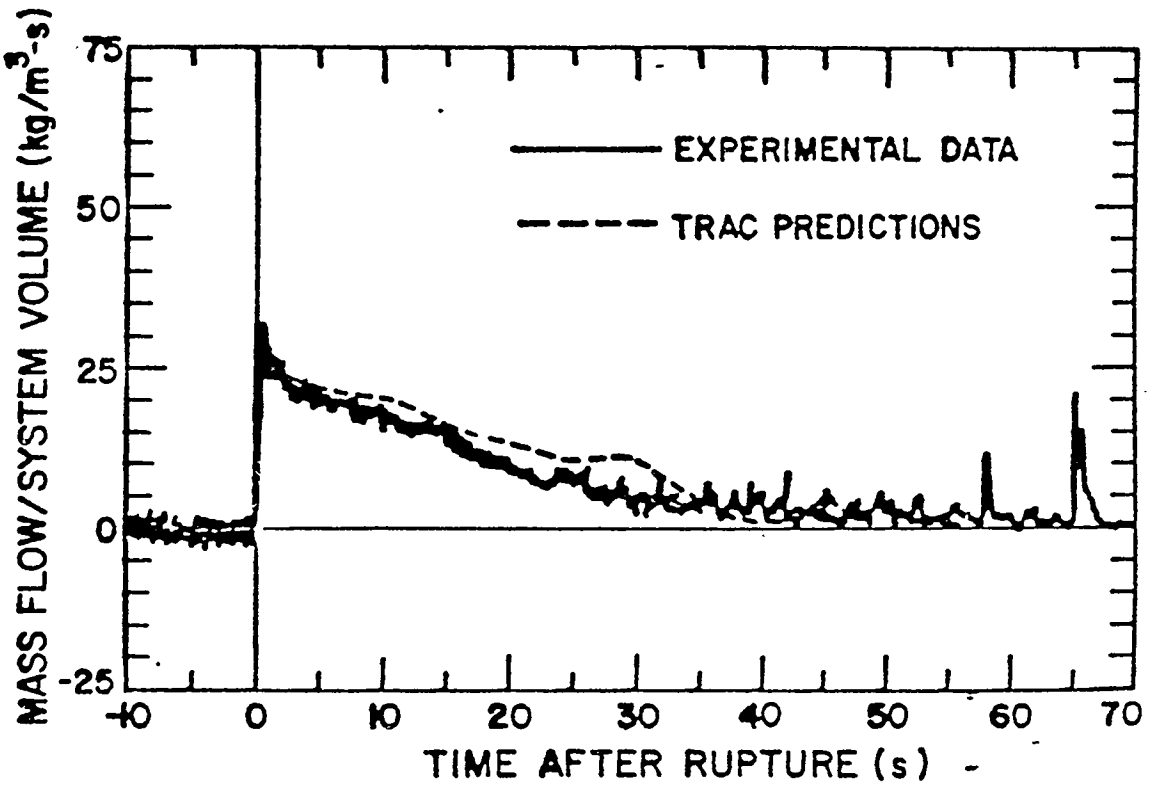

Fig. 18. Vessel-side break mass flow rate for LOFT Test L1-4.

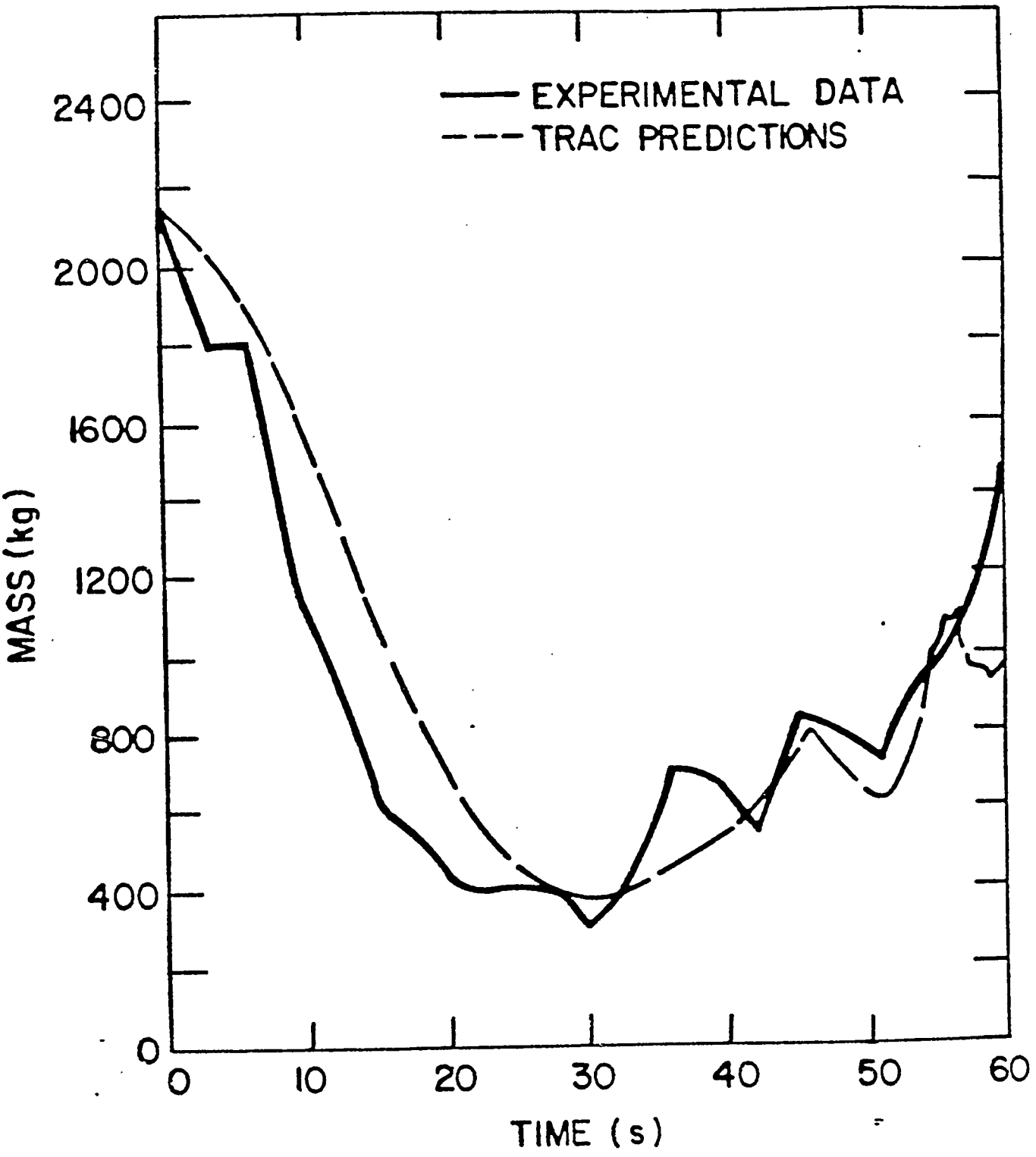

Fig. 19. Reactor vessel liquid mass for LOFT Test L1-4.

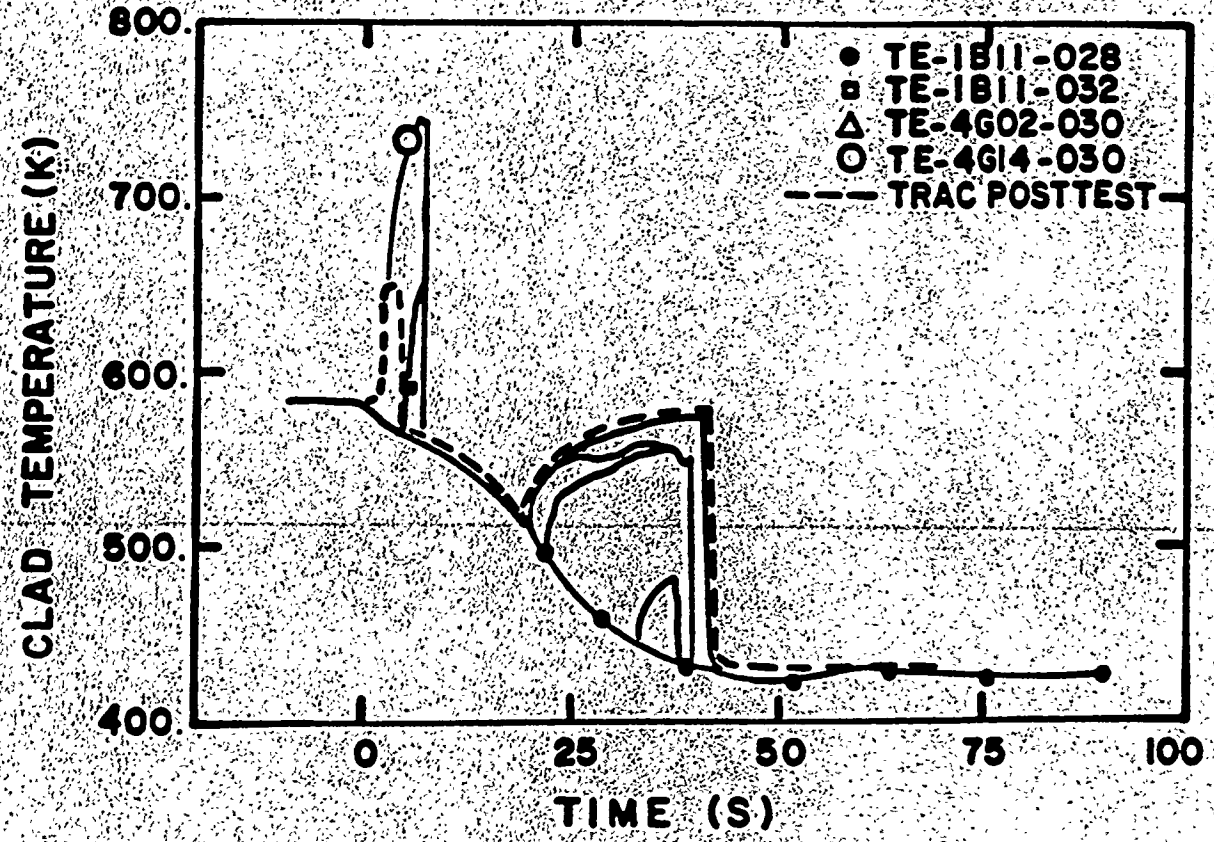

Fig. 20. Cladding temperature response near core midheight for low power rods in LOFT Test L2-2.

APPENDIX B-1

ADDITIONAL PLOTS FOR BASE CASE CALCULATION

$0 \leq T \leq 81$ minutes

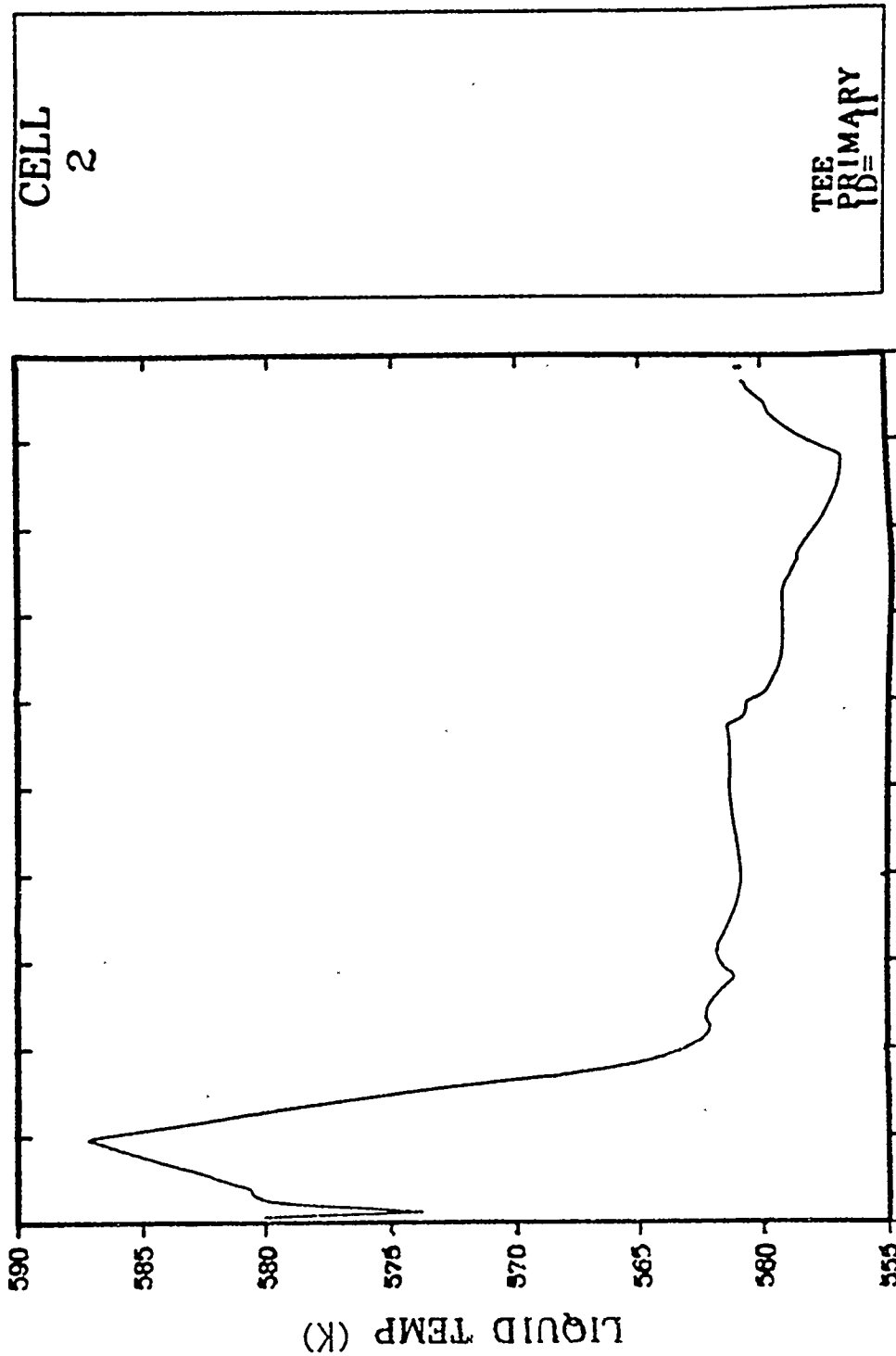

Fig. B-1.1. A Loop hot-leg liquid temperature.

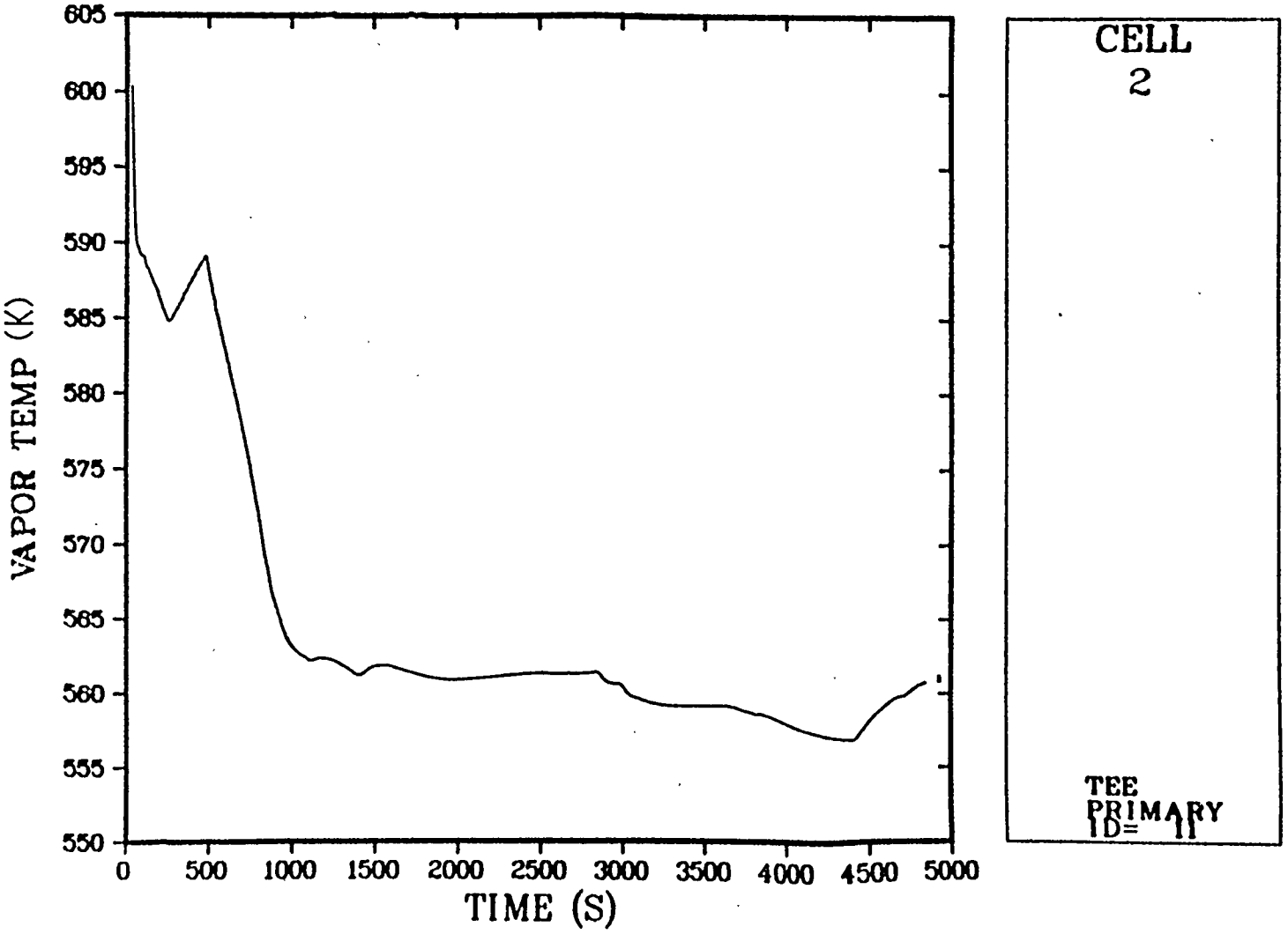

Fig. B-1.2. A Loop hot-leg vapor temperature.

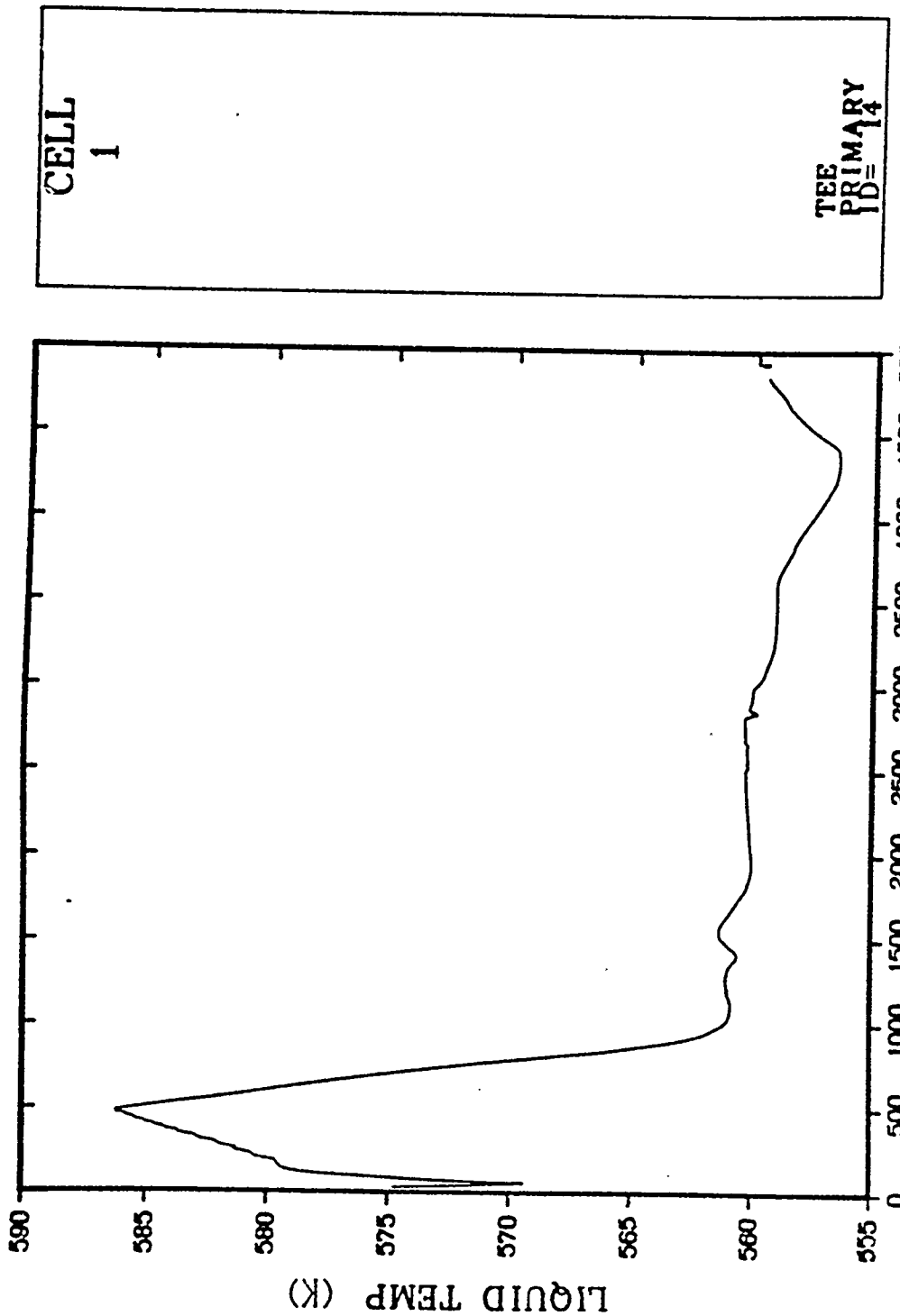

Fig. B-1.3. A Loop cold-leg liquid temperature.

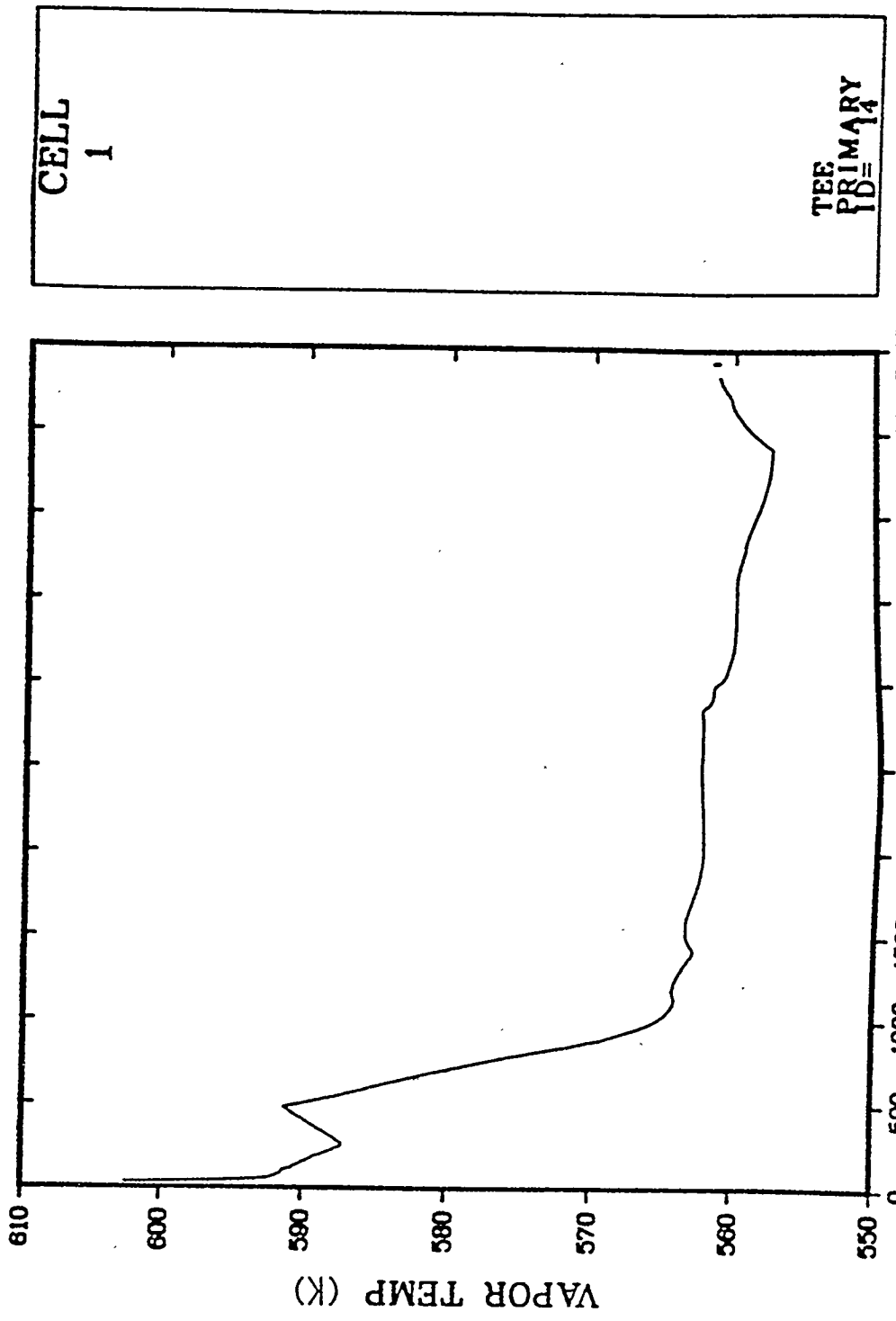

Fig. B-1.4. A Loop cold-leg vapor temperature.

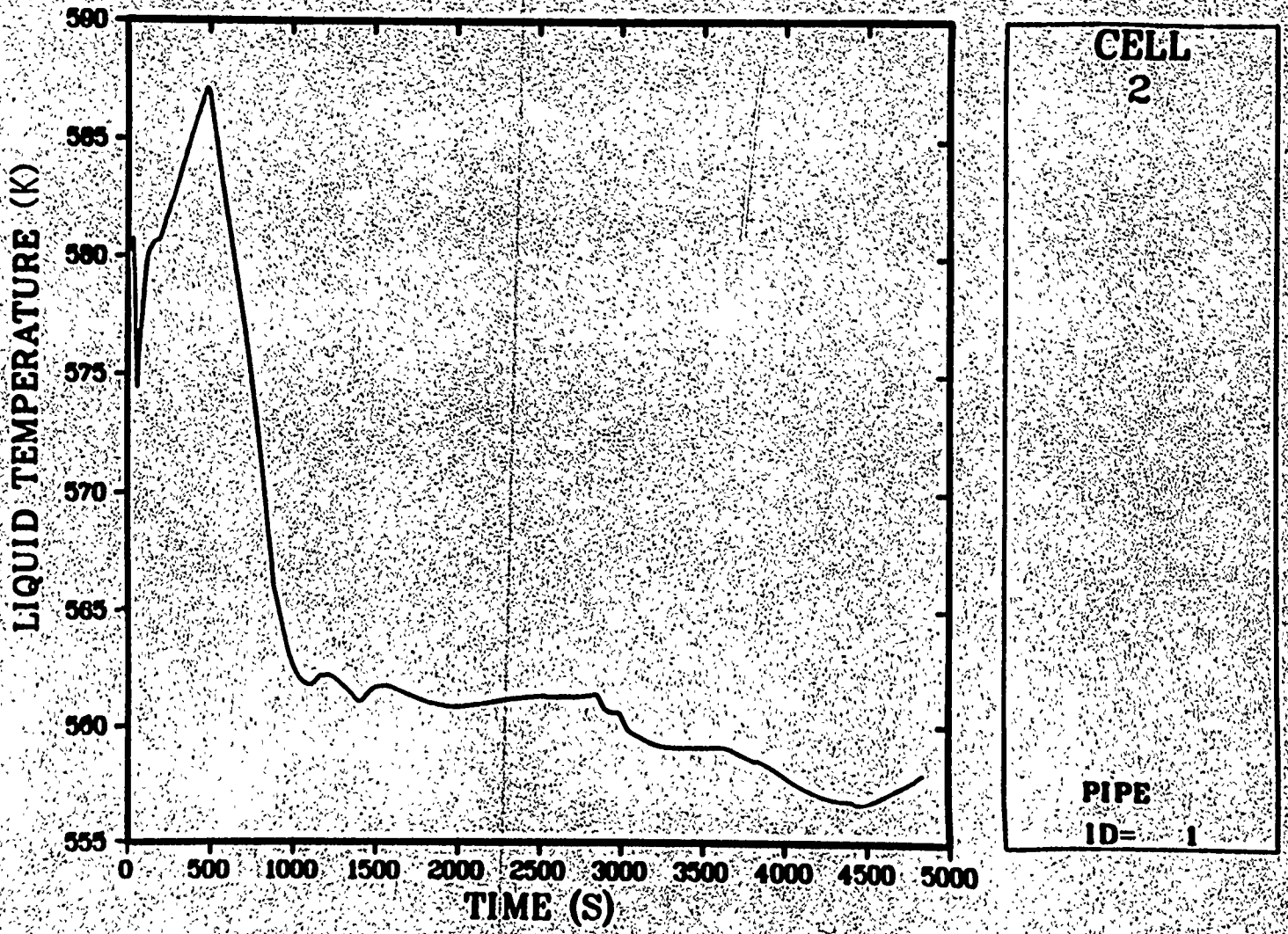

Fig. B-1.5. B Loop hot-leg liquid temperature.

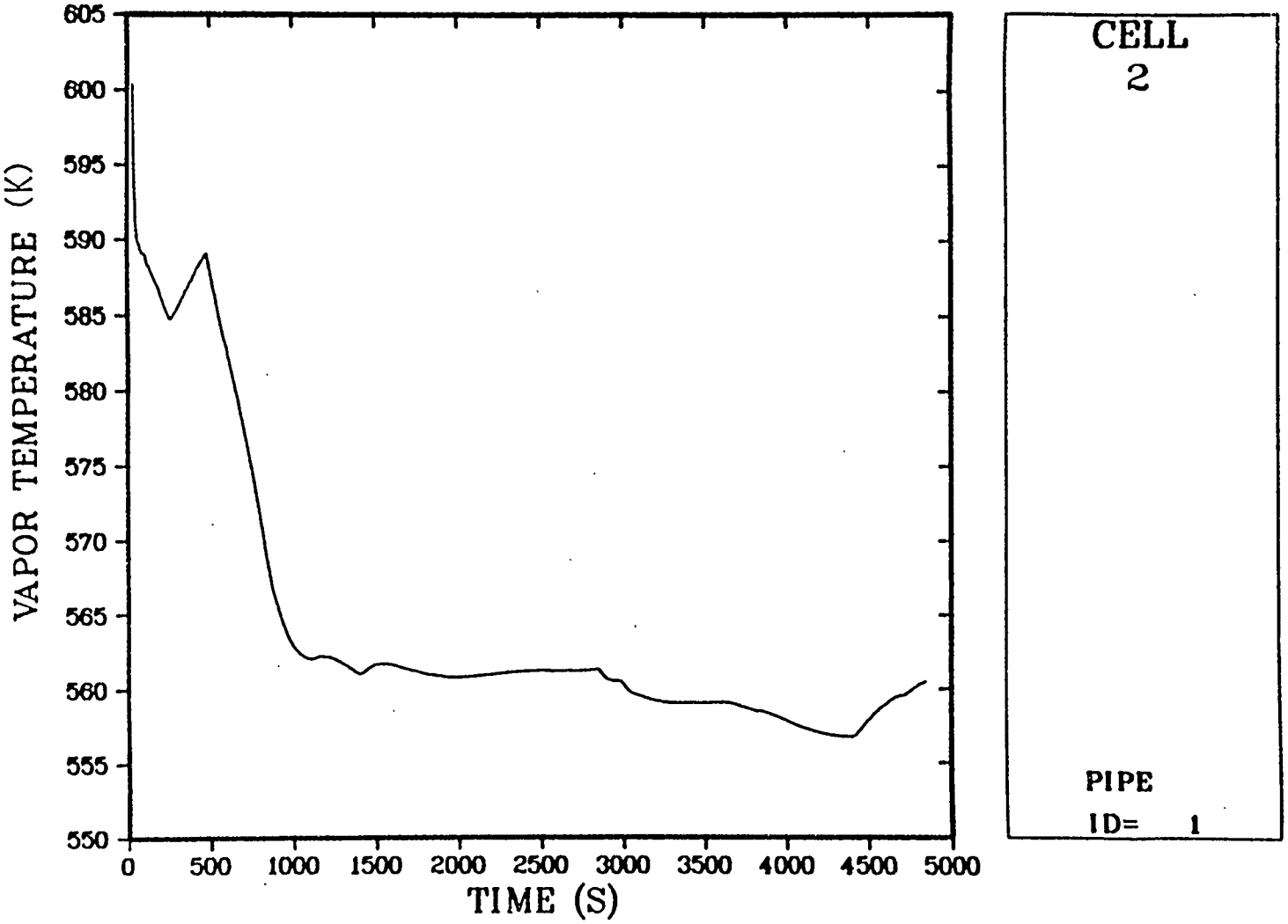

Fig. B-1.6. B Loop hot-leg vapor temperature.

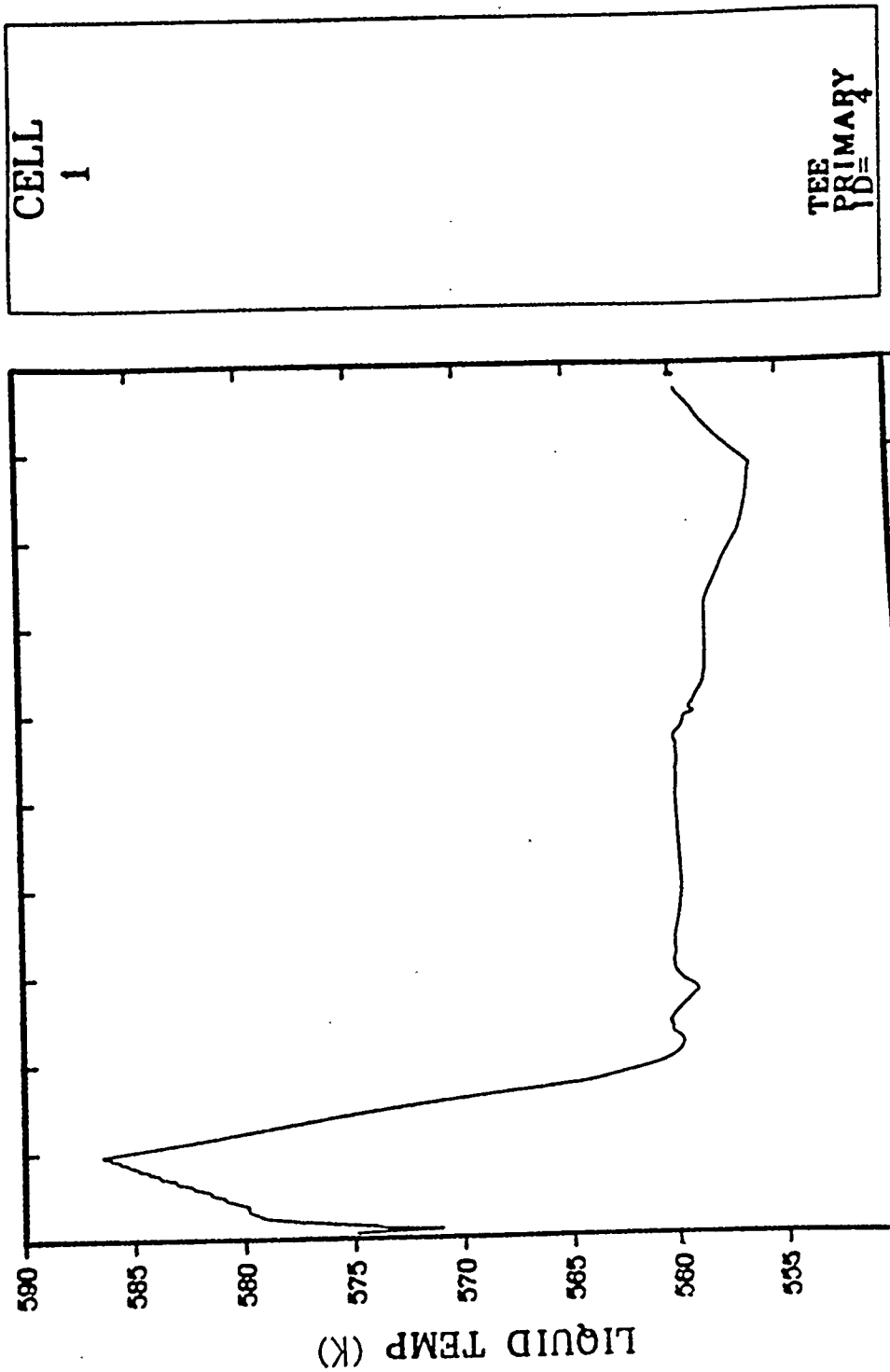

Fig. B-1.7. B Loop cold-leg liquid temperature.

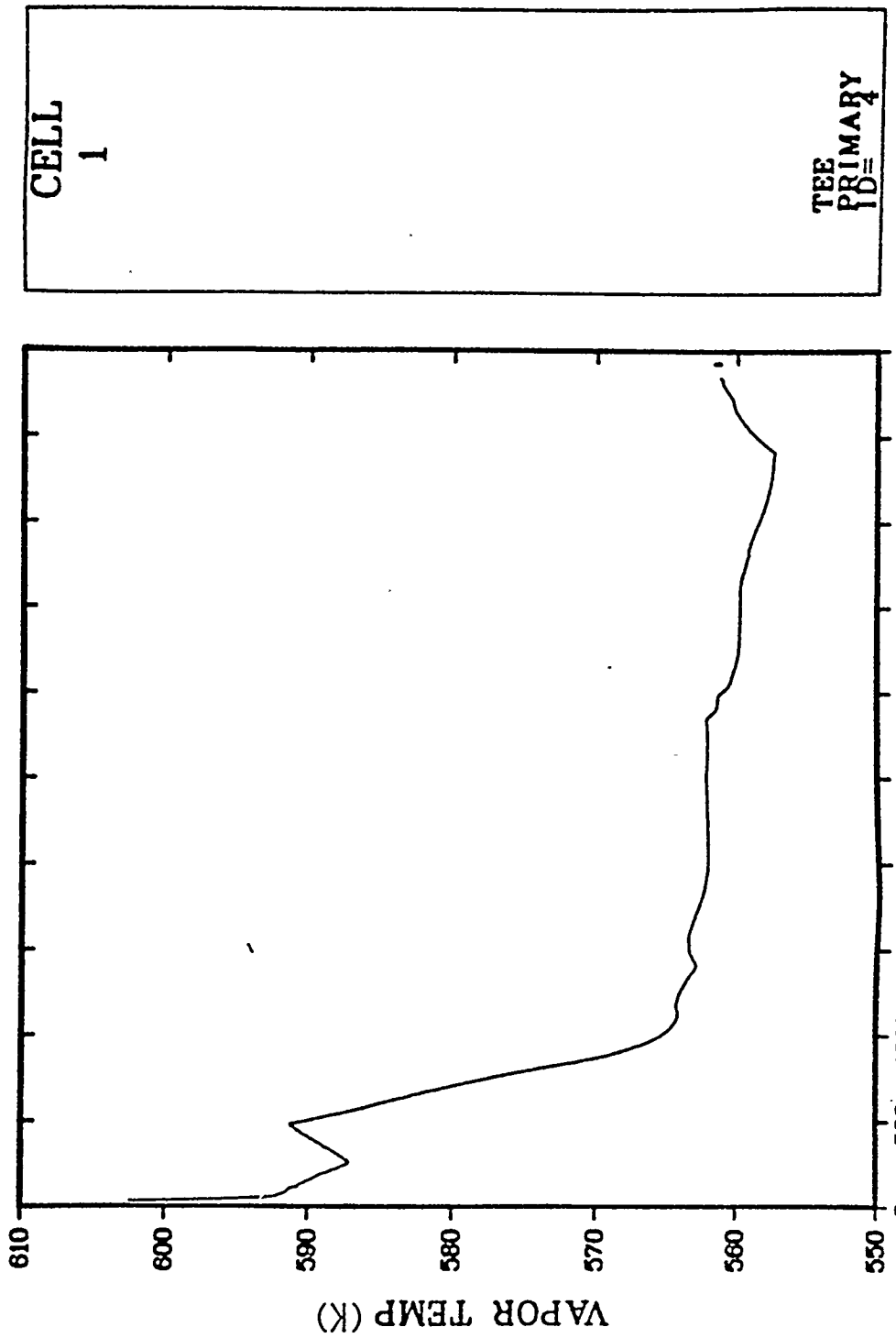

Fig. B-1.8. B Loop cold-leg vapor temperature.

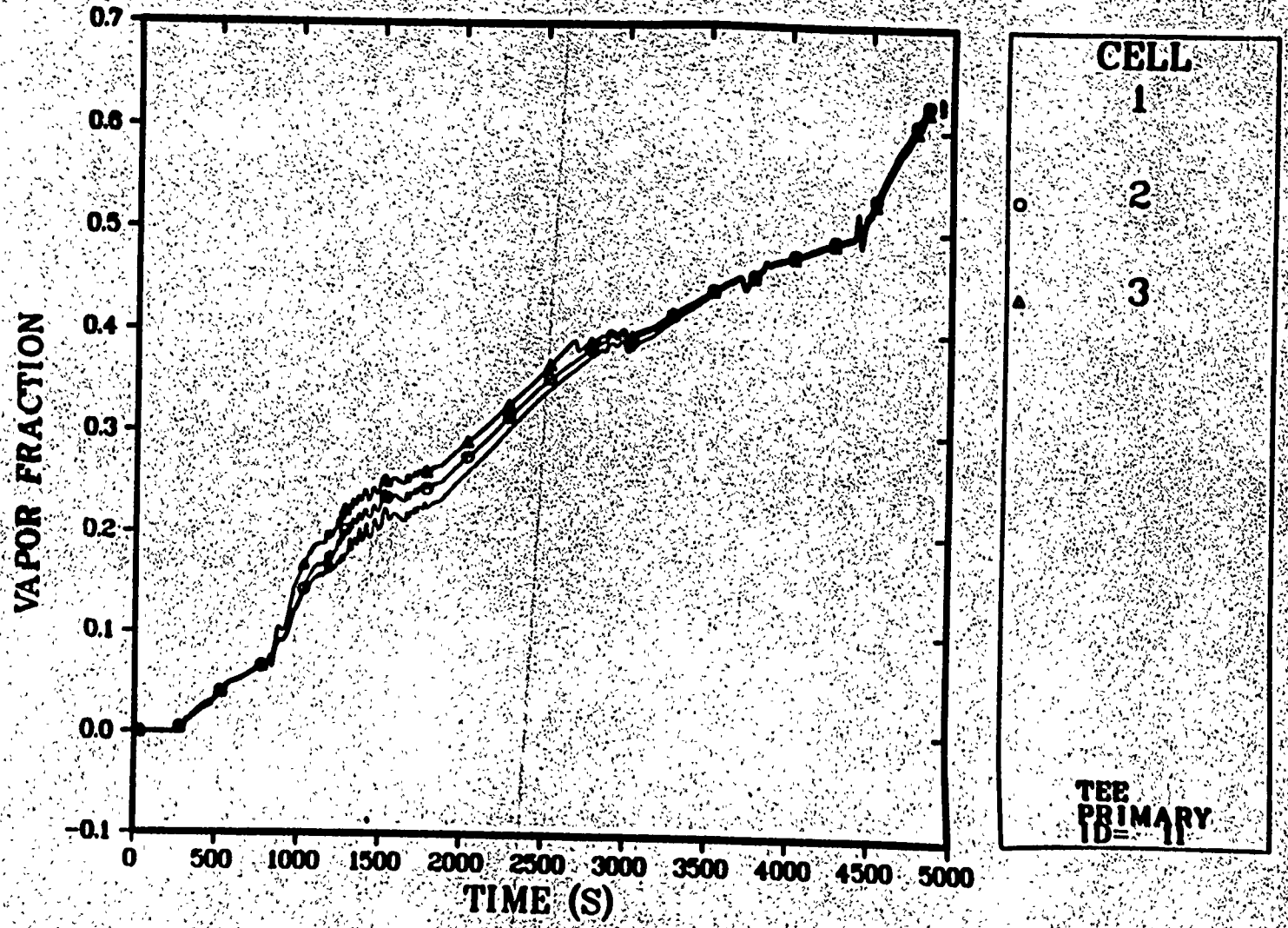

Fig. B-1.9. A Loop hot-leg void fraction distribution (Cells 1, 2, 3).

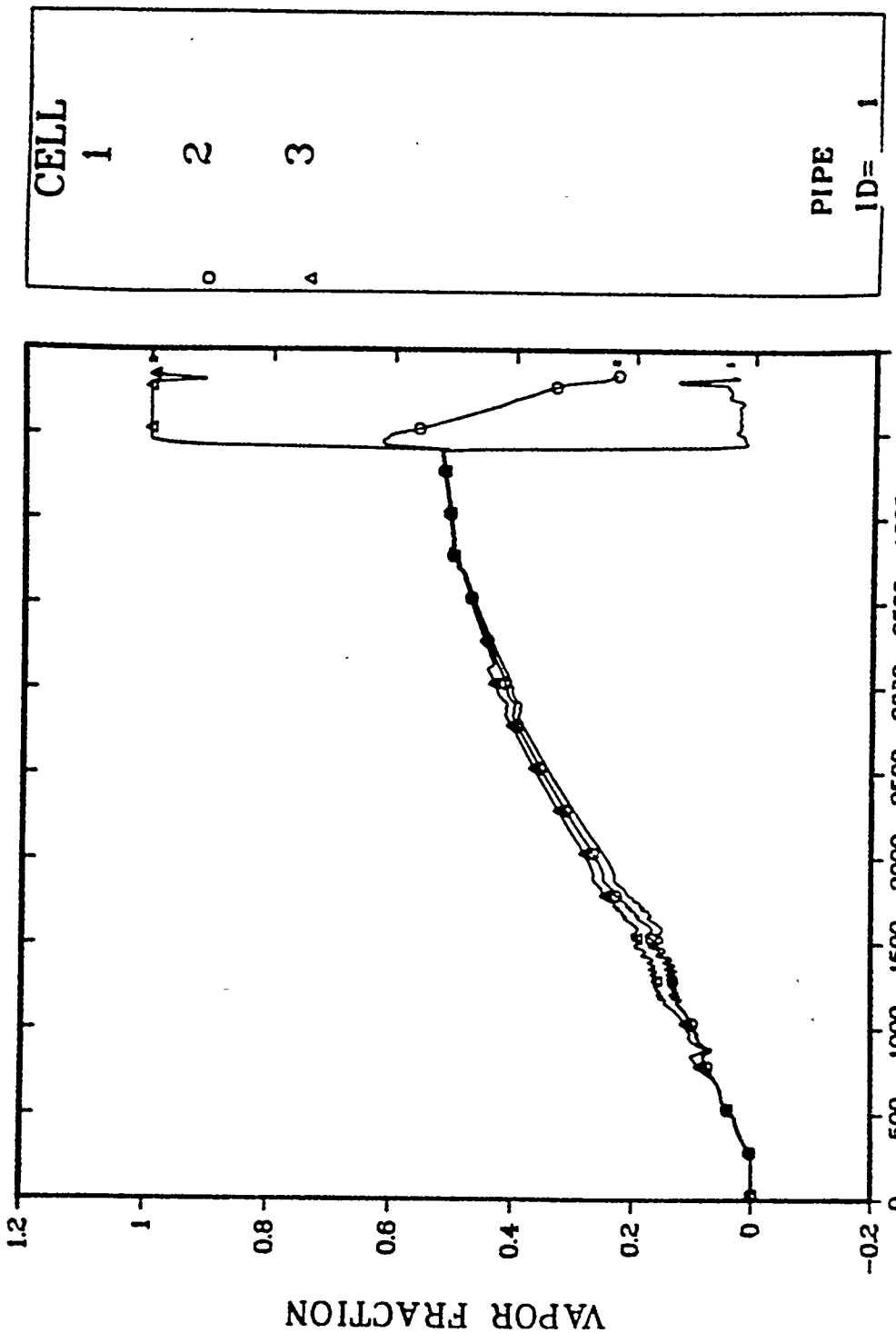

Fig. B-1.10. B Loop hot-leg void fraction distribution (Cells 1, 2, 3).

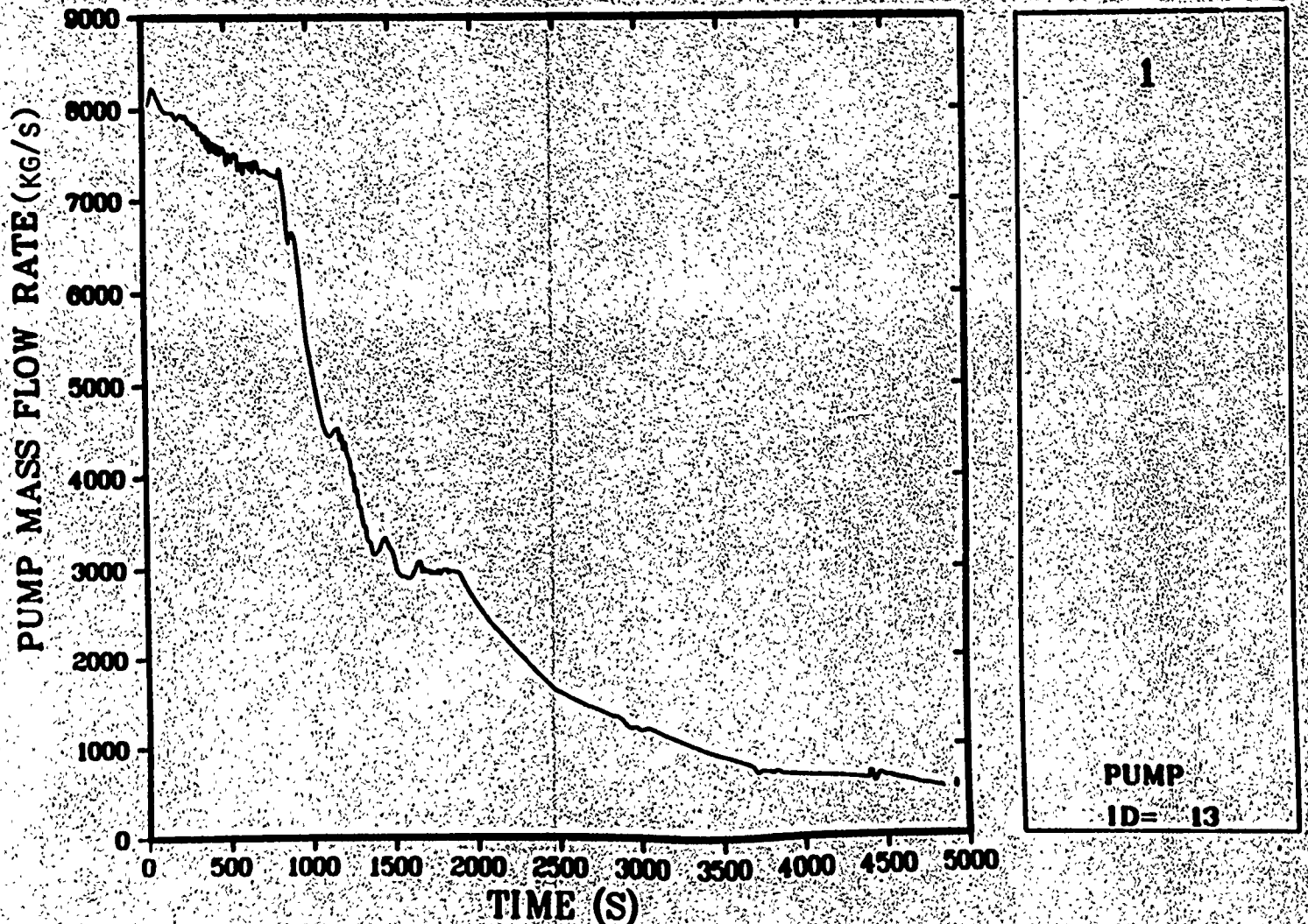

Fig. B-1.11. A Loop pump mass flow rate.

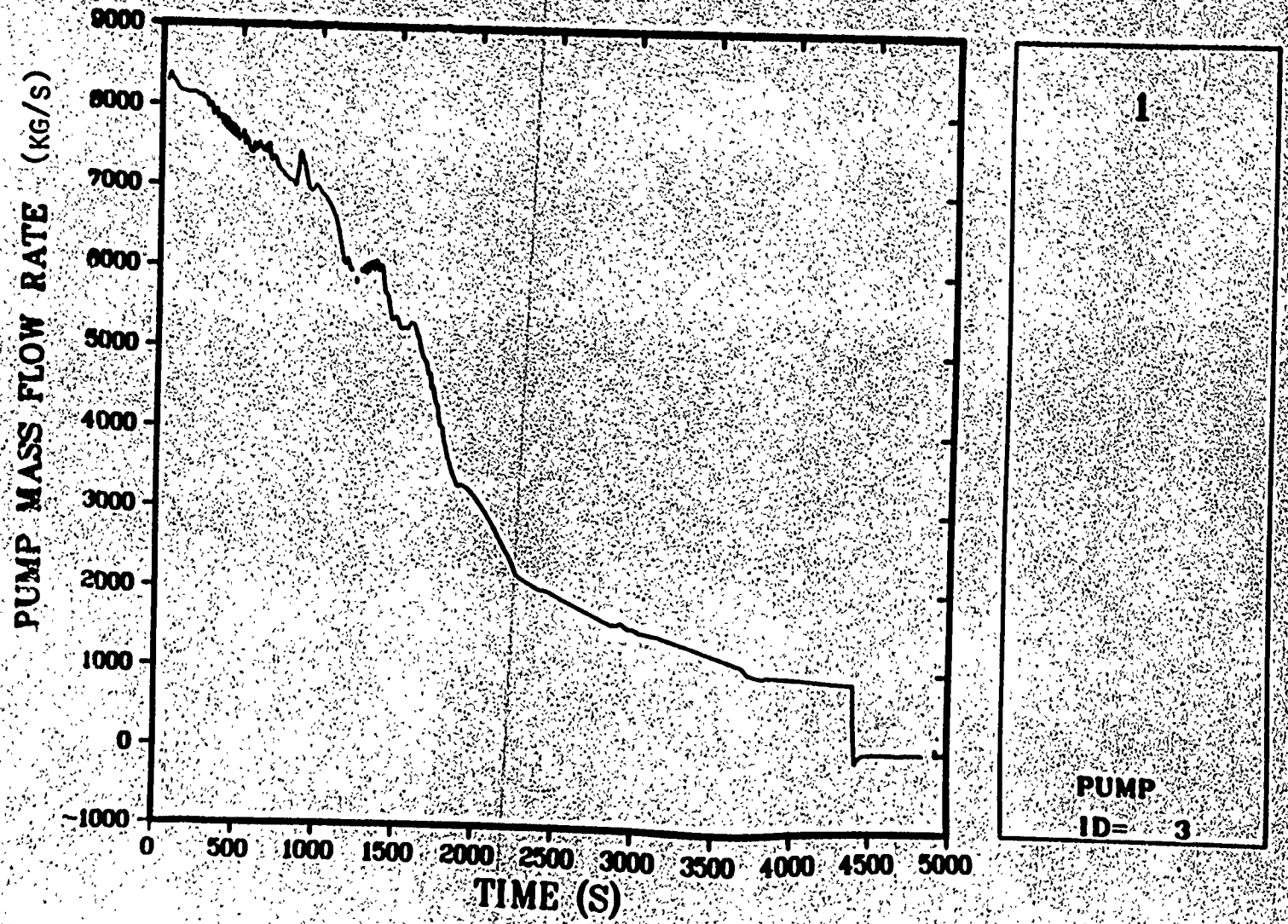

Fig. B-1.12. B Loop pump mass flow rate.

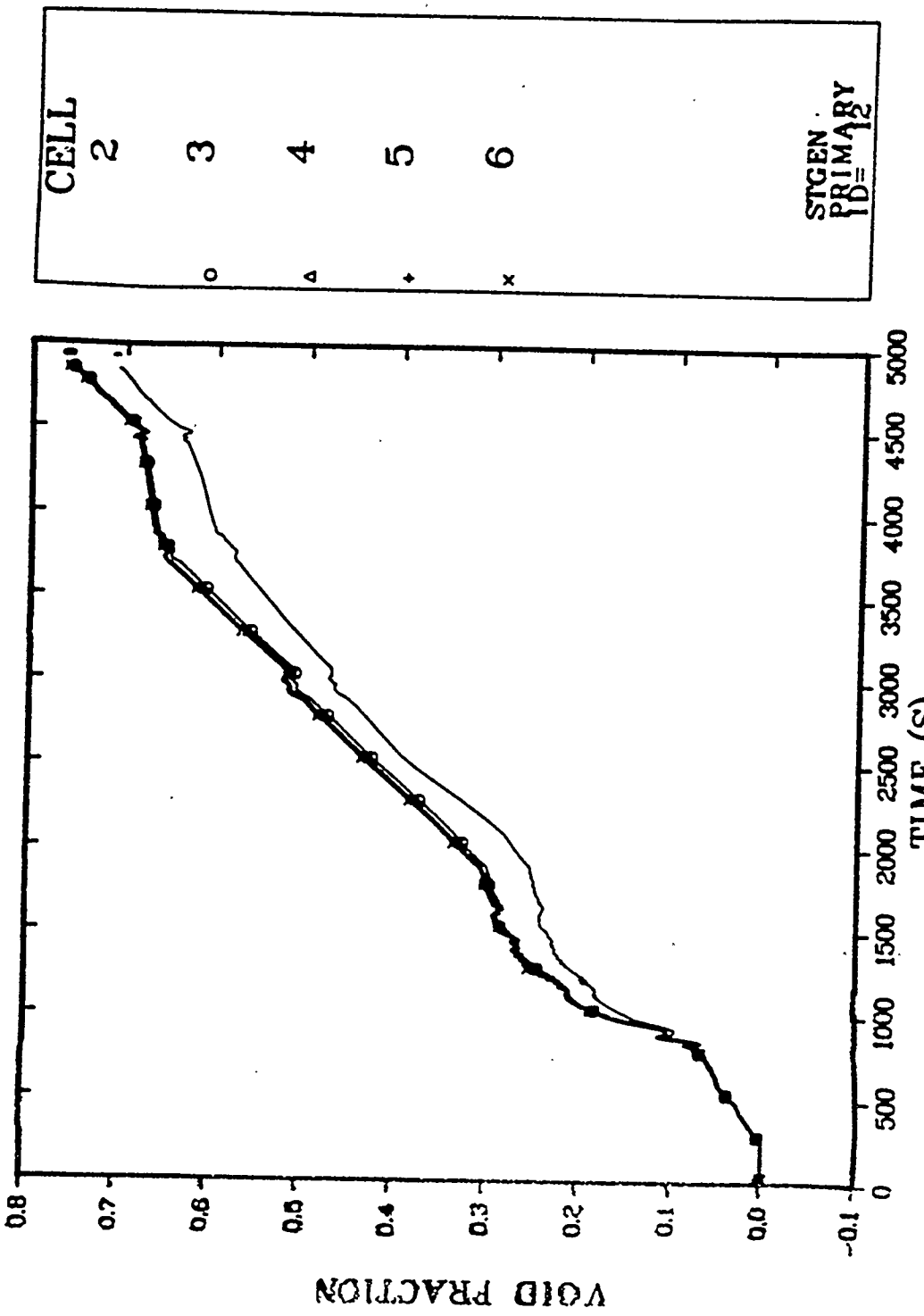

Fig. B-1.13. A Loop steam generator void fraction distribution.

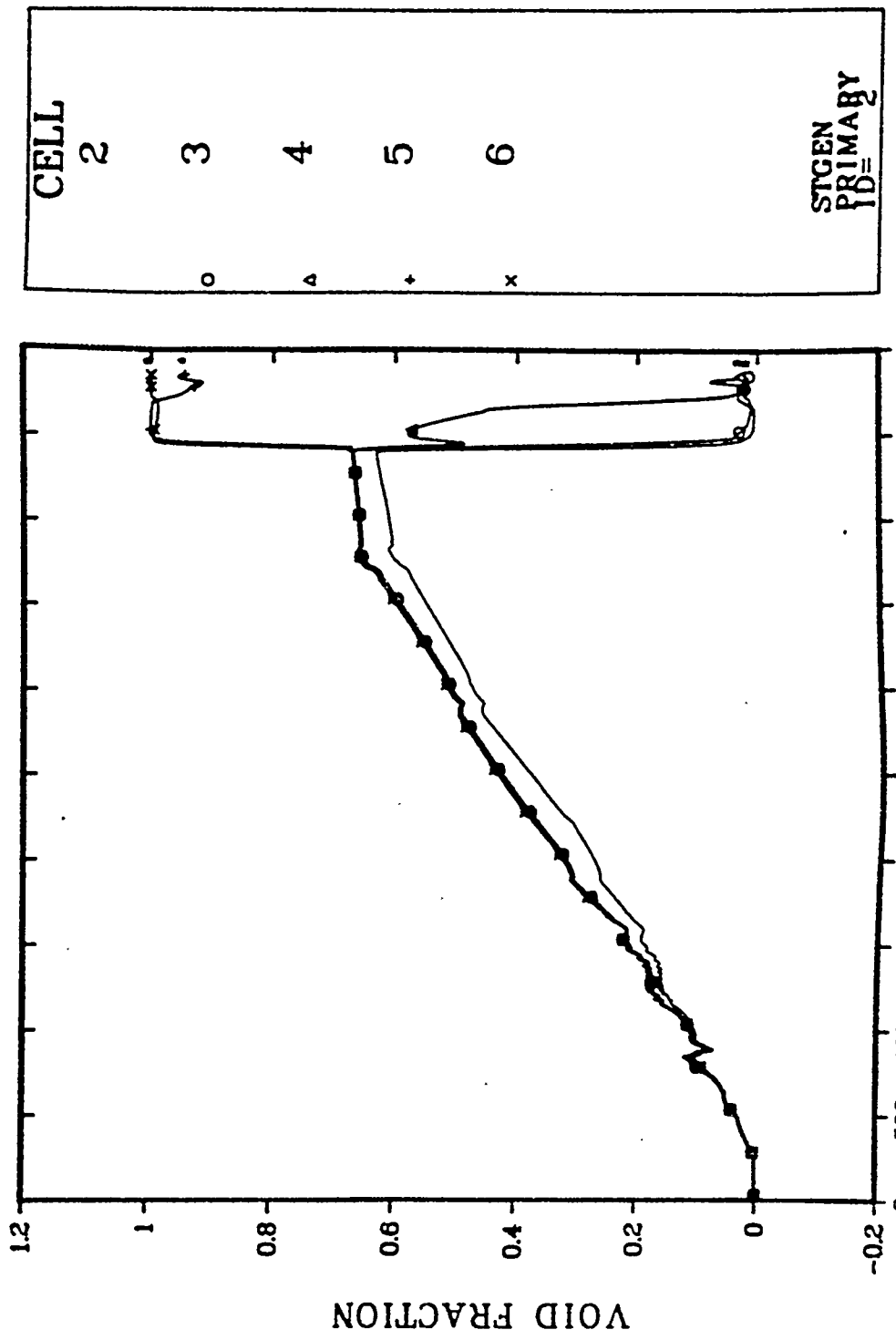

Fig. B-1.14. B Loop steam generator void fraction distribution.

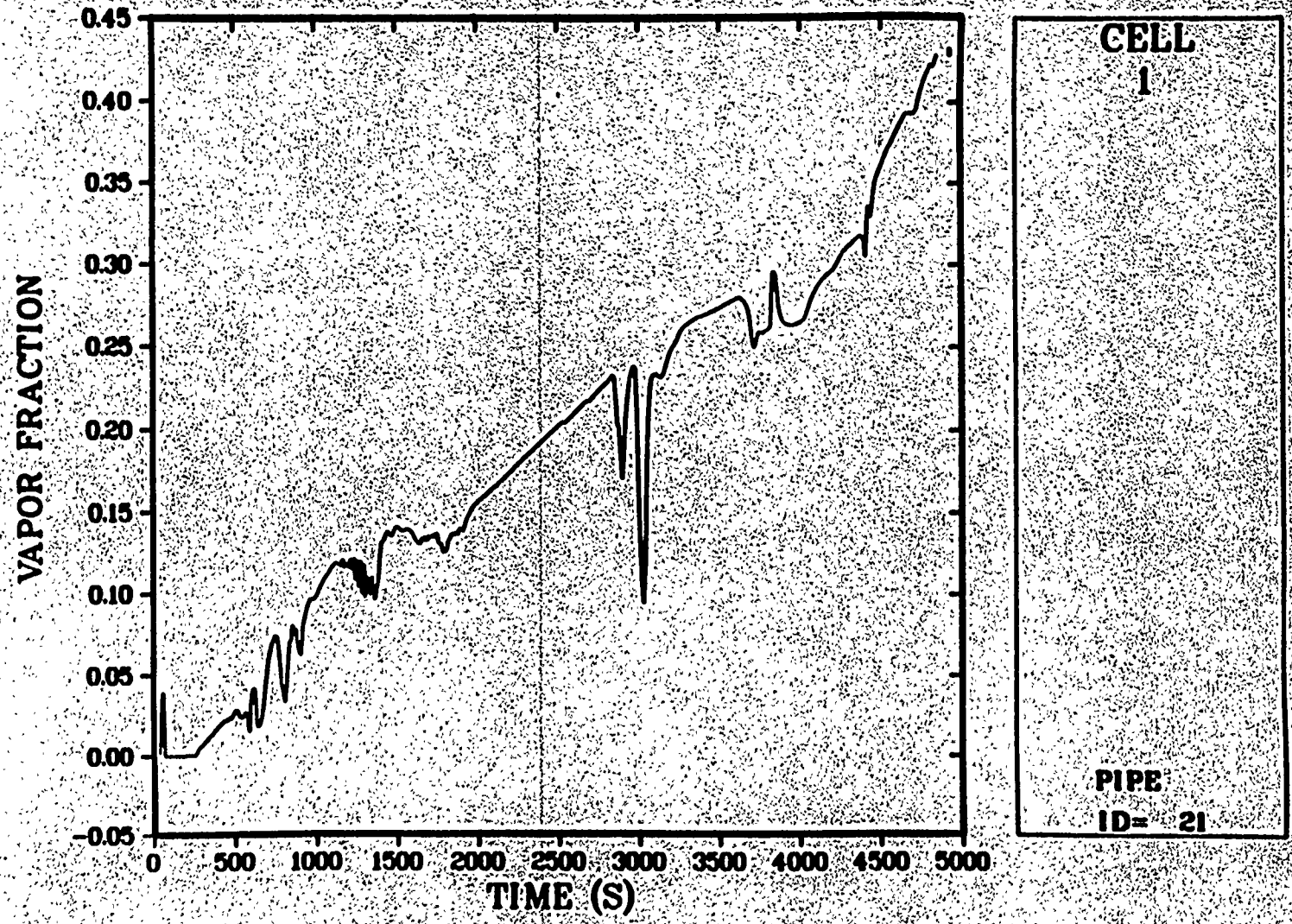

Fig. B-1.15. Pressurizer surge line void fraction.

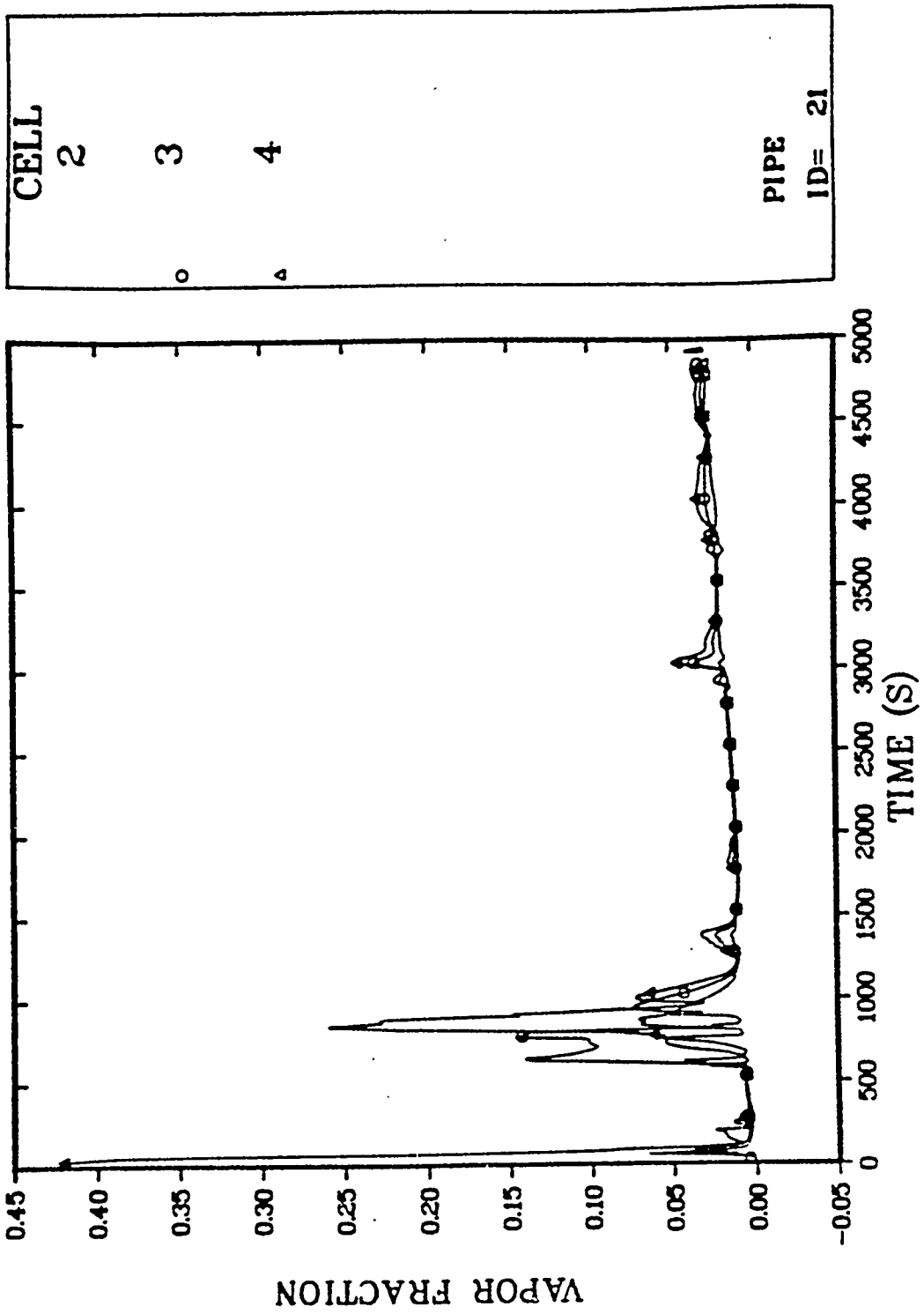

Fig. B-1.16. Pressurizer void fraction distribution (first 3 cells).

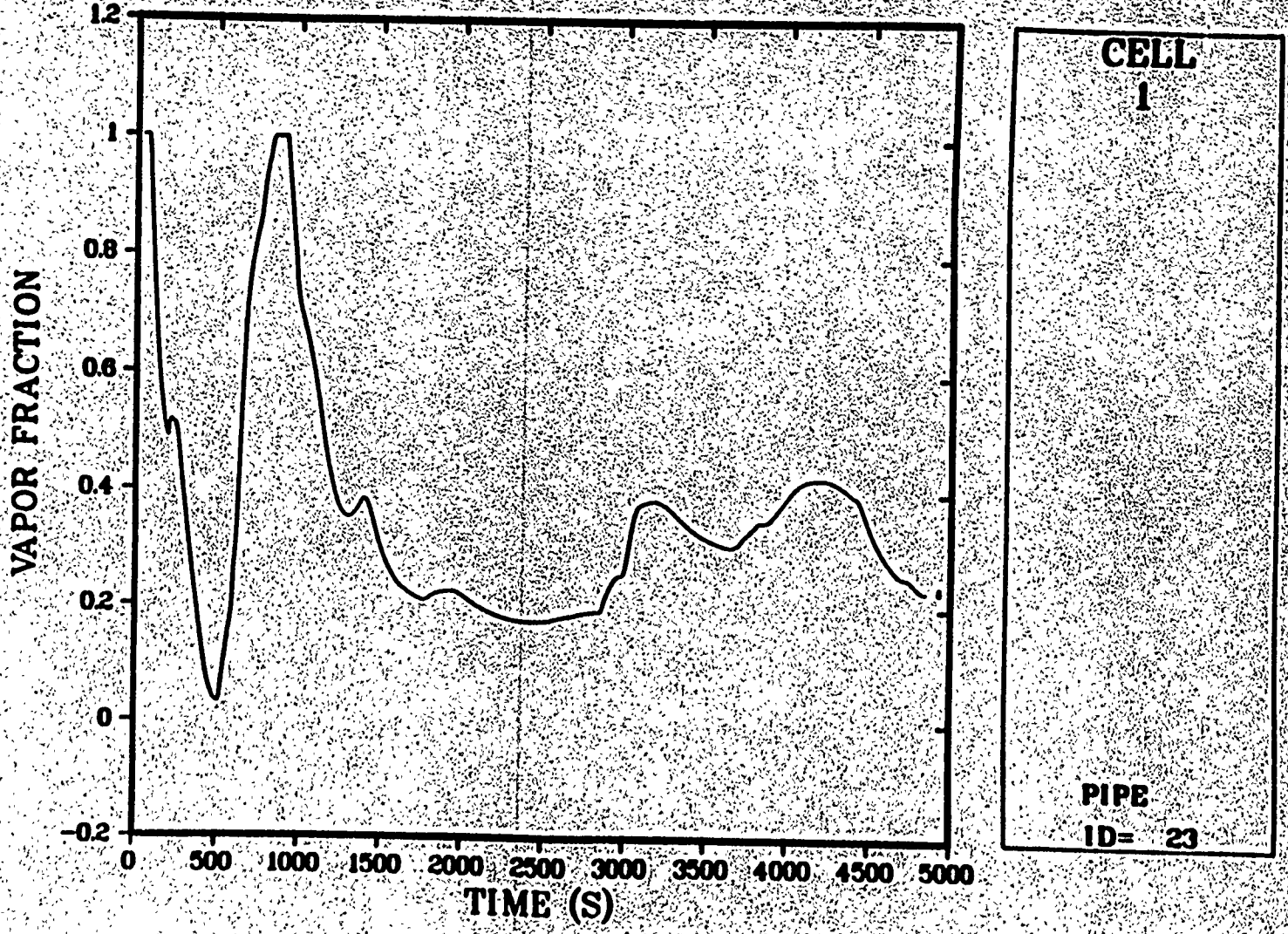

Fig. B-1.17. Pressurizer void fraction (top cell).

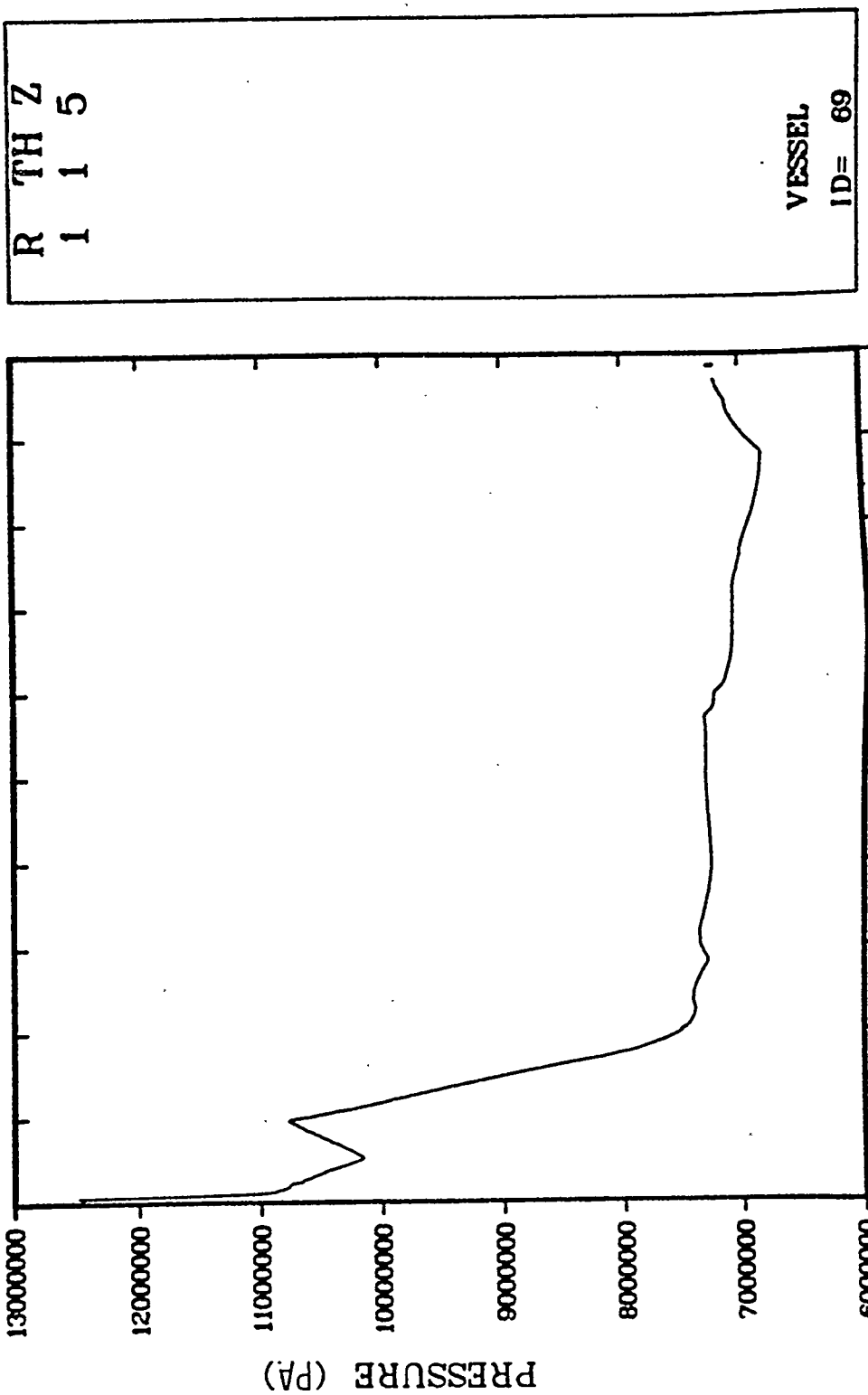

Fig. B-1.18. Upper plenum pressure.

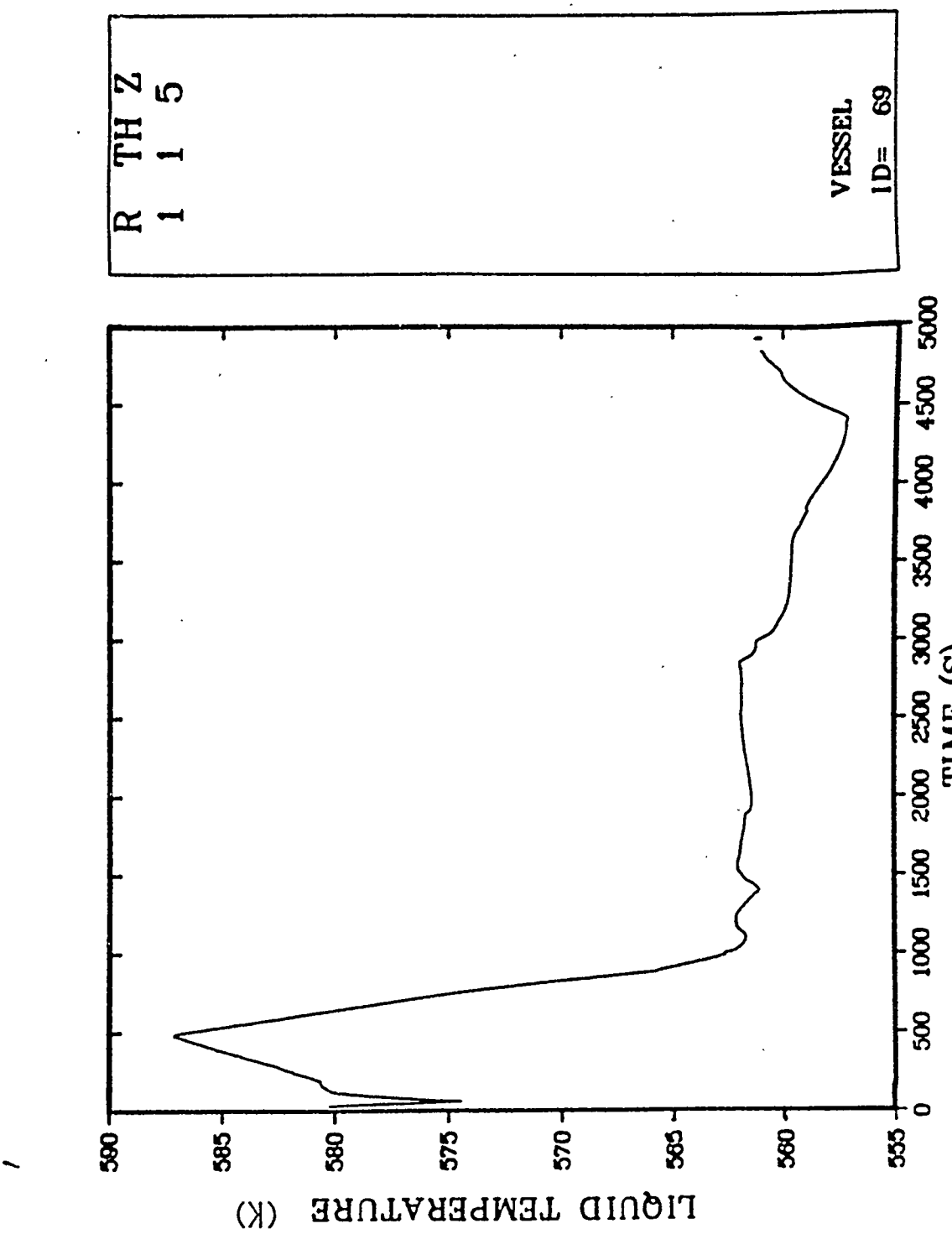

Fig. B-1.19. Upper plenum liquid temperature.

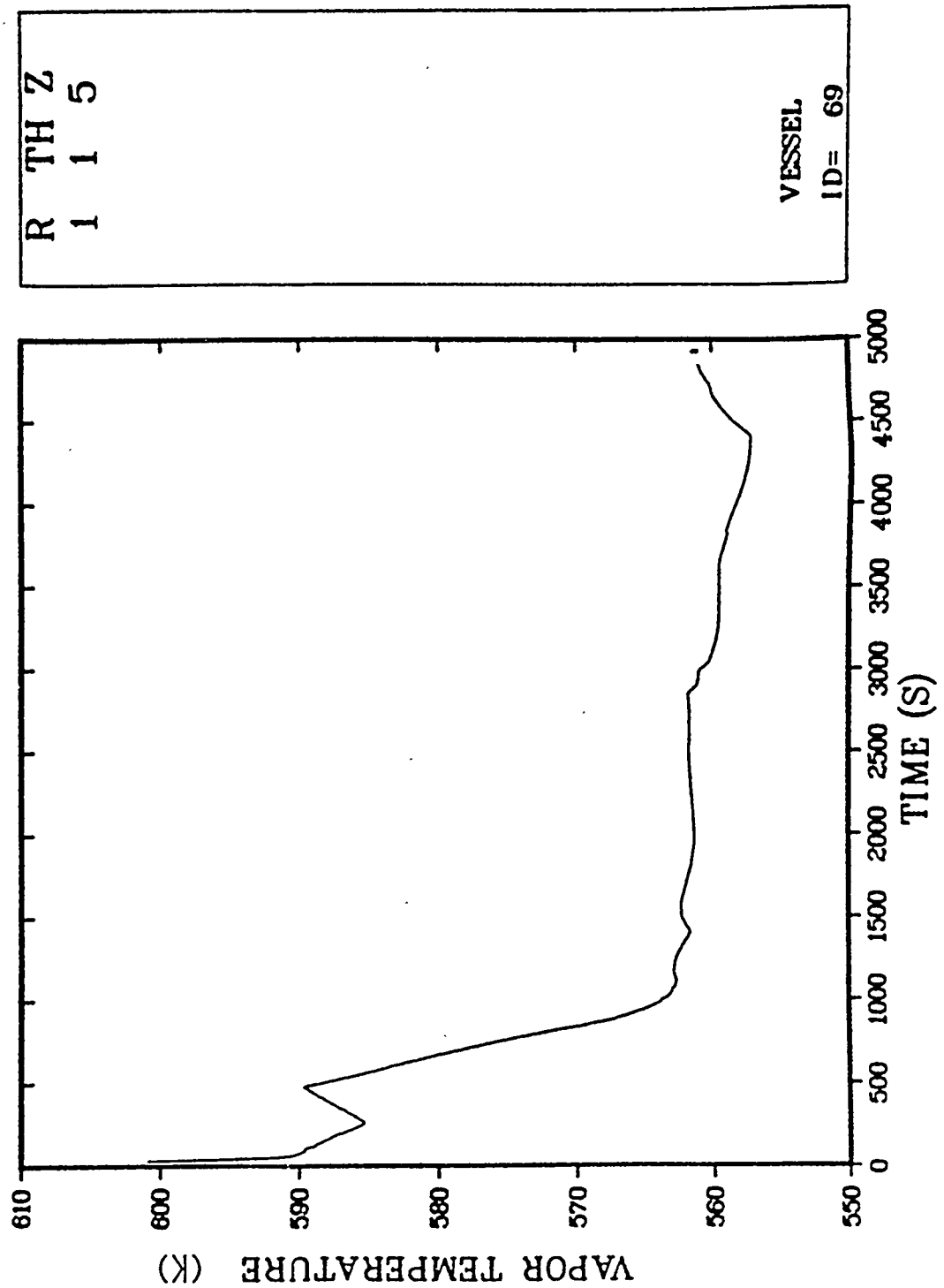

Fig. B-1.20. Upper plenum vapor temperature.

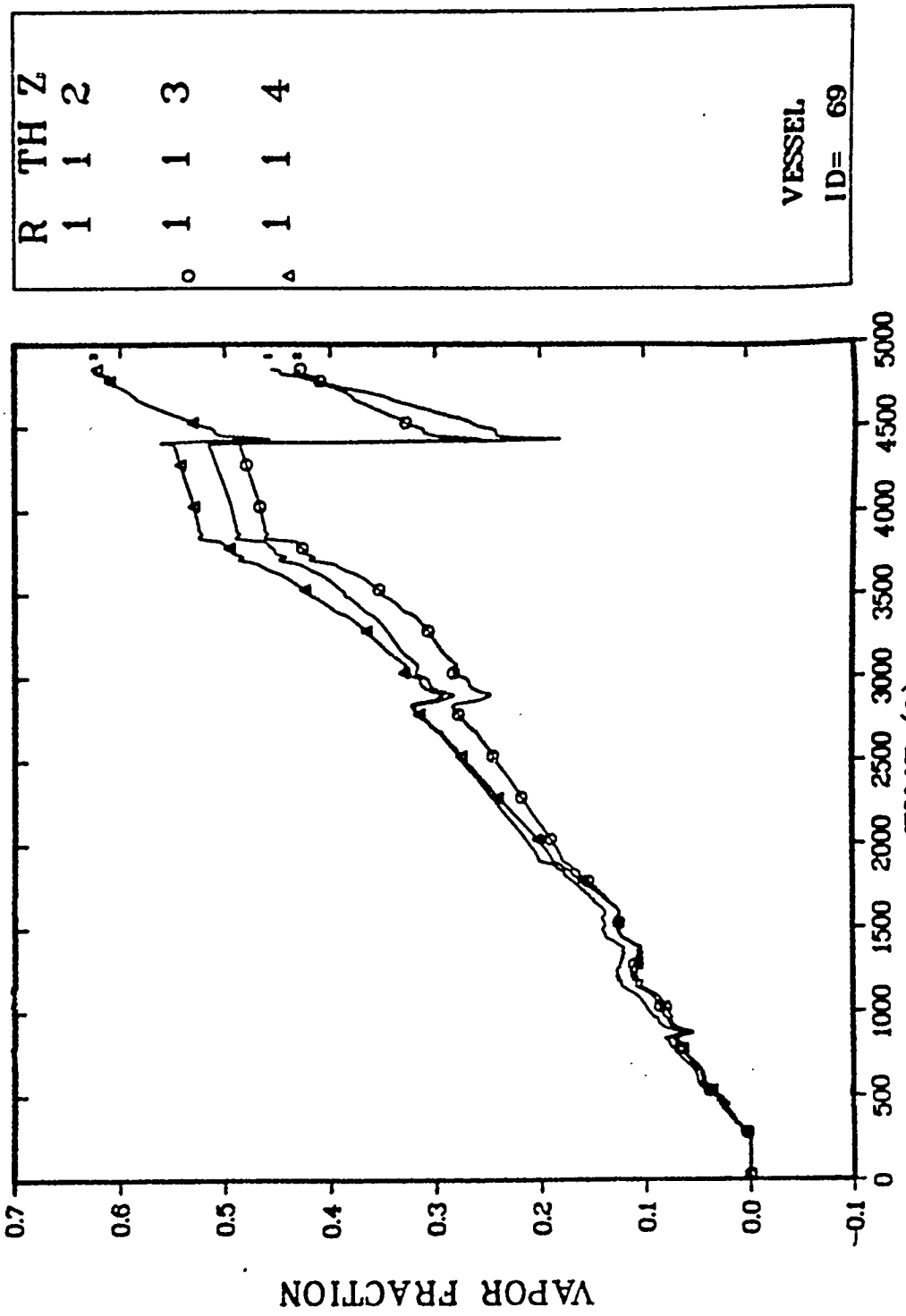

Fig. B-1.21. Core void fraction profile (axial direction - Cell 1).

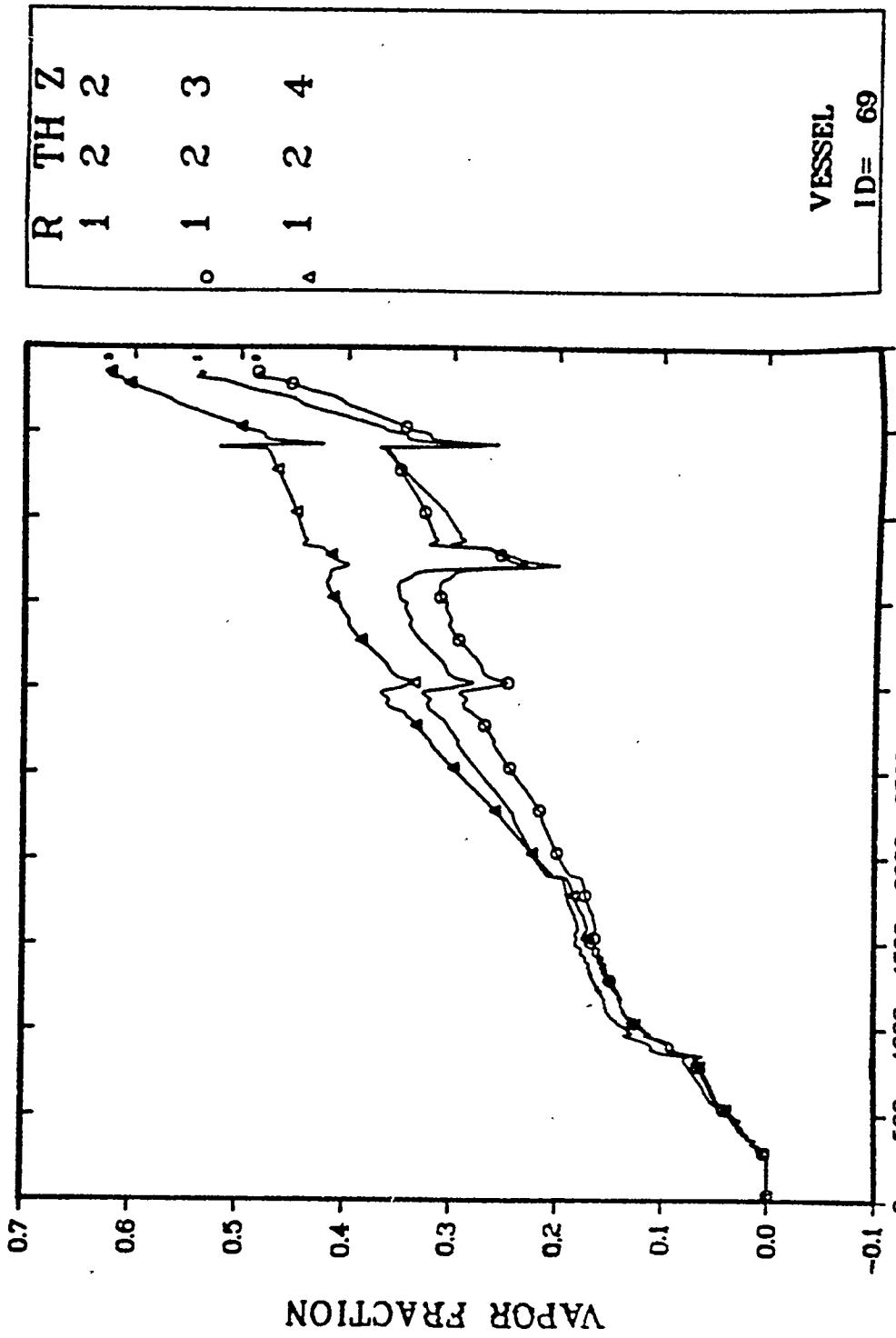

Fig. B-1.22. Core void fraction profile (axial direction - Cell 2).

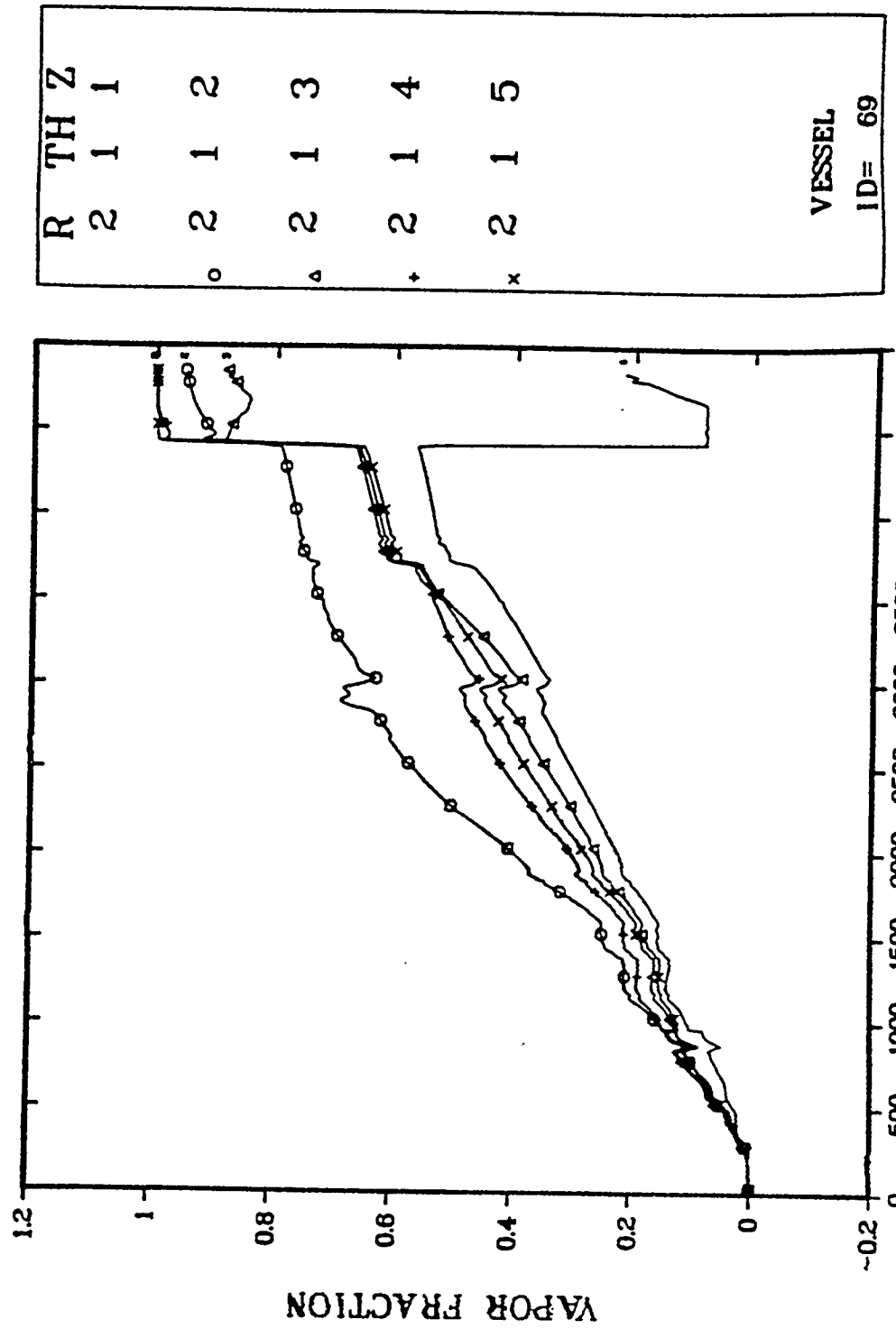

Fig. B-1.23. Downcomer void fraction profile.

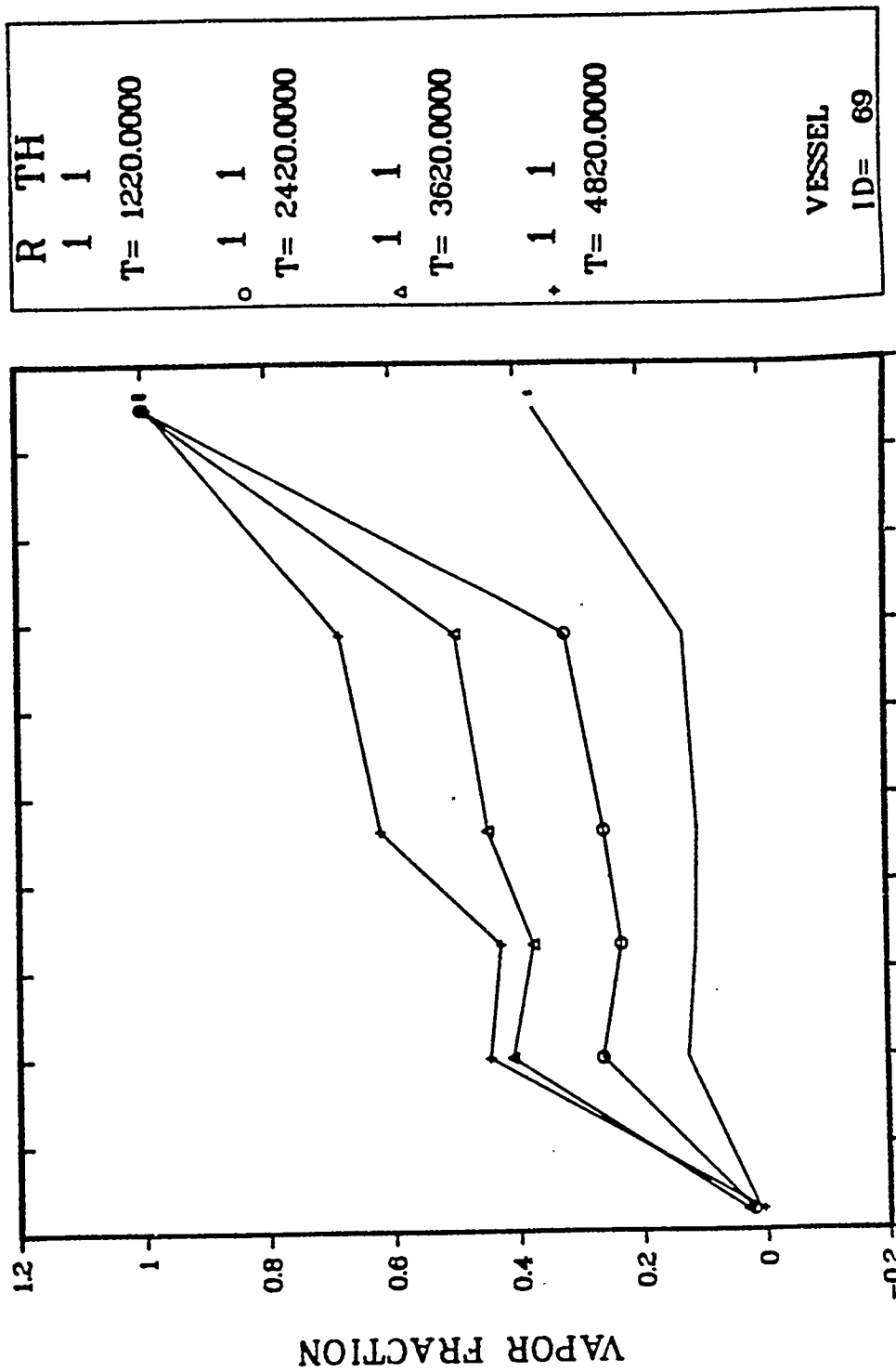

Fig. B-1.24. Vessel void fraction profile vs time.

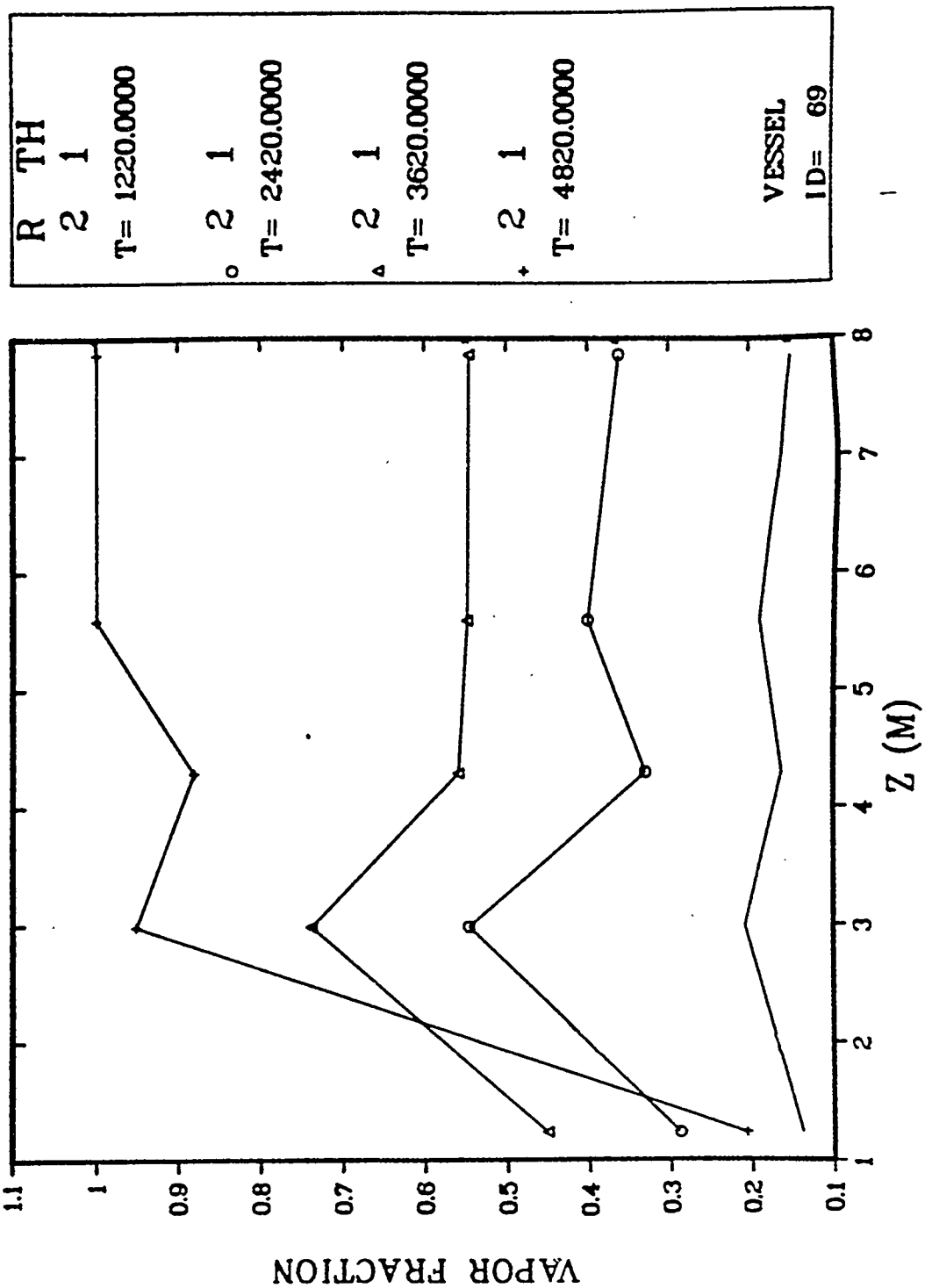

Fig. B-1.25. Downcomer void fraction profile vs time.

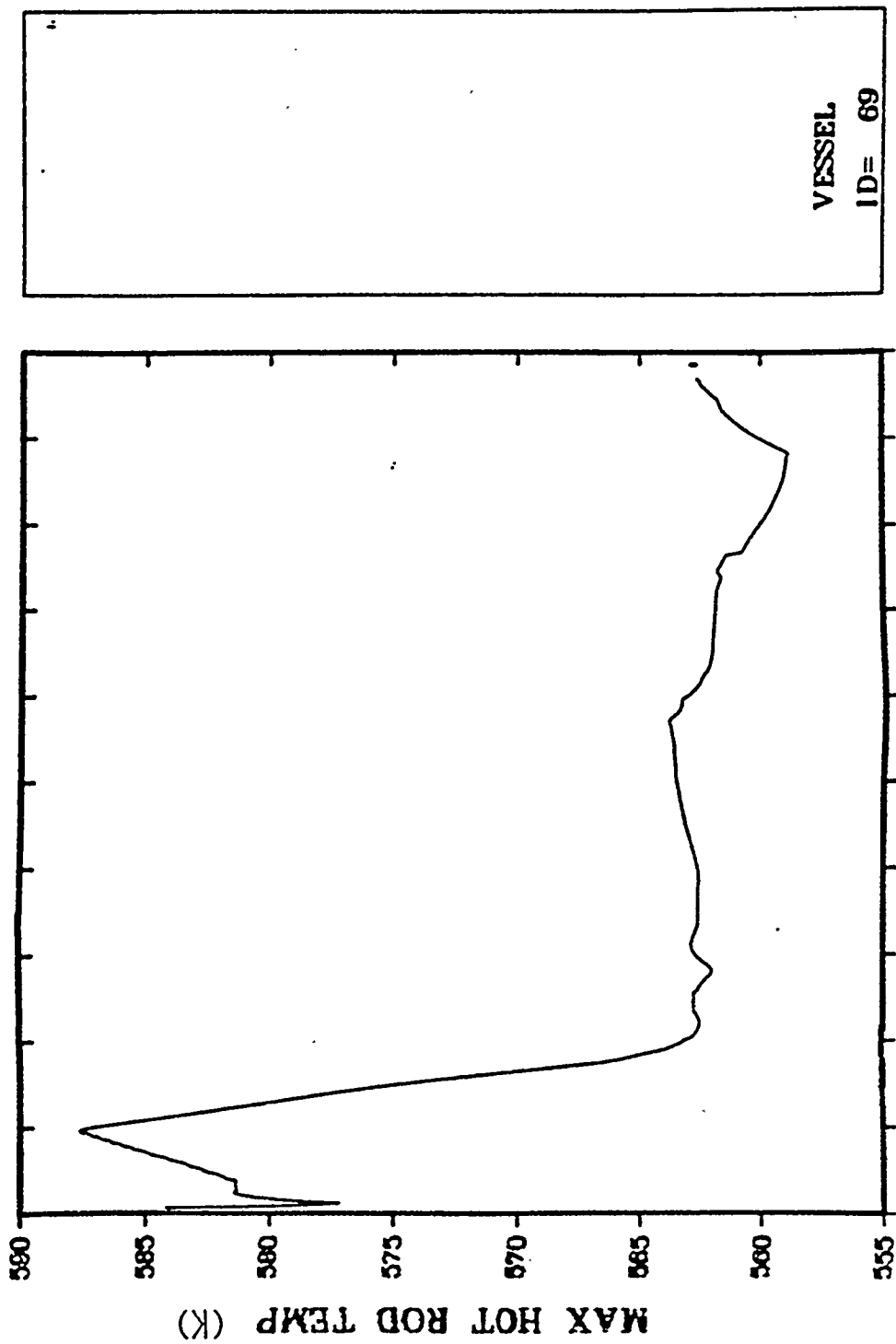

Fig. B-1.26. Maximum hot-rod temperature.

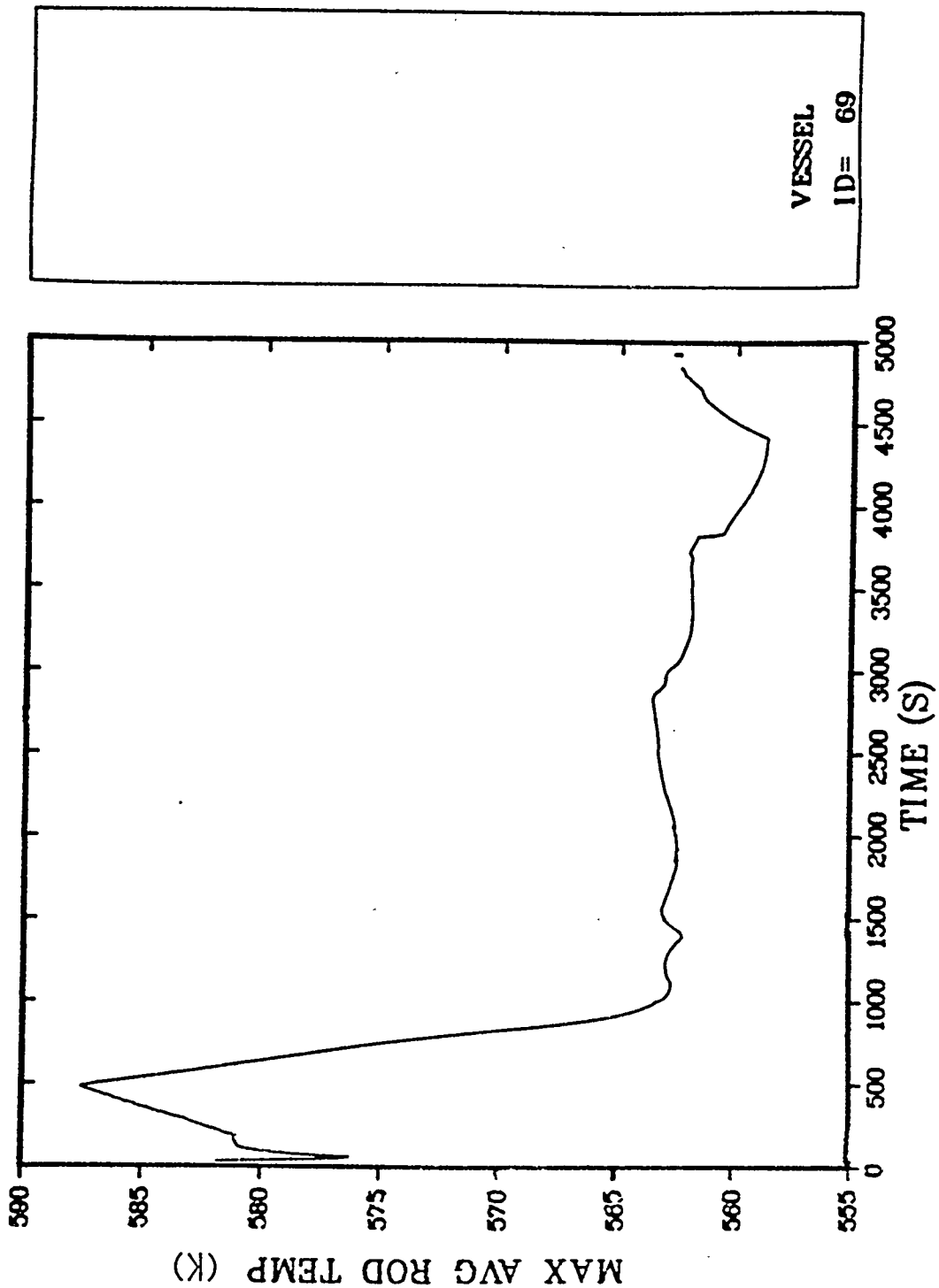

Fig. B-1.27. Maximum average rod temperature.

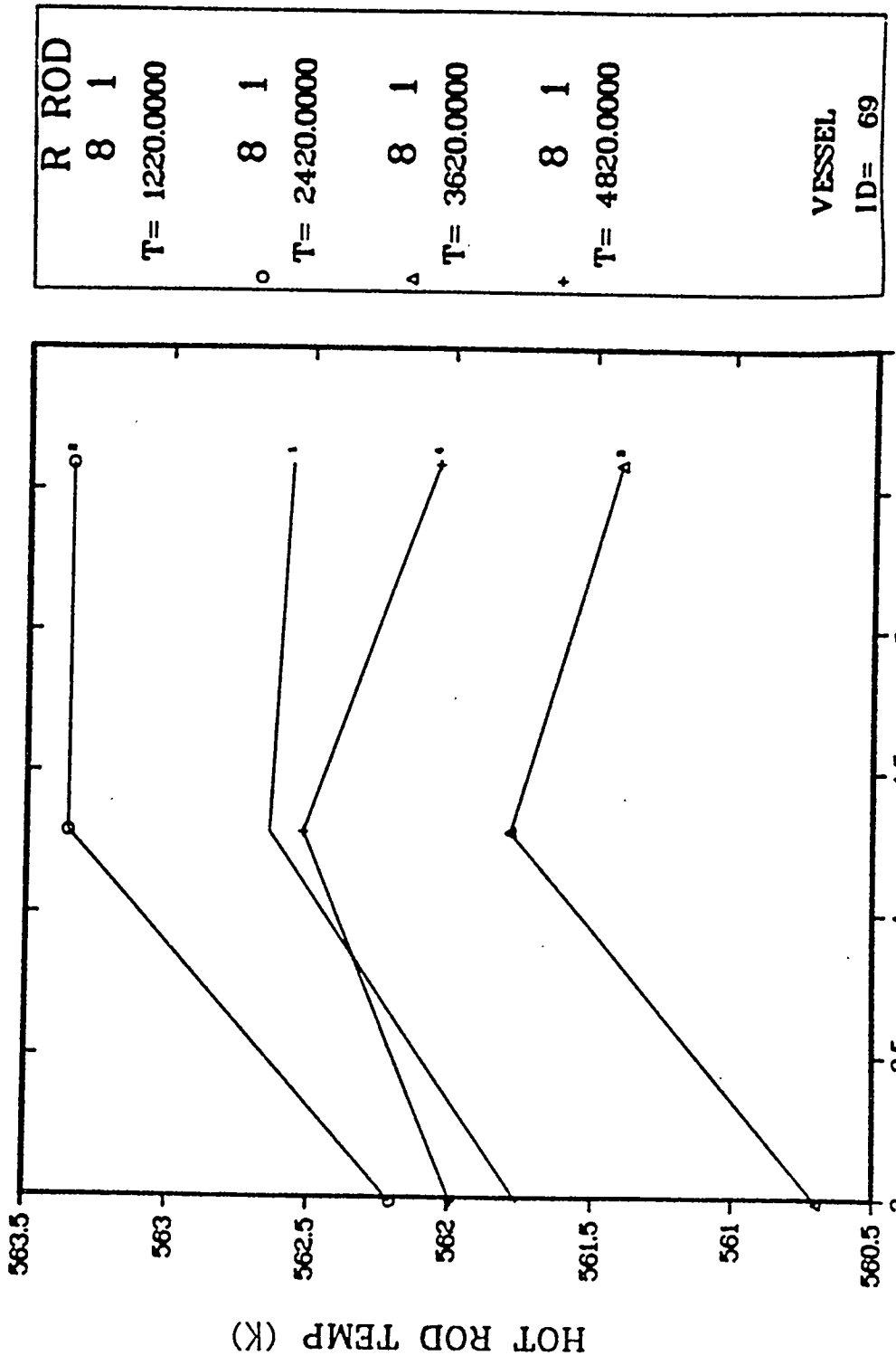

Fig. B-1.28. Hot-rod temperature profile vs time (Rod 1).

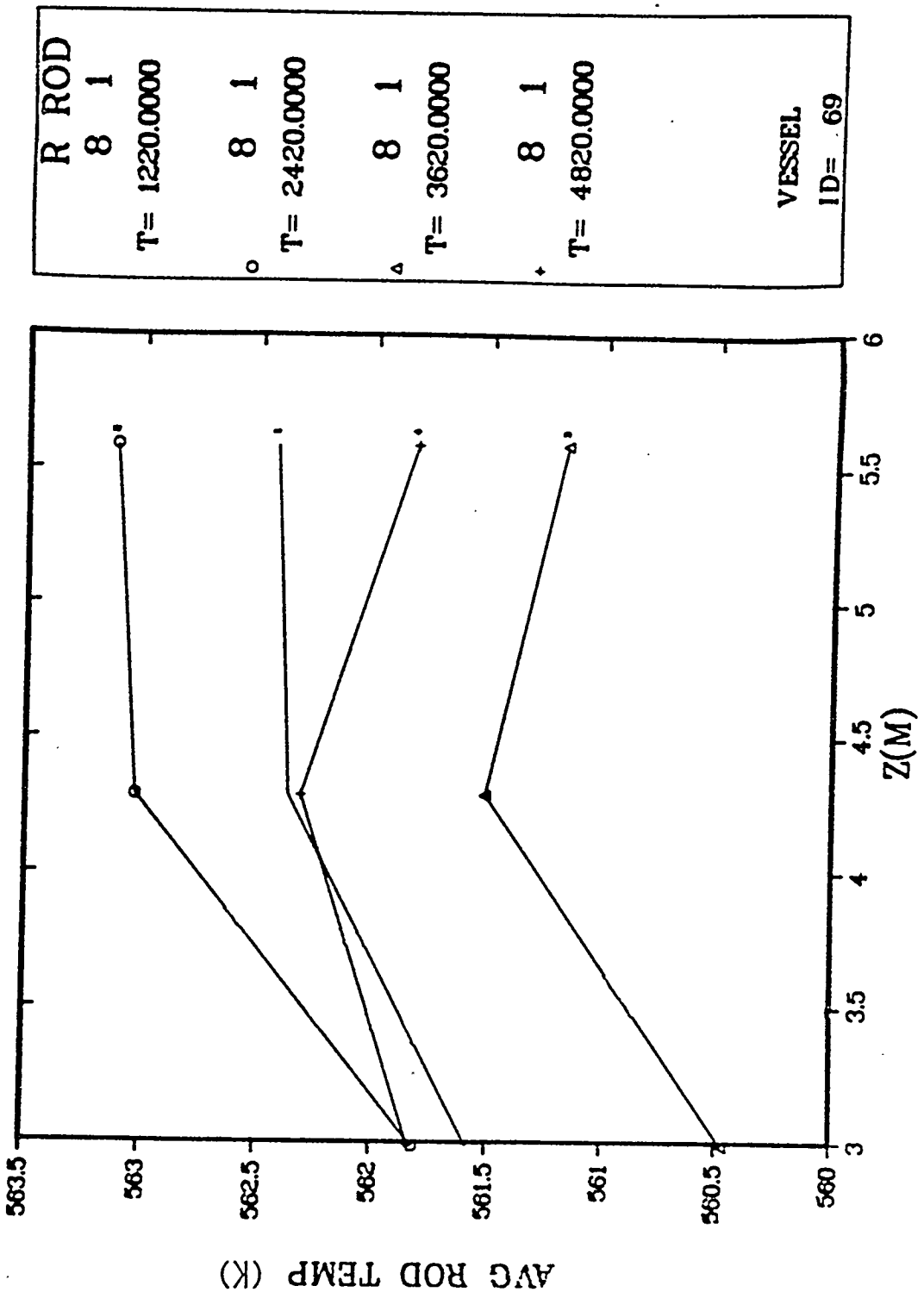

Fig. B-1.29. Average rod temperature profile vs time (Rod 1).

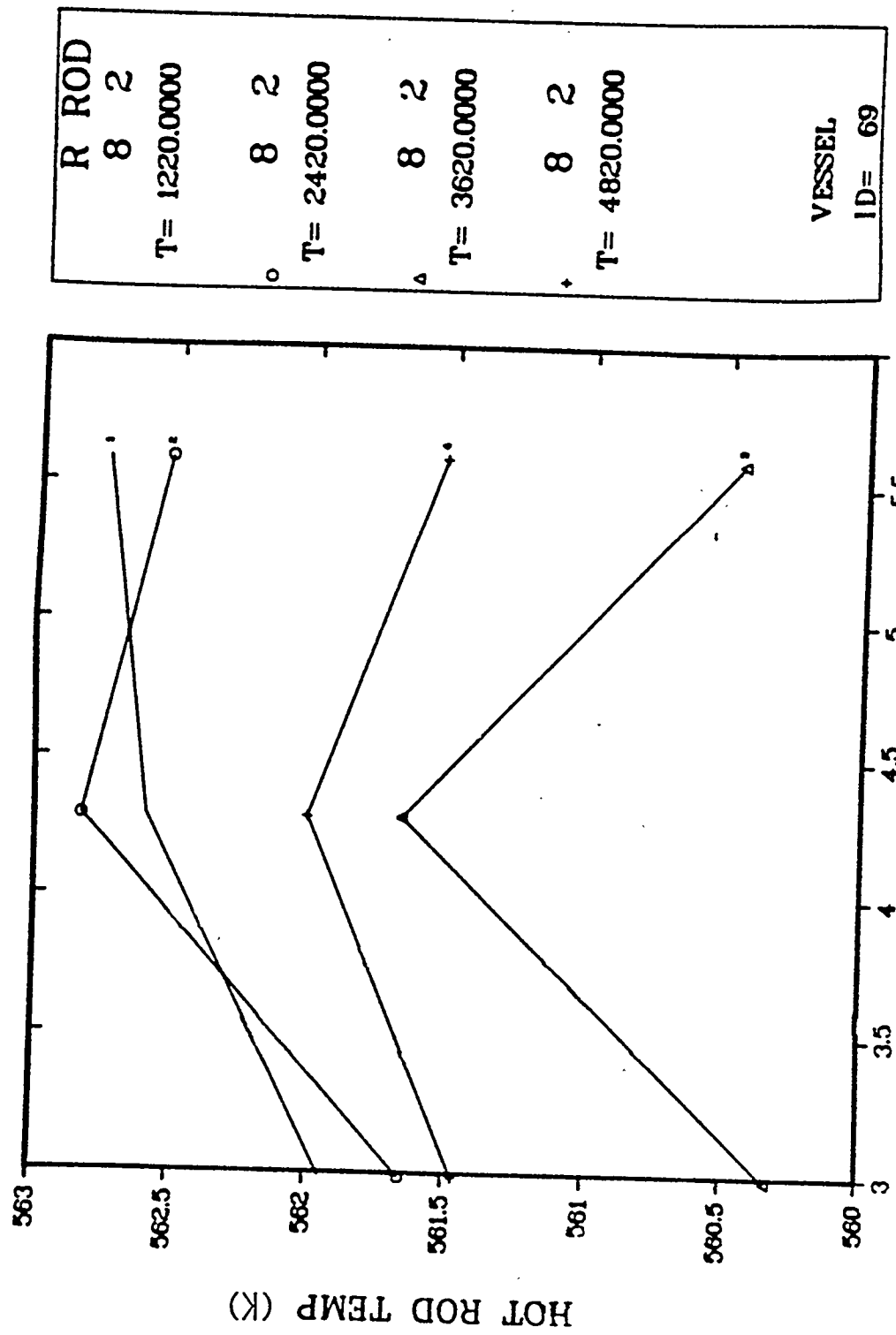

Fig. B-1.30. Hot-rod temperature profile vs time (Rod 2).

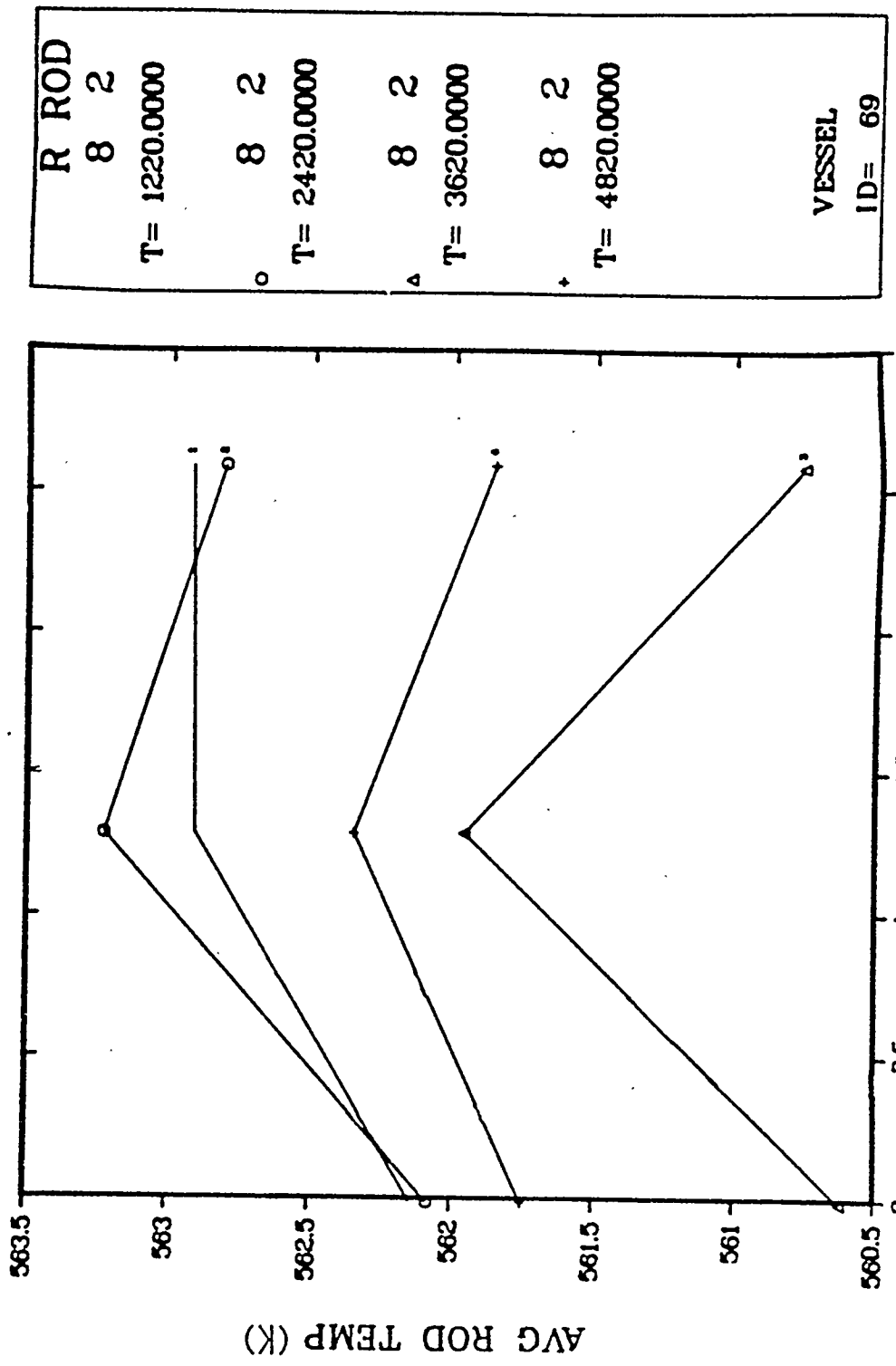

Fig. B-1.31. Average rod temperature profile vs time (Rod 2).

APPENDIX B-2

ADDITIONAL PLOTS FOR BASE CASE CALCULATION

81 minutes $\leq$ T $\leq$ 138 minutes

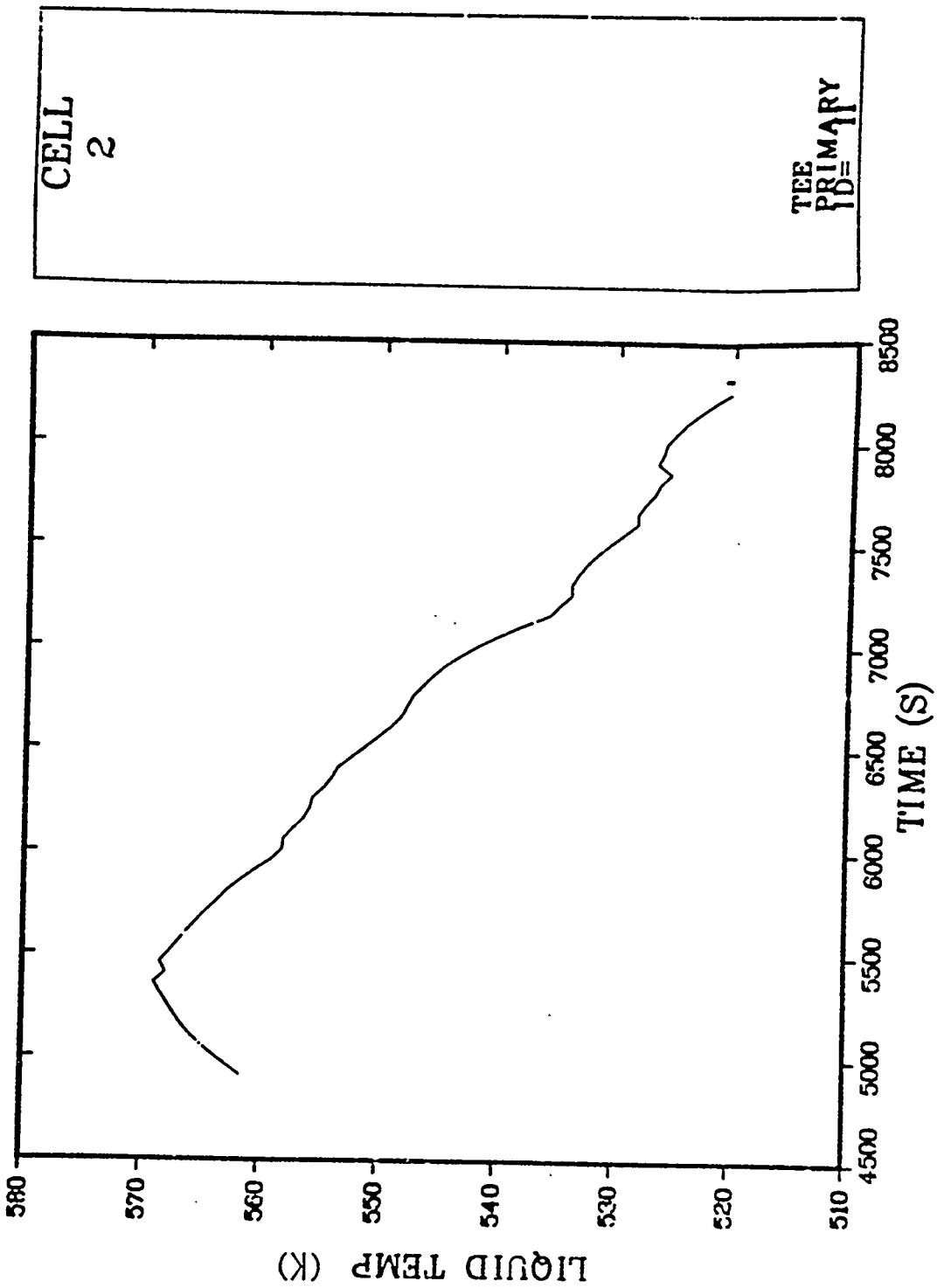

Fig. B-2.1. A Loop hot-leg liquid temperature.

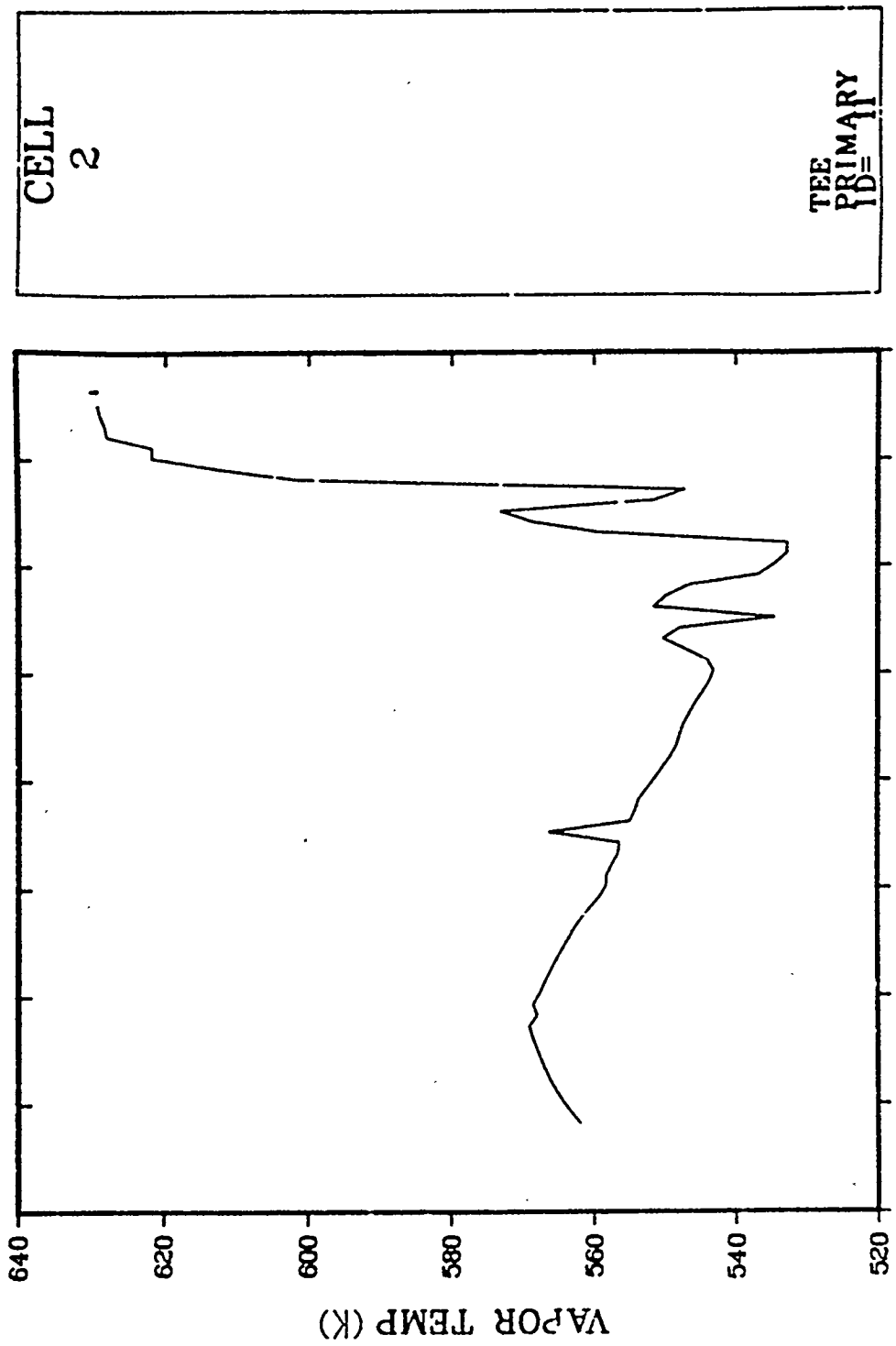

Fig. B-2.2. A Loop hot-leg vapor temperature.

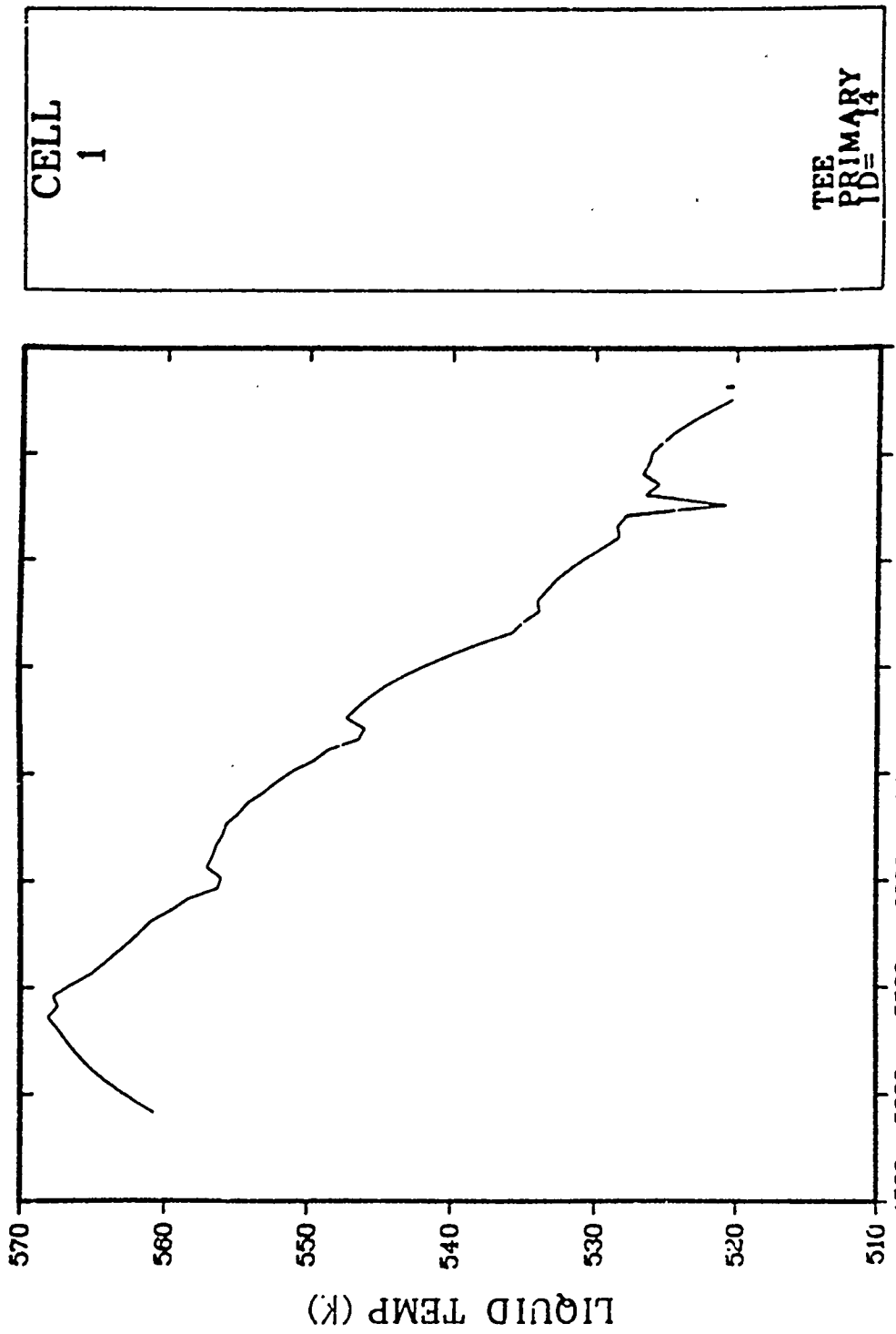

Fig. B-2.3. A Loop cold-leg liquid temperature.

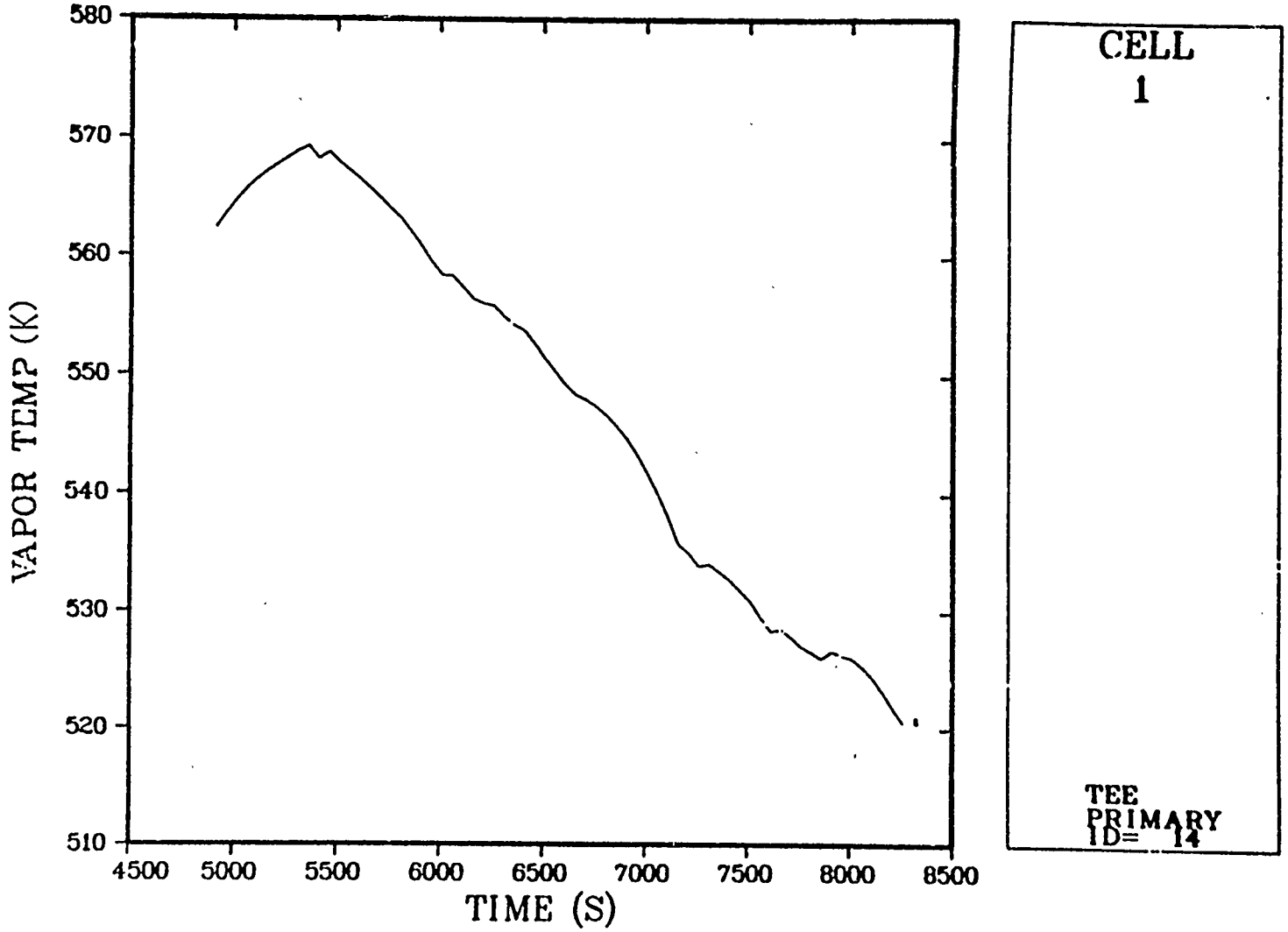

Fig. B-2.4. A Loop cold-leg vapor temperature.

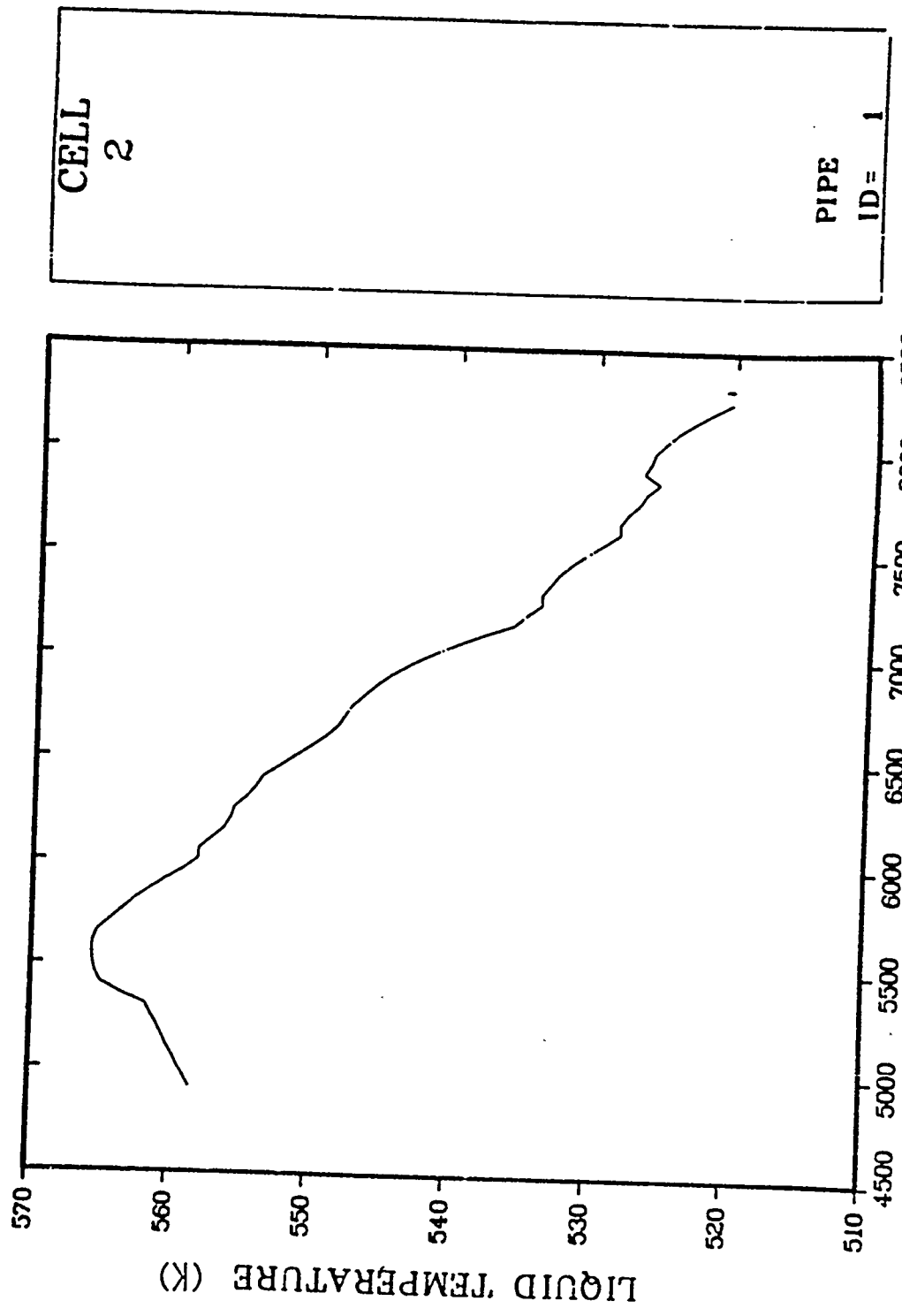

Fig. B-2.5. B Loop hot-leg liquid temperature.

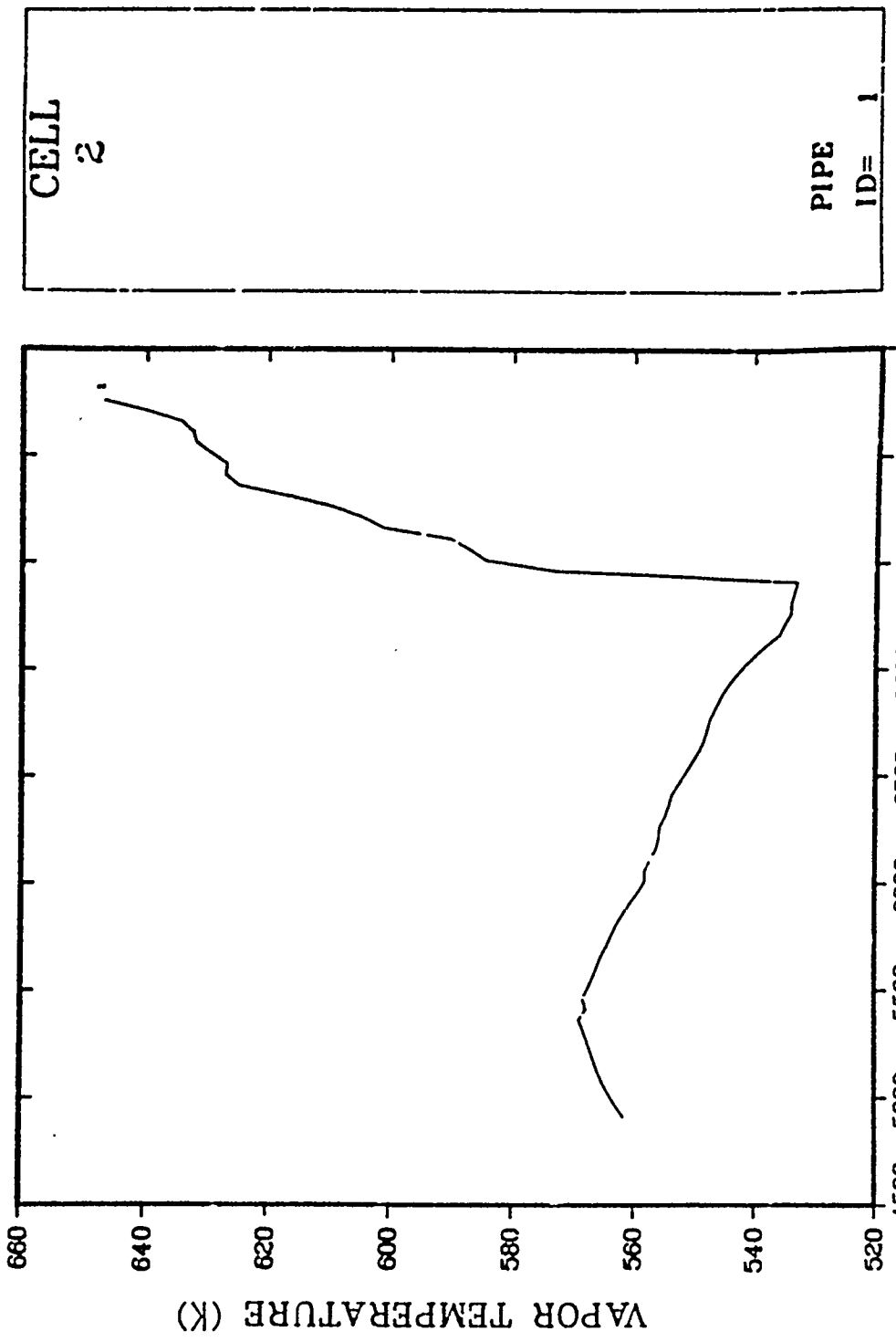

Fig. B-2.6. B Loop hot-leg vapor temperature.

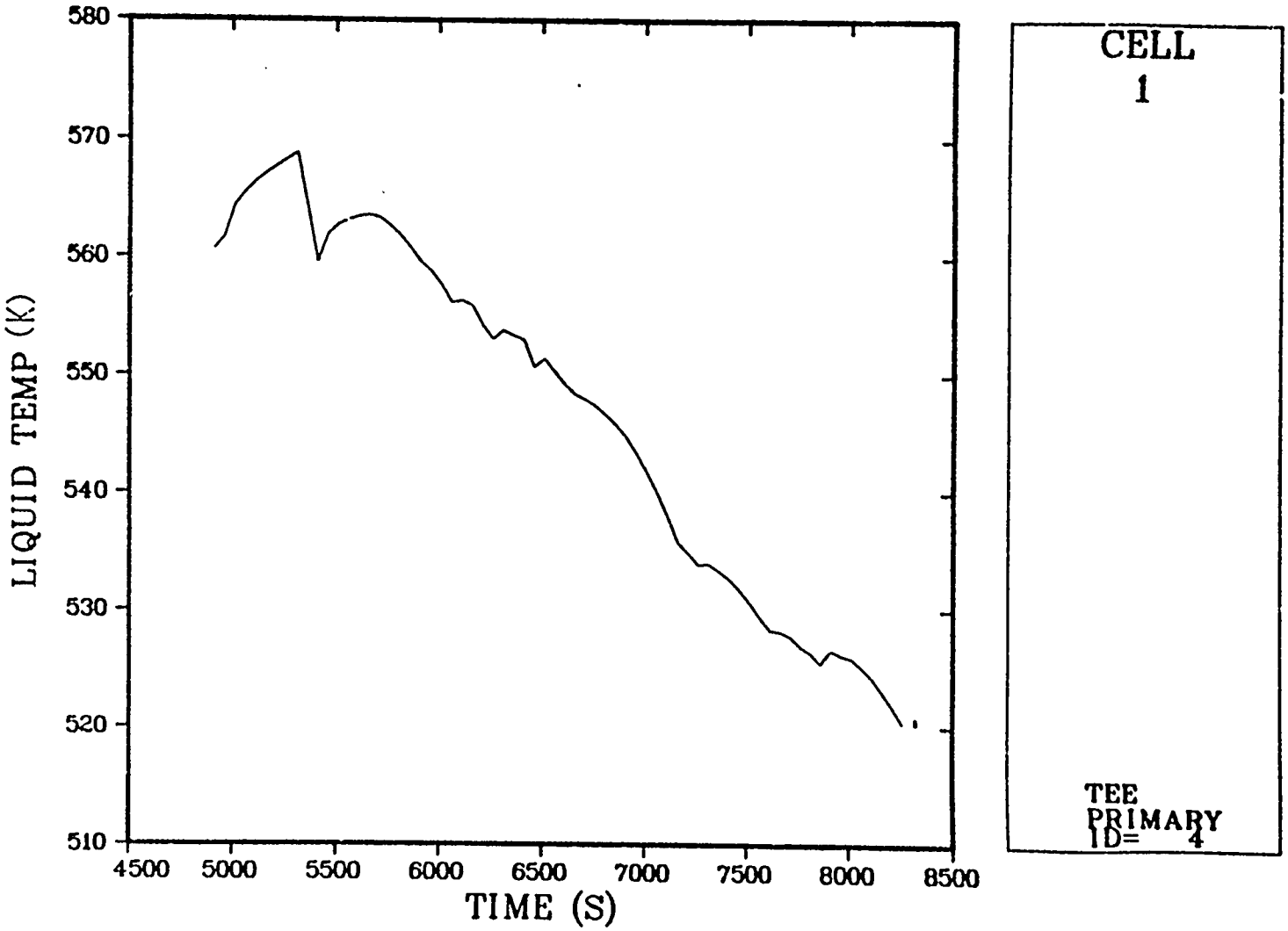

Fig. B-2.7. B Loop cold-leg liquid temperature.

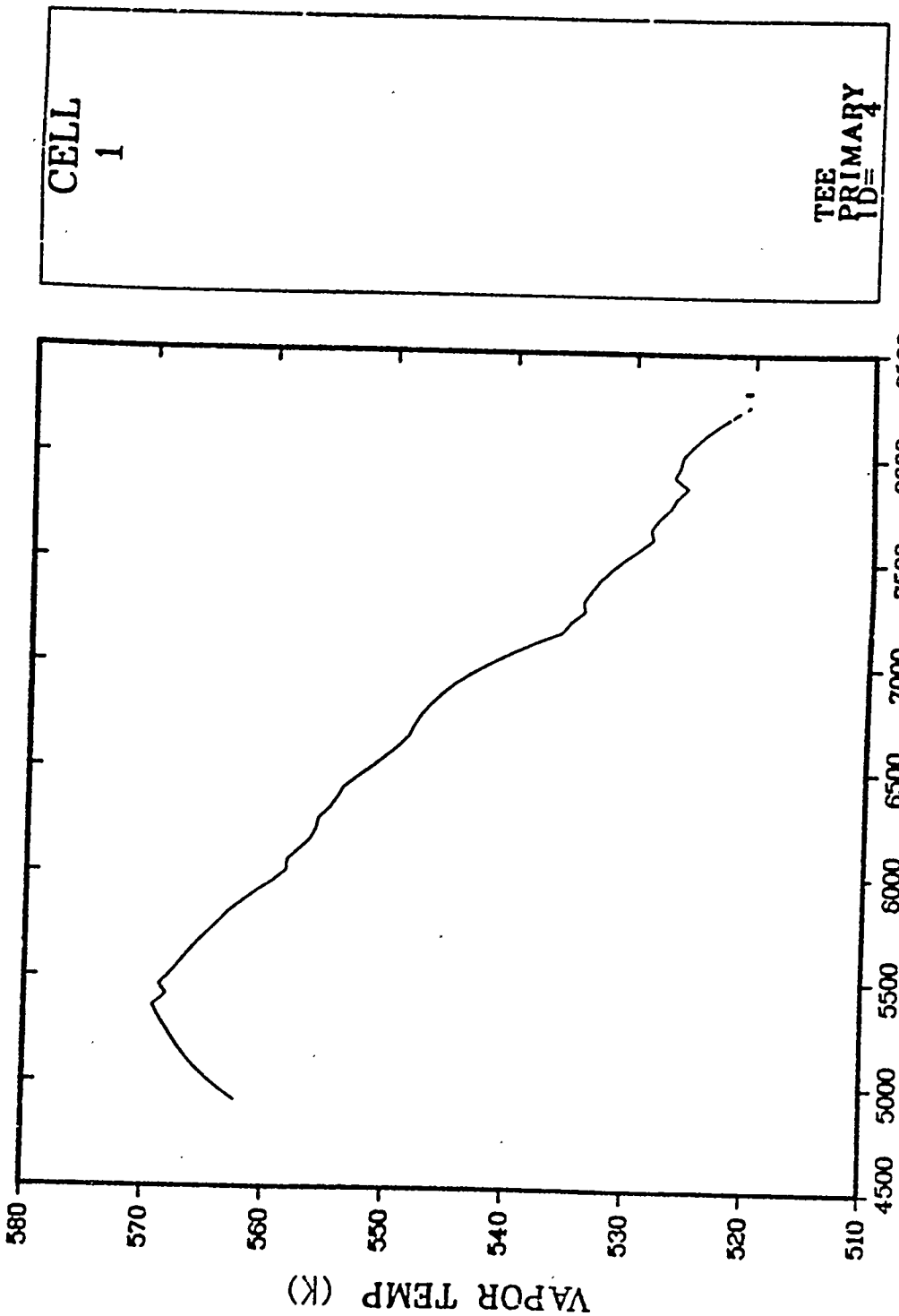

Fig. B-2.8. B Loop cold-leg vapor temperature.

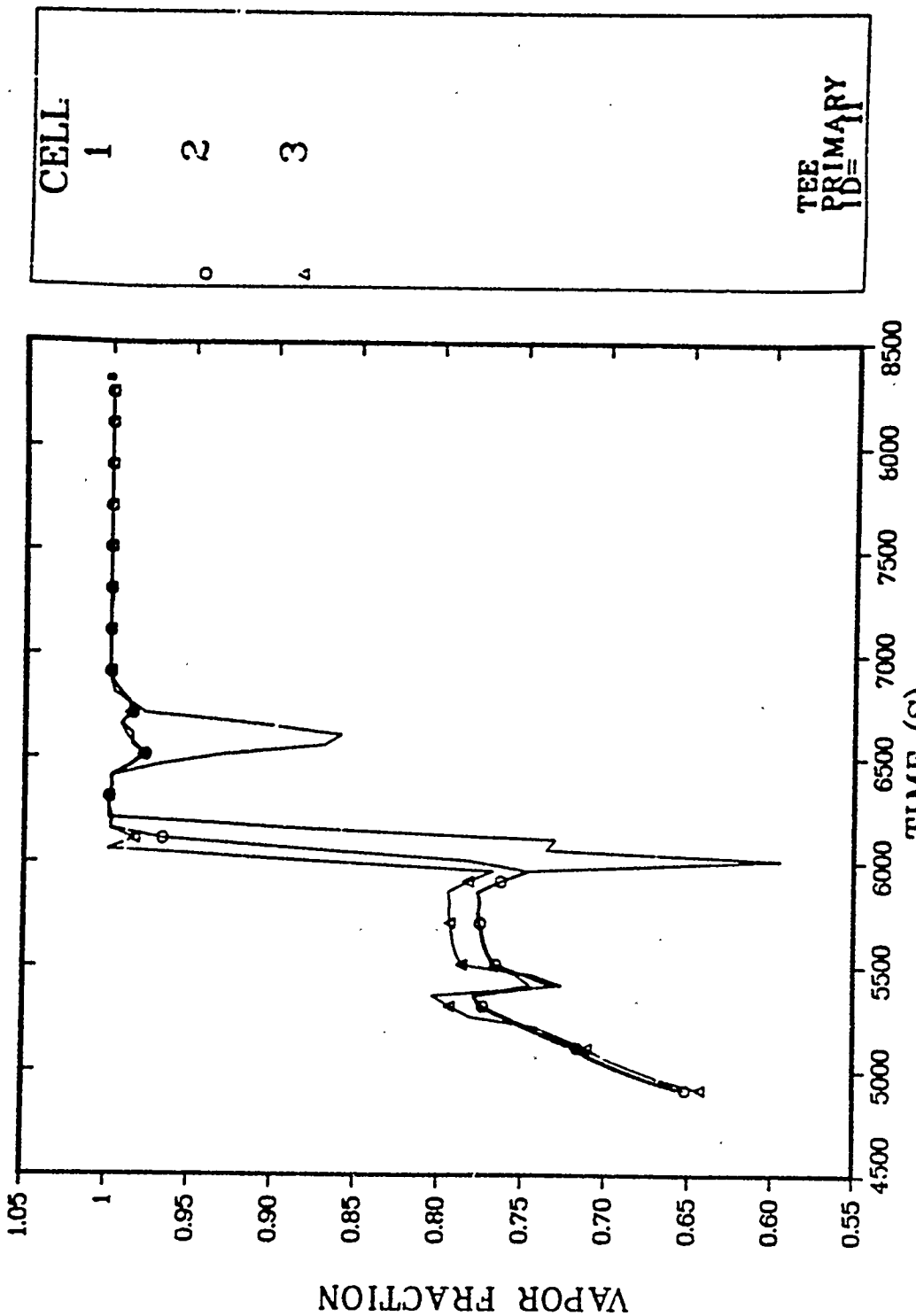

Fig. B-2.9. A Loop hot-leg void fraction distribution (Cells 1, 2, 3).

Fig. B-2.10. A Loop pump mass flow rate.

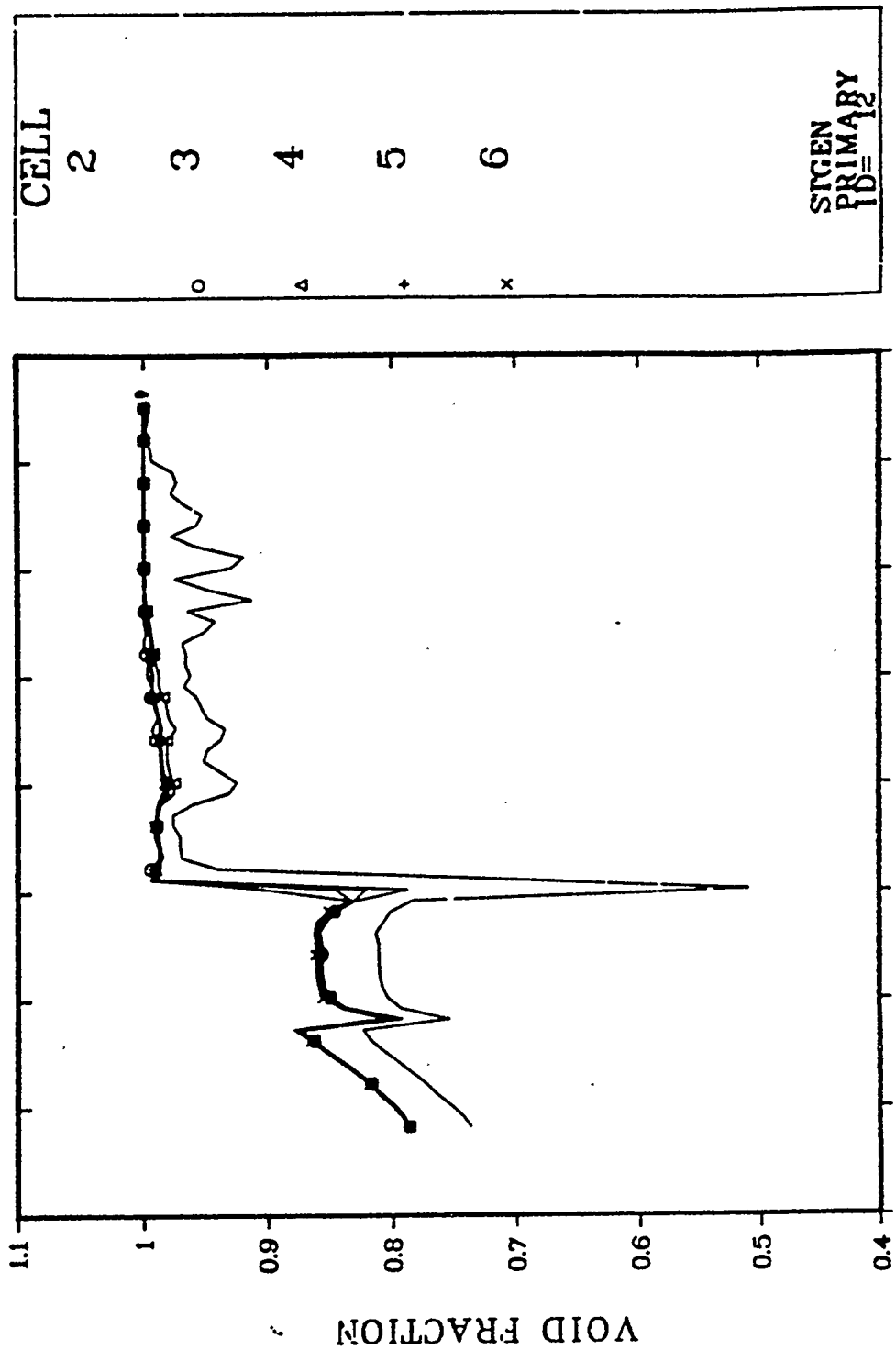

Fig. B-2.11. A Loop steam generator void fraction distribution.

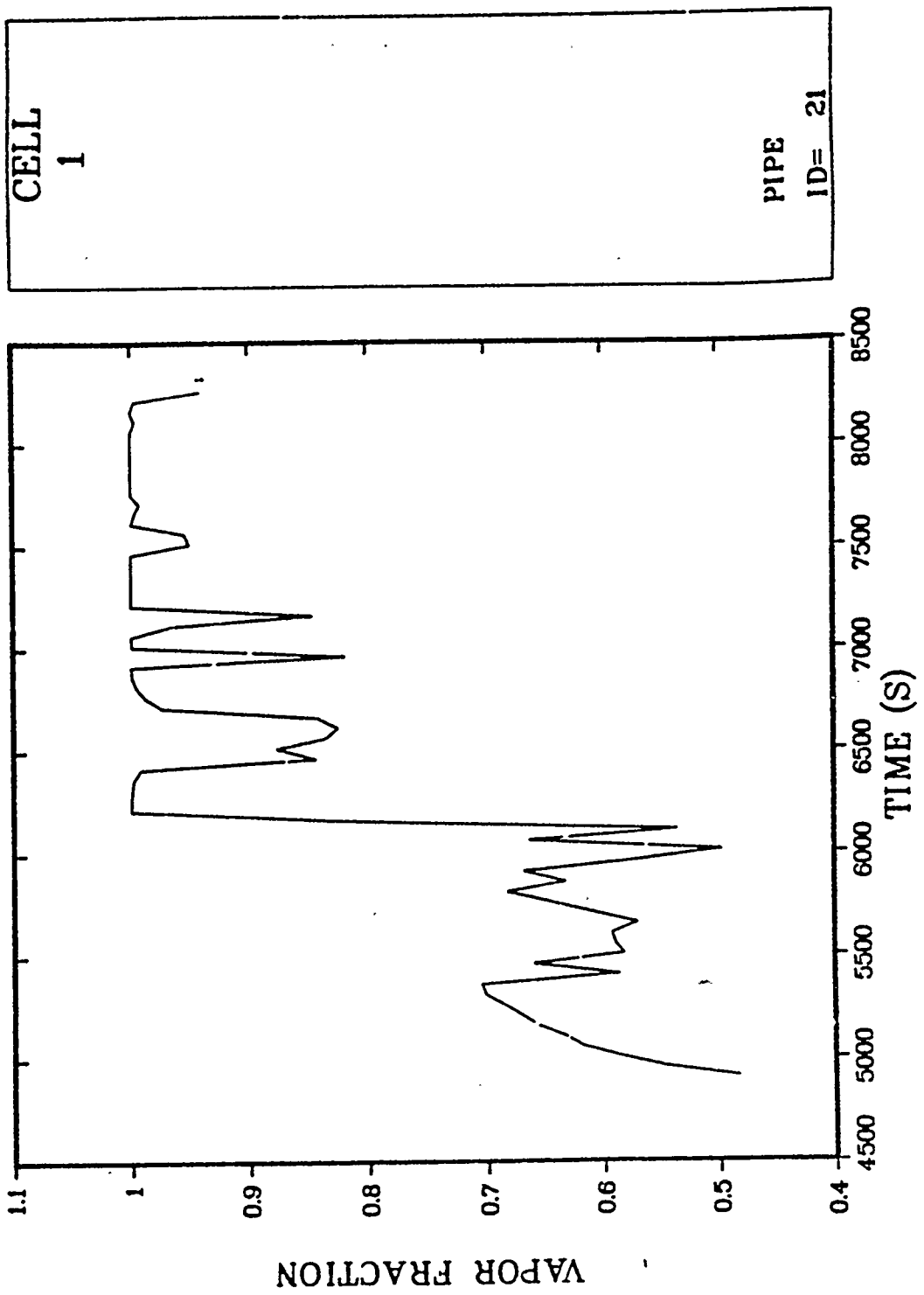

Fig. B-2.12. Pressurizer surge line void fraction.

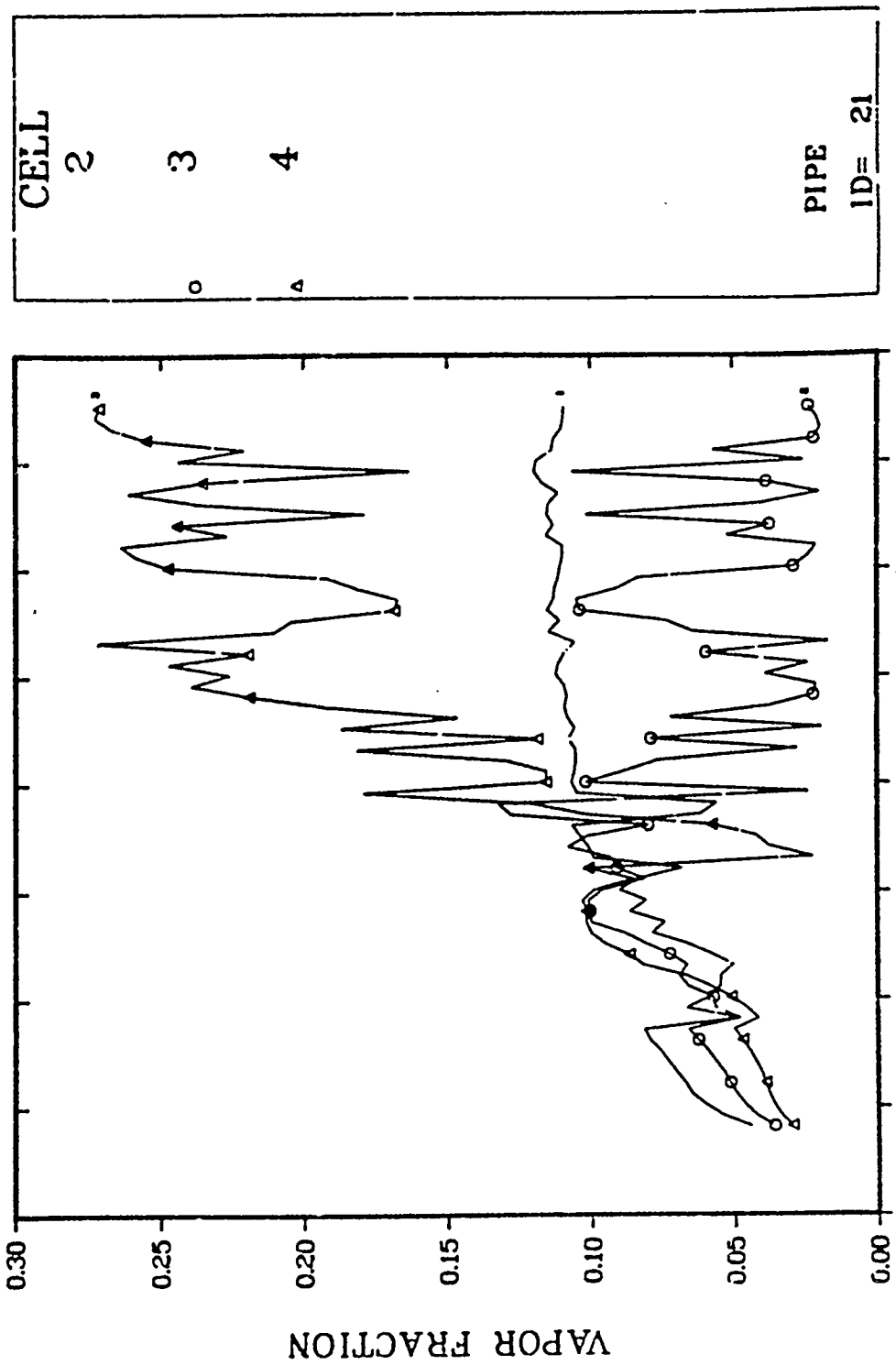

Fig. B-2.13. Pressurizer void fraction distribution (first 3 cells).

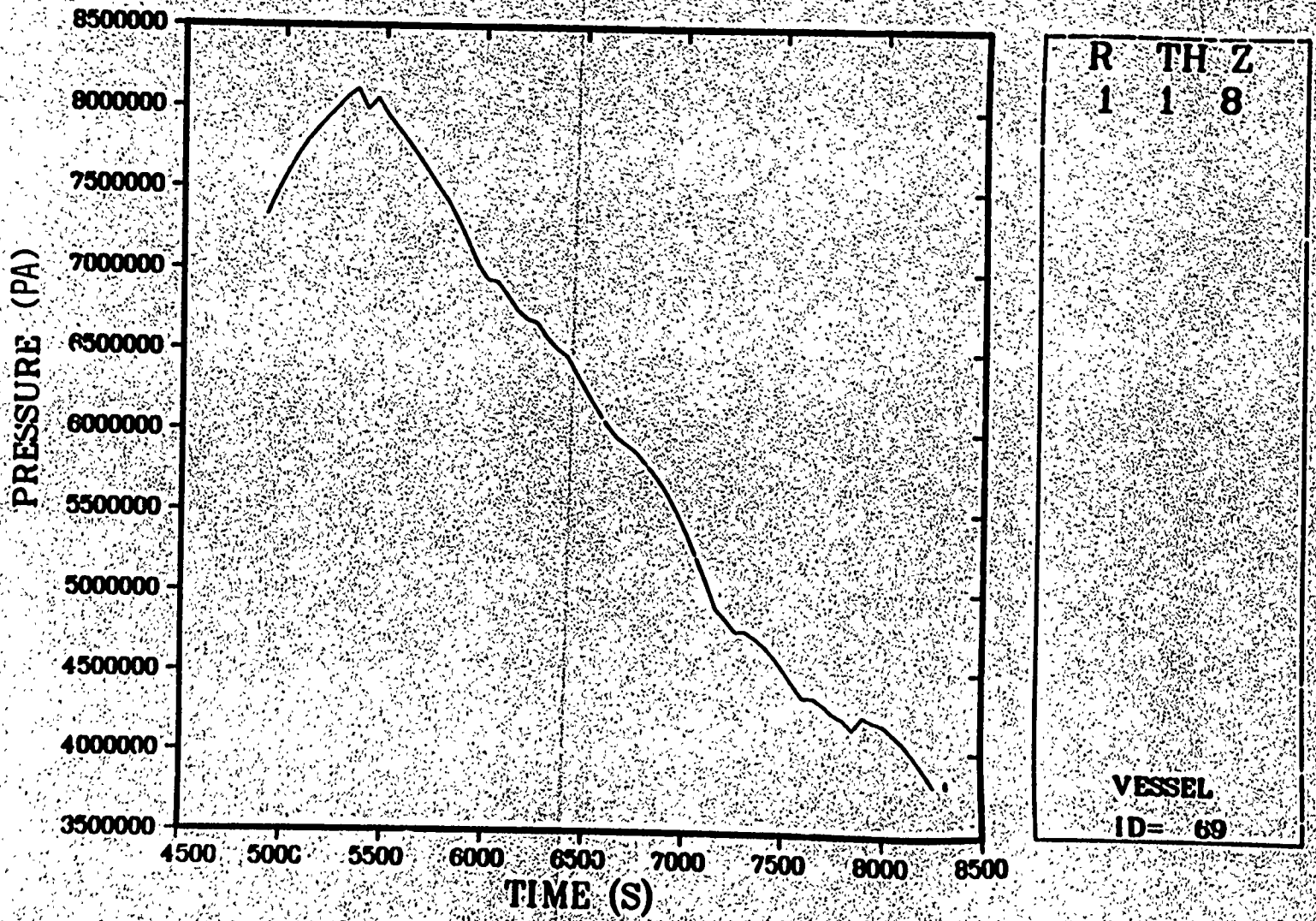

Fig. B-2.15. Upper plenum pressure.

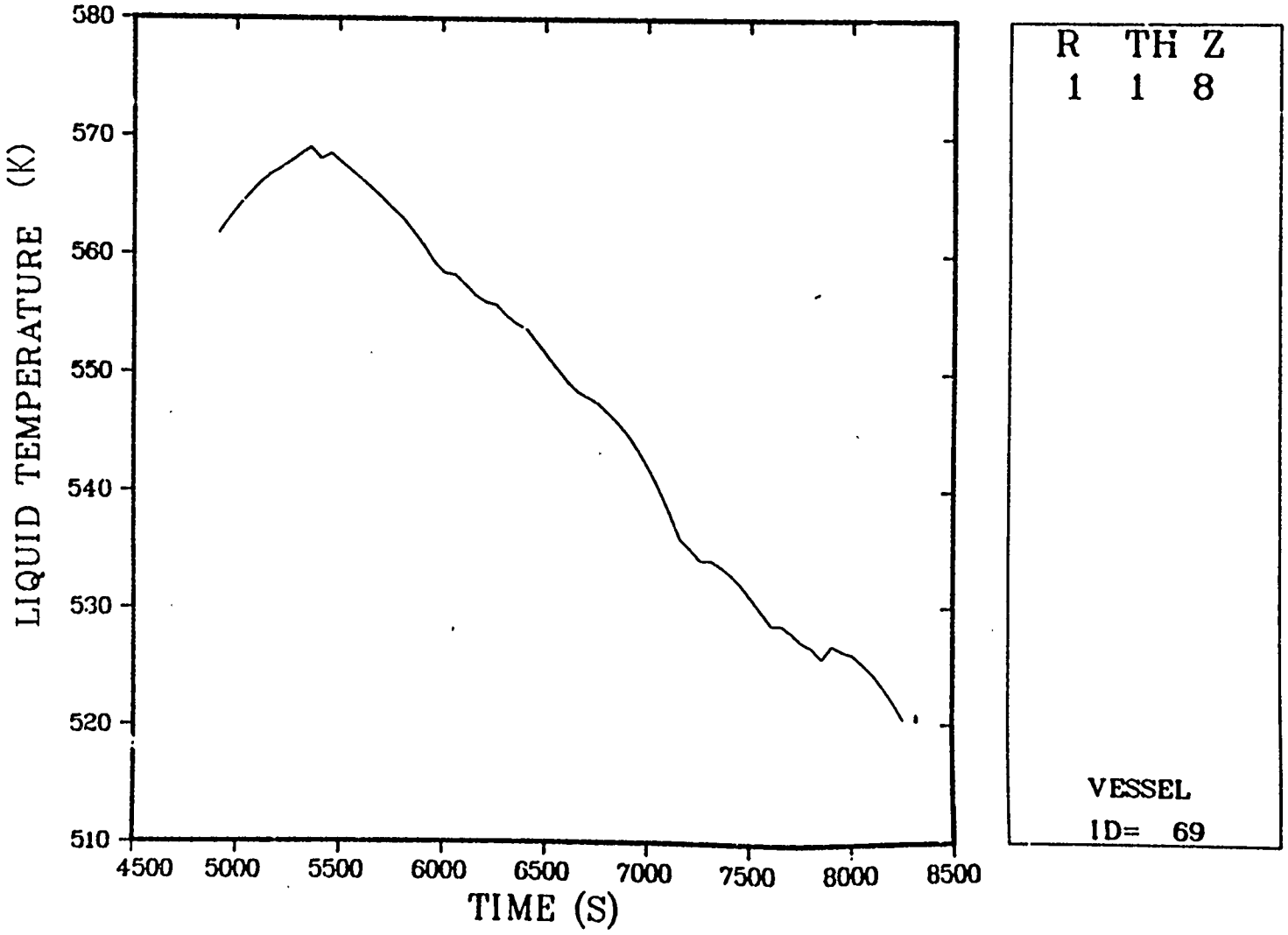

Fig. B-2.16. Upper plenum liquid temperature.

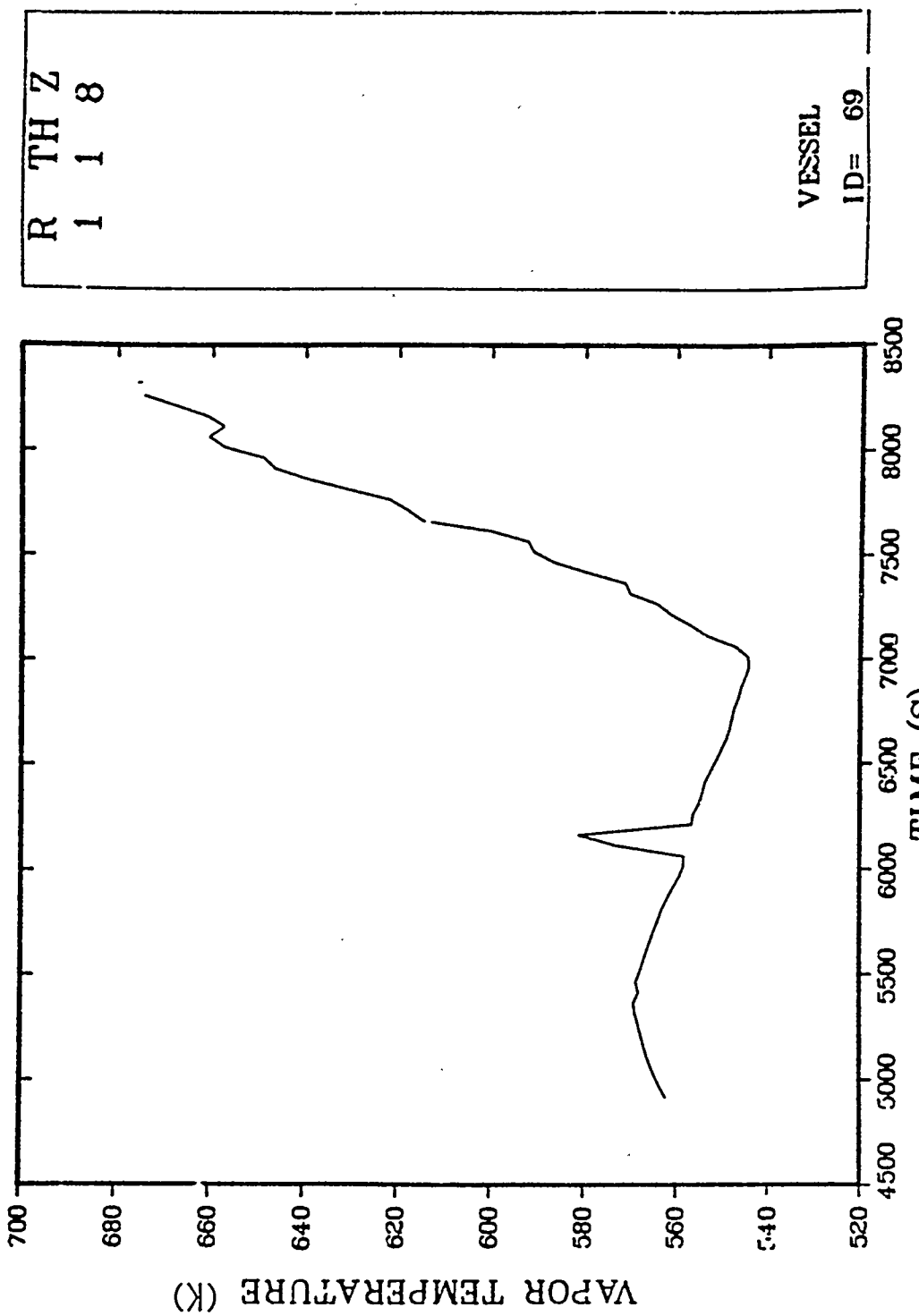

Fig. B-2.17. Upper plenum vapor temperature.

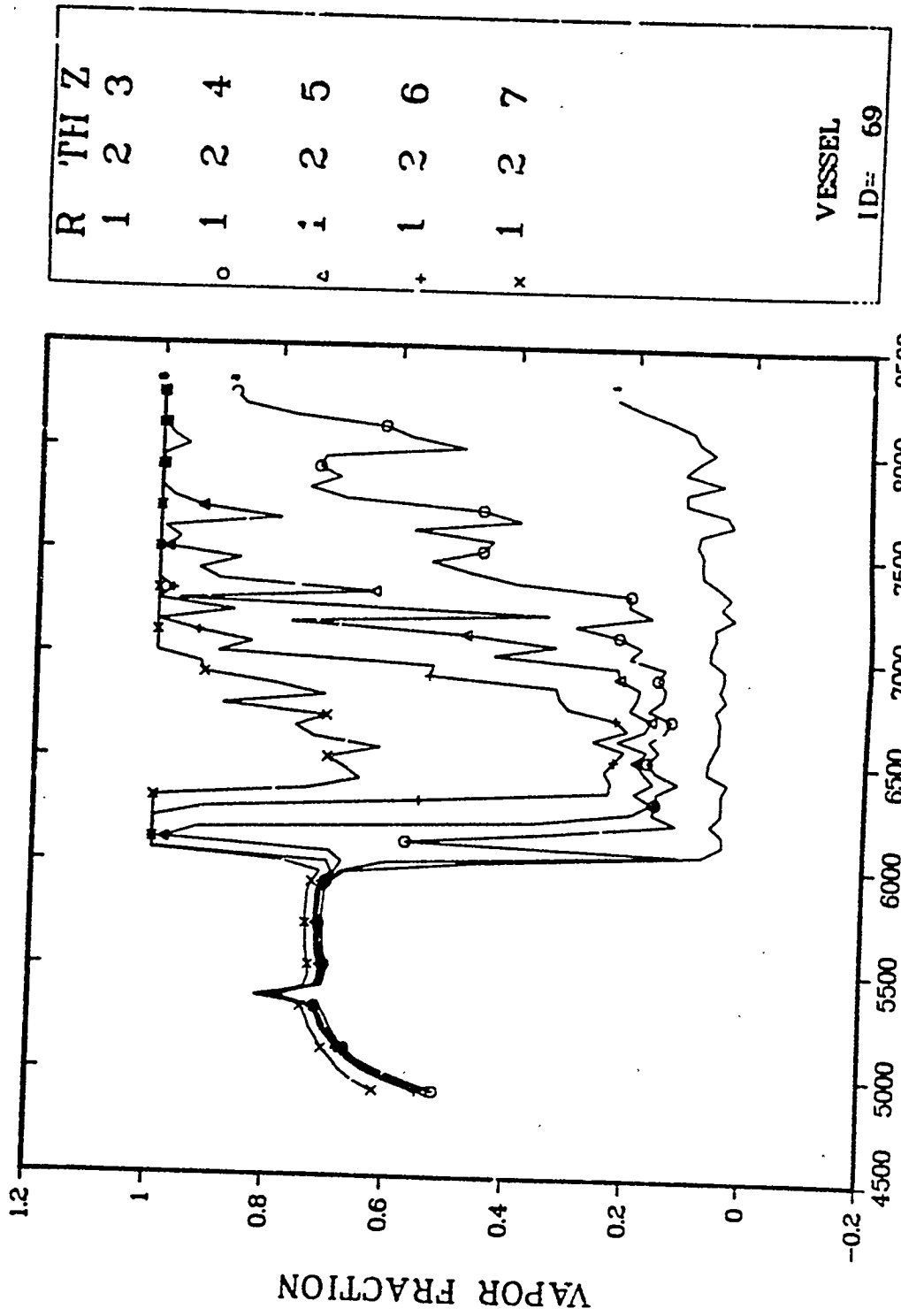

Fig. B-2.18. Core void fraction profile (axial direction).

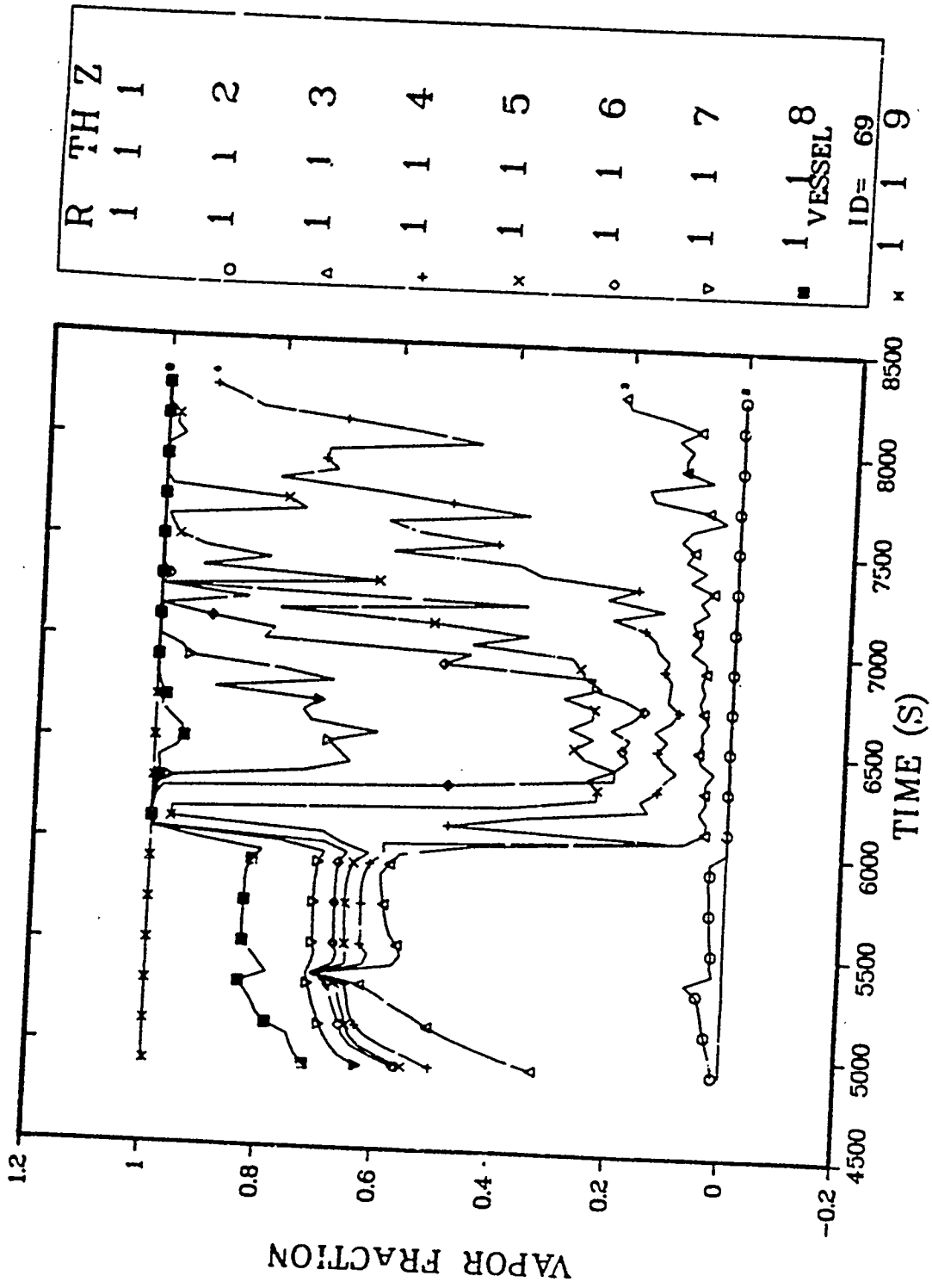

Fig. B-2.19. Vessel void fraction profile
(axial direction - first azimuthal cell).

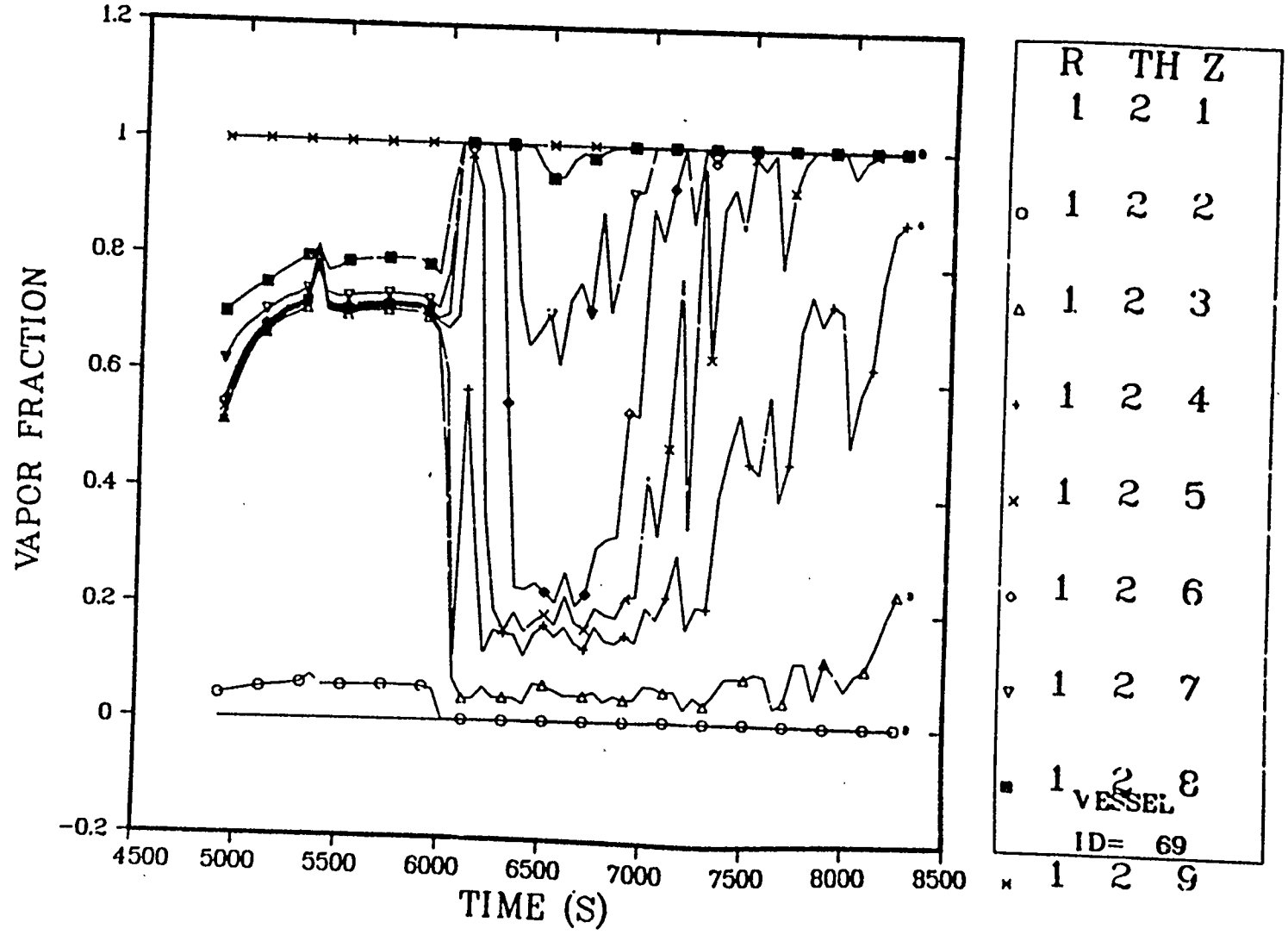

Fig. B-2.20. Vessel void fraction profile (axial direction - second azimuthal cell).

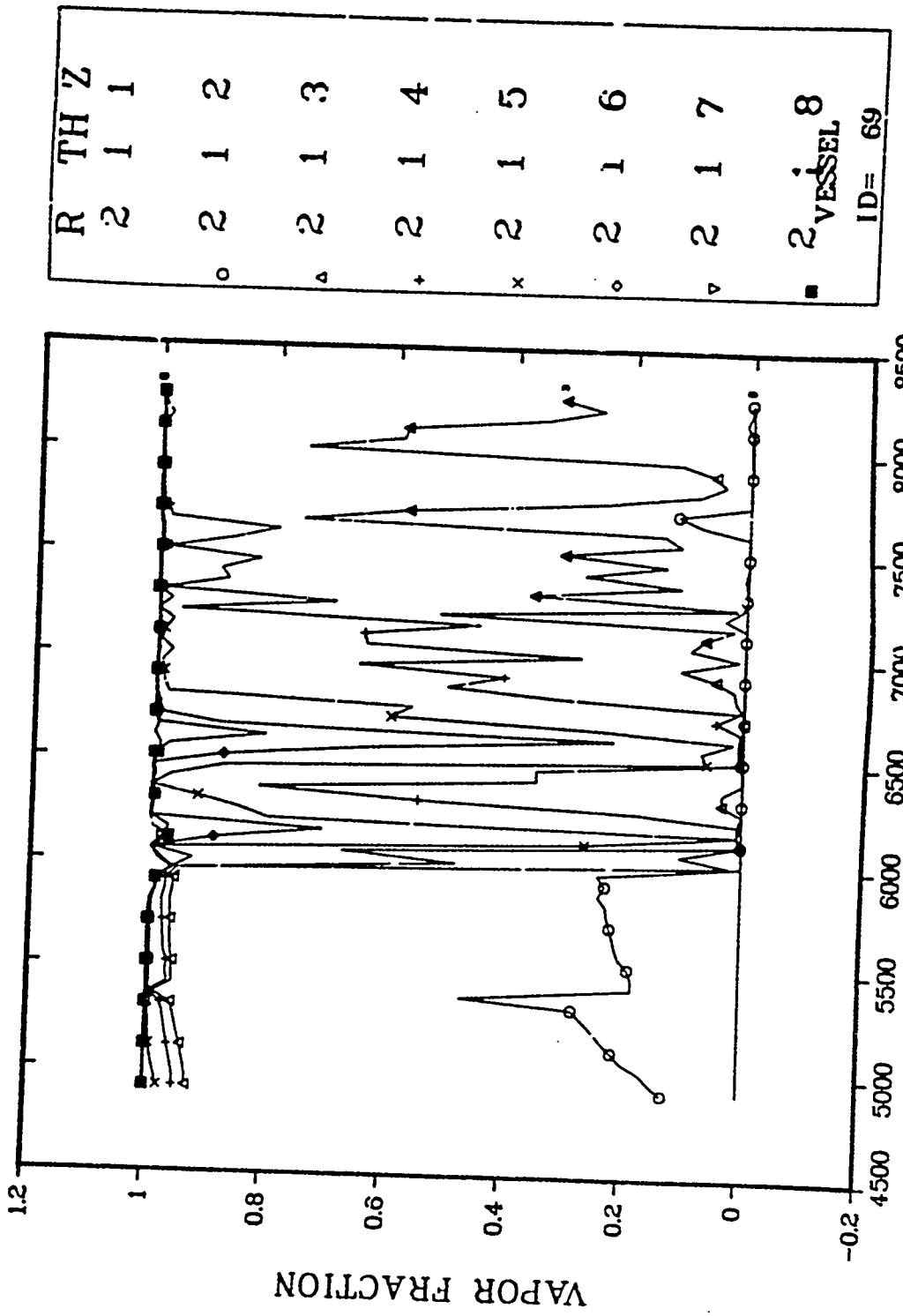

Fig. B-2.21. Downcomer void fraction profile (Cell 1).

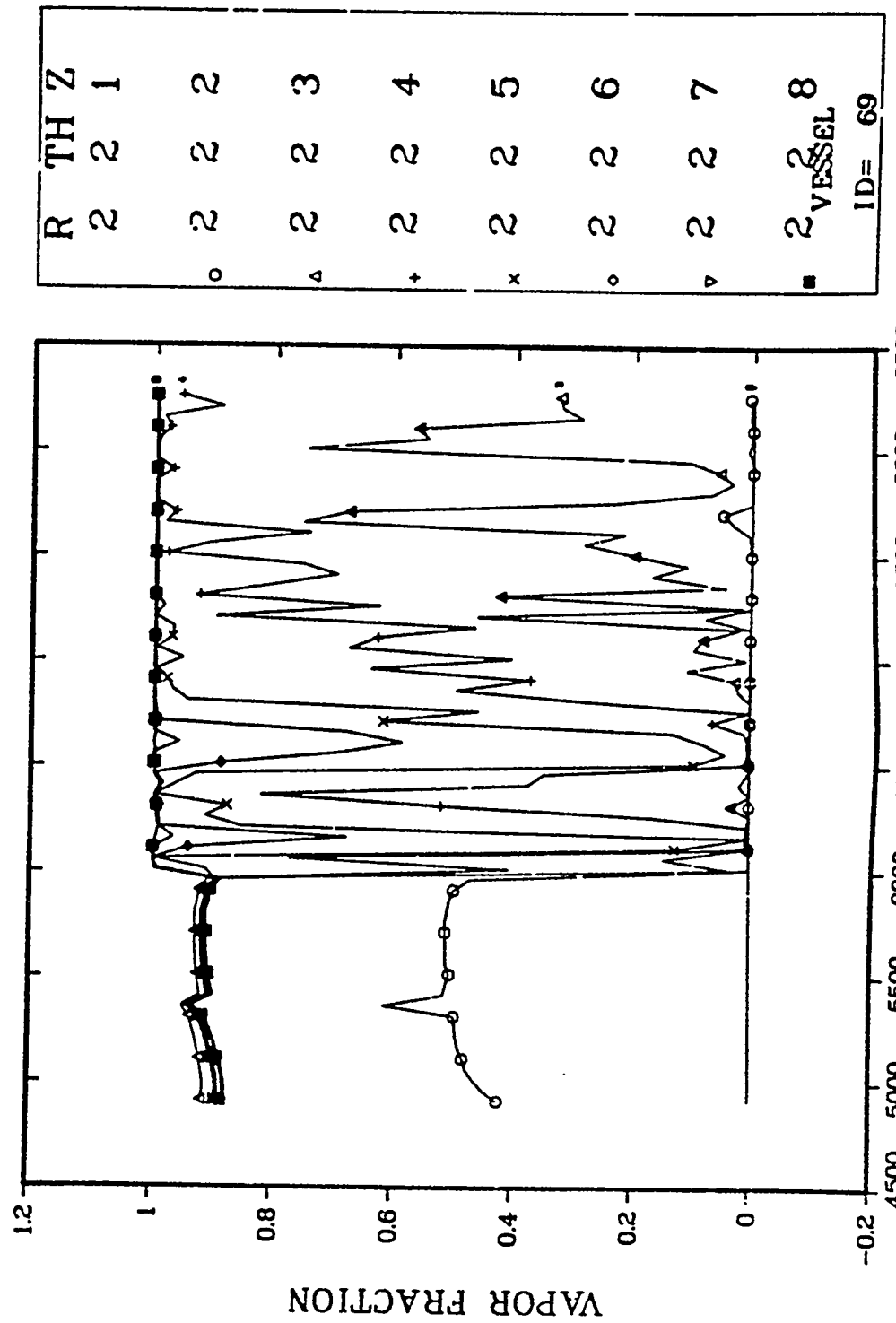

Fig. B-2.22. Downcomer void fraction profile (Cell 2).

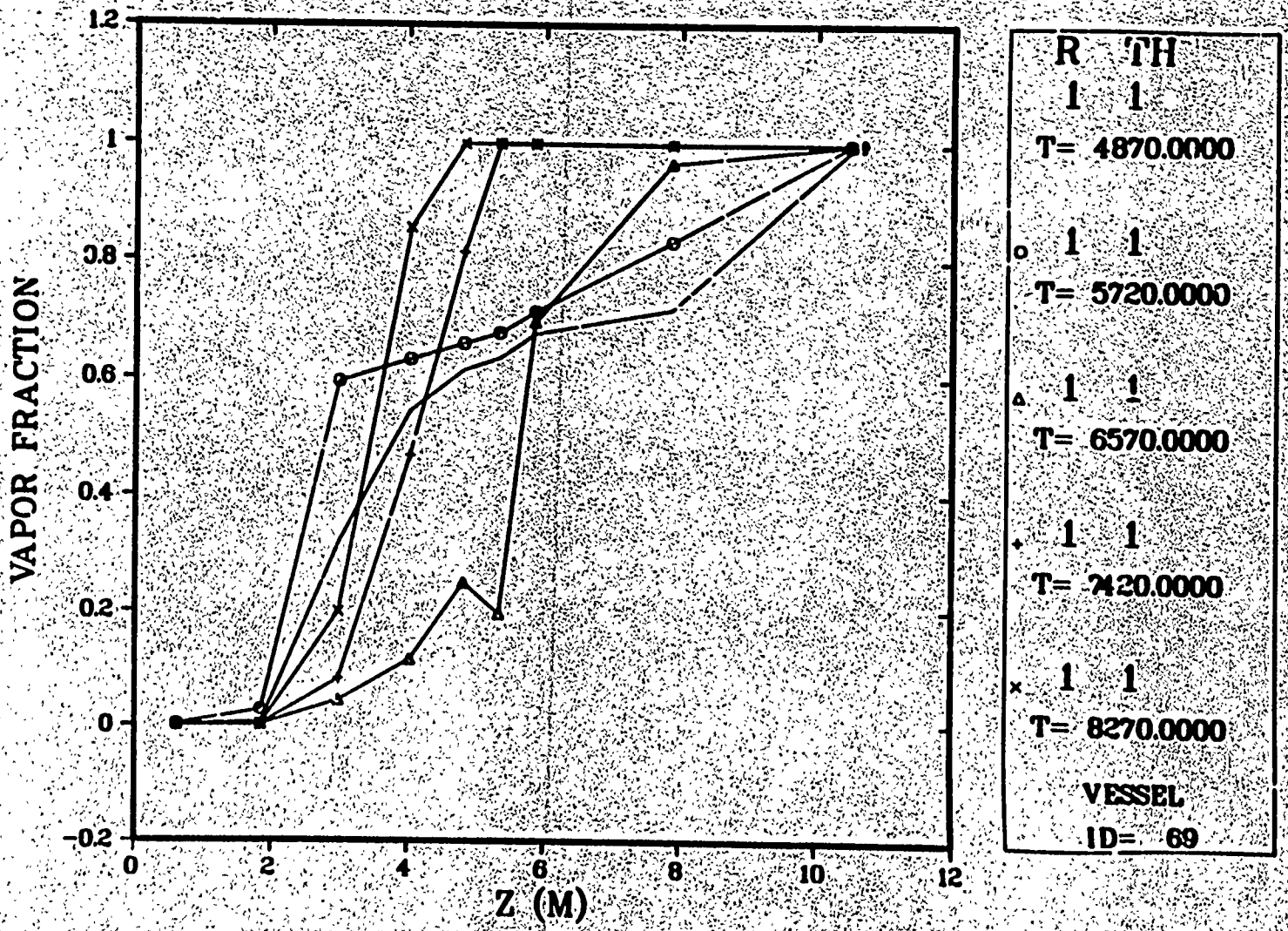

Fig. B-2-23. Vessel void fraction profile vs time (Cell 1).

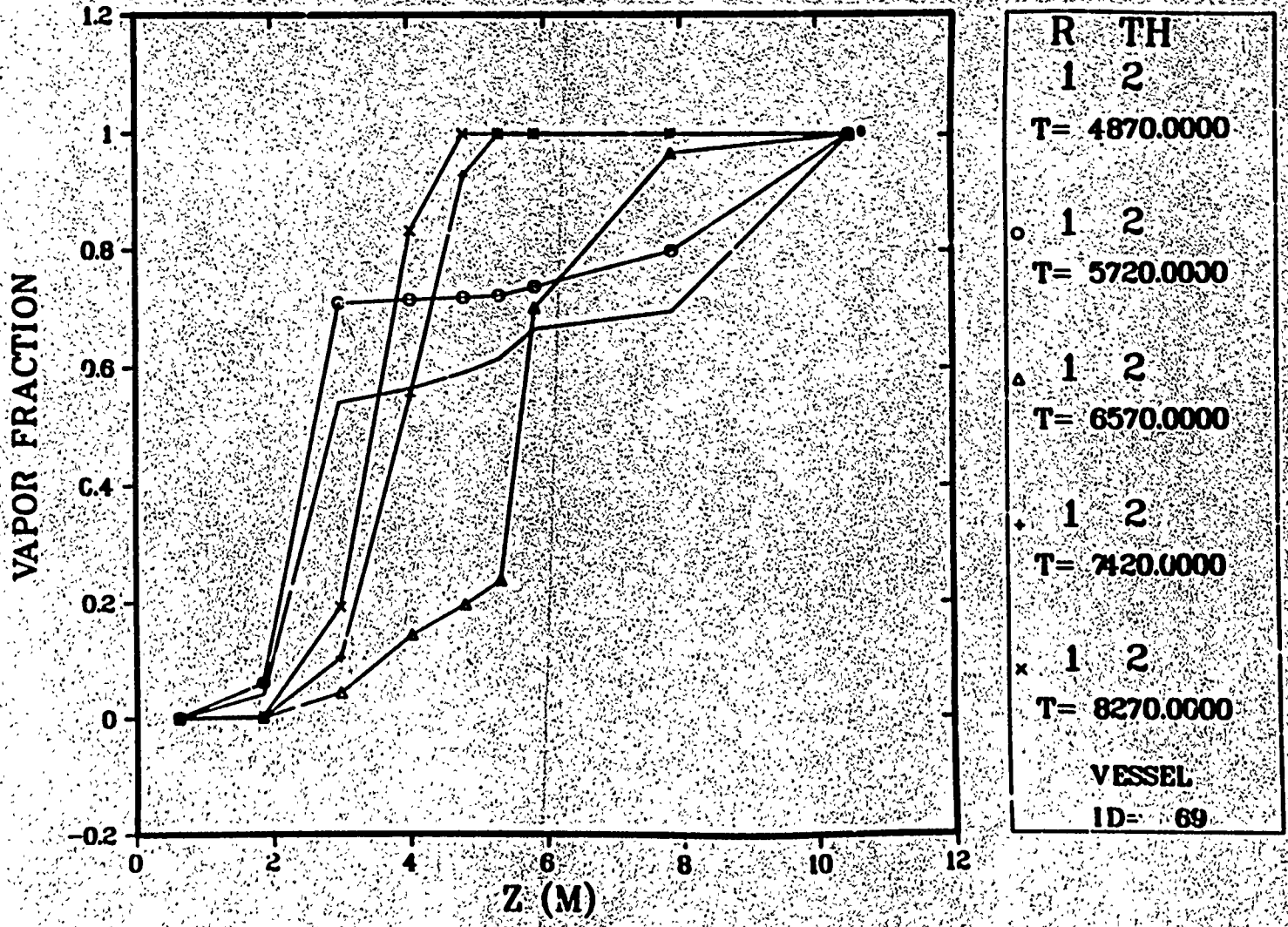

Fig. B-2.24. Vessel void fraction profile vs time (Cell 2).

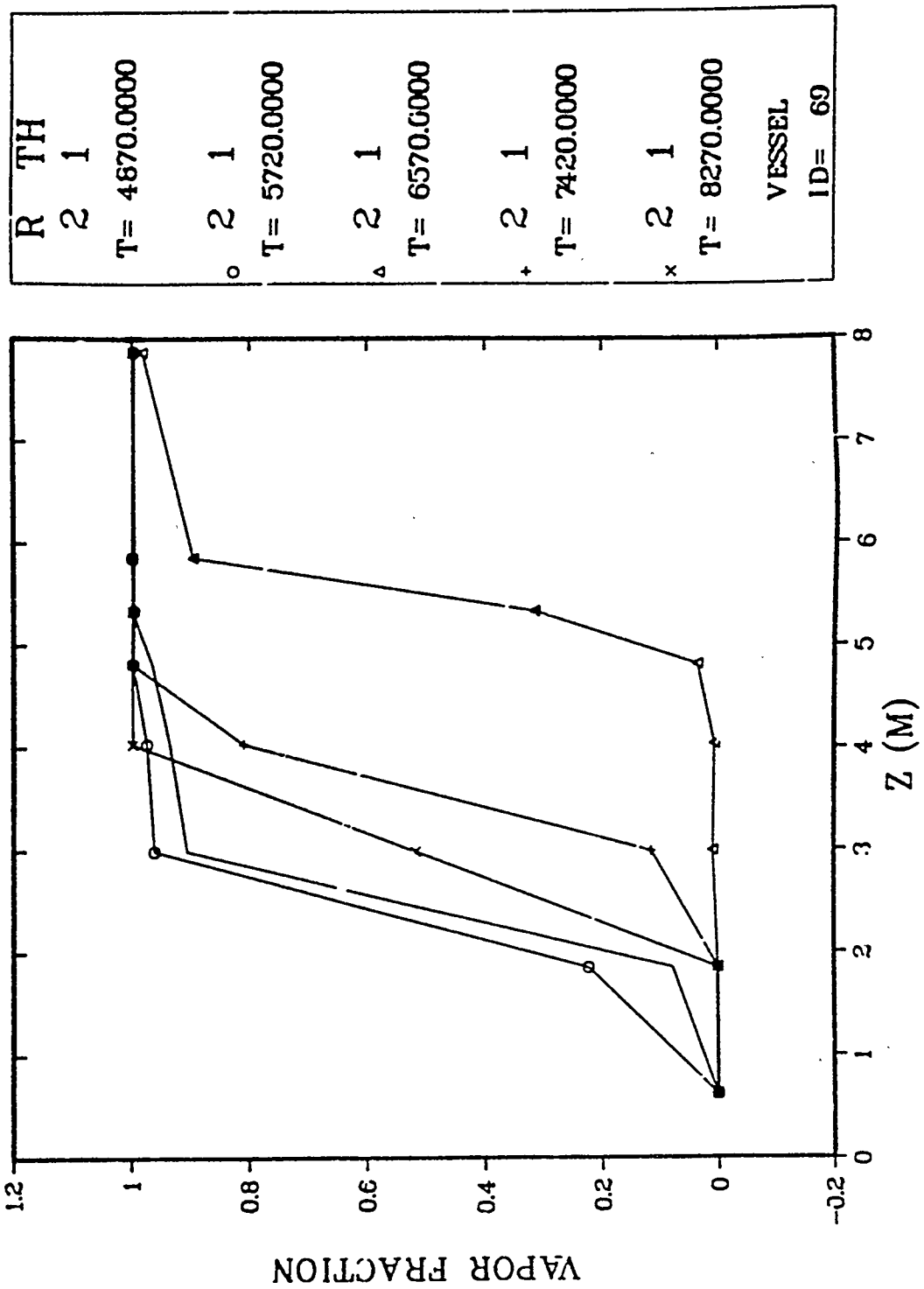

Fig. B-2.25. Downcomer void fraction profile vs time.

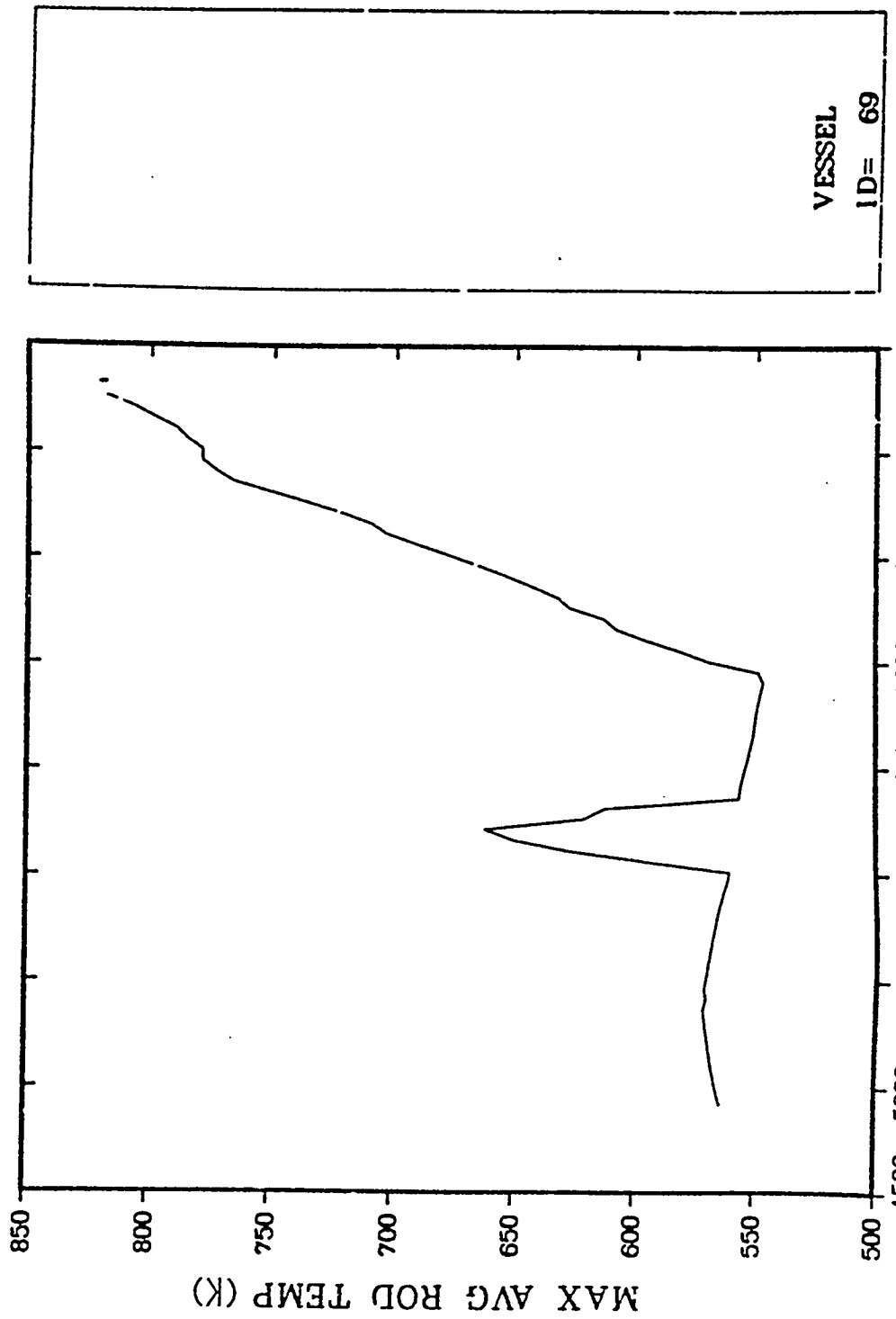

Fig. B-2.26. Maximum average rod temperature.

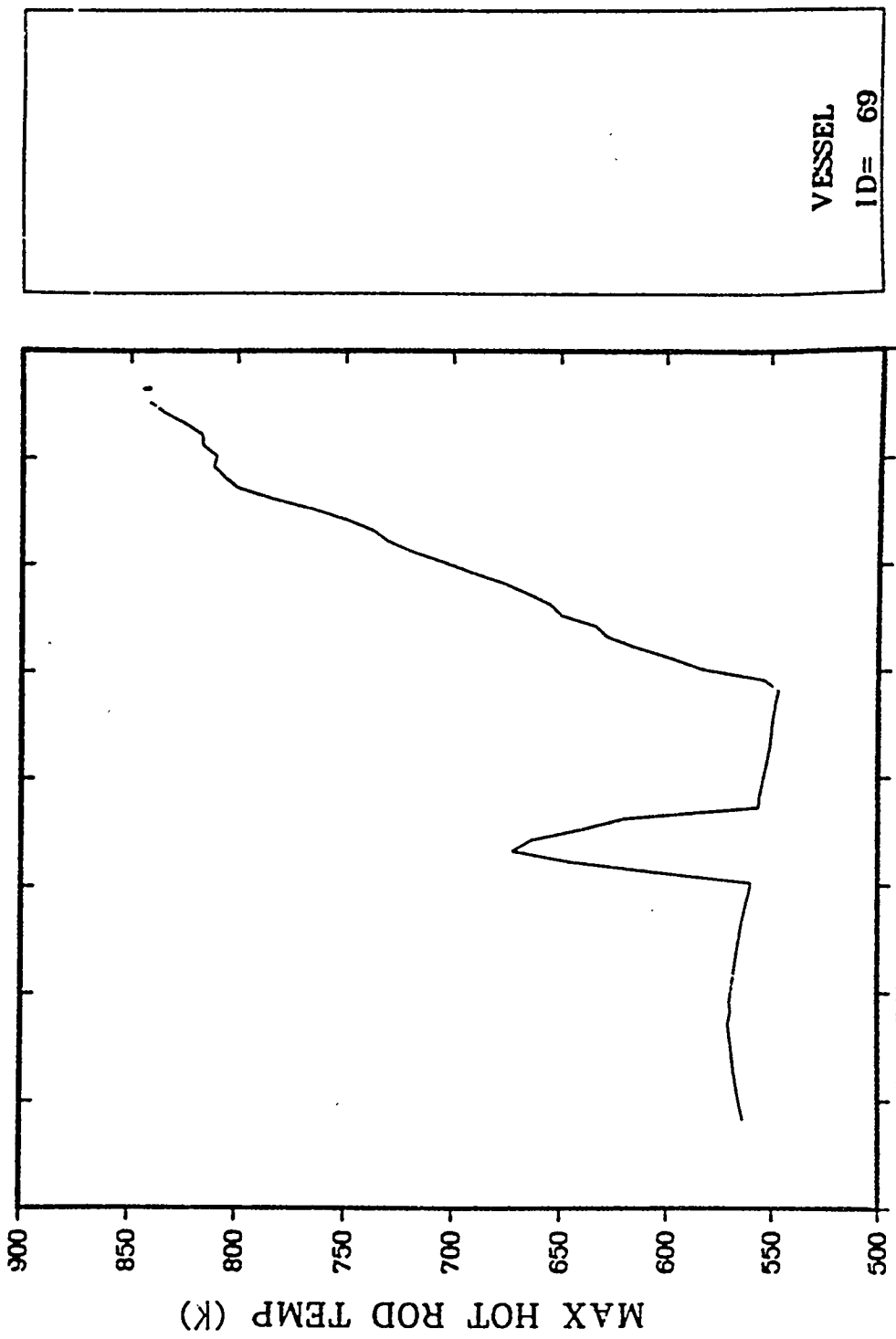

Fig. B-2.27. Maximum hot-rod temperature.

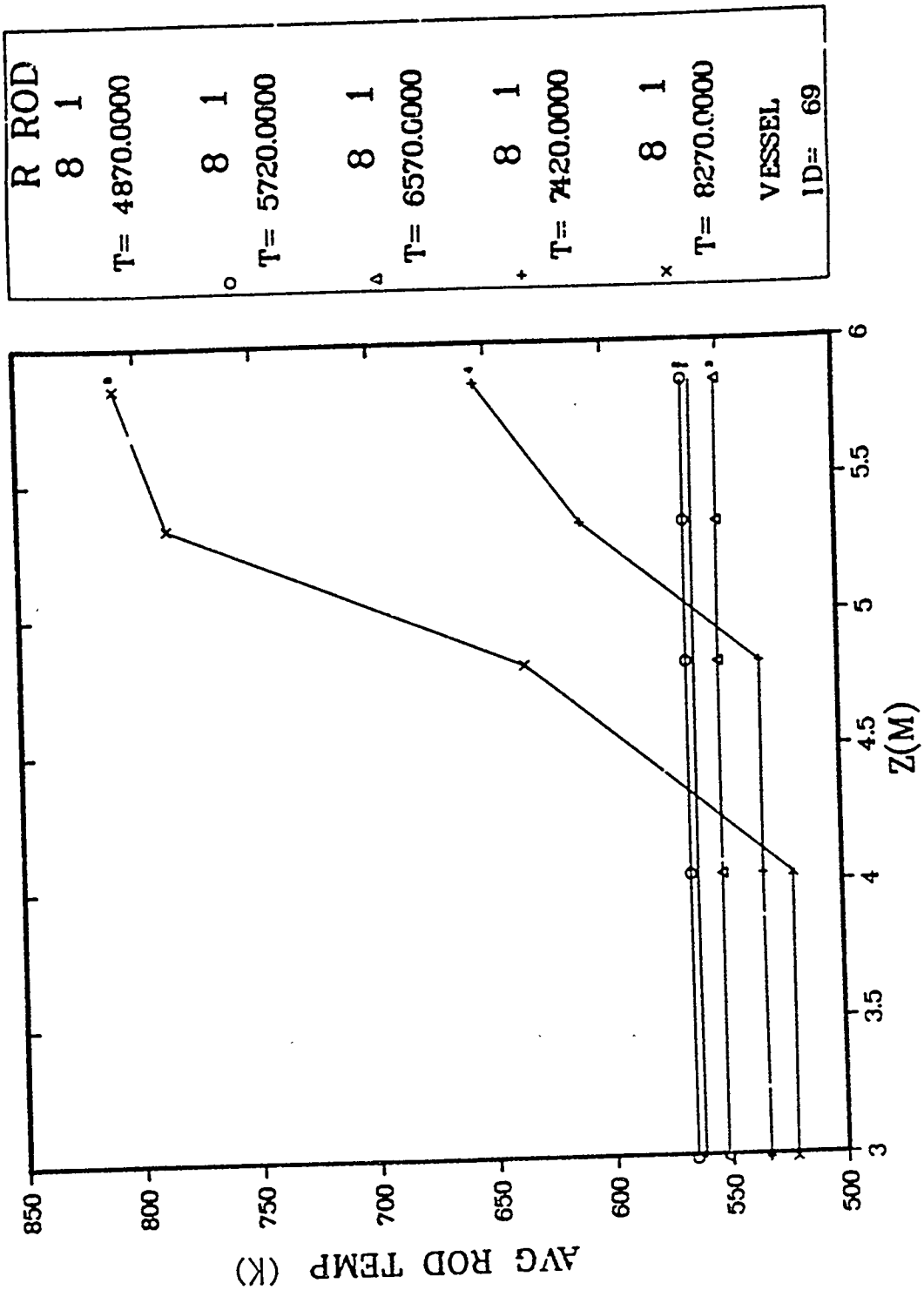

Fig. B-2.28. Average rod temperature profile vs time (Rod 1).

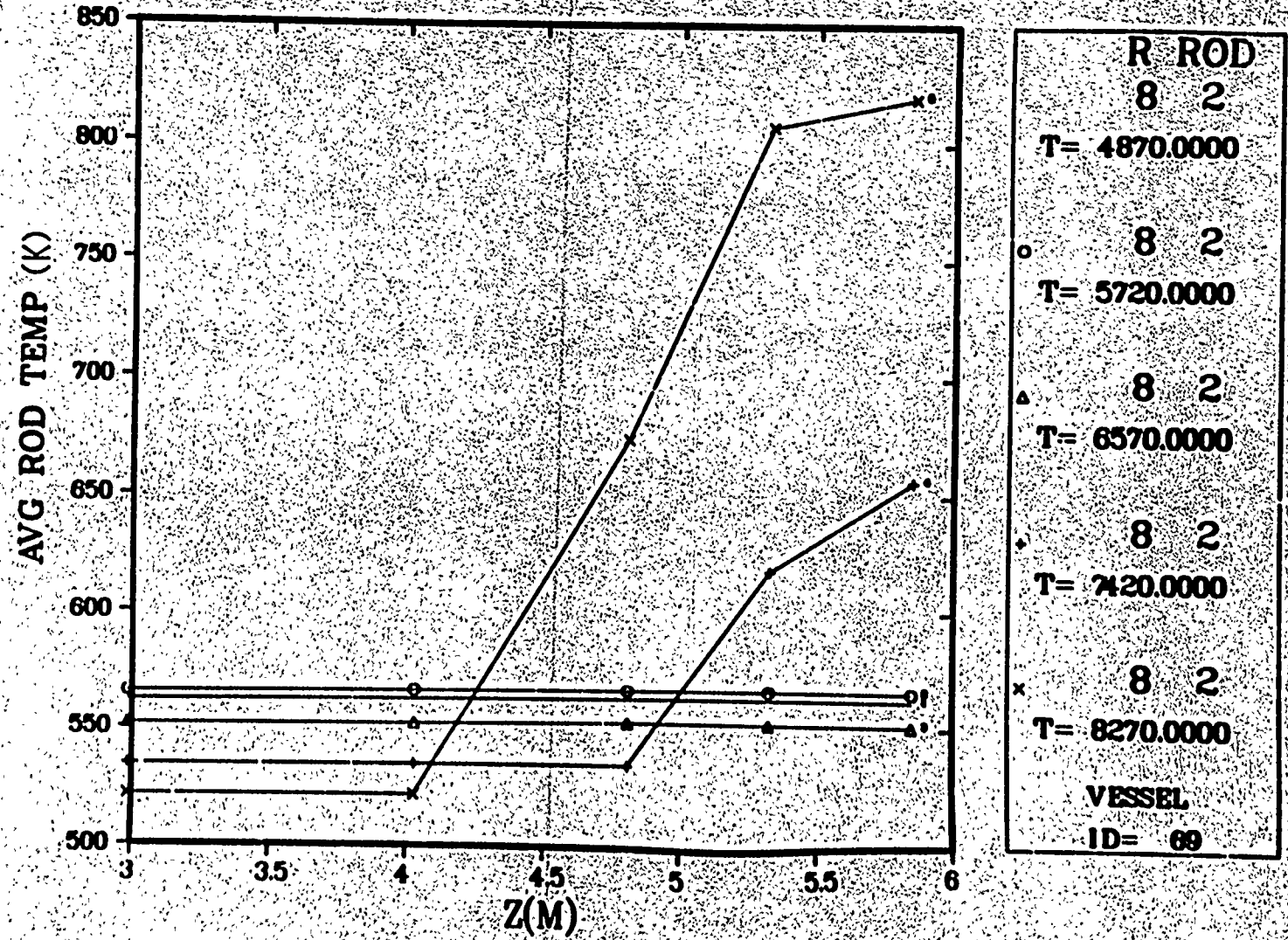

Fig. B-2.29. Average rod temperature profile vs time (Rod 2).

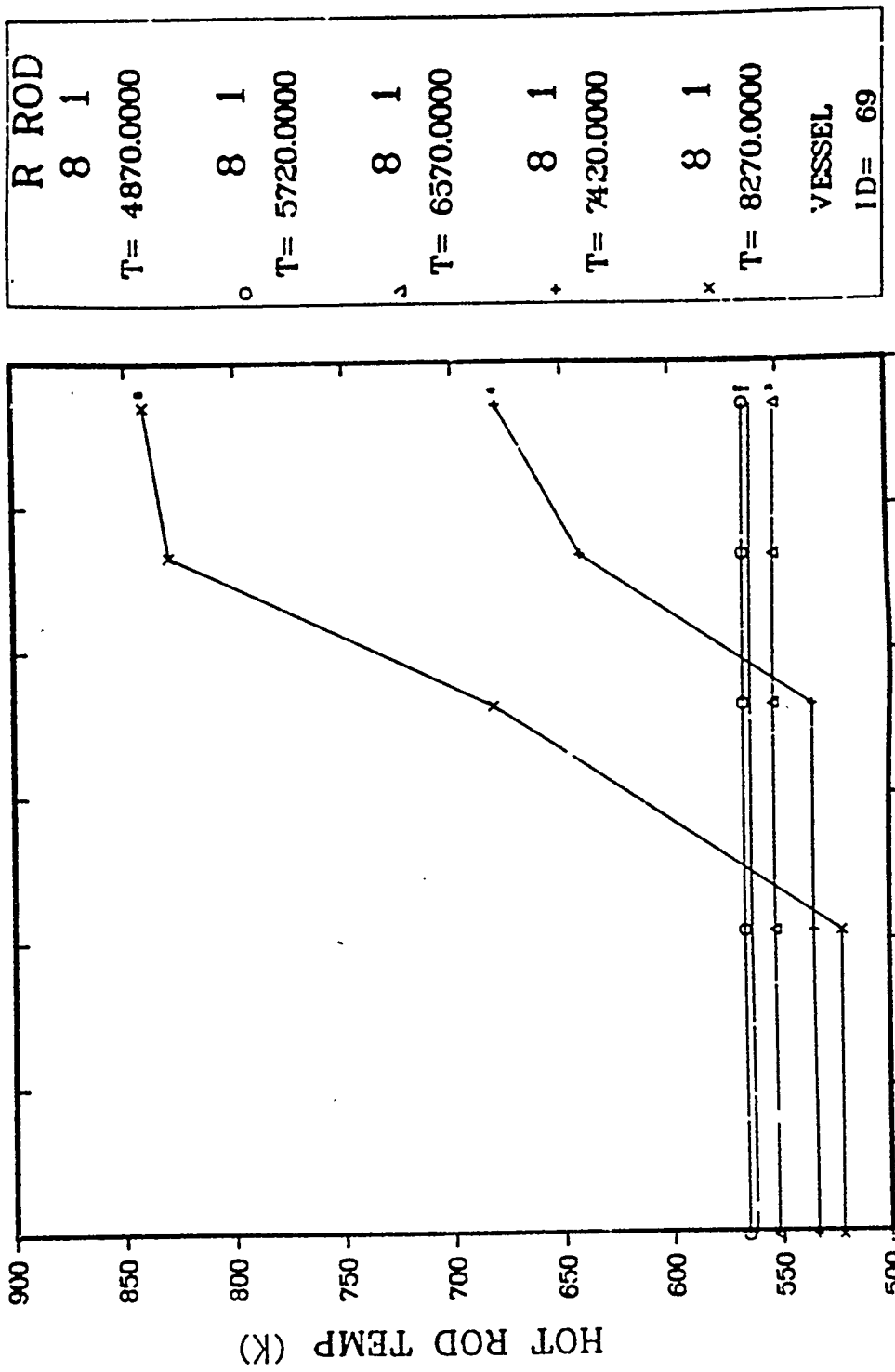

Fig. B-2.30. Hot-rod temperature profile vs time (Rod 1).

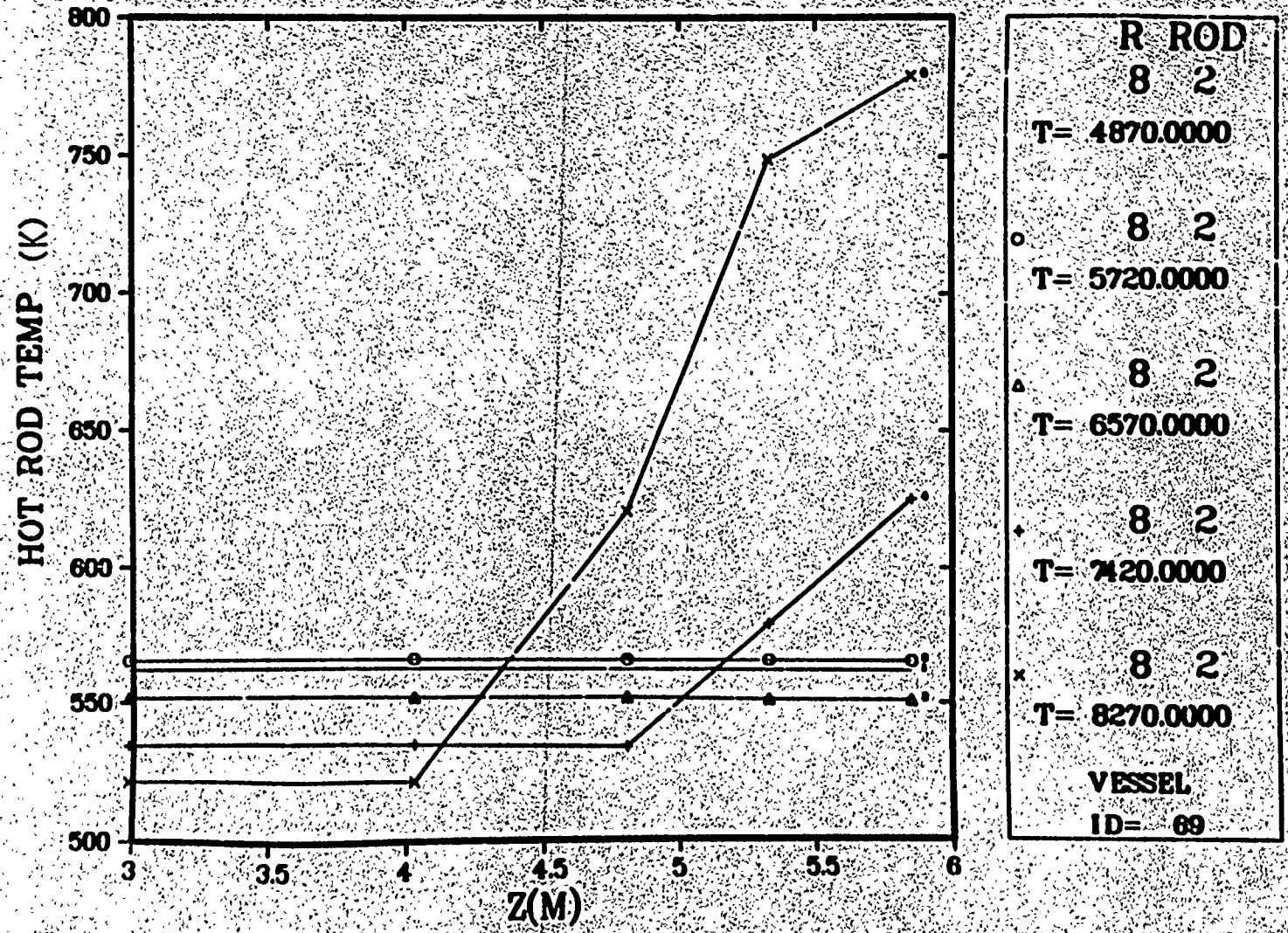

Fig. B-2.31. Hot-rod temperature profile vs time (Rod 2).

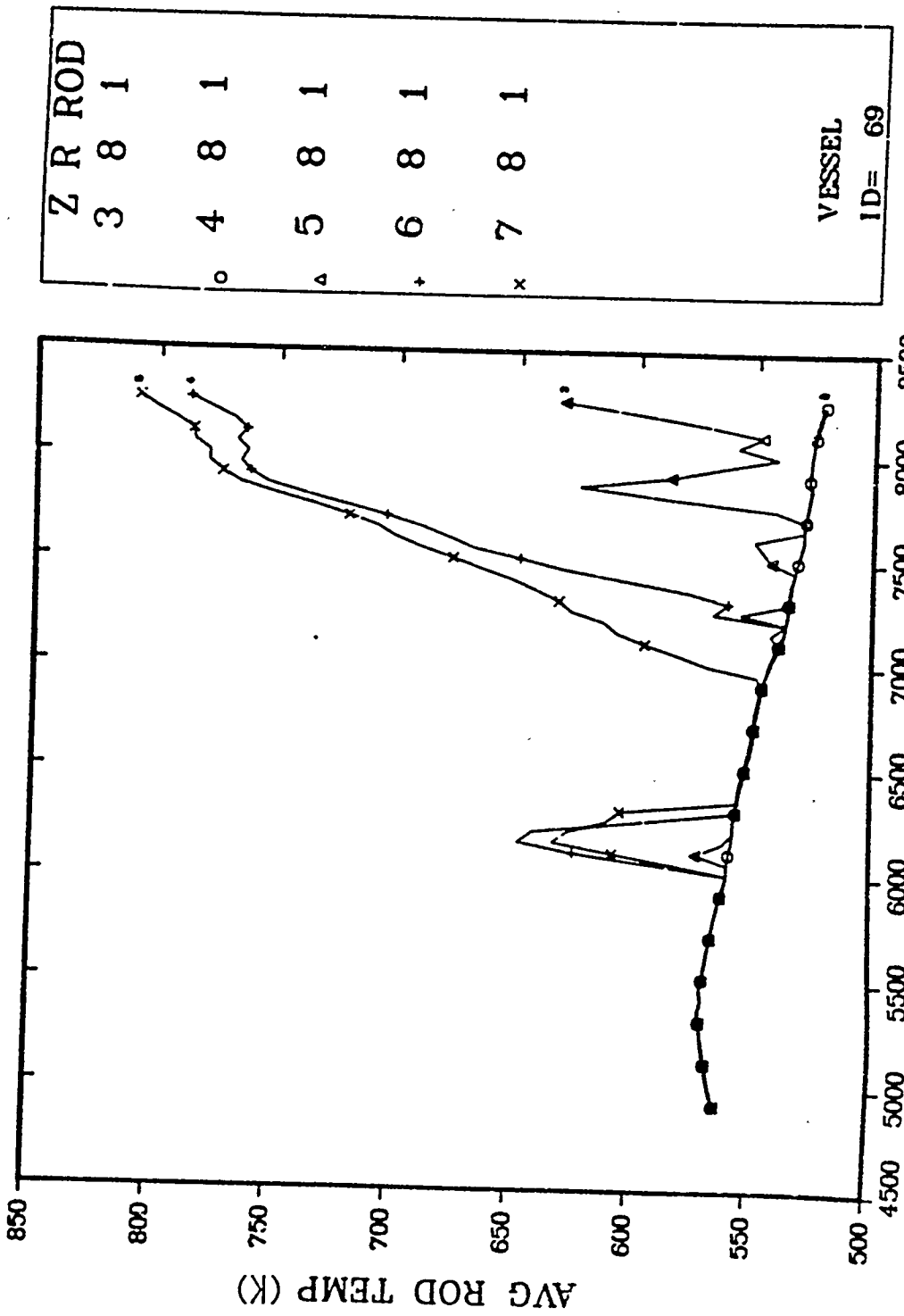

Fig. B-2.32. Average rod temperature axial profile (Rod 1).

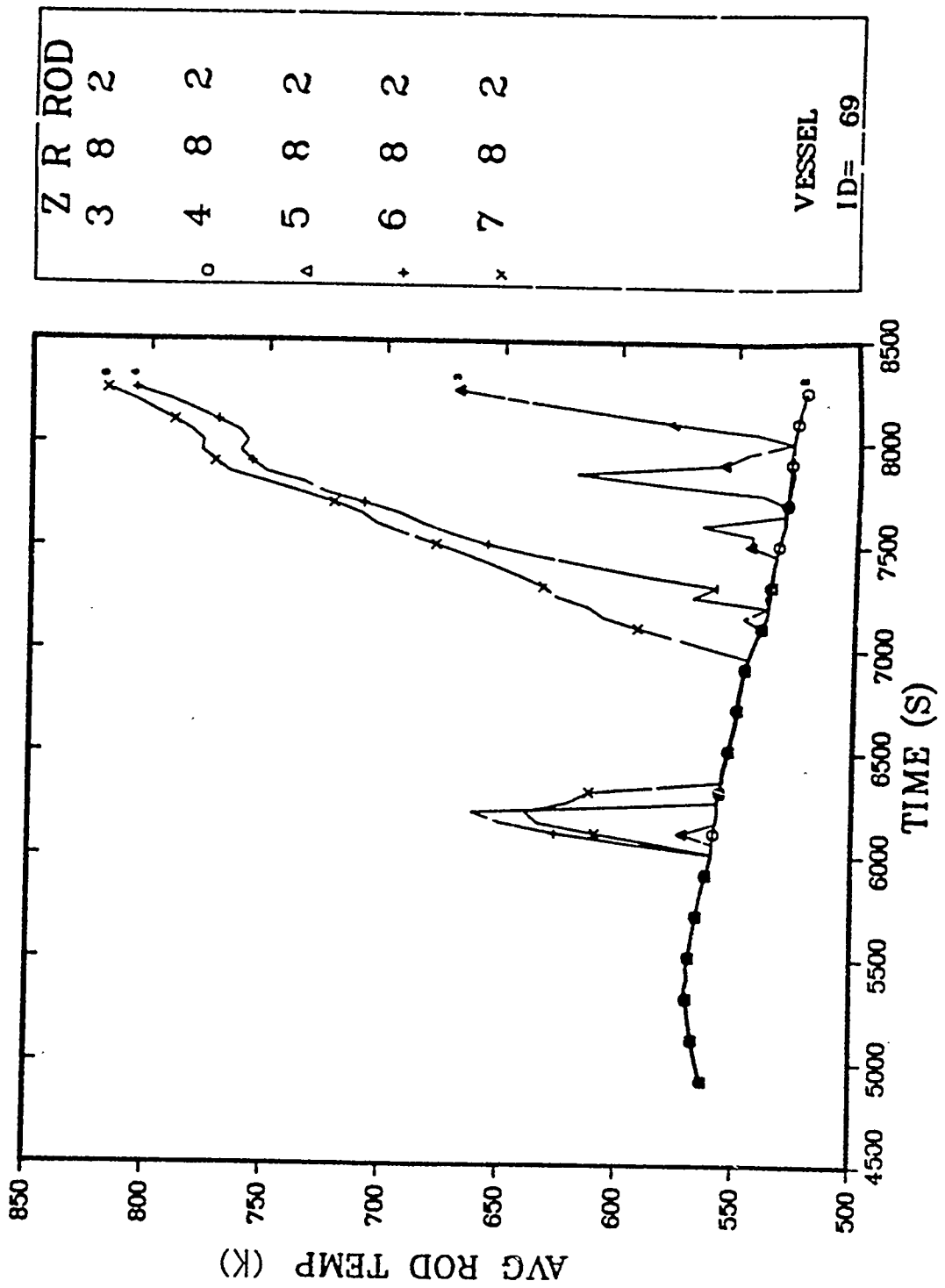

Fig. B-2.33. Average rod temperature axial profile (Rod 2).

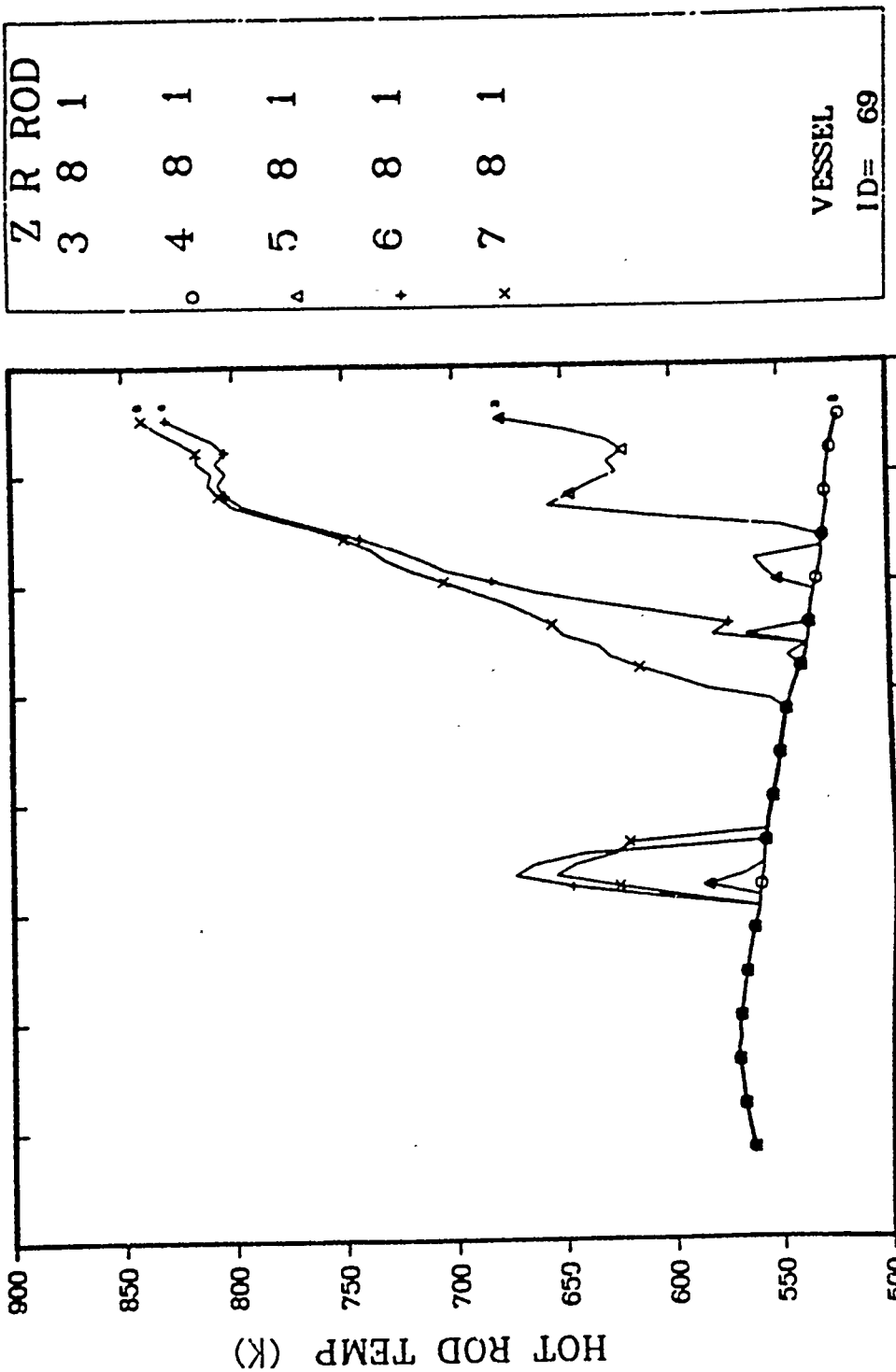

Fig. B-2.34. Hot-rod temperature axial profile (Rod 1).

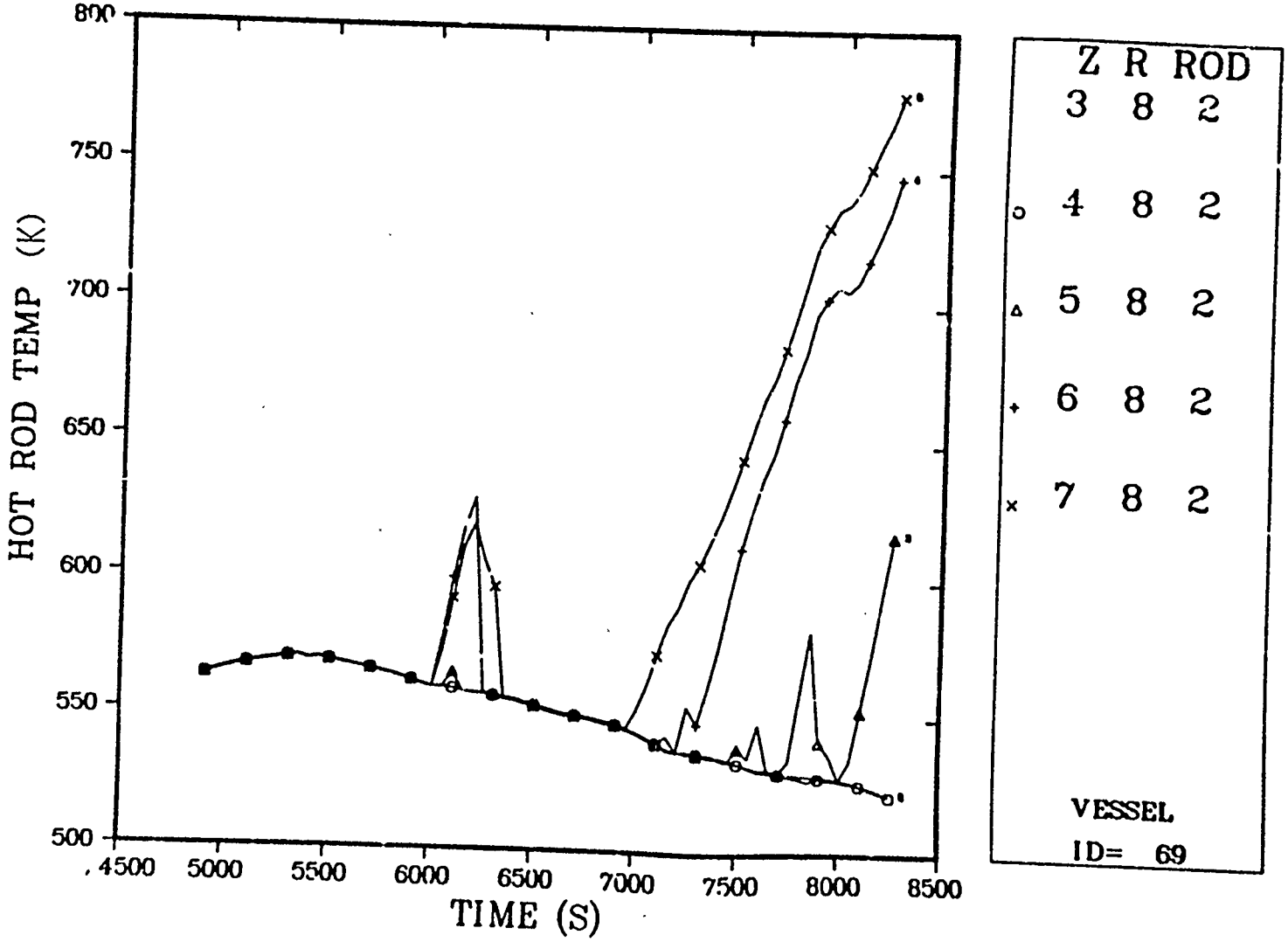

Fig. B-2.35. Hot-rod temperature axial profile (Rod 2).

APPENDIX B-3

ADDITIONAL PLOTS FOR BASE CASE CALCULATION

138 minutes < T < 180 minutes

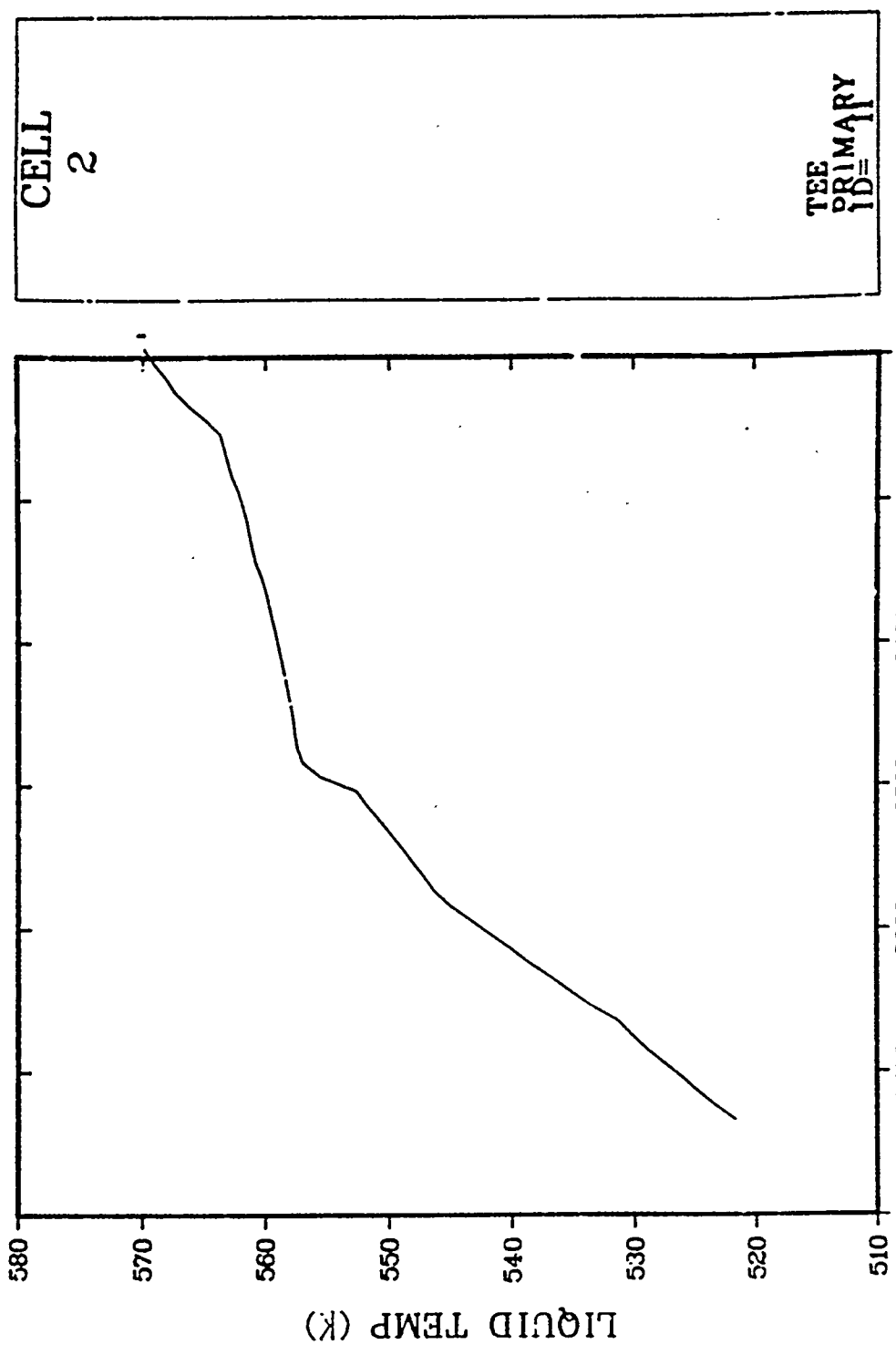

Fig. B-3.1. A Loop hot-leg liquid temperature.

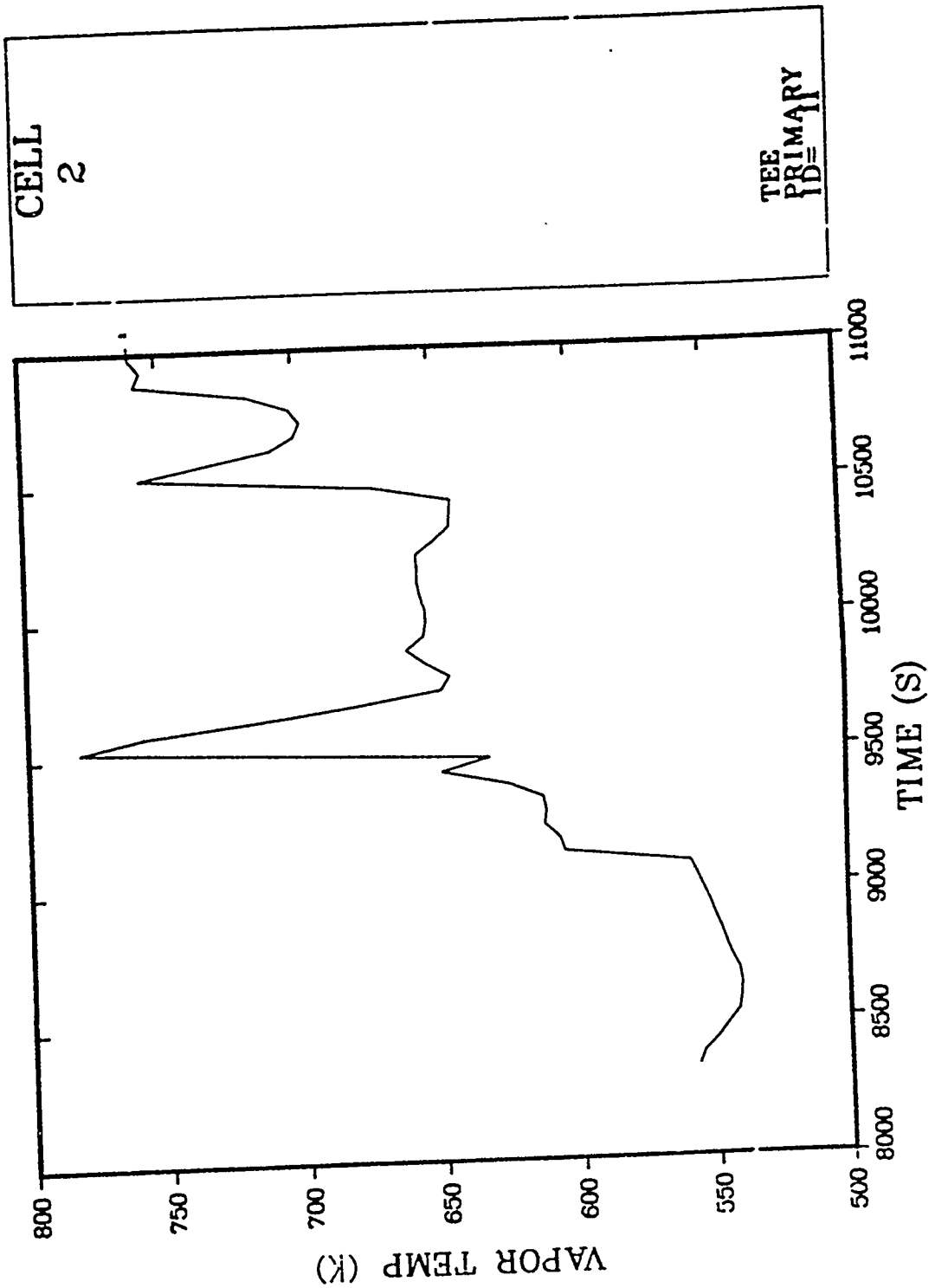

Fig. B-3.2. A Loop hot-leg vapor temperature.

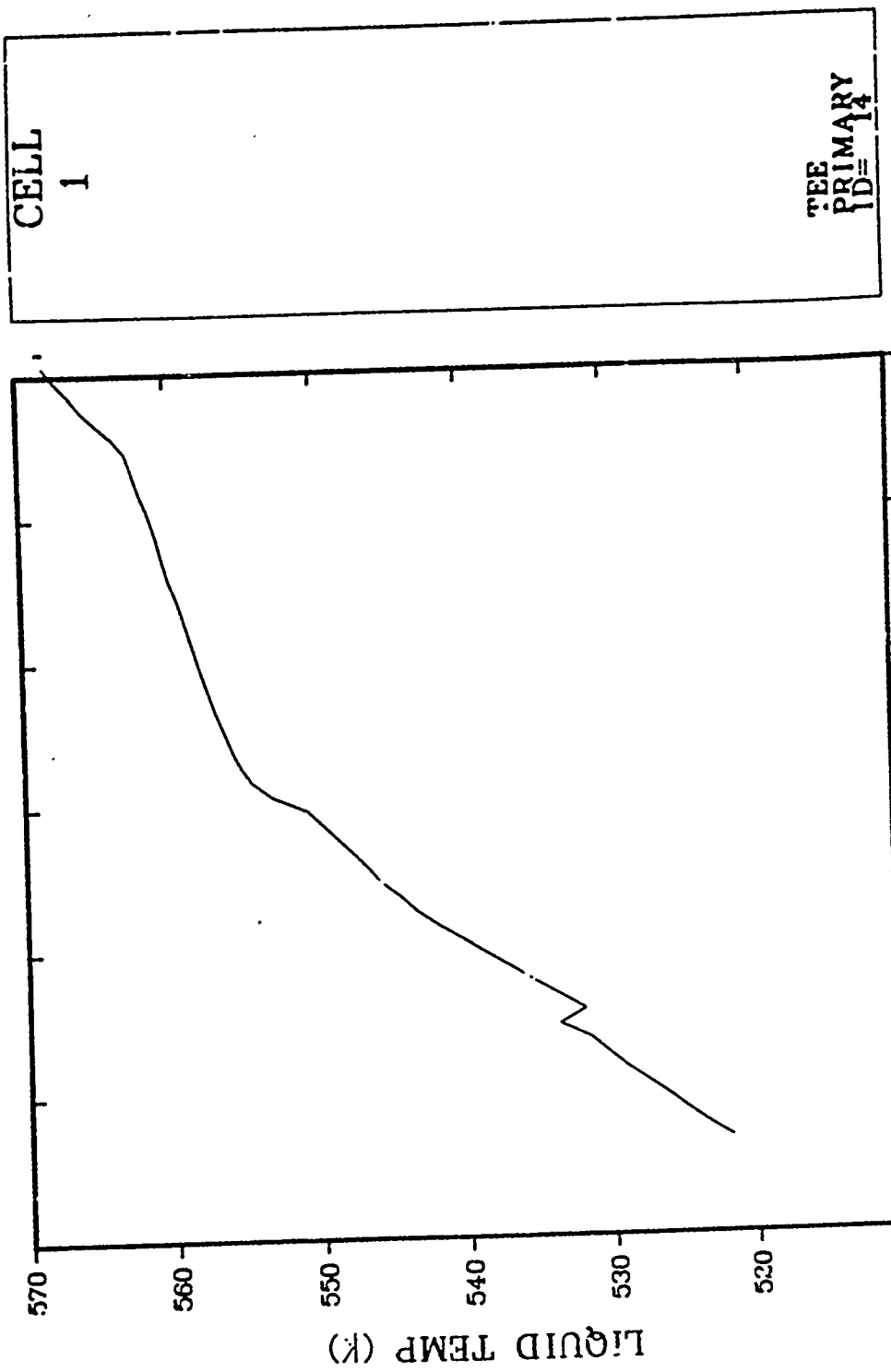

Fig. B-3.3. A Loop cold-leg liquid temperature.

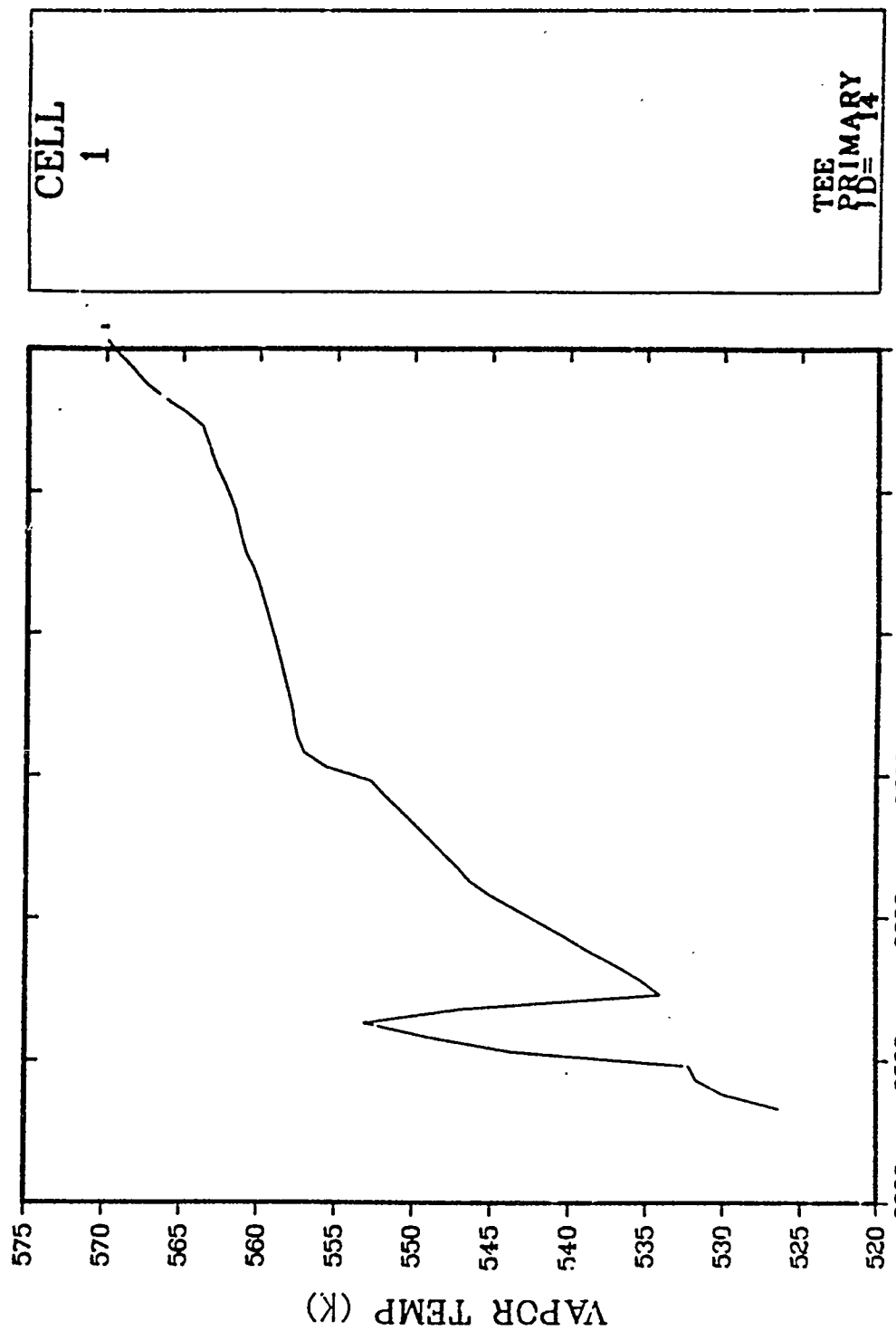

Fig. B-3.4. A Loop cold-leg vapor temperature.

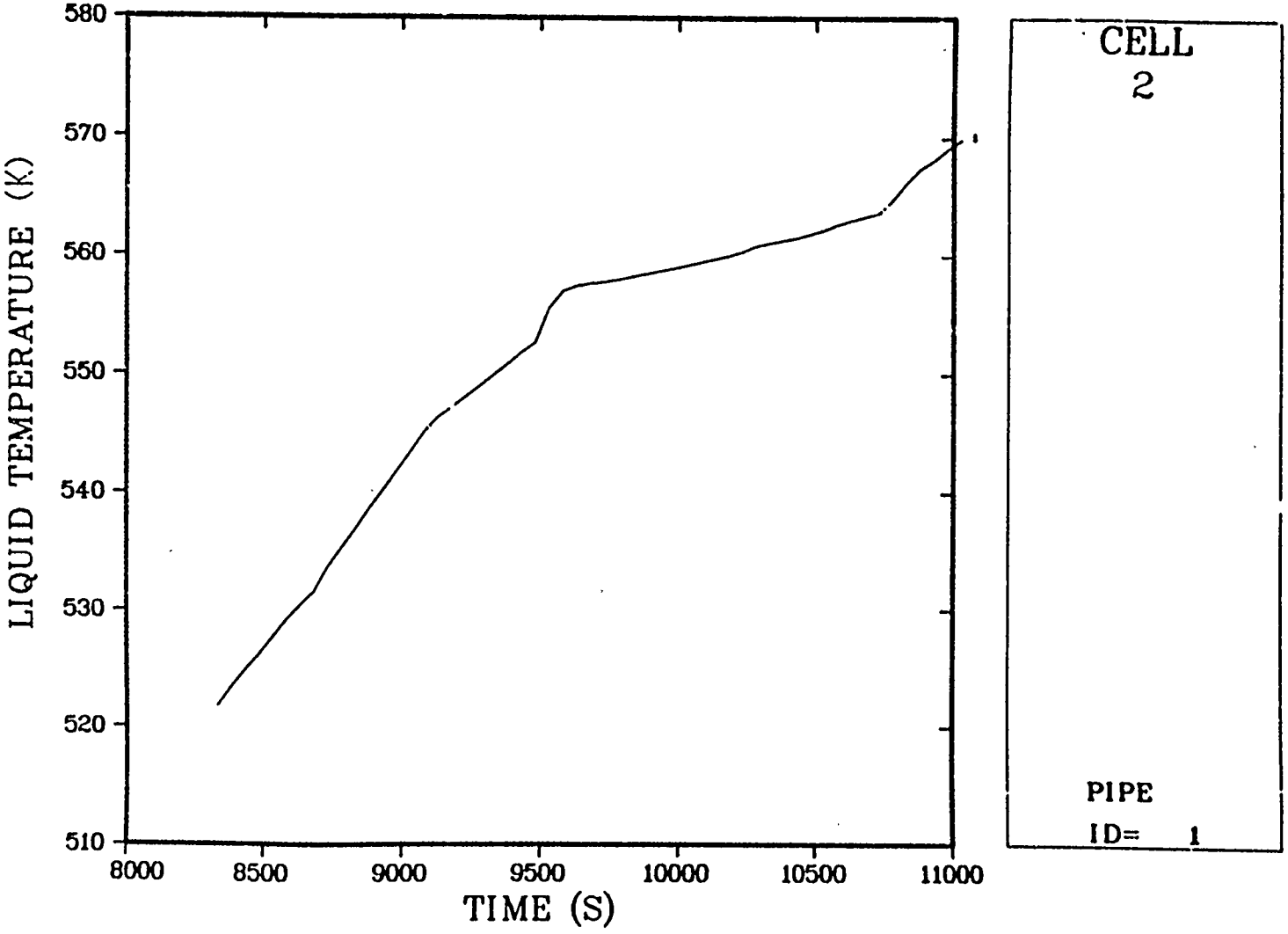

Fig. B-3.5. B Loop hot-leg liquid temperature.

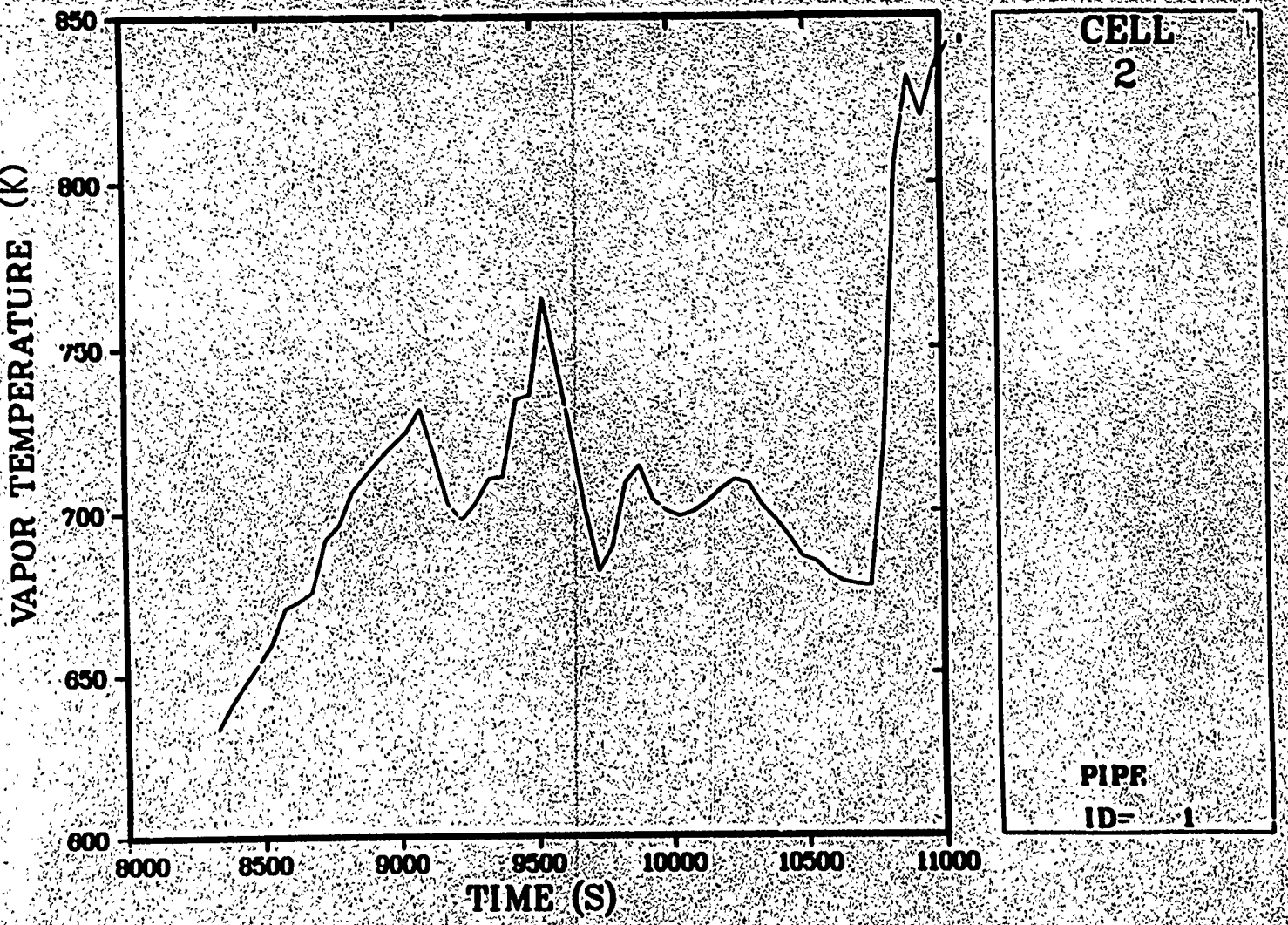

Fig. B-3.6. B Loop hot-leg vapor temperature.

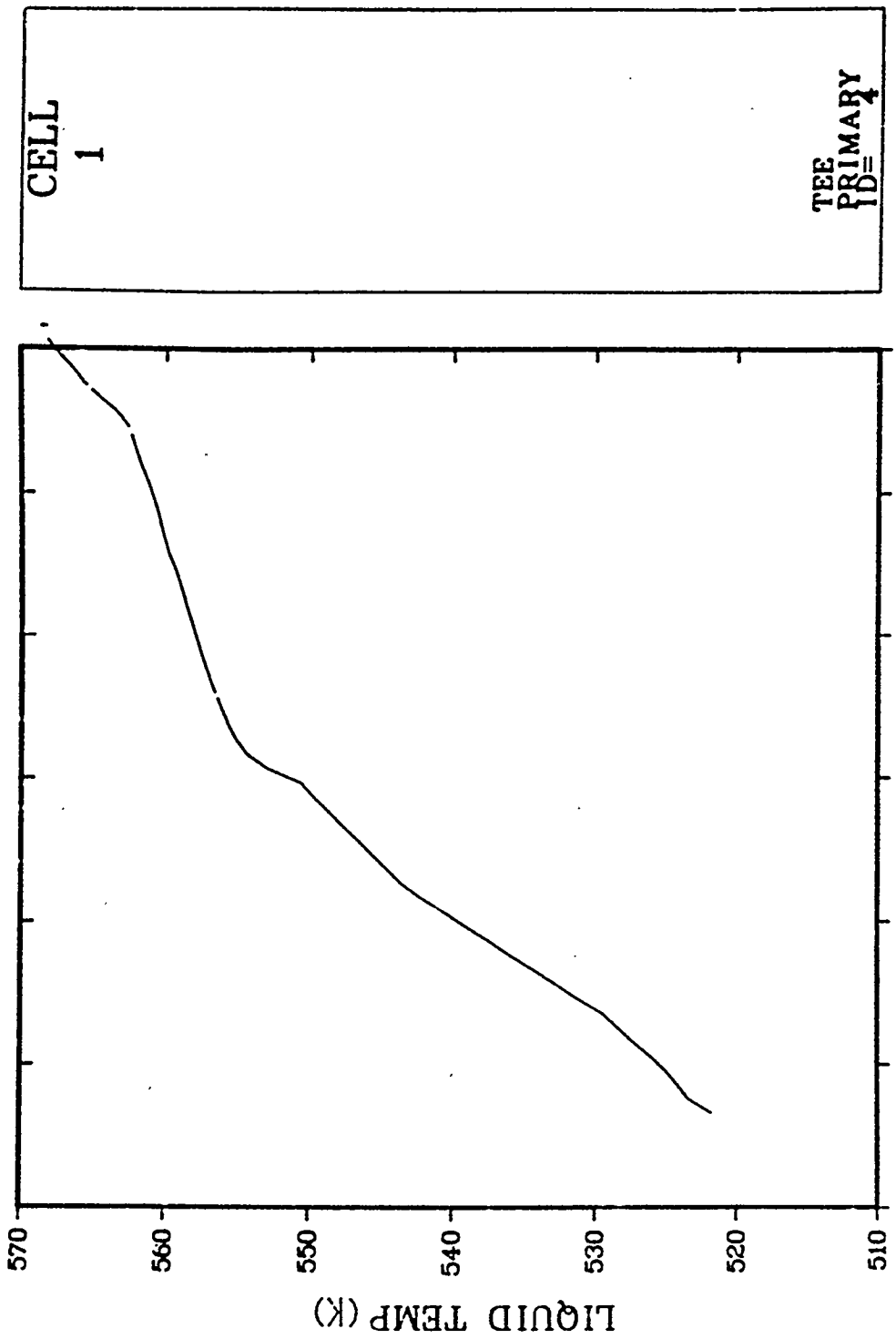

Fig. B-3.7. B Loop cold-leg liquid temperature.

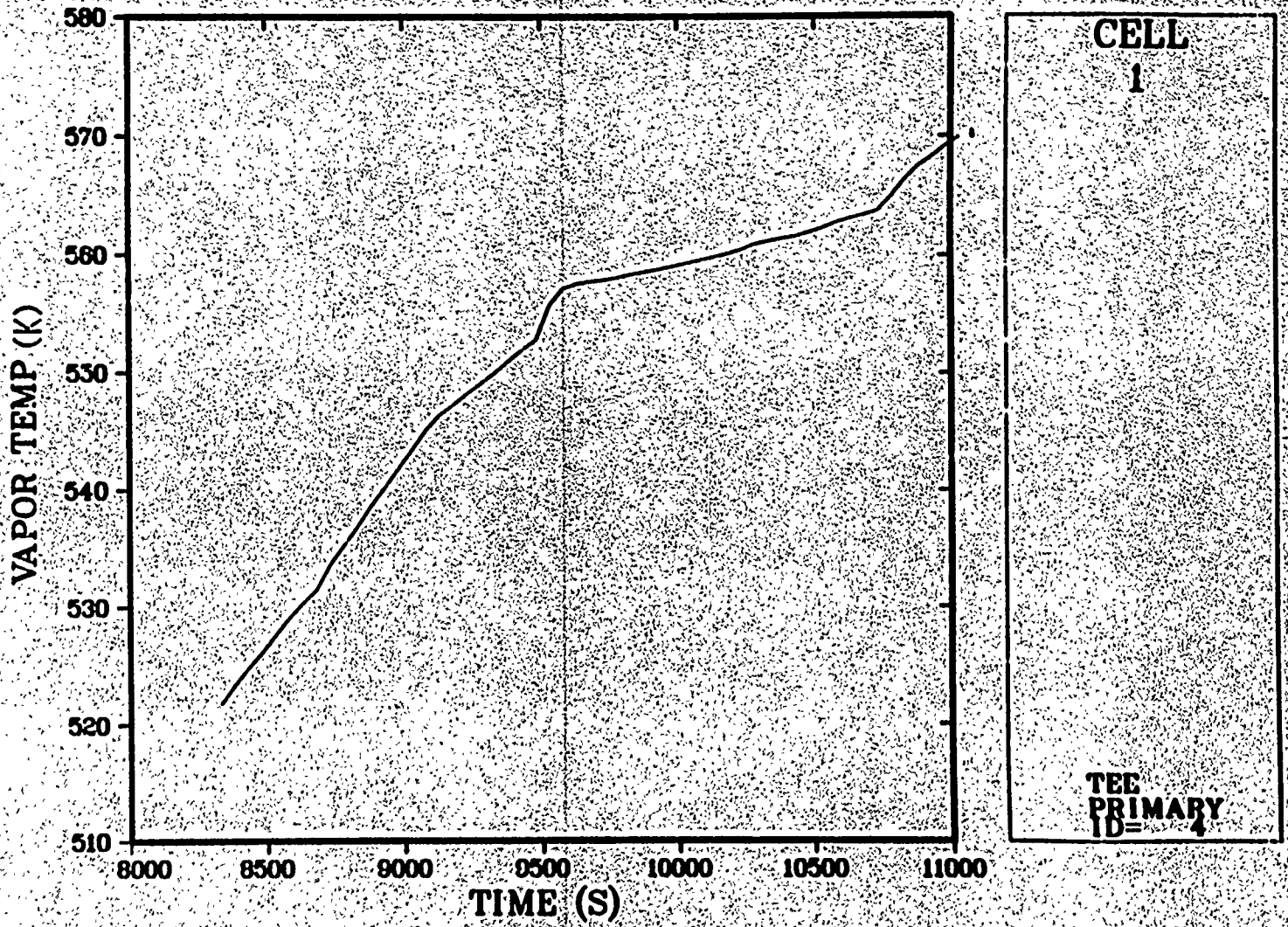

Fig. B-3.8. B Loop cold-leg vapor temperature.

Fig. B-3.9. A Loop hot-leg void fraction distribution (Cells, 1,2,3).

Fig. B-3.10. B Loop hot-leg void fraction distribution (Cells 1,2,3).

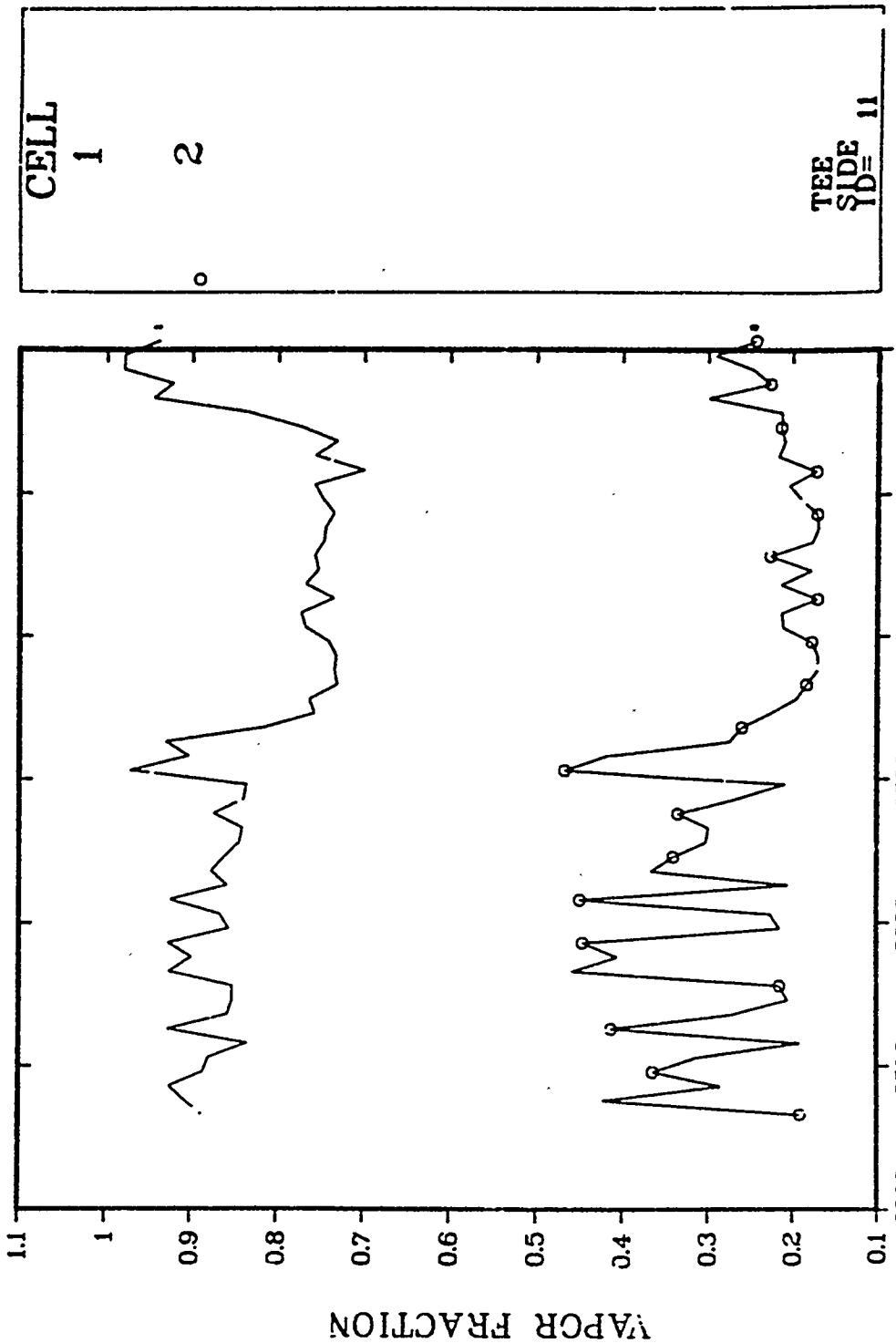

Fig. B-3.11. Pressurizer surge line void distribution (Cells 1,2).

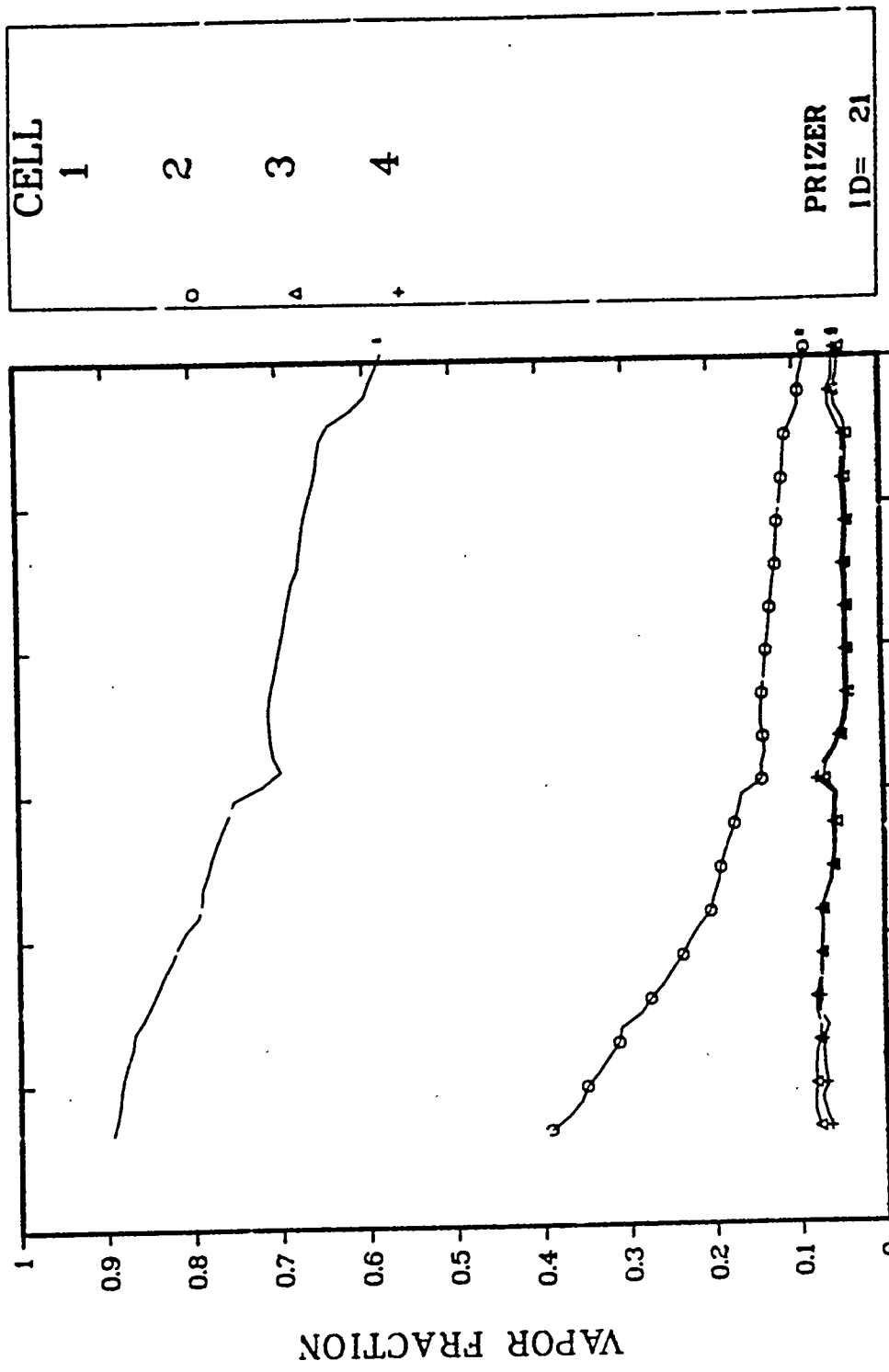

Fig. B-3.12. Pressurizer void fraction distribution.

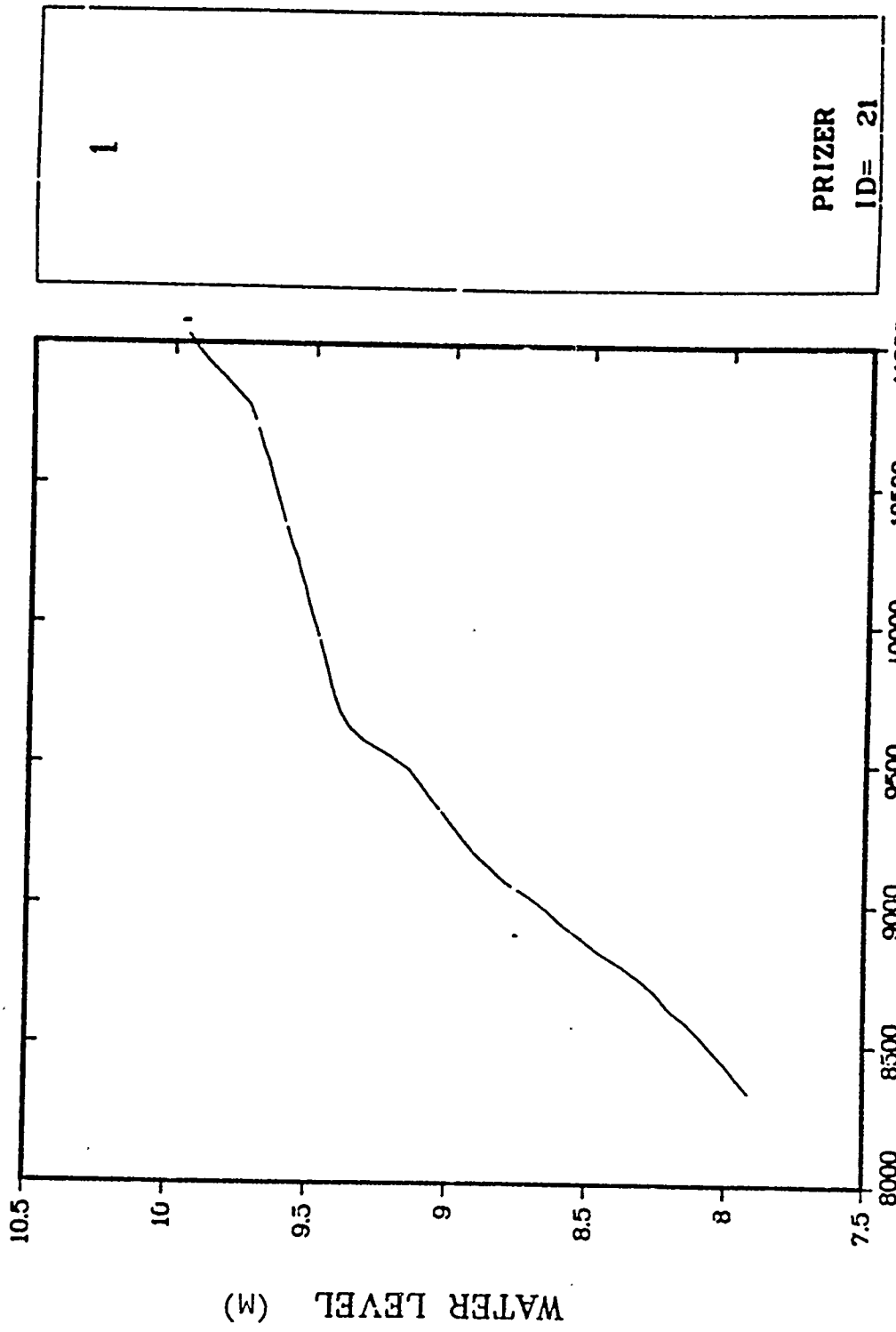

Fig. B-3.13. Pressurizer water level.

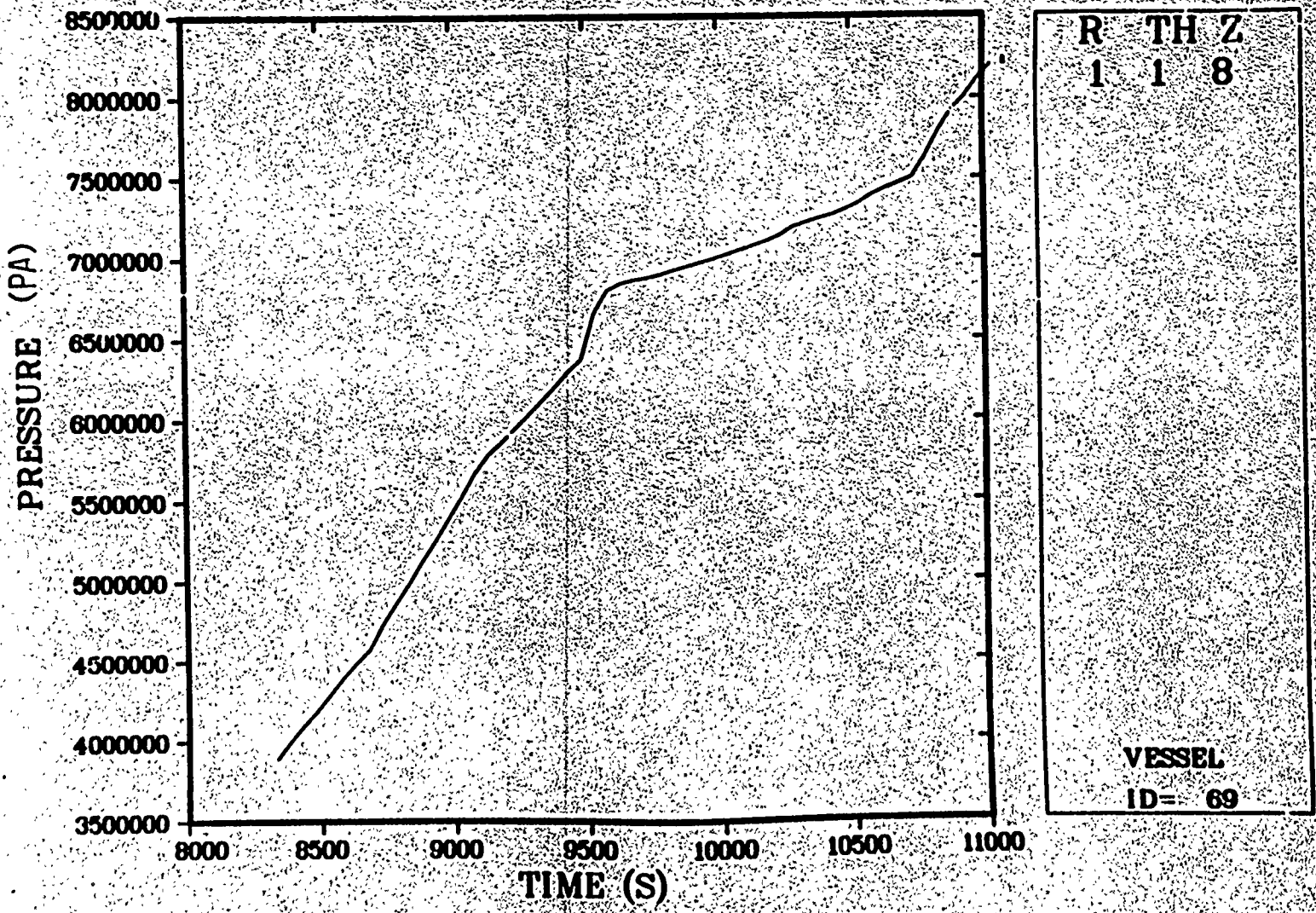

Fig. B-3.14. Upper plenum pressure.

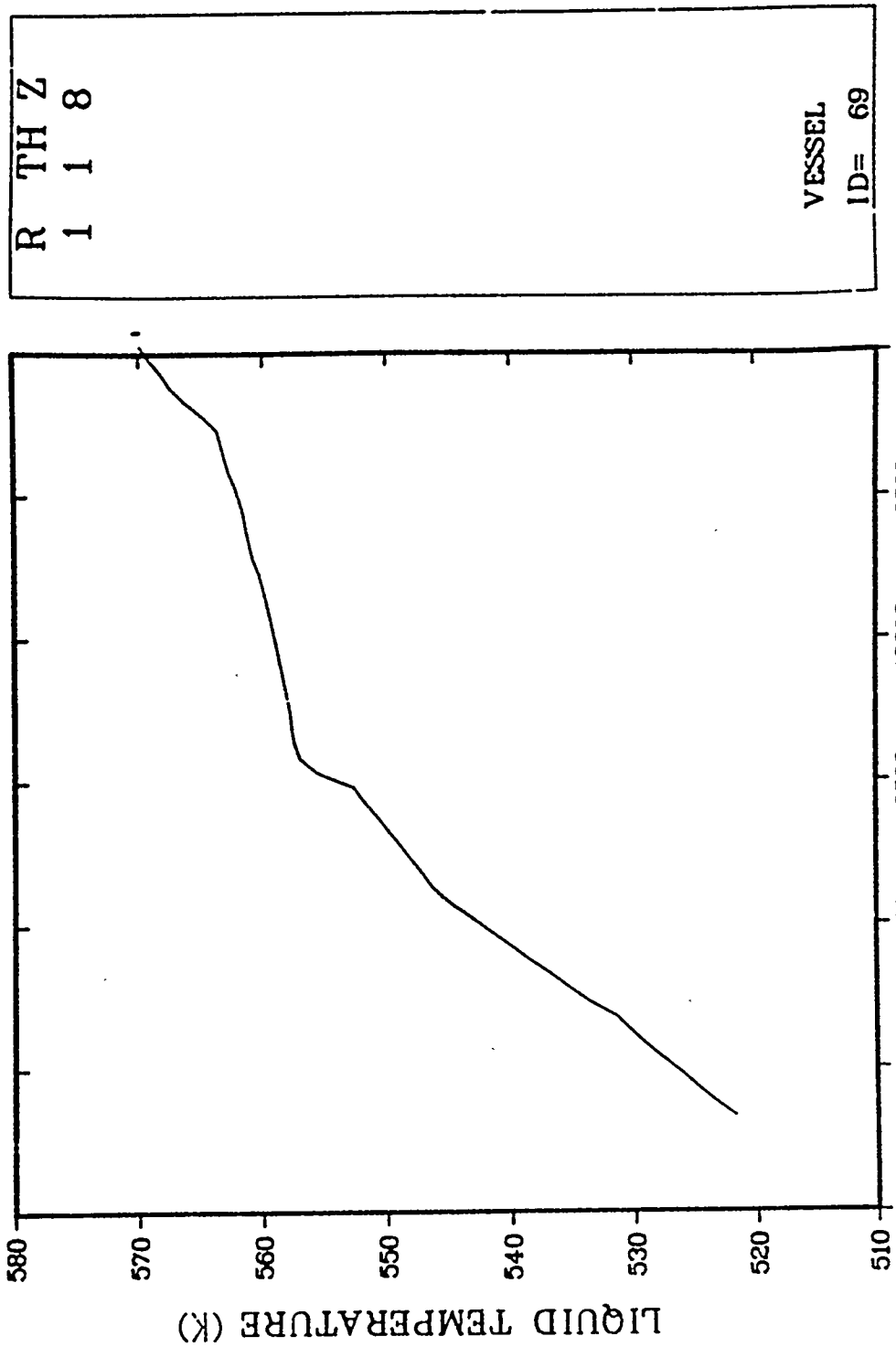

Fig. B-3.15. Upper plenum liquid temperature.

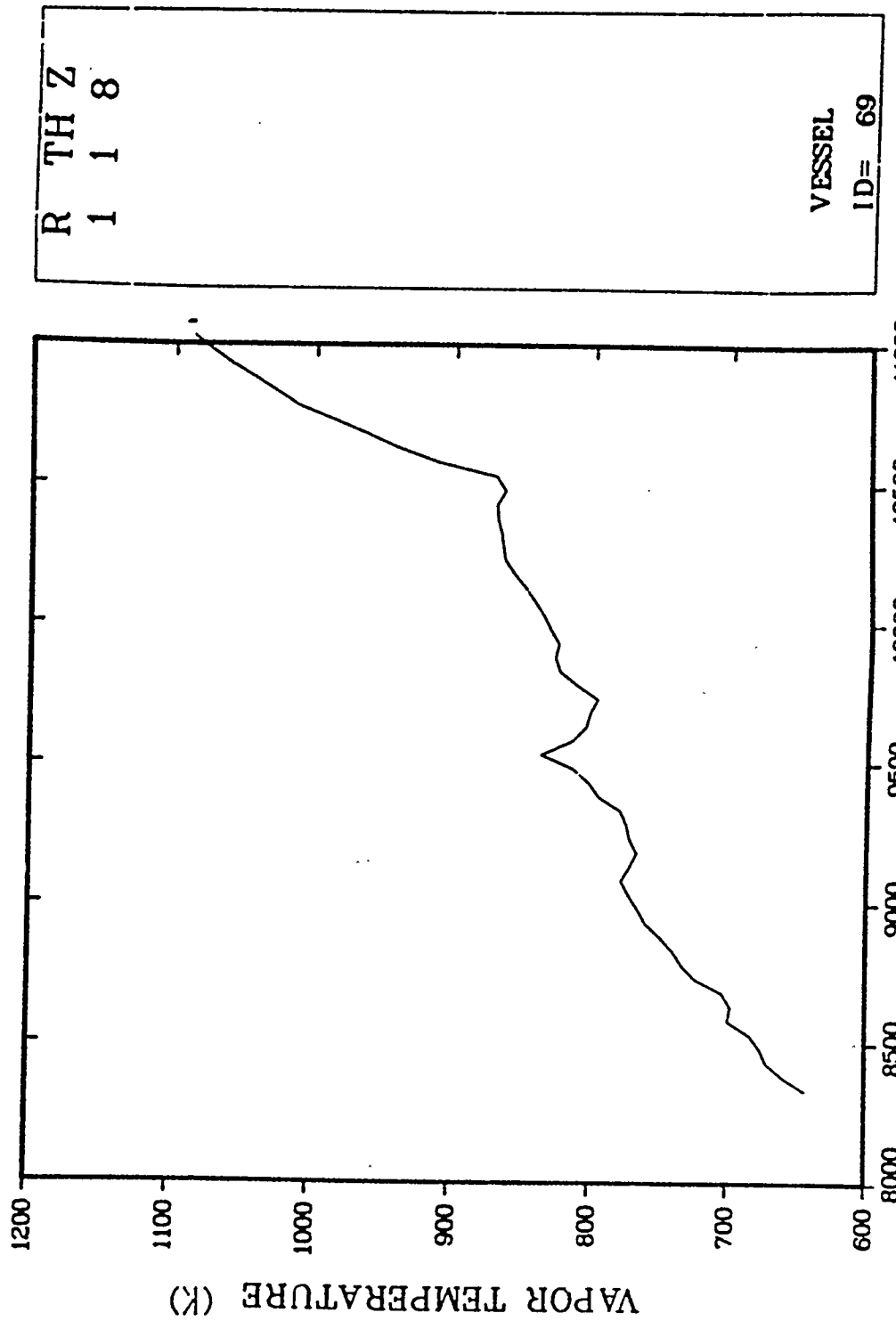

Fig. B-3.16. Upper plenum vapor temperature.

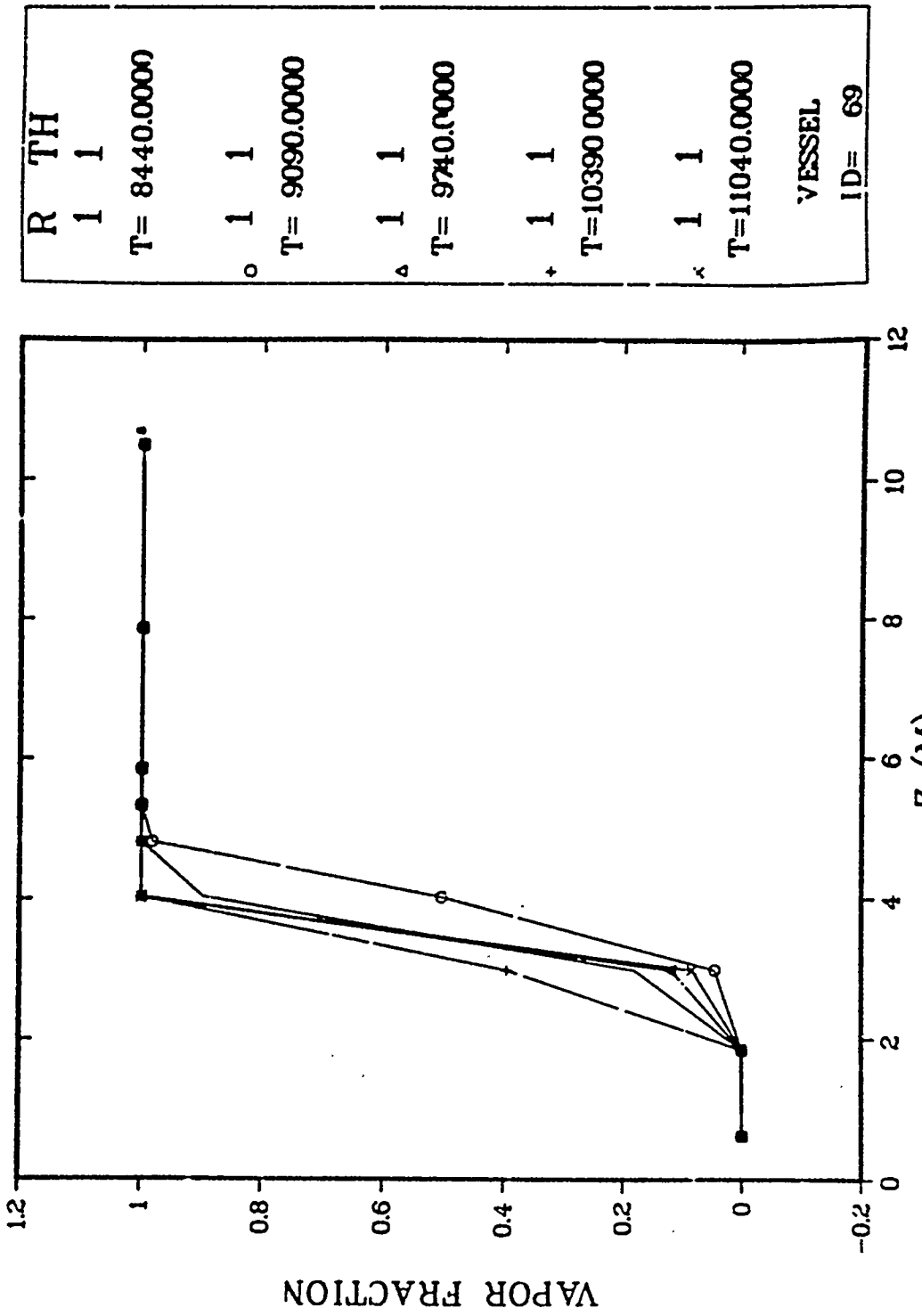

Fig. B-3.17. Vessel void fraction axial profile vs time (Cell 1).

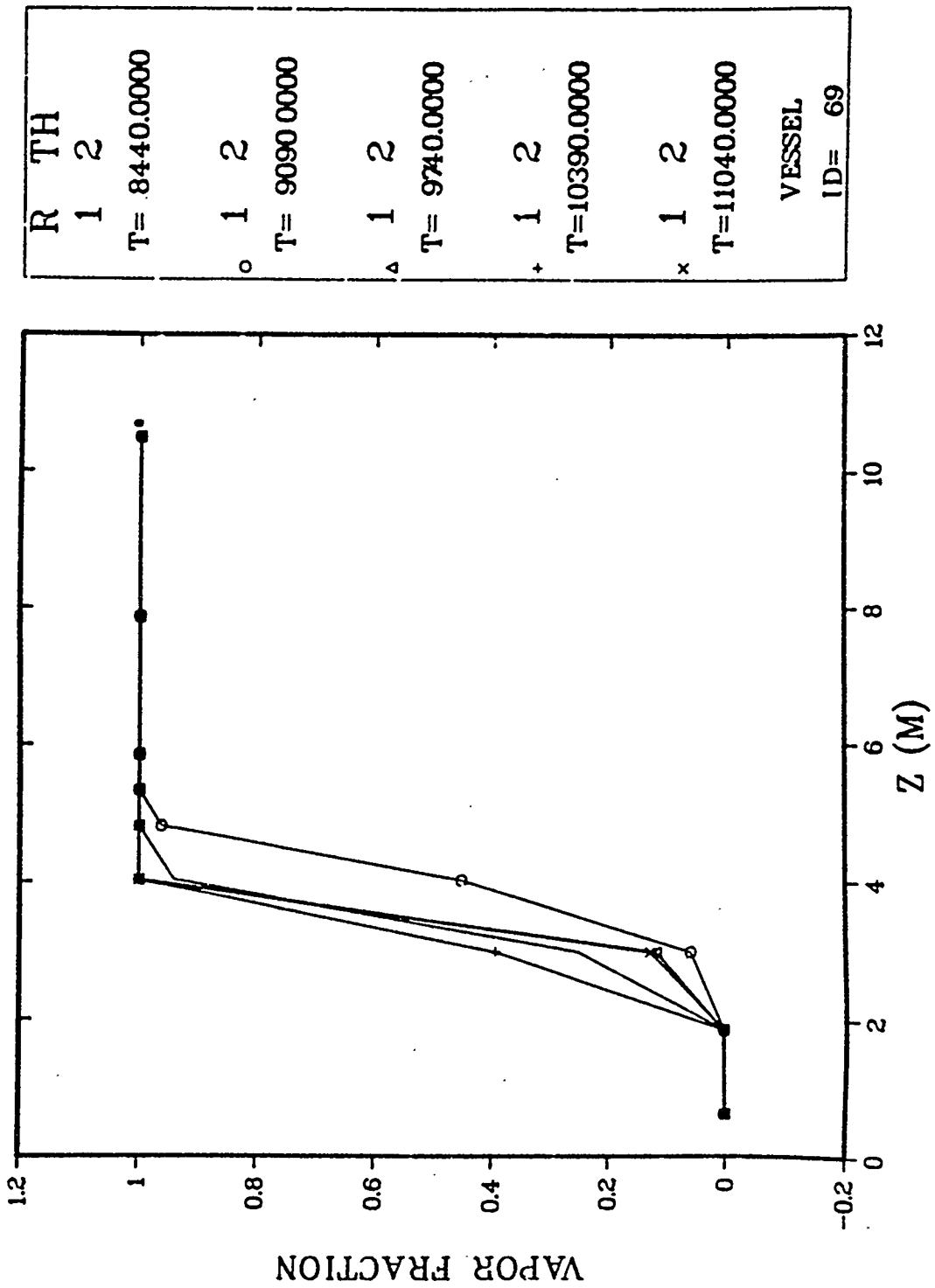

Fig. B-3.18. Vessel void fraction axial profile vs time (Cell 2).

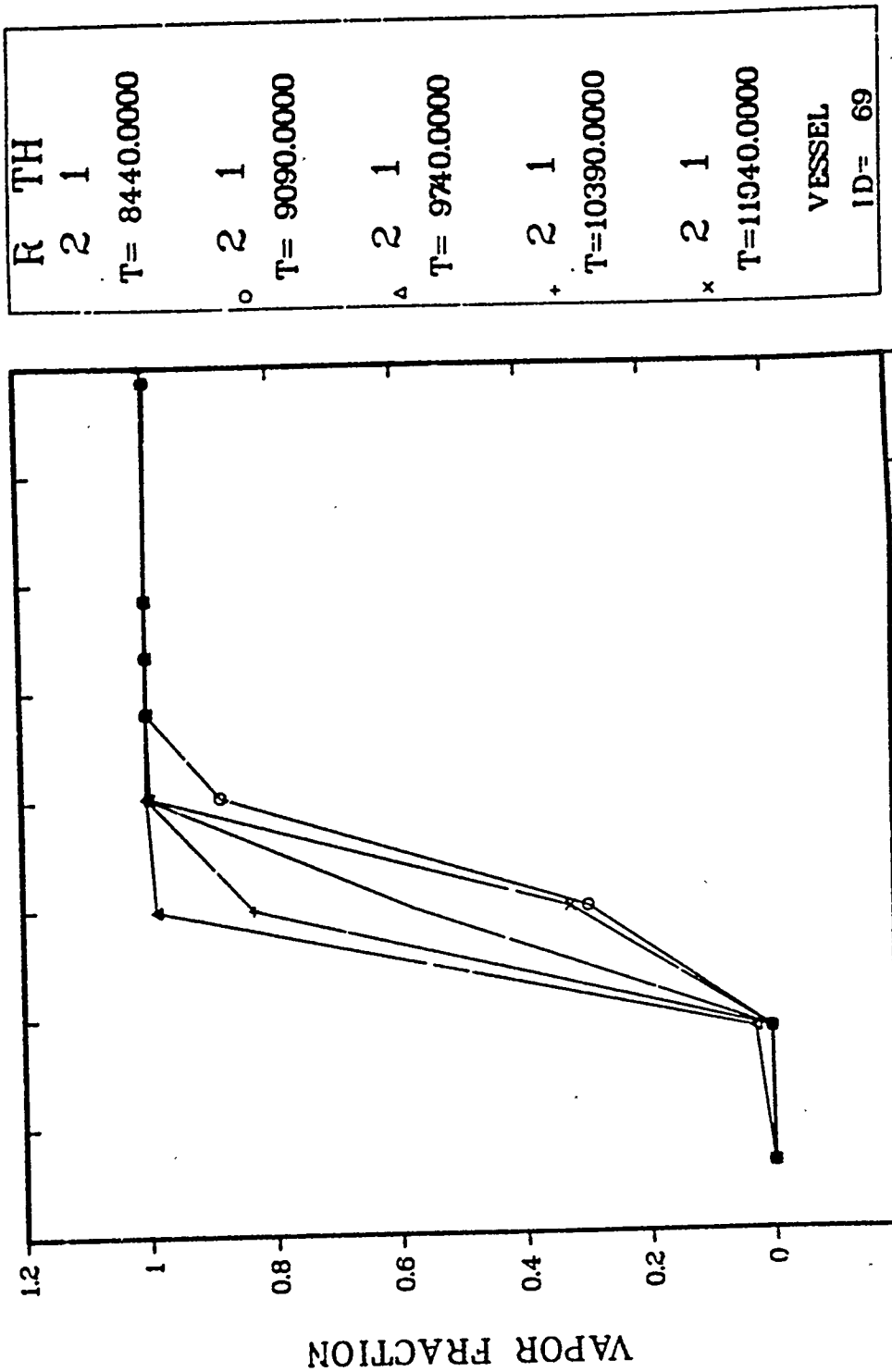

Fig. B-3.19. Downcomer void fraction axial profile vs time.

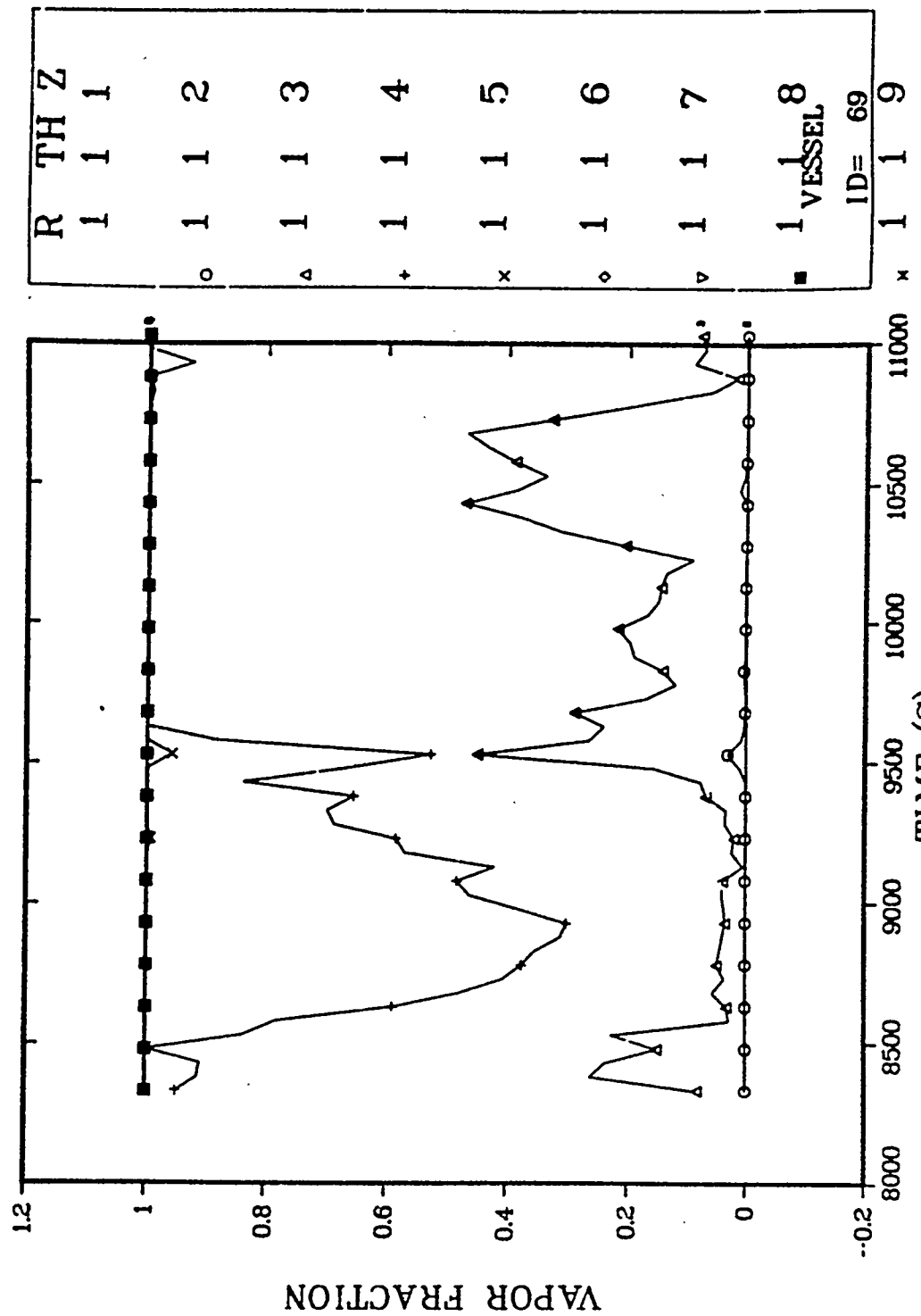

Fig. B-3.20. Vessel void fraction axial profile (Cell 1).

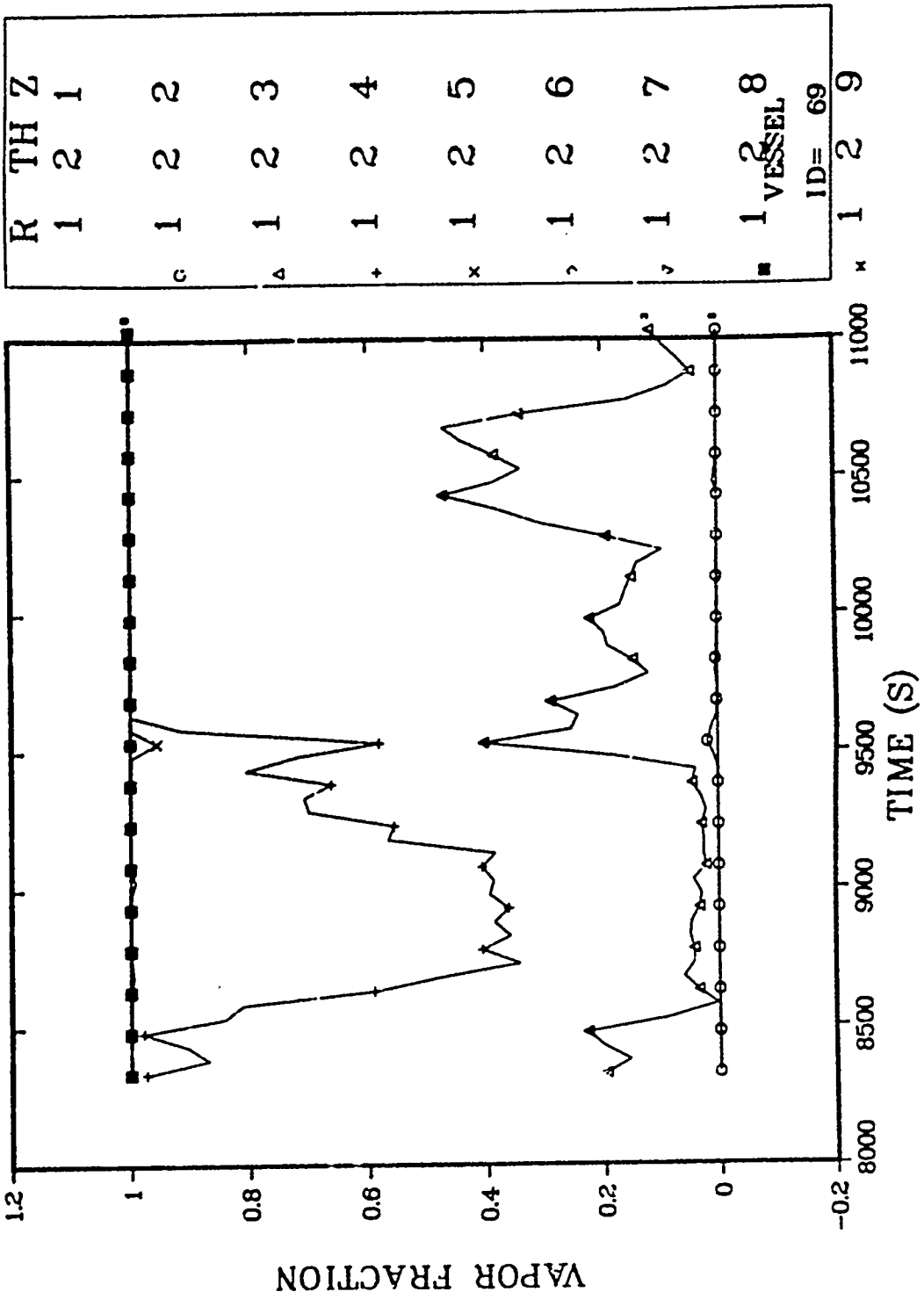

Fig. B-3.21. Vessel void fraction axial profile (Cell 2).

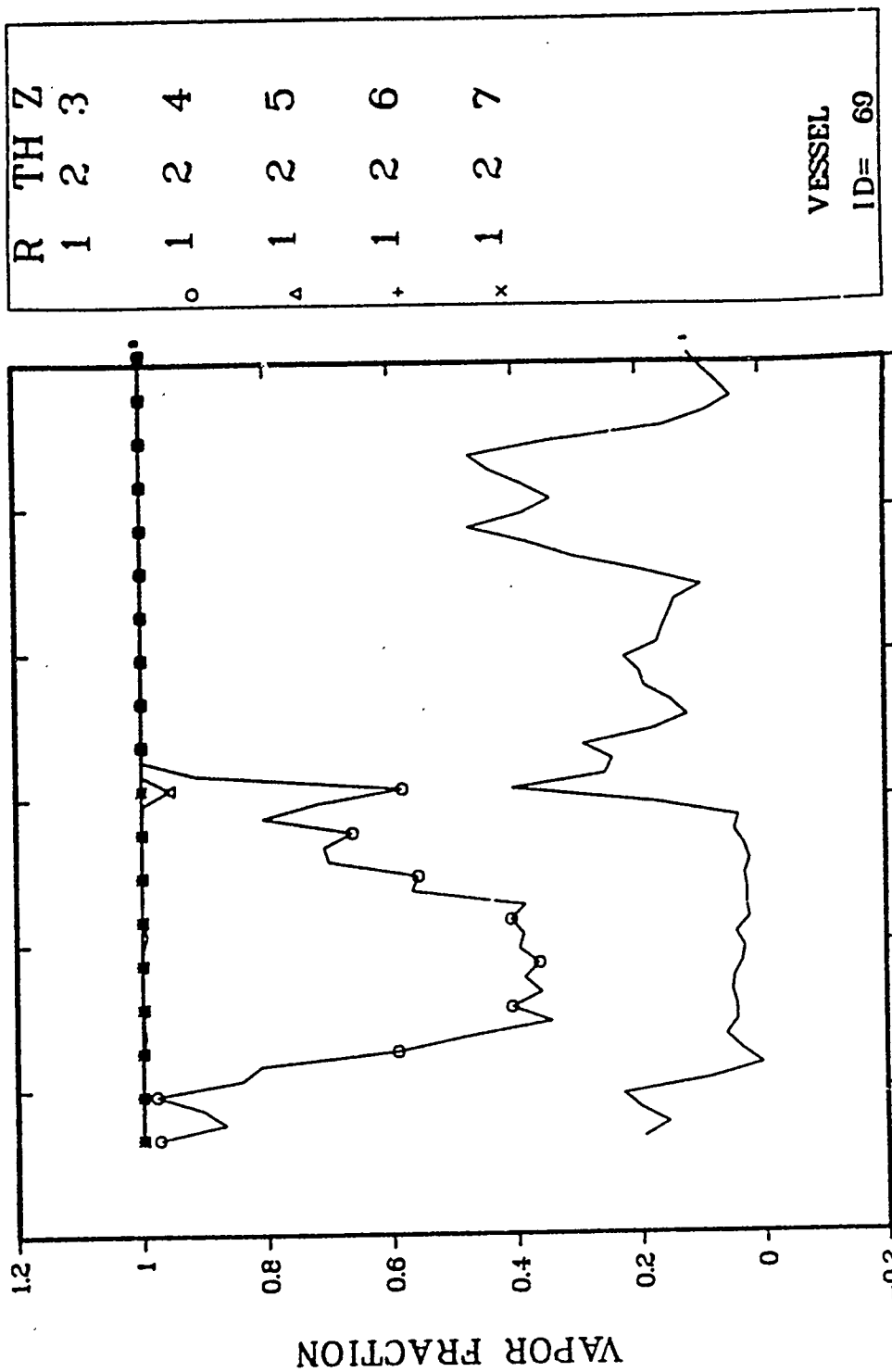

Fig. B-3.22. Core void fraction axial profile (Cell 2).

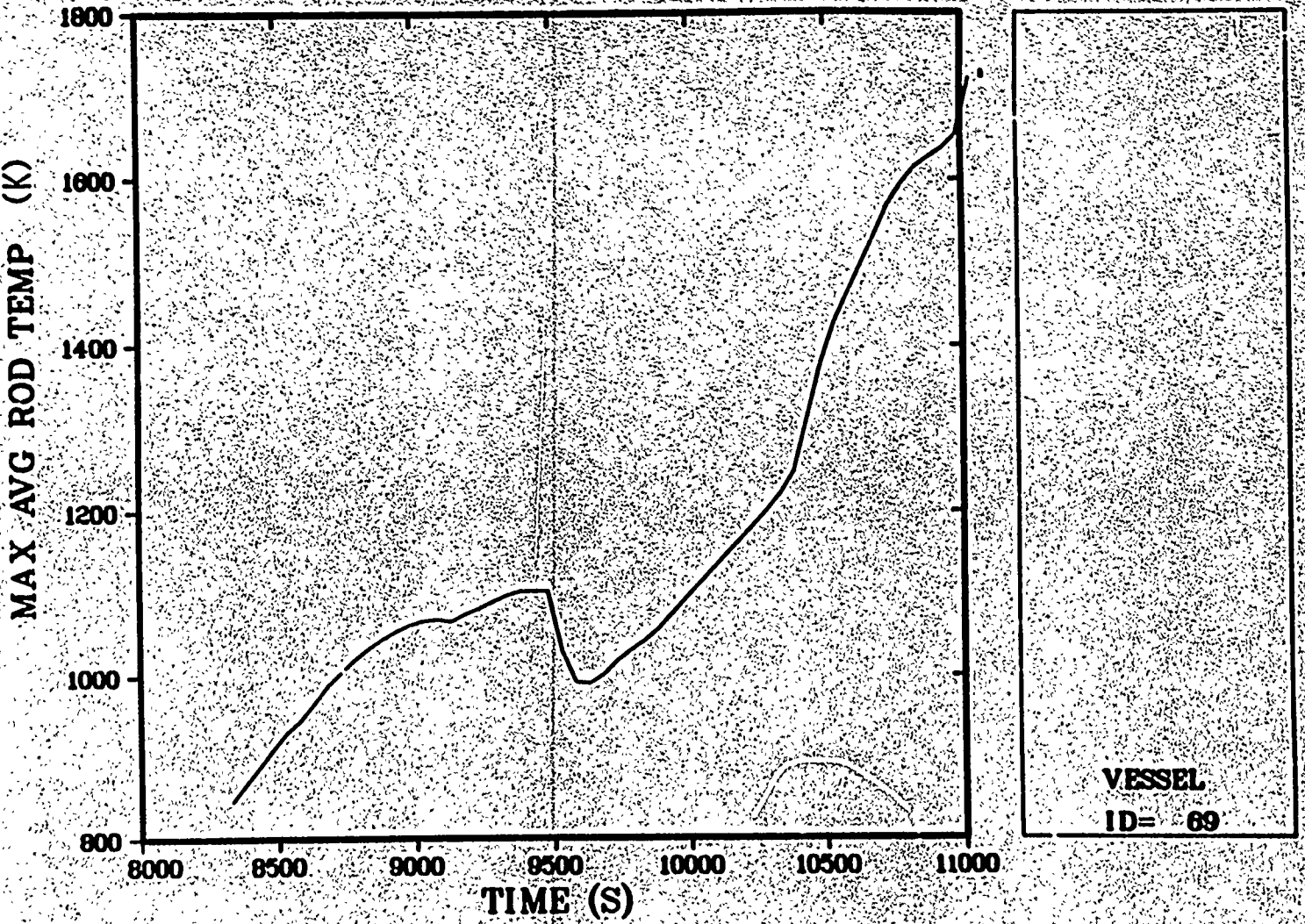

Fig. B-3.23. Maximum average rod temperature.

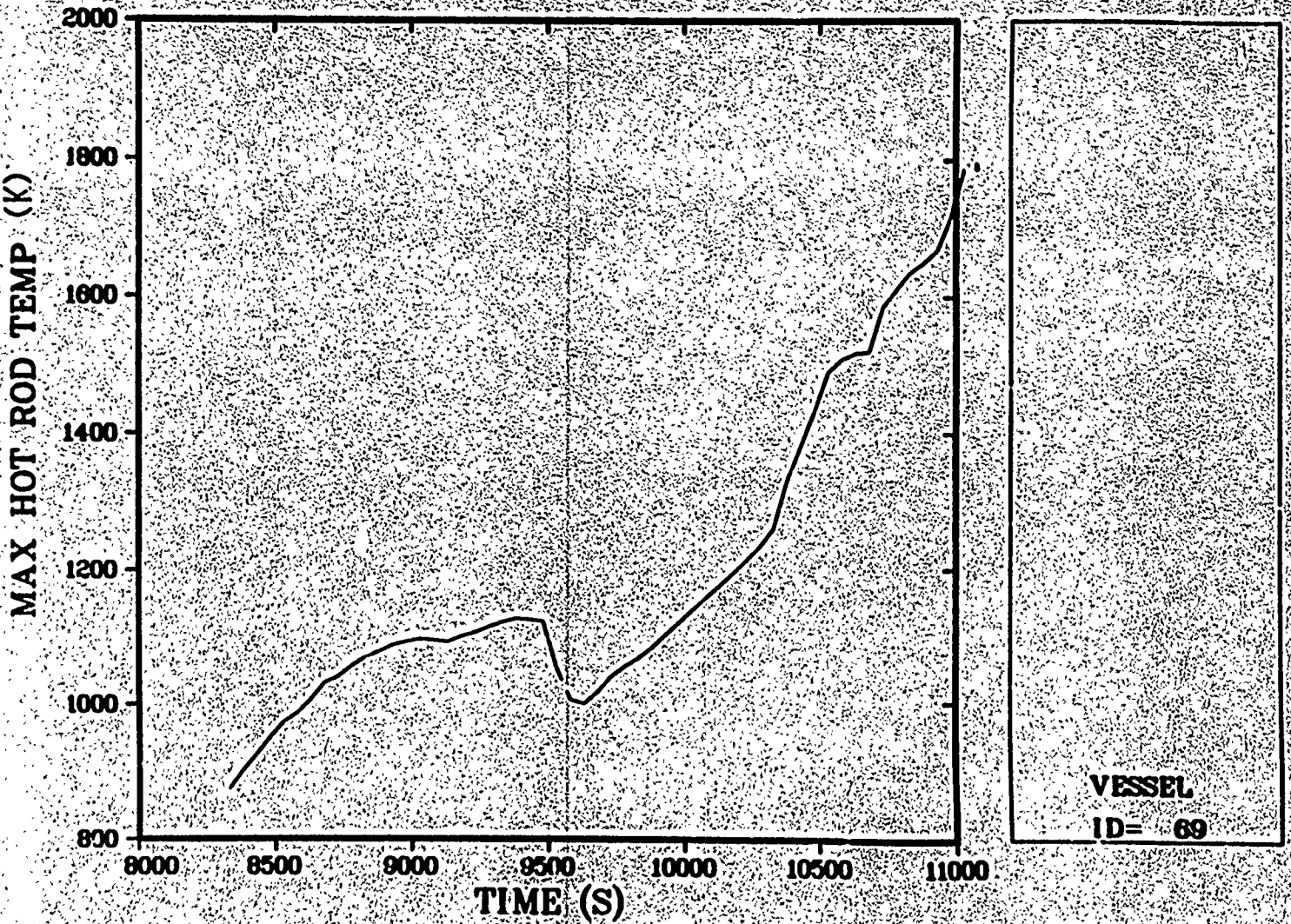

Fig. B-3.24. Maximum hot-rod temperature.

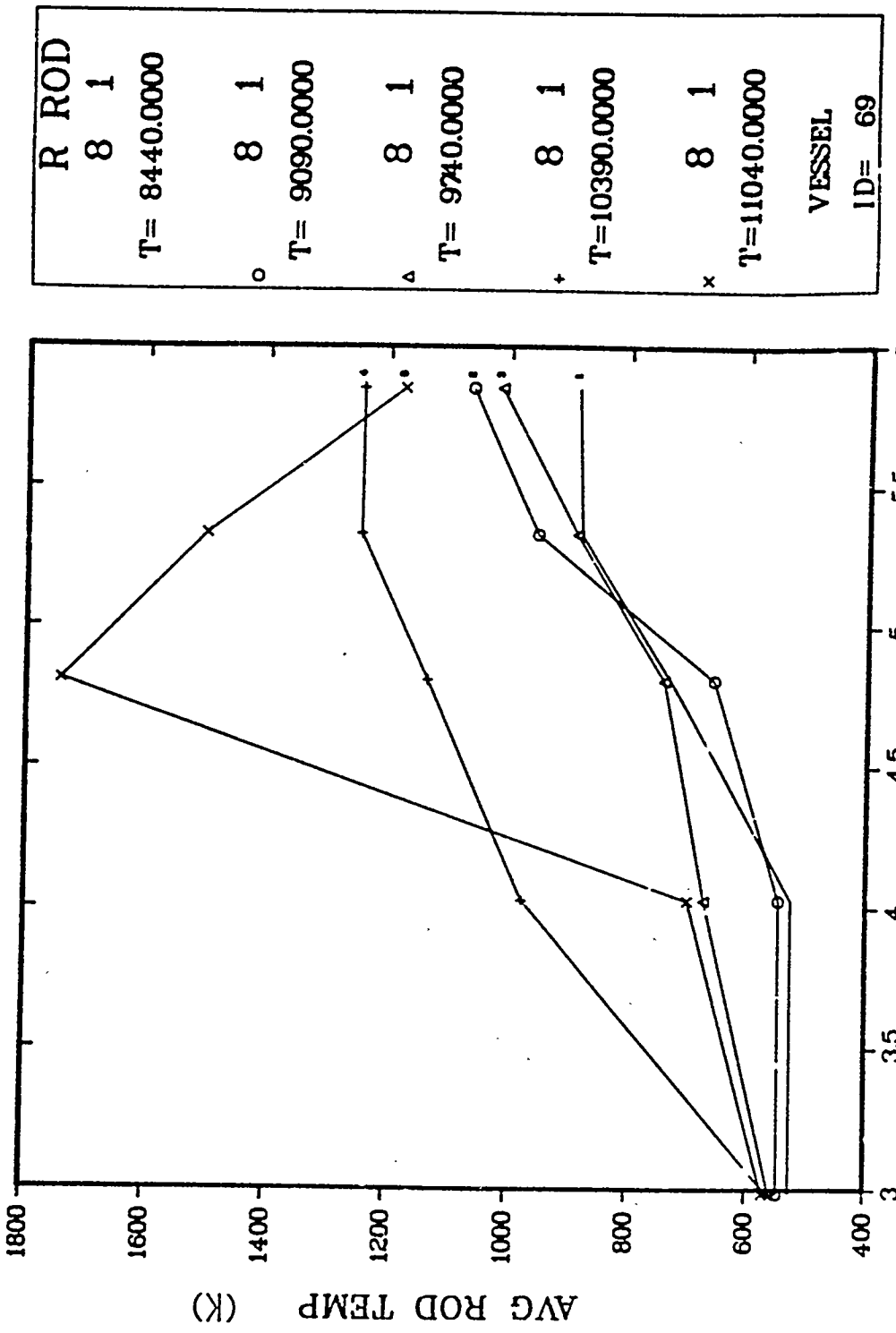

Fig. B-3.25. Average rod temperature axial profile vs time (Rod 1).

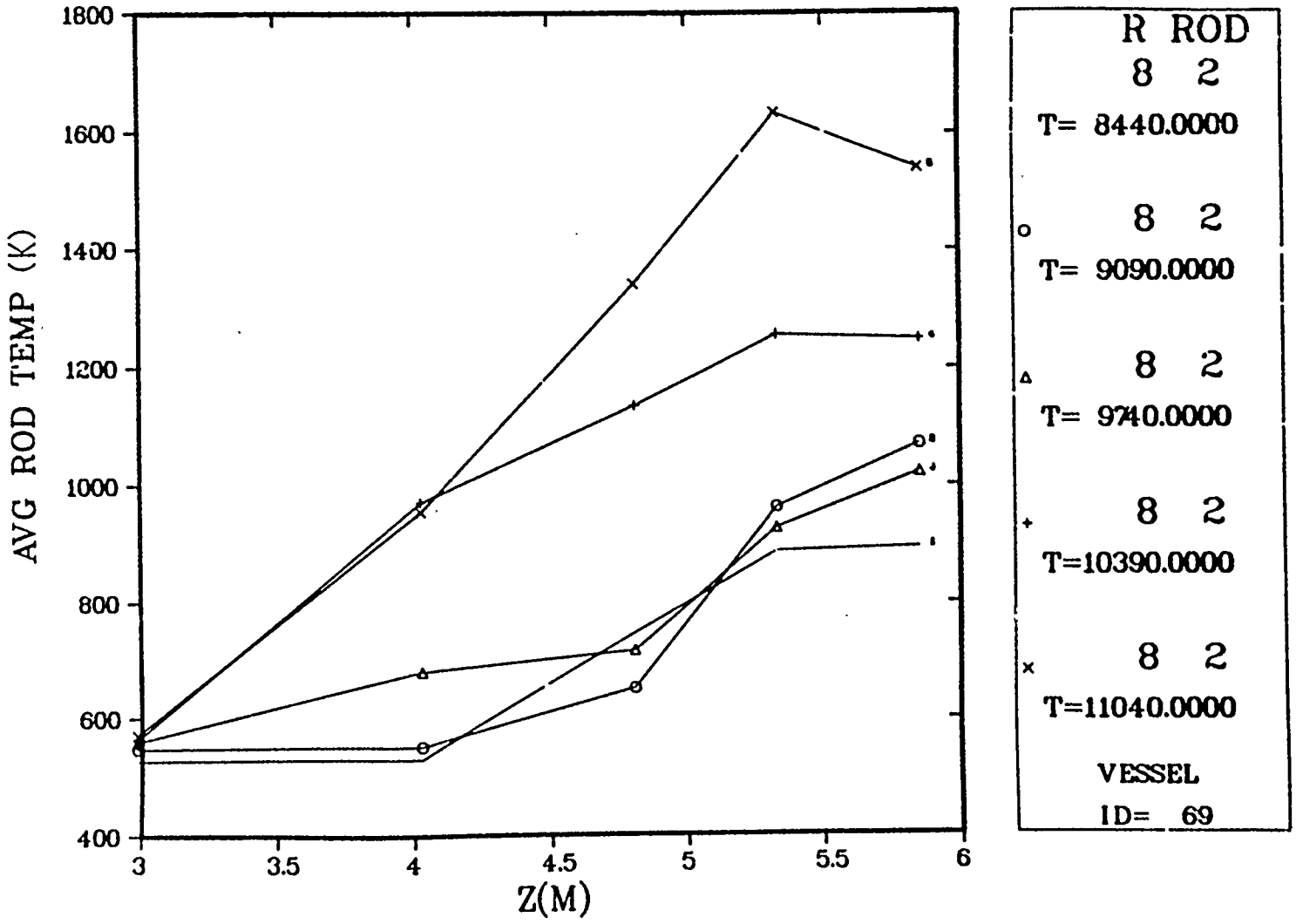

Fig. B-3.26. Average rod temperature axial profile vs time (Rod 2).

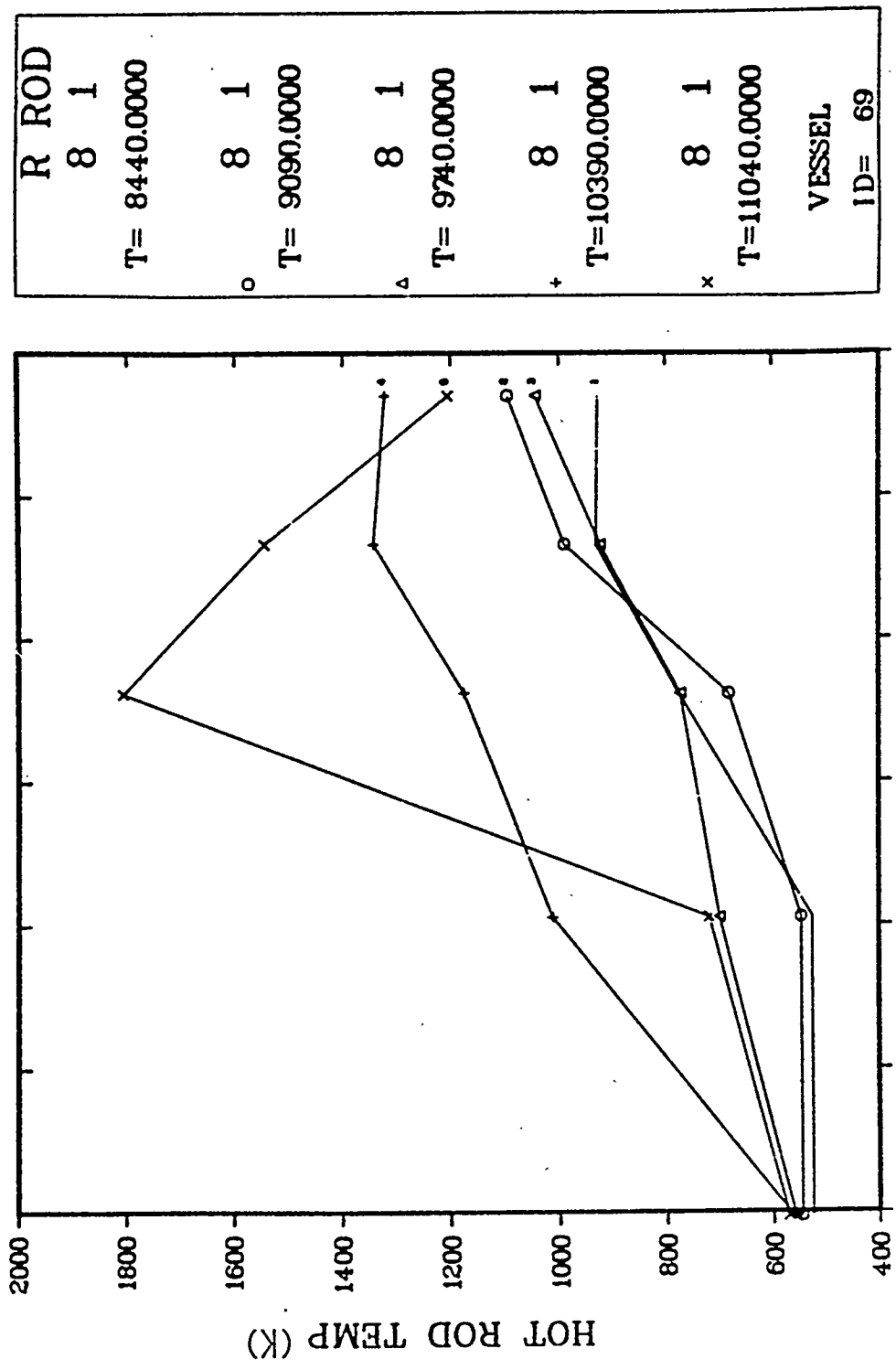

Fig. B-3.27. Hot-rod temperature axial profile vs time (Rod 1).

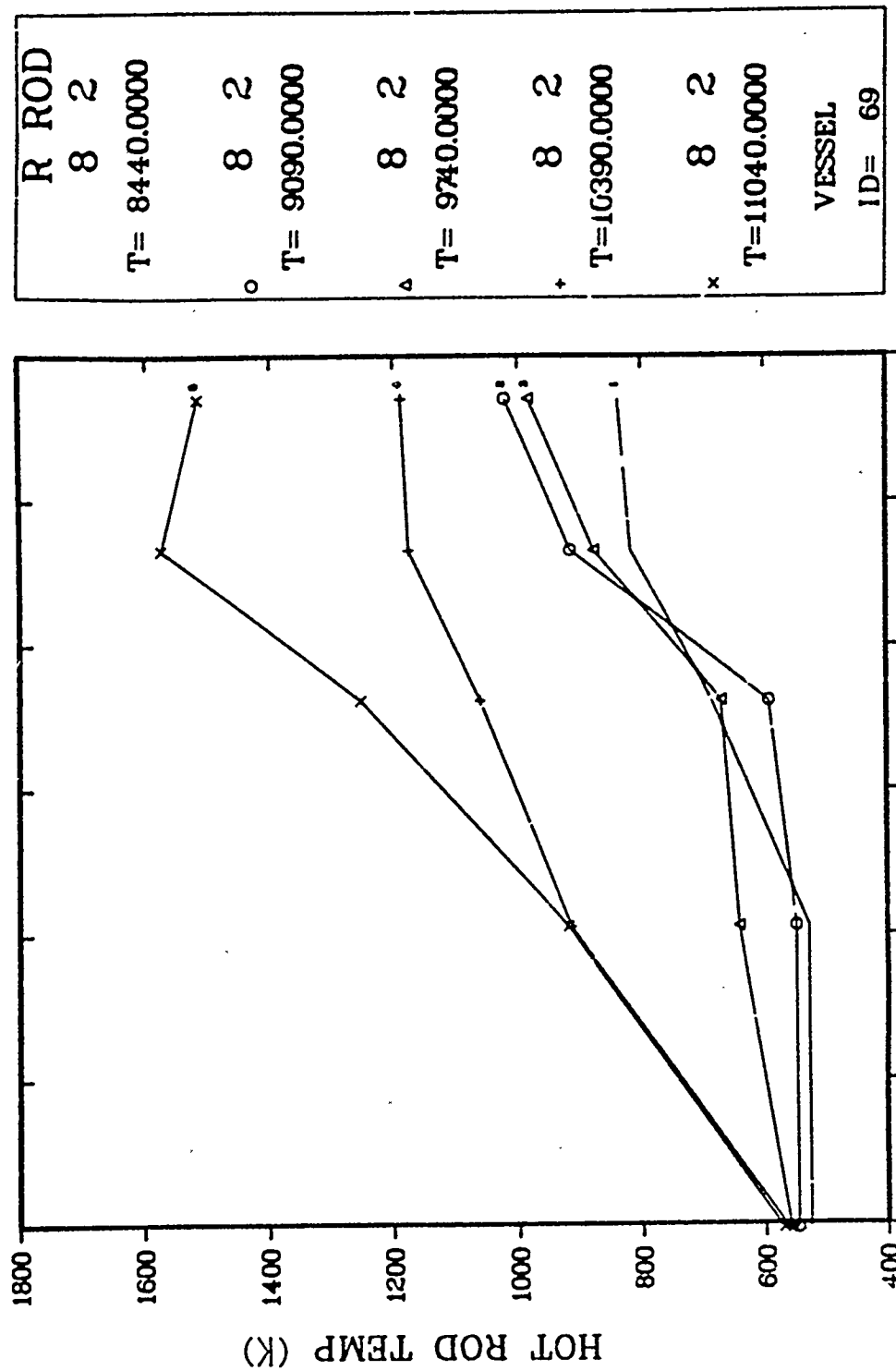

Fig. B-3.28. Hot-rod temperature axial profile vs time (Rod 2).

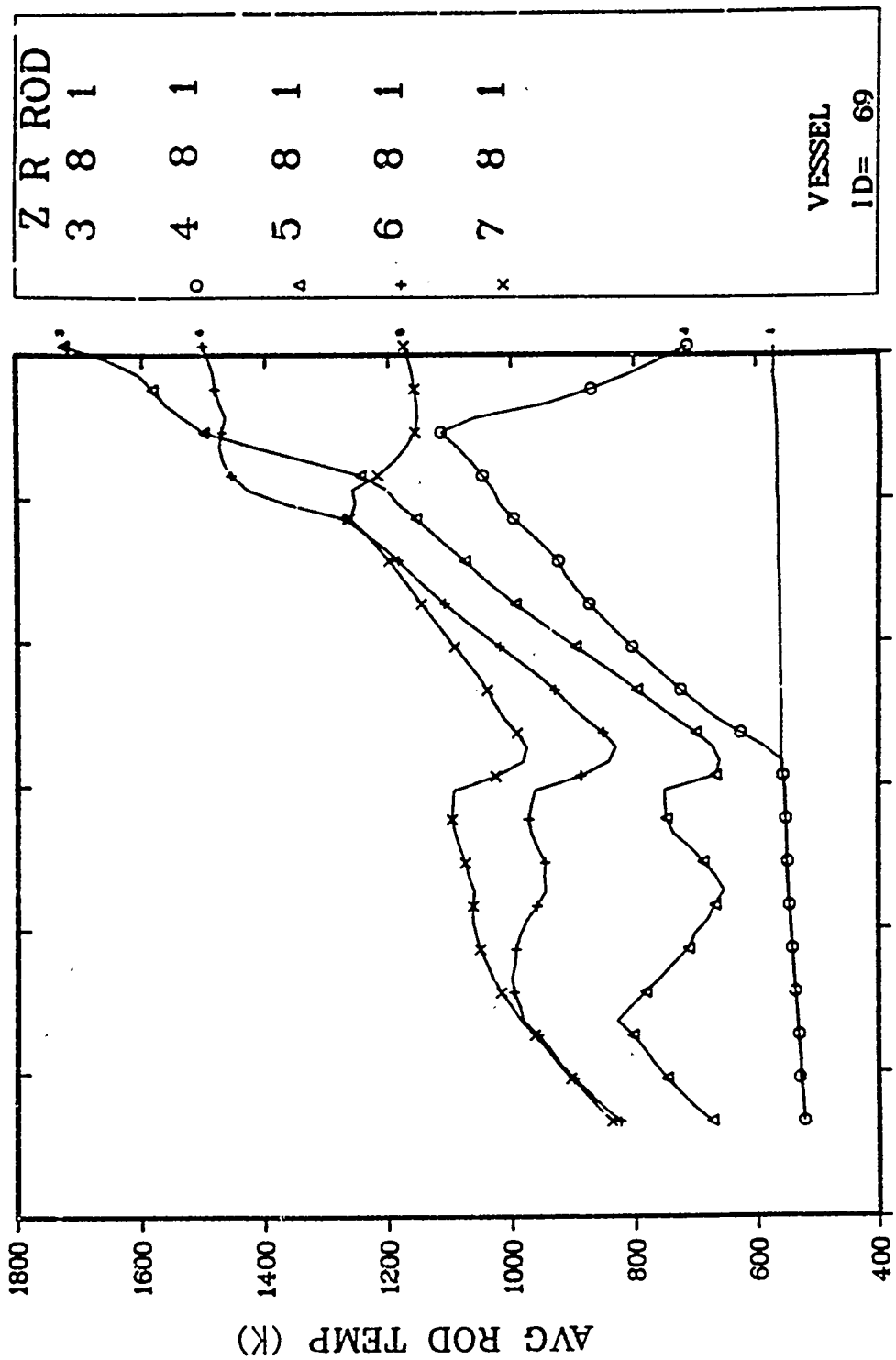

Fig. B-3.29. Average rod temperature axial profile (Rod 1).

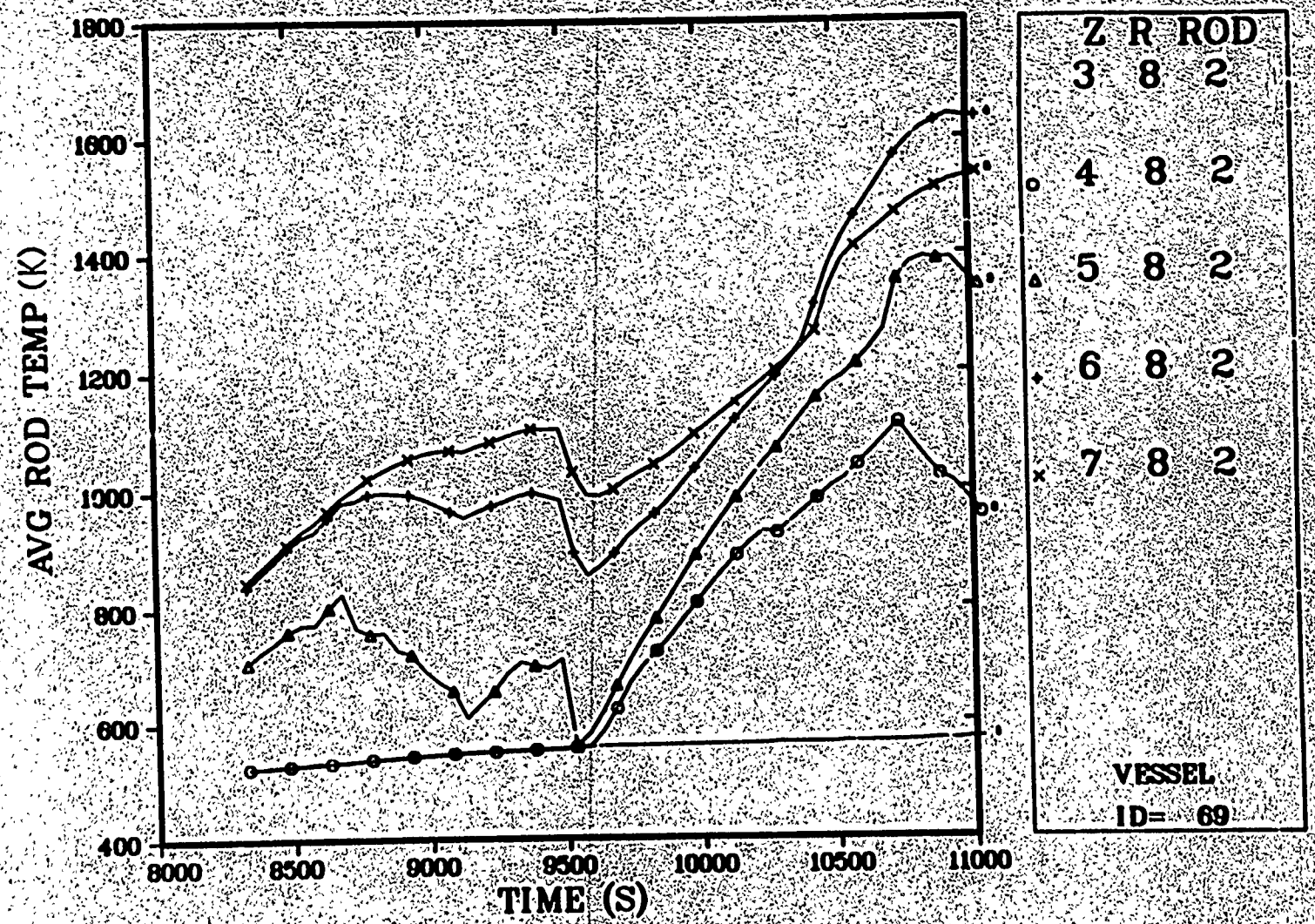

Fig. B-3.30. Average rod temperature axial profile (Rod 2).

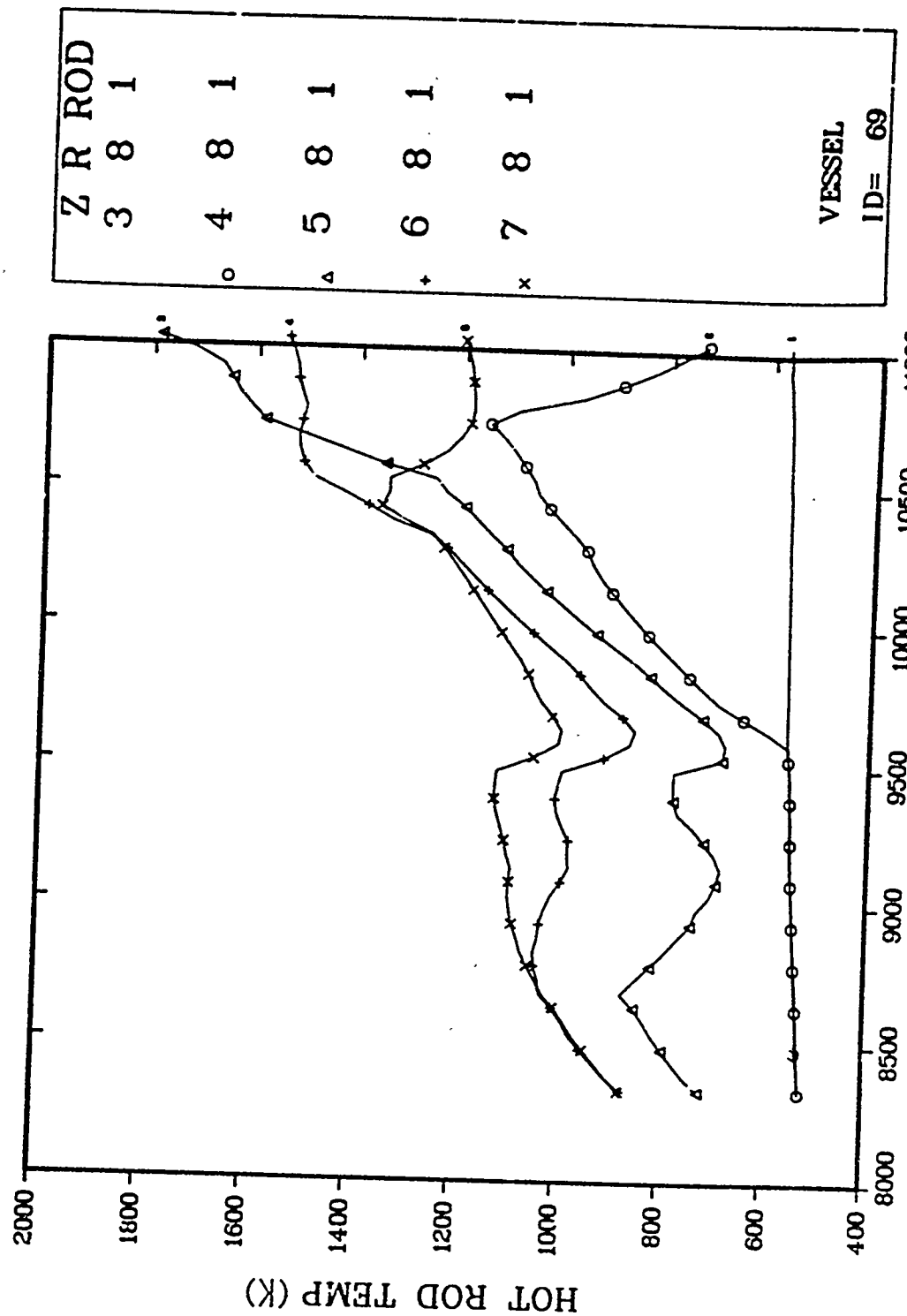

Fig. B-3.31. Hot-rod temperature axial profile (Rod 1).

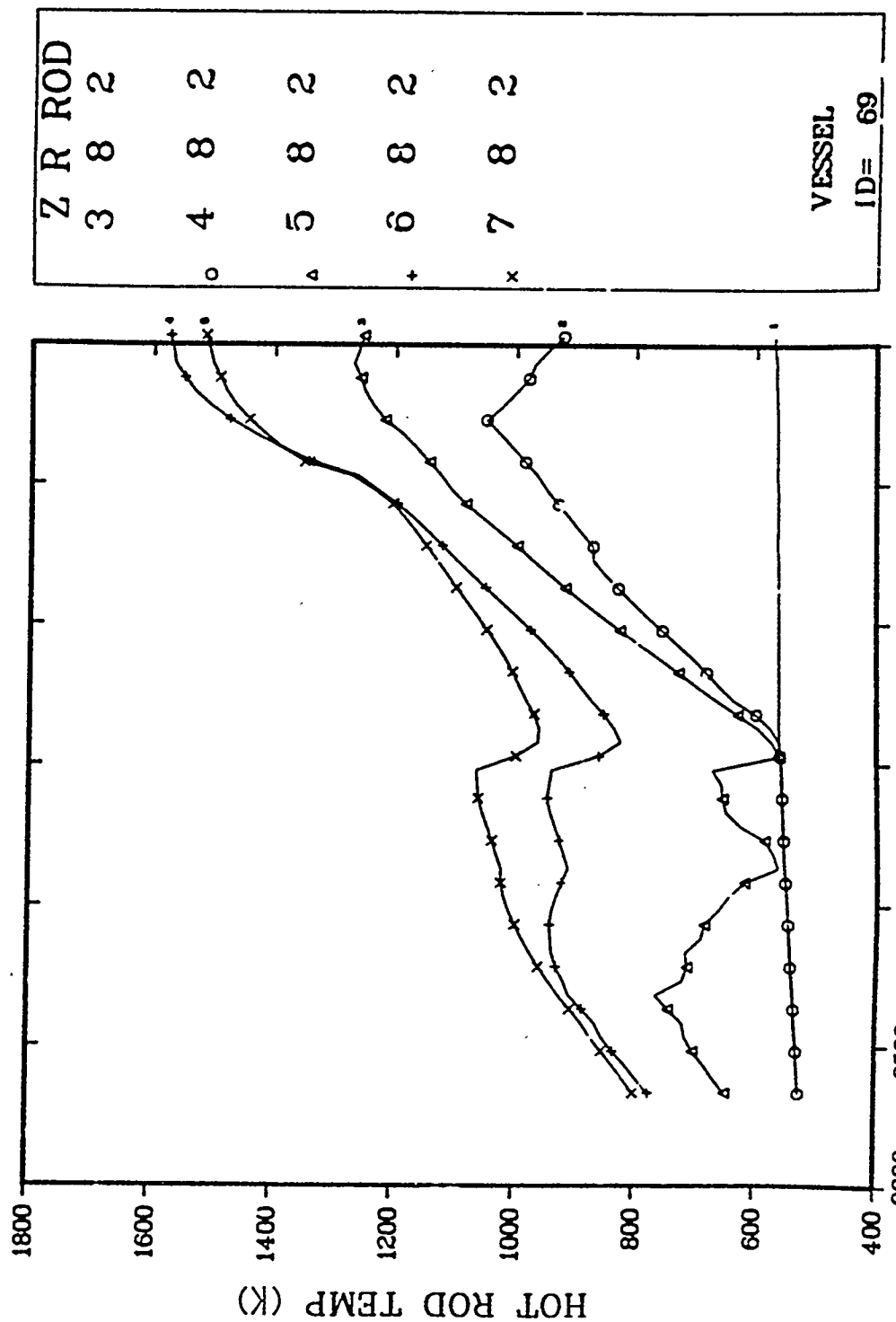

Fig. B-3.32. Hot-rod temperature axial profile (Rod 2).